Advanced Magnetoelastic and Magnetocaloric Materials for Device Applications

Ravi L. Hadimani

Wolfson Centre for Magnetics,

School of Engineering,

Cardiff University

December 2009

Submitted in accordance with the requirements for the degree of Doctor of Philosophy.

ProQuest LLC
789 East Eisenhower Parkway
P.O. Box 1346
Ann Arbor, MI 48106-1346

Dedicated to my parents:

Dr. Lingappa M. Hadimani and Mrs. Saroja L. Hadimani

Acknowledgement

During the course of completing the project objectives, many people assisted me and offered their support; I would like to express my sincere appreciation to my supervisor Prof. D. C. Jiles who helped me with his expertise in magnetics and guided me in right directions in spite of his busy schedule. I would also extend my appreciation to my second supervisor Dr. Y. Melikhov who helped me with his academic and moral support and to Dr. J. E. Snyder for useful discussions which contributed to the solutions of some of my problems in the project. I would like to acknowledge Dr. D. Fort and Dr. S. Koohpayeh of Materials and Metallurgy Department of Birmingham University who helped me carry out sample preparation, heat treatment and Laue measurements. I would like to thank Prof. H. Davies and Ms. N Mohd Saiden for helping me in carrying out high magnetic field measurements at the University of Sheffield. I would like to express my gratitude to the Royal Society for providing me studentship for three years to work on this project. I would also express my gratitude to IEEE Magnetic Society, UK Magnetic Society and Institute of Physics who supported me financially to present my work in various international conferences during my studies.

It would have not been possible for me to come all the way from India and take up this course without the inspiration and financial support from my parents and siblings. I would like to thank my fiancée Katarina Pastvova who supported me in every aspect of my life in order to help me in completing the project and my thesis. Last but not the least I would like to thank all my friends who have helped me directly or indirectly to complete this project with a sense of satisfaction.

Abstract

Magnetocaloric and magnetoelastic materials can be utilised in various device applications and have a potential to increase their efficiency by a considerable amount. In this thesis, $Gd_5(Si_xGe_{1-x})_4$ is extensively researched on its magnetic properties such as magnetic phase transition temperature, magnetostriction, magnetoresistance and anisotropy.

Field induced phase transition in $Gd_5(Si_xGe_{1-x})_4$ was observed in several compositions and the rate of change of the first order phase transition temperature was determined to be approximately 5 K/Tesla. Various methods of transition temperature measurements were compared and the Arrott plot technique was determined to be accurate method for magnetocaloric materials. An advanced technique based on Arrott plots was developed to estimate the second order phase transition temperature when it is suppressed by the first order phase transition. This technique was also extended to estimate the transition temperature of mixed phase alloys. Field induced phase transition at high temperature using high magnetic field measurements up to 9 Tesla were carried out on two compositions of $Gd_5(Si_xGe_{1-x})_4$ for $x=0.5$ and $x=0.475$ to validate the Arrott plot technique.

Magnetostriction measurements were carried out on $Gd_5(Si_xGe_{1-x})_4$ for various compositions. Fine structure was observed in the magnetostriction measurement in single crystal and polycrystalline $Gd_5Si_{1.95}Ge_{2.05}$ samples but not on other compositions, which might be due to the presence of a secondary phase. It was demonstrated that a giant magnetostriction of the order of 1813 ppm could be obtained by varying the temperature using a Peltier cell and removing the requirement of bulky equipment such as Physical Properties Measurement System (PPMS).

Magnetoresistance was measured for various compositions and an irreversible increase in resistivity was observed which depended linearly on the number of thermal cycles passing through the first order phase transition temperature. The irreversibly increased resistivity was recovered by holding the samples at high temperature for a long period of time of up to 3 days. A theoretical model was developed to explain the recovery in the resistance and was experimentally verified.

First order magnetocrystalline anisotropy constant K_1, easy and hard axes of the single crystal $Gd_5Si_{2.7}Ge_{1.3}$ sample were determined using magnetic moment as a function of angle of rotation of the sample at room temperature. Dependence of the first order phase transition temperature on the angle of rotation of the single crystal $Gd_5Si_2Ge_2$ sample was determined to be negligible.

Additionally polycrystalline samples of $Gd_5Si_{1.8}Ge_{2.2}$ and $Gd_5Si_{1.9}Ge_{2.1}$ were prepared by arc-melting and heat treatment was carried out on these samples in accordance with the literature to remove residual secondary phases in the sample at the Materials and Metallurgy Department of the Birmingham University. XRD measurements were carried out on these samples to confirm the crystal structure.

Table of Contents

List of Figures

List of Tables

List of Abbreviations and Symbols

AMR	Active magnetic refrigeration
B	Magnetic induction
Btu	Bitumen unit
CMR	Carnot magnetic refrigeration
DOE	Department of Energy
$Dy_5Si_{2.5}Ge_{1.5}$	Dysprosium silicon germanium
Dy_5Si_4	Dysprosium silicide
e	Charge on electron
EDS	Energy dispersion spectroscopy
Er_5Si_4	Erbium silicide
FeMnAs	Iron manganese arsenic
Gd	Gadolinium
$Gd_{1-x}Sm_xMn_2Si_2$	Gadolinium samarium manganese silicon
$Gd_5(Si_xGe_{1-x})_4$	Gadolinium Silicon Germanium
Gd_5T_4	Gadolinium silicide/germanide/gallium/tin
Ge	Germanium
h	Enthalpy
H	Magnetic field
H_F	Final magnetic field
H_I	Initial magnetic field
H_s	Saturation magnetic field
I	Current

k	Proportionality constant
K_0	Zero order anisotropy constant
K_1	First order anisotropy constant
K_2	Second order anisotropy constant
k_B	Boltzmann constant
K_s	Shape anisotropy constant
kWh	Kilo watt hour
L	Length
LaFeSi	Lanthanum iron silicon
M	Magnetic moment
M	Magnetisation
M	Molecular field constant
m_a	Magnetic moment along 'a' axis
m_b	Magnetic moment along 'b' axis
m_c	Magnetic moment along 'c' axis
MFM	Magnetic force microscopy
M-H	Magnetisation as a function of magnetic field
MnAs	Manganese arsenide
MPMS	Magnetic properties measurement system
n	Number of degrees of freedom
N	Number of dislocations
N_0	Initial number of dislocations
N_a	Demagnetisation factor along 'a' axis
N_c	Demagnetisation factor along 'c' axis
Ni_2MnGa	Nickel manganese gallium
NiMnFe	Nickel manganese iron

N_s	Charge carrier density
p	Pressure
P	Probability
ppm	parts per million
PPMS	Physical properties measurement system
q	Electric charge
R	Resistance
RKKY	Rudermann-Kittel-Kasuya-Yosida
$RMnO_3$	Rare earth manganese oxide
s	Arrhenius constant
S	Entropy
SEM	Scanning electron microscopy
Si	Silicon
Sm	Magnetic component of entropy
Sm_5Ge_4	Samarium germanide
SQUID	Superconducting quantum interference device
T	Temperature
t	Time
T^*_C	Second order phase transition temperature of the orthorhombic phase
T_{ad}	Adiabatic temperature
T_{av}	Average temperature
Tb_5Ge_4	Terbium germanide
$Tb_5Si_{2.25}Ge_{1.75}$	Terbium silicon germanium
Tb_5Si_4	Terbium silicide
T_c	Curie Temperature
T_{FO}	First order phase transition temperature

V	Voltage
V_H	Hall voltage
XRD	X-ray diffraction
α_1	Cosine of magnetisation with respect to 'a' axis
α_2	Cosine of magnetisation with respect to 'b' axis
α_3	Cosine of magnetisation with respect to 'c' axis
β	Critical component of H/M for compensation of above and below transition temperature
β_1	Cosine of magnetostriction w ith respect to 'a' axis
β_2	Cosine of magnetostriction w ith respect to 'b' axis
β_3	Cosine of magnetostriction with respect to 'c' axis
γ	Critical component of M for compensation of above and below transition temperature
Δ	Change in the parameter
ΔE	Threshold energy
ε	Strain
λ	Magnetostriction
λ_0	Spontaneous magnetostriction
λ_{100}	Magnetostriction along [100] direction
λ_{111}	Magnetostriction along [111] direction
λ_s	Saturation magnetostriction
μ	Permeability
μ_0	Permeability of air
μ_B	Bohr magneton
ρ	Resistivity
ρ_0	Initial resistivity

σ	Stress
τ	Mean free time of collision of electrons
χ	Susceptibility

Chapter 1: Introduction

1.1 Introduction

Increasing the efficiency of devices and hence reducing the energy consumption to save the environmental pollution is the order of the day. There is a tremendous benefit to be obtained from improving the efficiency of refrigeration and air conditioning. The domestic refrigeration energy consumption accounts for 7% of the total energy consumption in the United States of America [1] and 6% in the United Kingdom [2]. Industrial refrigeration and office space air conditioning will add up to an even higher percentage of energy consumption.

The normal liquid vapour refrigerators have a Carnot efficiency of 30% which is half the Carnot efficiency of current gadolinium based magnetic refrigerators [3]. With the invention of giant magnetocaloric effect in $Gd_5(Si_xGe_{1-x})_4$, there has been extensive research on magnetocaloric materials and magnetic refrigeration. Magnetic refrigerators built with the new giant magnetocaloric materials such as $Gd_5(Si_xGe_{1-x})_4$ and NiMnFe will have efficiency even higher than the 60% Carnot efficiency. There is a scope to reduce the energy consumption of the refrigeration sector by more than half which is equivalent to saving of $3.5\text{x}10^{15}$ Btu ($1.02\text{x}10^{12}$ kWh $\approx$ 30 billion dollars) [4] for the United States and $6.75\text{x}10^{6}$ Tonnes of Oil Equivalent ($87.7\text{x}10^{9}$ kWh $\approx$ 10.5 billion pounds) [5] for the United Kingdom by switching from normal liquid vapour to magnetic refrigeration. Apart from savings in energy, magnetic refrigerators also offer other benefits such as being non hazardous to the ozone layer.

$Gd_5(Si_xGe_{1-x})_4$ exhibits one of the highest giant magnetocaloric effects at the first order phase transition close to room temperature. It is important to study the properties of $Gd_5(Si_xGe_{1-x})_4$ in order to improve the performance of magnetic refrigerators. $Gd_5(Si_xGe_{1-x})_4$ also exhibits other

unusual properties at the first order phase transition such as giant magnetoresistance of $\Delta R/R = 25\%$ [6], colossal magnetostriction of the order of 10,000 ppm [7]. These extreme properties occur close to room temperature for compositions in the range $0.5 < x < 0.575$ which can be utilised in various engineering applications. These properties can be controlled by variation of temperature, magnetic field and composition which offer versatility to potential applications. There are few journal publications on thin films and nano structures of $Gd_5(Si_xGe_{1-x})_4$. The extreme properties at the first order phase transition might be even larger for the thin films or nano structures of $Gd_5(Si_xGe_{1-x})_4$. Further research into this area might yield very interesting and ground breaking properties for various engineering applications such as micro cooling and magnetic data recording.

In this thesis the properties of $Gd_5(Si_xGe_{1-x})_4$ have been thoroughly investigated with various measurements. The measurement results on its unusual properties arising from the first order phase transition have been discussed in detail in various chapters dedicating each chapter for a certain property. In Chapter 2, the phase diagram, crystal structure, Widmanstatten lines and measurements carried out on field induced first order phase transition have been discussed. Since the unusual properties in $Gd_5(Si_xGe_{1-x})_4$ arise from the first order phase transition, it is important to study this phase transition as described in Chapter 3. Various techniques of determining transition temperatures have been investigated. The Arrott plot was found to be more accurate technique to determine Curie temperature of magnetocaloric materials than inflection point or line projection method. An advanced technique based on Arrott plots has been developed for the first time to determine the projected second order phase transition temperature of the orthorhombic phase when it is suppressed by the first order phase transition. The Arrott plot technique was further used to estimate the transition temperature of individual phases in the mixed phase alloy of $Gd_5(Si_xGe_{1-x})_4$. High field measurements were carried out to verify the Arrott plot technique.

In Chapter 4, the magnetocaloric effect is discussed in detail. Methods of estimation of magnetocaloric effect have been discussed. Heat capacity measurements with zero applied field showing the phase transitions are presented. Problems affecting the heat capacity measurements using the old puck have been discussed and a new heat capacity puck has been reviewed. In Chapter 5 magnetostriction in $Gd_5(Si_xGe_{1-x})_4$ has been discussed. Measurements showing the fine structure observation in magnetostriction measurements have been presented. It was demonstrated that a giant thermally induced strain/ magnetostriction in $Gd_5Si_{2.09}Ge_{1.91}$ can be obtained by varying the temperature using a Peltier cell that has removed the requirement of bulky equipments such as PPMS (Physical Properties Measurement System) to obtain the giant magnetostriction/thermally induced strain at the first order phase transition.

In Chapter 6 electrical transport properties of $Gd_5(Si_xGe_{1-x})_4$ have been investigated. Various measurements are presented showing an irreversible increase in the resistivity of the samples due to thermal cycling across the first order phase transition. It was shown that thermally cycling the $Gd_5(Si_xGe_{1-x})_4$ samples through the first order phase transition causes irreversible micro-structural changes such as increase in dislocation density and micro-cracks which were seen through irreversible changes in coercivity and resistivity of the material. This is important as the magnetic material in the magnetic refrigerator will be cycled through its first order phase transition nearly a billion times in the life span of the refrigerator of approximately 15 years [8]. The irreversibly increased resistivity was recovered by holding the samples at higher temperatures. A model was developed to explain the resistivity recovery in these samples and was experimentally verified. In Chapter 7 magnetocrystalline anisotropy constant, easy axis and hard axis were determined using magnetic moment vs. rotation angle and magnetic moment vs. magnetic field measurements. The effect of orientation of single crystal samples with the applied magnetic field on the transition temperature was determined. In Chapter 8 conclusions and future work are presented.

Overall, the unusual properties of $Gd_5(Si_xGe_{1-x})_4$ are investigated in detail by various measurements. Advanced techniques are developed to estimate transition temperature when it is not possible to determine them experimentally. A new theoretical model has been developed to explain the resistivity recovery in $Gd_5(Si_xGe_{1-x})_4$ samples and this has been experimentally verified. This research has enabled the future investigators with new analytical tools and new insight into the preparation of the $Gd_5(Si_xGe_{1-x})_4$ system.

References

[1] A. Meier, "Refrigerator energy use in the laboratory and in the field", Energy and Buildings, **22**, pp. 233-243, (1995).

[2] Department of Trade and Industry, "Energy Consumption in the United Kingdom", National statistics, http://www.berr.gov.uk/files/file11250.pdf, pp. 9 and 24, (2002). Retrieved, November 2009

[3] C. Zimm, A. Jastrab, A. Sternberg, V. K. Pecharsky, K. Gscheidner, Jr., M. Osborne and I. Anderson, Adv. Cryog. Eng., **43, pp.** 1759, (1998).

[4] Energy Information Administration, DOE, "*Energy Consumption, Expenditures, and Emissions Indicators 1949-2008*", http://www.eia.doe.gov/emeu/aer/pdf/pages/sec1_13.pdf, Retrieved, November 2009

[5] Department of Energy and Climate Change, "Energy consumption in the UK: overall data tables 2009", http://www.decc.gov.uk/en/content/cms/statistics/publications/ecuk/ecuk.aspx Retrieved, November 2009.

[6] E. M. Levin, V. K. Pecharsky, K. A. Gschneidner, Jr., and G. J. Miller, "*Magnetic-field and temperature dependencies of the electrical resistance near the magnetic and crystallographic first-order phase transition of* $Gd_5(Si_2Ge_2)$.", Phys. Rev. B, **60**, pp. 7993-7997, (2001).

[7] L. Morellon, P. A. Algarabel, M. R. Ibarra, J. Blasco, B. Garcı´a-Landa, Z. Arnold, F. Albertini, "*Magnetic-field-induced structural phase transition in* $Gd_5(Si_{1.8}Ge_{2.2})$", Phys. Rev. B, **58**, R14721, (1998)

[8] K. Gscheidner, Jr., Magnetocalorics and Magnetic Cooling Meeting at EuroMat Conference, Glasgow, 10 September 2009.

Chapter 2: $Gd_5(Si_xGe_{1-x})_4$

2.1 Introduction

$Gd_5(Si_xGe_{1-x})_4$ (Gadolinium Silicon Germanium) was discovered by F. Holtzberg [1] and G. S. Smith [2, 3] in 1967 at IBM Watson Research Centre and Lawrence Radiation Laboratory respectively. Holtzberg was the first to show that $Gd_5(Si_xGe_{1-x})_4$ was ferromagnetic close to room temperature for certain values of x. $Gd_5(Si_xGe_{1-x})_4$ did not attract much attention until the discovery of the giant magnetocaloric effect by Pecharsky and Gschneidner from Ames Laboratory in 1997 [4, 5, 6, 7]. The number of publications on $Gd_5(Si_xGe_{1-x})_4$ have increased exponentially since then [8]. Holtzberg *et. al.* [1] reported that there exists an intermediate phase between silicon and germanium rich regions whose crystal structure is not orthorhombic. Pecharsky *et al.* identified the intermediate structure as the monoclinic structure and have studied the $Gd_5(Si_xGe_{1-x})_4$ system for various values of $0< x < 1$ [9, 10,11].

$Gd_5(Si_xGe_{1-x})_4$ exhibits a first order phase transition close to room temperature for the composition $x<0.575$ [9] from a low temperature orthorhombic phase to high temperature monoclinic phase which is accompanied by a large volumetric change in the crystal lattice. This change in the volume results in change in various magnetic, thermal and electrical properties of the material. These changes in properties are very large compared to those that occur close to the second order phase transition. Table 2.1 gives the change in properties due to the first order phase transition and their potential applications. Various groups have studied these extreme properties (except thermal conduction property), but except for the magnetic refrigerator by Lu *et. al.* [16] no devices have been built using $Gd_5(Si_xGe_{1-x})_4$.

The energy conversion efficiency of magnetic refrigerators reported by Zimm *et al.* [17] was as high as 60% of Carnot efficiency, which is much larger than the 30% achieved in conventional liquid/vapour cycle refrigeration. This finding has drawn attention to the magnetocaloric effect

especially to $Gd_5(Si_xGe_{1-x})_4$ as it exhibits one of the highest magnetocaloric effects near room temperature.

Table 2.1 Properties changes due to the first order phase transition and their applications

Property	Change in the property due to the first order phase transition	Potential Applications
Magnetocaloric Effect	**17° C for a field change of 5 Tesla [12]**	**Magnetic refrigerator, micro coolers, etc**
Magnetostriction	**10,000 ppm [13, 14]**	**Actuators, sensors, etc.**
Magnetoresistance	**25% [15]**	**Data recording heads, sensors etc.**
Thermal Conductivity	**??**	**??**

$Gd_5(Si_xGe_{1-x})_4$ is also one of the potential candidate material for actuator applications. It exhibits a colossal magnetostriction of 10,000 ppm along 'a' axis which is much larger than commercially available magnetostriction actuator material Terfenol-D which exhibits a linear magnetostriction of 2000 ppm and 0 ppm volumetric magnetostriction [18]. There are few papers in the literature on the magnetostrictive applications of $Gd_5(Si_xGe_{1-x})_4$. One of the reasons could be that for high frequency applications sudden changes in the magnetic fields can cause eddy current losses in $Gd_5(Si_xGe_{1-x})_4$ as it is a good electrical conductor. Nersessian *et al.* [19] tried to overcome this problem by preparing a composite of ball milled $Gd_5Si_2Ge_2$ (x=0.5) particles in a resin matrix but the maximum strain obtained by them was 1300 ppm.

There are not many reports in the literature on development of devices utilising giant magnetoresistance change in $Gd_5(Si_xGe_{1-x})_4$. There is a scope for further investigation into the developmental side of magnetoresistive sensors using $Gd_5(Si_xGe_{1-x})_4$.

2.2 Phase Diagram

$Gd_5(Si_xGe_{1-x})_4$ has different magnetic phases depending on temperature and composition as expressed through the value of x. This can be represented in the form of a phase diagram. Understanding of the phase diagram has evolved since it was first introduced by Pecharsky and Gschneidner of the Ames Laboratory, USA [6]. This is because certain regions in the phase diagram showed mixed phase regions and evaluating the exact value of x for the boundaries of this region was difficult. Fig 2.1 shows the first phase diagram that was published in 1997 [6] which does not show any mixed phase regions close to between orthorhombic I (Gd_5Si_4 type) and monoclinic phase but only between orthorhombic II (Sm_5Ge_4) and monoclinic phase values of x. Fig 2.2 shows one of the intermediate phase diagrams that was not published but was circulated as a private communication to selected researchers, and shows various phases for different compositions at temperatures higher than 350 K to 1000 K. [20].

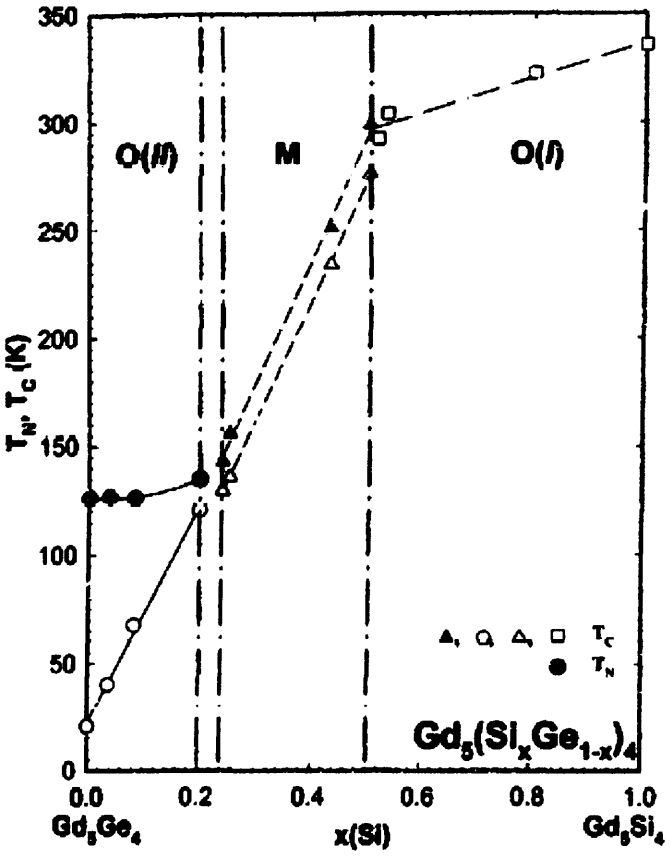

Fig 2.1 The first phase diagram published in 1997 with fewer compositions investigated [6].

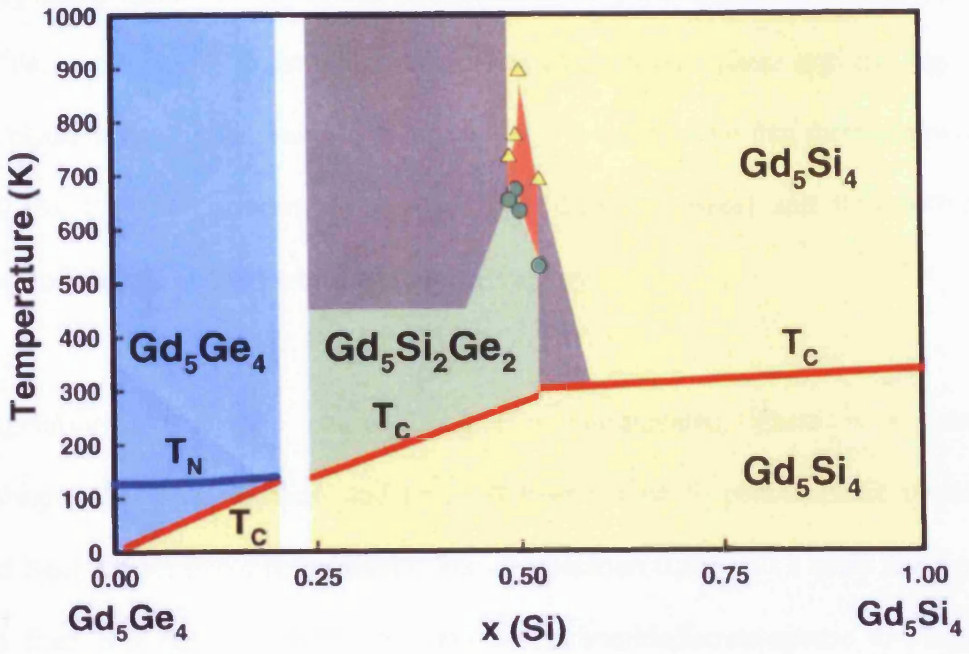

Fig. 2.2 Phase diagram showing different phases at various compositions at temperatures higher than 350 K [20].

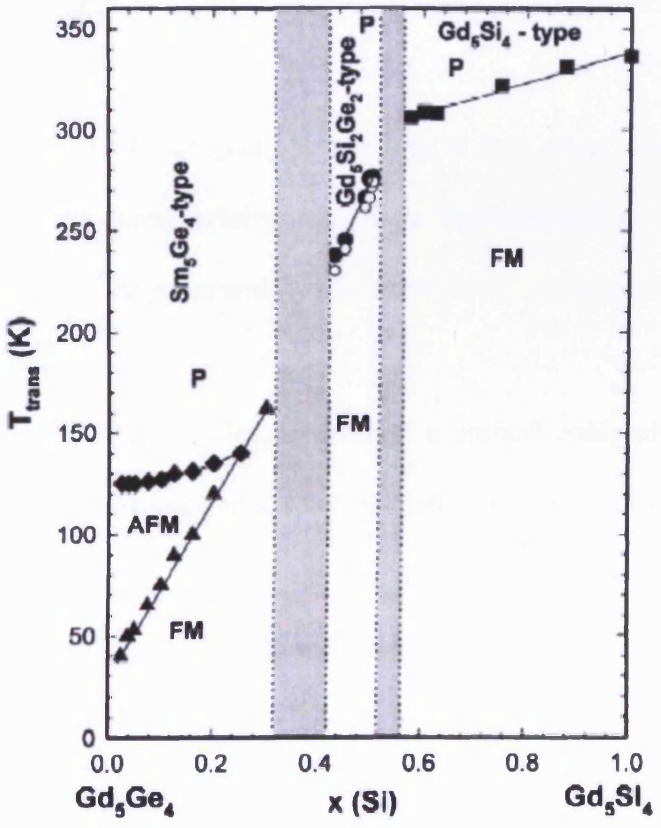

Fig 2.3 Latest phase diagram of $Gd_5(Si_xGe_{1-x})_4$ considering the mixed phase [9].

The latest phase diagram shows various compositions have been investigated to determine the exact values of the compositions to draw the boundaries of the mixed phase regions. Fig. 2.3 shows the complete phase diagram that was published in 2003. It can be seen that there are two mixed phase regions $0.3<x<0.4$ [9] (between Sm_5Ge_4 and $Gd_5Si_2Ge_2$ phases) and $0.51<x<0.575$ (between $Gd_5Si_2Ge_2$ and Gd_5Si_4 phases) which are shaded in grey.

For composition $x<0.25$, the phase diagram is complicated. There is a ferromagnetic to antiferromagnetic phase transition and an antiferromagnetic to paramagnetic phase transition at Curie and Neel temperatures respectively. For composition $0.25<x<0.3$ there is a first order phase transition from low temperature Gd_5Si_4 type orthorhombic/ferromagnetic to high temperature Sm_5Ge_4 type orthorhombic/paramagnetic. This region of the phase diagram is termed the "germanium rich region" and it is not investigated widely as the first order phase transition temperature at which the extreme change in properties exists is much lower than room temperature.

For composition $0.4<x<0.51$, $Gd_5(Si_xGe_{1-x})_4$ exhibits a first order phase transition from low temperature Gd_5Si_4 type orthorhombic/ferromagnetic to high temperature monoclinic phase close to room temperature. Hence it is the most widely studied region in the phase diagram.

For composition $0.575<x<1$, $Gd_5(Si_xGe_{1-x})_4$ exhibits a second order phase transition from low temperature Gd_5Si_4 type orthorhombic/ferromagnetic to high temperature Gd_5Si_4 type orthorhombic/paramagnetic phase above room temperature. There is no change in the crystal structure of the material at this phase transition; hence the change in properties is not so large as at the first order phase transition. The mixed phase for the composition $0.3<x<0.4$ is composed of Sm_5Ge_4 type orthorhombic and $Gd_5Si_2Ge_2$ type monoclinic phases simultaneously at all temperatures. The mixed phase for the composition $0.51<x<0.575$ consists of $Gd_5Si_2Ge_2$ type monoclinic and Gd_5Si_4 type orthorhombic phases simultaneously at all temperatures.

Table 2.2 Magnetic ordering temperature and magnetocaloric properties of $Gd_5(Si_xGe_{1-x})_4$ phases [21].

	Composition	Curie Temperature (K)	Neel Temperature (K)	Magnetocaloric Effect	
				Isothermal entropy change, ΔS, (mJ/cm^3K)	Adiabatic temperature change, ΔT
Sm_5Ge_4 Orthorhombic	Gd_5Si_4	336	–	61.7	8.8
	$Gd_5Si_{3.5}Ge_{0.5}$	331	–	55.0	7.3
	$Gd_5Si_{3.0}Ge_{1.0}$	323	–	65.0	8.6
	$Gd_5Si_{2.5}Ge_{1.5}$	313	–	70.7	8.5
	$Gd_5Si_{2.06}Ge_{1.94}$	306	–	70.5	8.0
Monoclinic	**$Gd_5Si_{2.0}Ge_{2.0}$**	**276**	**–**	**140**	**15.0**
	$Gd_5Si_{1.72}Ge_{2.28}$	**246**	**–**	**298**	**18.8**
	$Gd_5Si_{1.0}Ge_{3.0}$	**140**	**–**	**538**	**11.8**
	$Gd_5Si_{0.9}Ge_{3.1}$	**130**	**–**	**240**	**10.5**
Gd_5Si_4 Orthorhombic	$Gd_5Si_{0.8}Ge_{3.2}$	121	135	166	9.2
	$Gd_5Si_{0.33}Ge_{3.67}$	68	128	287	11.2
	$Gd_5Si_{0.15}Ge_{3.85}$	40	127	177	8.8
	Gd_5Ge_4	20	125	128	7.2

Transition temperatures of all the compositions including the Neel temperatures along with the adiabatic temperature change and isothermal entropy change at the Curie temperature are shown in Table 2.2. It is noticeable that the magnetocaloric effect in terms of both adiabatic temperature change and isothermal entropy change is highest for the compositions that exhibit the $Gd_5Si_2Ge_2$ type monoclinic phase.

2.3 Lattice Structure

The lattice structure of $Gd_5(Si_xGe_{1-x})_4$ is different for different values of x [6]. It can be divided into three main structures in accordance with the phase diagram: Sm_5Ge_4 type orthorhombic, Gd_5Si_4 type orthorhombic and $Gd_5Si_2Ge_2$ type monoclinic. The crystal structure is formed from the basic slabs for all values of x. Each unit cell in all the above mentioned structures consists of two slabs and accounts for 36 atoms.

Fig. 2.4 (a) shows a projection along 'b' axis which is common to all the structures showing slabs with gadolinium atoms in blue and silicon and germanium in red or green. Fig. 2.4 (b), (c) and (d) shows projection along 'c' axis for Sm_5Ge_4 type orthorhombic, Gd_5Si_4 type orthorhombic and $Gd_5Si_2Ge_2$ type monoclinic structures respectively [6, 9].

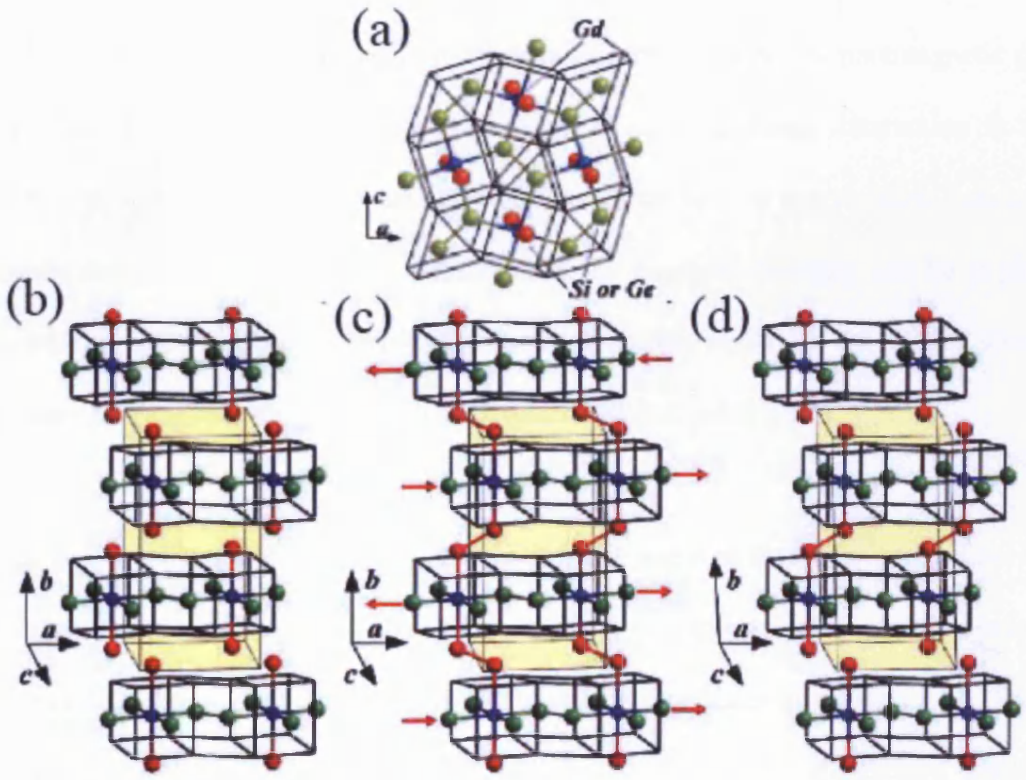

Fig 2.4 Crystal structures of $Gd_5(Si_xGe_{1-x})_4$: (a) projection of slabs along 'b' axis which is common to all the structures. (b), (c) and (d) are projections along c axis of Sm_5Ge_4 type orthorhombic, Gd_5Si_4 type orthorhombic and $Gd_5Si_2Ge_2$ type monoclinic structures respectively [6, 9].

The low temperature orthorhombic Gd_5Si_4 type structure which exists below the Curie temperature for all the compositions has covalent type of bonding between Si and Si or Ge and Ge atoms connecting every slab (Fig. 2.4(c)). A similar kind of covalent bonding exists between Si and Si or Ge and Ge atoms in $Gd_5Si_2Ge_2$ type monoclinic structures but only between the alternating slabs (Fig. 2.4(d)). Sm_5Ge_4 type orthorhombic structure does not have any covalent type of bonding between the slabs (Fig. 2.4(b)). It is interesting to note that ferromagnetism exists only when the covalent type bonds exist between all the slabs which happens only when the crystal structure is Gd_5Si_4 type orthorhombic. Hence crystallography and magnetic order are closely related.

Lanthanide systems (rare earth metals and compounds) exhibit magnetism due to indirect RKKY (Ruderman-Kittel-Kasuya-Yosida) interaction by unpaired inner shell 4*f* electrons through the outer shell 6*s* electrons [22]. In $Gd_5(Si_xGe_{1-x})_4$ system the RKKY interaction exists but doesn't explain the abrupt first order phase transition from the ferromagnetic to the paramagnetic phases. This can be explained by the existence of a Gd-Si/Ge-Gd super-exchange interaction in the Gd_5Si_4 type orthorhombic structure [22, 23, and 24]. When all or half of the covalent bonds are broken the super-exchange is broken, hence the reduction in magnetic moment can be explained [23]. The magnetic moment in pure gadolinium is lower than $Gd_5(Si_xGe_{1-x})_4$ for $x>0.57$ which is due to the existence of super-exchange interaction between Gd-Si/Ge-Gd.

Crystallographic data including the non orthogonal angle of the monoclinic phase was determined by Pecharsky *et. al.* [9] using room temperature X-ray diffraction. The monoclinic structure has a very small deviation in angle γ from the orthorhombic structure angle γ by $\approx 3°$. The lattice volume of Sm_5Ge_4 type orthorhombic structure is larger than monoclinic structure which is larger than Gd_5Si_4 type orthorhombic structure. Table 2.3 shows the lattice parameters for various compositions at room temperature including the unit cell volume and the angle of the monoclinic structure.

Table 2.3 Crystallographic data of $Gd_5(Si_xGe_{1-x})_4$ for various compositions and for heat treated samples in monoclinic phase [9].

Crystallographic data of the single phase $Gd_5(Si_zGe_{1-z})_4$ alloys as determined from Rietveld refinement

Composition	Space group	Lattice parameters (Å)			γ(°)	Unit cell volume (Å^3)
		a	*b*	*c*		
Sm_5Ge_4-type structure						
Gd_5Ge_4 [a]	*Pnma*	7.6968(5)	14.831(1)	7.7851(1)	–	888.7(2)
$Gd_5(Si_{0.005}Ge_{0.995})_4$	*Pnma*	7.6967(6)	14.831(1)	7.7819(6)	–	888.3(2)
$Gd_5(Si_{0.025}Ge_{0.975})_4$	*Pnma*	7.6953(5)	14.830(1)	7.7829(6)	–	888.2(2)
$Gd_5(Si_{0.038}Ge_{0.962})_4$	*Pnma*	7.6951(5)	14.826(1)	7.7816(5)	–	887.8(2)
$Gd_5(Si_{0.050}Ge_{0.950})_4$	*Pnma*	7.6939(5)	14.827(1)	7.7812(6)	–	887.7(2)
$Gd_5(Si_{0.075}Ge_{0.925})_4$	*Pnma*	7.6893(5)	14.822(1)	7.7782(5)	–	886.5(2)
$Gd_5(Si_{0.083}Ge_{0.917})_4$ [a]	*Pnma*	7.689(1)	14.822(1)	7.777(2)	–	886.4(2)
$Gd_5(Si_{0.100}Ge_{0.900})_4$	*Pnma*	7.6881(7)	14.822(1)	7.7763(7)	–	886.2(2)
$Gd_5(Si_{0.125}Ge_{0.875})_4$	*Pnma*	7.6858(4)	14.817(1)	7.7752(5)	–	885.5(2)
$Gd_5(Si_{0.150}Ge_{0.850})_4$	*Pnma*	7.6868(5)	14.819(1)	7.7738(6)	–	885.4(2)
$Gd_5(Si_{0.160}Ge_{0.840})_4$ [a]	*Pnma*	7.6797(4)	14.816(1)	7.7713(5)	–	884.2(2)
$Gd_5(Si_{0.225}Ge_{0.775})_4$ [a]	*Pnma*	7.6745(4)	14.811(1)	7.7670(4)	–	882.8(2)
$Gd_5(Si_{0.253}Ge_{0.747})_4$ [a]	*Pnma*	7.6689(6)	14.804(1)	7.7609(6)	–	881.1(2)
$Gd_5(Si_{0.300}Ge_{0.700})_4$	*Pnma*	7.6617(6)	14.801(1)	7.7604(6)	–	880.1(2)
$Gd_5(Si_2Ge_2)$-type structure						
$Gd_5(Si_{0.430}Ge_{0.570})_4$ [a]	$P112_1/a$	7.5906(7)	14.810(1)	7.7864(8)	93.146(5)	874.0(2)
1570 K/1 h	$P112_1/a$	7.5932(6)	14.812(1)	7.7843(7)	93.202(4)	874.1(2)
$Gd_5(Si_{0.450}Ge_{0.550})_4$	$P112_1/a$	7.5904(7)	14.810(1)	7.7830(4)	93.191(4)	873.6(3)
1570 K/1 h	$P112_1/a$	7.5910(6)	14.811(1)	7.7828(4)	93.197(4)	873.7(2)
$Gd_5(Si_{0.488}Ge_{0.512})_4$	$P112_1/a$	7.5859(6)	14.808(1)	7.7817(6)	93.173(2)	872.8(2)
1570 K/1 h	$P112_1/a$	7.5873(5)	14.808(1)	7.7819(5)	93.216(3)	872.9(2)
$Gd_5(Si_{0.495}Ge_{0.505})_4$	$P112_1/a$	7.5835(6)	14.807(1)	7.7815(6)	93.182(4)	872.4(2)
1570 K/1 h	$P112_1/a$	7.5845(6)	14.807(1)	7.7802(7)	93.205(4)	872.4(2)
$Gd_5(Si_{0.500}Ge_{0.500})_4$ [a]	$P112_1/a$	7.5854(7)	14.802(2)	7.7800(8)	93.176(4)	872.5(3)
1570 K/1 h	$P112_1/a$	7.5863(6)	14.810(1)	7.781(6)	93.200(4)	872.8(2)
$Gd_5(Si_{0.503}Ge_{0.497})_4$	$P112_1/a$	7.5825(5)	14.806(1)	7.7798(6)	93.182(4)	872.1(2)
1570 K/1 h	$P112_1/a$	7.5838(6)	14.806(1)	7.7797(7)	93.199(4)	872.1(2)
Gd_5Si_4-type structure						
$Gd_5(Si_{0.575}Ge_{0.425})_4$	*Pnma*	7.5119(5)	14.788(1)	7.7963(4)	–	866.0(2)
$Gd_5(Si_{0.600}Ge_{0.400})_4$	*Pnma*	7.5084(5)	14.782(1)	7.7956(5)	–	865.2(2)
$Gd_5(Si_{0.625}Ge_{0.375})_4$	*Pnma*	7.5059(5)	14.775(1)	7.7839(5)	–	863.2(2)
$Gd_5(Si_{0.750}Ge_{0.250})_4$	*Pnma*	7.4972(5)	14.765 (1)	7.7709(5)	–	860.2(2)
$Gd_5(Si_{0.800}Ge_{0.200})_4$ [a]	*Pnma*	7.4963(9)	14.765(2)	7.771(1)	–	860.1(3)
$Gd_5(Si_{0.875}Ge_{0.125})_4$	*Pnma*	7.4902(5)	14.7522(9)	7.7559(5)	–	857.0(2)
Gd_5Si_4 [a]	*Pnma*	7.4822(4)	14.7396(7)	7.7453(4)	–	854.2(1)

2.4 Widmanstatten Lines

There has been a great interest in the microstructure of $Gd_5(Si_xGe_{1-x})_4$ due to the exhibition of extreme and unusual properties at the first order phase transition. Szade *et al.* [25] reported the existence of regular straight lines in the microstructure of single $Gd_5(Si_xGe_{1-x})_4$ samples which were not identified. A later study by Meyers e*t al.* [26] using Scanning Electron Microscopy (SEM) and

Energy Dispersion Spectroscopy (EDS) reported an increase in content of Gd and O but a decrease in Si and Ge and identified the regular system of lines as a secondary phase in the form of Widmanstatten lines. The secondary phase was hypothesised by Meyers *et al.* [26] to be rods of $Gd_5(Si/Ge)_3$ which was later confirmed by other researchers [27, 28].

Widmanstatten structures are formed by a solid state precipitation reaction from a supersaturated solution which are normally in the form of regular rods or needles. Widmanstatten lines were first reported by Widmanstatten in 1808 appearing on a nickel-iron meteorite when its polished surface was etched by nitric acid. These structures were normally observed along a specific set of $\{h\ k\ l\}$ directions. Fig. 2.5 shows Widmanstatten lines in single crystal $Gd_5Si_2Ge_2$ (x=0.5) sample, (a) shows a lower magnification of the lines in the sample observed (b) shows a higher magnification of the lines crossing each other. They normally show a constant aspect ratio with lengths of up to 100 μm and width of less than 1 μm.

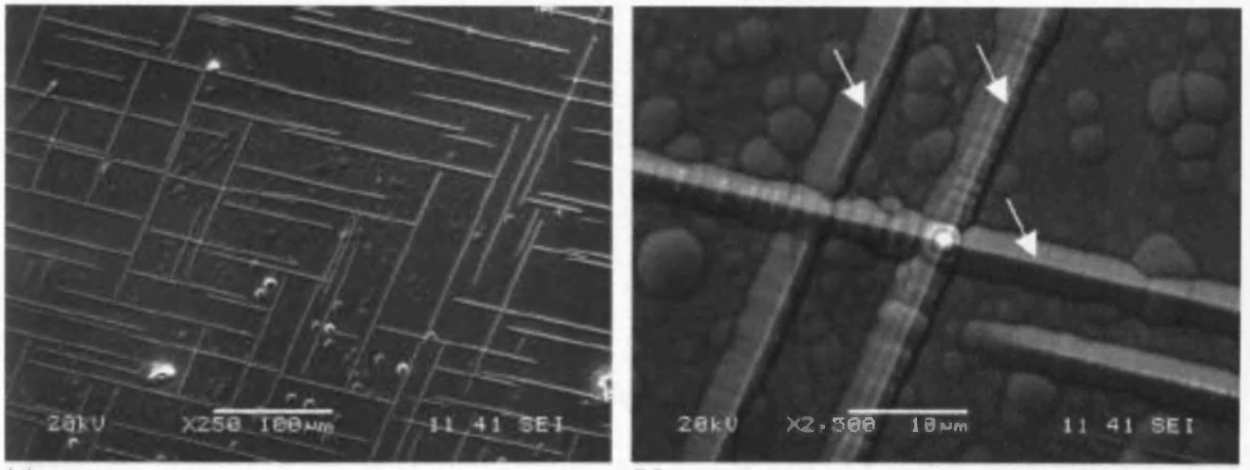

Fig. 2.5 SEM images of Widmanstatten lines on the surface of a single crystal $Gd_5Si_2Ge_2$ (x=0.5) sample (a) showing low magnification and (b) showing a high magnification of the lines [27].

Widmanstatten lines in $Gd_5(Si_xGe_{1-x})_4$ samples intersect each other at angle of 80° [25, 27]. Ugurlu *et al.* [27, 29] studied the orientation and alignment of Widmanstatten lines in single crystal $Gd_5Si_2Ge_2$ (x=0.5) samples with respect to the crystal lattice indices. When the single crystal is

viewed along [001] direction the lines appear to align with [010] and [100] directions. And when viewed along [100] direction they appear to align with [010] and [001] directions. When the single crystal is aligned in [010] and viewed the Widmanstatten lines appear to make 50° and 40° to [001] and [100] respectively as shown in Fig. 2.6.

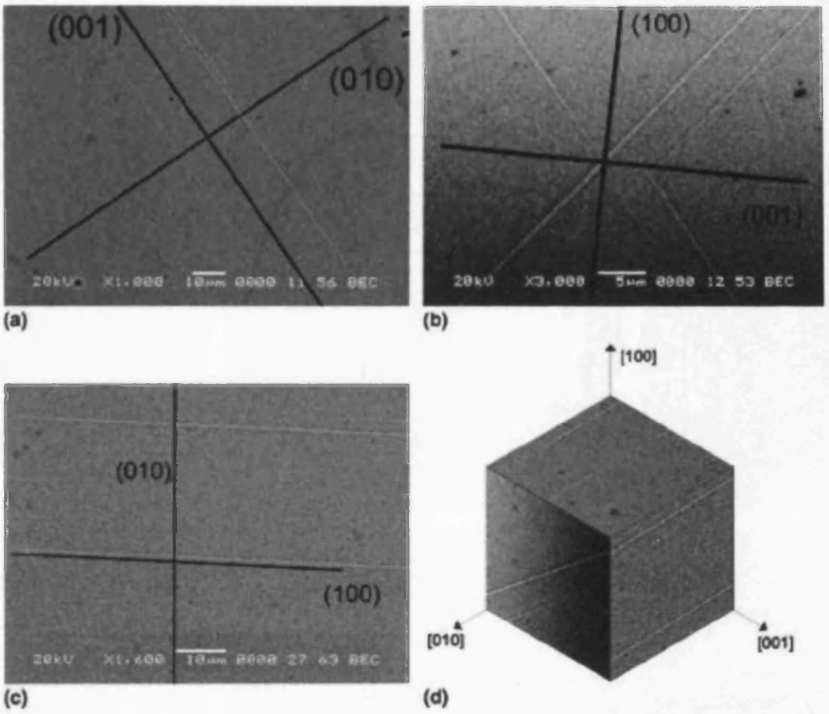

Fig 2.6 Alignment of Widmanstatten lines along major crystal indices (a) when viewed along 'a' axis (b) when viewed along 'b' axis; lines making 50° and 40° to [001] and [100] respectively and (c) when view along 'c' axis. [27]

Ugurlu *et al.* [30] conducted further study of Widmanstatten lines on other rare earth systems and reported the observation similar to $Gd_5(Si_xGe_{1-x})_4$ samples. Fig. 2.7 shows Widmanstatten lines observation through Scanning Electron Microscope (SEM) of (a) Gd_5Si_4, (b) Gd_5Ge_4, (c) $Gd_5Si_2Ge_2$, (d) Dy_5Si_4, (e) $Dy_5Si_{2.5}Ge_{1.5}$, (f) $Dy_5Si_{3.0}Ge_{1.0}$, (g) Tb_5Si_4, (h) Tb_5Ge_4, (i) Er_5Si_4, (j) $Tb_5Si_{2.25}Ge_{1.75}$. It was confirmed by Energy Dispersive Spectroscopy (EDS) in all the above systems that the Widmanstatten lines are formed by secondary phase of $R_5(Si/Ge)_3$ where R stands for the rare earths of Gd, Dy, Tb and Er.

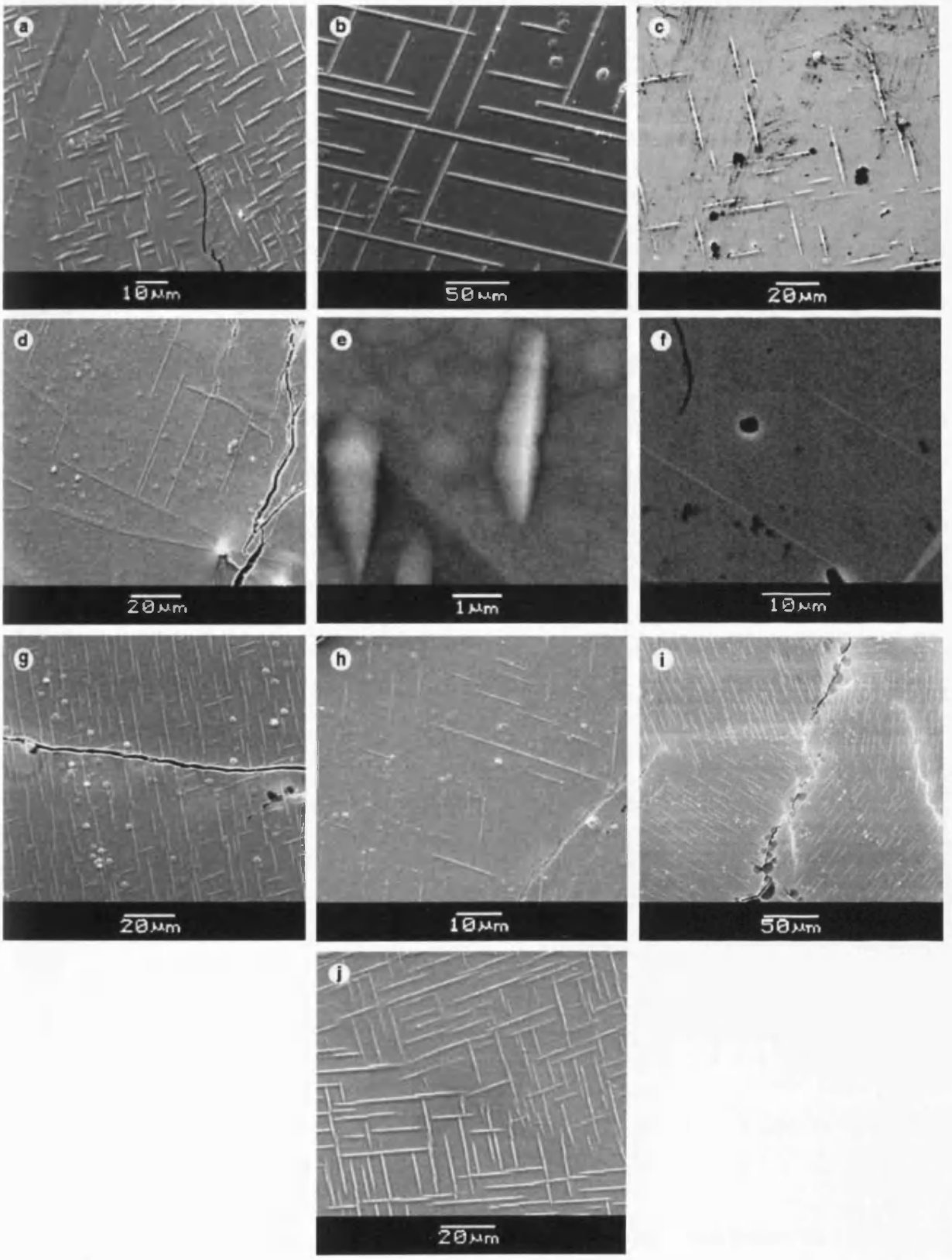

Fig. 2.7 Widmanstatten lines observation through Scanning Electron Microscope (SEM) of (a) Gd_5Si_4, (b) Gd_5Ge_4, (c) $Gd_5Si_2Ge_2$, (d) Dy_5Si_4, (e) $Dy_5Si_{2.5}Ge_{1.5}$, (f) $Dy_5Si_{3.0}Ge_{1.0}$, (g) Tb_5Si_4, (h) Tb_5Ge_4, (i) Er_5Si_4, (j) $Tb_5Si_{2.25}Ge_{1.75}$. [30]

2.5 Phase Transition

There are various types of phase transformations such as solid-liquid-gaseous phase transitions, crystallographic phase transitions and magnetic phase transitions. During any phase transition, Gibbs free energy is continuous but its derivatives can be discontinuous. If the n^{th} derivative of the Gibbs free energy is discontinuous then it is called n^{th} order phase transition [31, 32]. Magnetic phase transitions are mainly classified into two categories; first order phase transitions and second order phase transitions. This classification is done based on whether the magnetic Gibbs free energy has a discontinuity at its first or second derivatives.

Most of the phase transitions we come across are first order phase transitions i.e. solidification of molten metal, evaporation of liquids, etc. which have a discontinuity in the entropy. Some of the salient features of first order phase transition are:

a.) The thermal first order phase transition will exhibit super heating and super cooling effects during the phase transition

b.) The thermal first order phase transition will be accompanied by latent heat

c.) The thermal first order phase transition will have co-existence of liquid and solid phases

d.) The first order phase transition exhibits hysteresis

The first order phase transition obeys the Clausius-Clapeyron equation [33] which is shown below

$$\frac{dT}{d(\ln P)} = \frac{RT^2}{\Delta h} \tag{2.1}$$

where R is the universal gas constant, Δh is the enthalpy change of vaporisation for liquid-vapour transformation, T is the temperature and P is the pressure.

Different characteristics of the first order phase transition considering the main parameters of a thermodynamic system are shown in Fig. 2.8 [34]. Gibbs free energy as a function of temperature is

shown in Fig. 2.8 (a) where it can be seen that the curve is continuous but its derivative which is entropy is discontinuous in Fig. 2.8 (b). Volume and heat capacity vs. temperature in Fig.2.8 (c) and (d) also show discontinuity respectively.

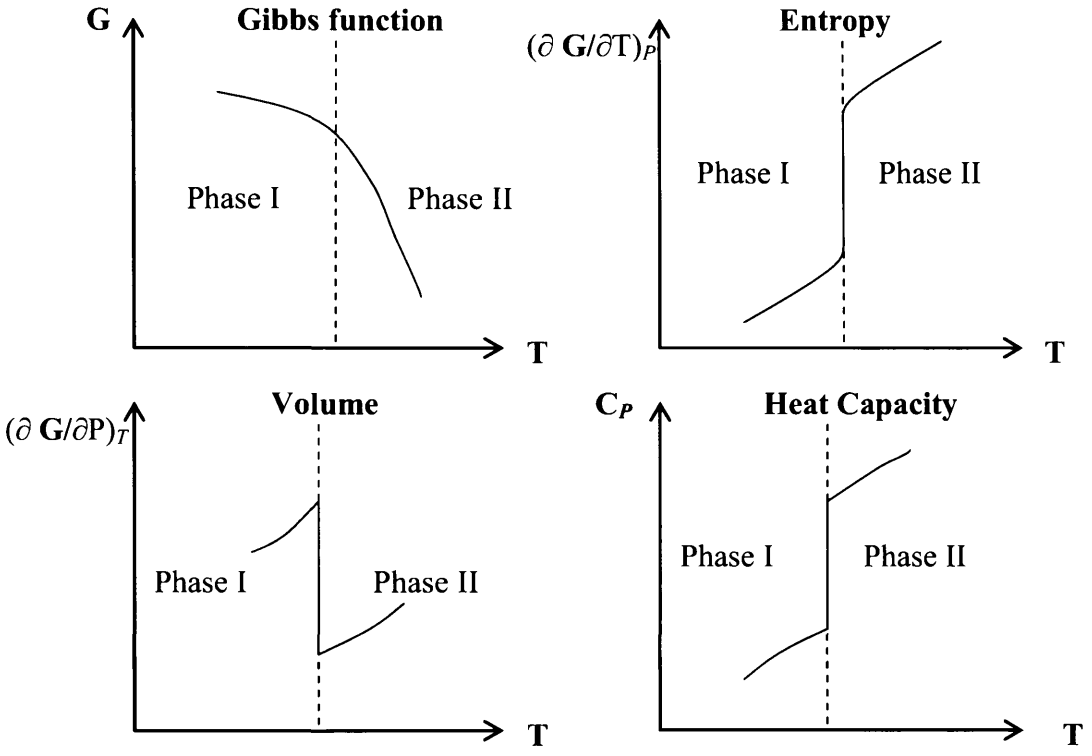

Fig. 2.8 Characteristics of a first order phase transition of a thermodynamic system (a) Gibbs Energy, (b) Entropy, (c) Volume and (d) Heat Capacity as a function of temperature [34].

Second order phase transition is gradual as stated before. The magnetic phase transition from a paramagnetic phase to ferromagnetic phase in most of the ferromagnetic materials is a second order phase transition. In ferromagnetic materials there is a competition between thermal energy and exchange (spin interaction) energy. Thermal energy overcomes spin interaction energy for a temperature much above the Curie temperature, T_c and the magnetisation, M becomes zero. For temperatures slightly above T_c there is a short range interaction between the spins and it needs a strong magnetic field to increase the magnetisation. At temperatures lower than the critical

temperature there is a spontaneous magnetisation in the material and any small magnetic field on the material increases the magnetisation drastically. Some of the salient features of second order phase transition are:

a.) Second order phase transitions do not exhibit super heating and super cooling effects during the phase transition

b.) Second order phase transitions do not exhibit latent heat

c.) Second order phase transitions do not have co-existence of two phases that are involved in the transition

d.) Second order phase transitions do not exhibit hysteresis

The main characteristics of a second order phase transition for bulk materials are shown in Fig. 2.9. It can be seen that the magnetisation changes gradually from low temperature ferromagnetic to high temperature paramagnetic. The volume changes at the transition. The entropy also changes at the transition temperature of the second order phase transition. The heat capacity shows a lambda anomaly at the transition temperature in a second order phase transition. It can be seen that there is no discontinuity in all these properties.

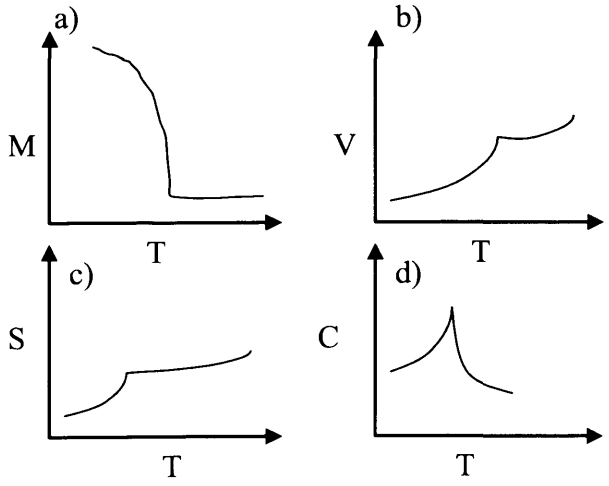

Fig. 2.9 Bulk property behaviour characteristics of a second order phase transition. a) Magnetisation, b) Volume measurement, c) Entropy measurement and d) Heat capacity measurement as functions of temperature [35].

2.6 Material Preparation

All the single crystal and polycrystalline samples except polycrystalline $Gd_5Si_{1.9}Ge_{2.1}$ and $Gd_5Si_{1.8}Ge_{2.2}$ were obtained from the Ames Laboratory, US Department of Energy. The single crystal samples were prepared by the Bridgman method using 99.996 % pure gadolinium (weight basis), 99.9999 % pure silicon (weight basis) and 99.999 % germanium (weight basis). The samples were annealed at 2000° C for one hour and then indexed by Lauve back scattered electron diffraction as describe in Appendix III. Polycrystalline samples were prepared by arc melting. The initial materials used for polycrystalline samples were commercial grade gadolinium (99.9 % pure by weight) and 99.9999 % pure silicon (weight basis) and 99.999 % germanium (weight basis). The samples were cut by electrical discharge machining (EDM) and standard metallographic techniques were used for polishing. Indexing of single crystal sample was carried out For sample preparation of polycrystalline $Gd_5Si_{1.9}Ge_{2.1}$ and $Gd_5Si_{1.8}Ge_{2.2}$ refer Appendix I and II.

2.7 Field Induced Phase Transition

$Gd_5(Si_xGe_{1-x})_4$ exhibits a field induced first order phase transition for $x<0.57$. When the $Gd_5(Si_xGe_{1-x})_4$ samples are in paramagnetic/monoclinic or paramagnetic/Sm_5Ge_4 type orthorhombic phase above the Curie point, by application of a certain amount of magnetic field one can induce the first order phase transition to a ferromagnetic/orthorhombic phase. The amount of field required to induce the phase transition depends on temperature of the sample. Higher magnetic field is needed when the samples are at higher temperatures above the Curie point. Fig. 2.10 shows the measurement of longitudinal magnetic moment vs. magnetic field for various temperatures of a single crystal $Gd_5Si_{1.95}Ge_{2.05}$ ($x=0.475$). It can be seen that the amount of field needed for 290 K isotherm is larger than 5 Tesla to induce the first order phase transition which is above the range of the Magnetic Properties Measurement System (MPMS) used for the measurements in this study. The rate of change of transition field with respect to temperature was measured to be nearly 1 Tesla/5 K (2000 Oe/K).

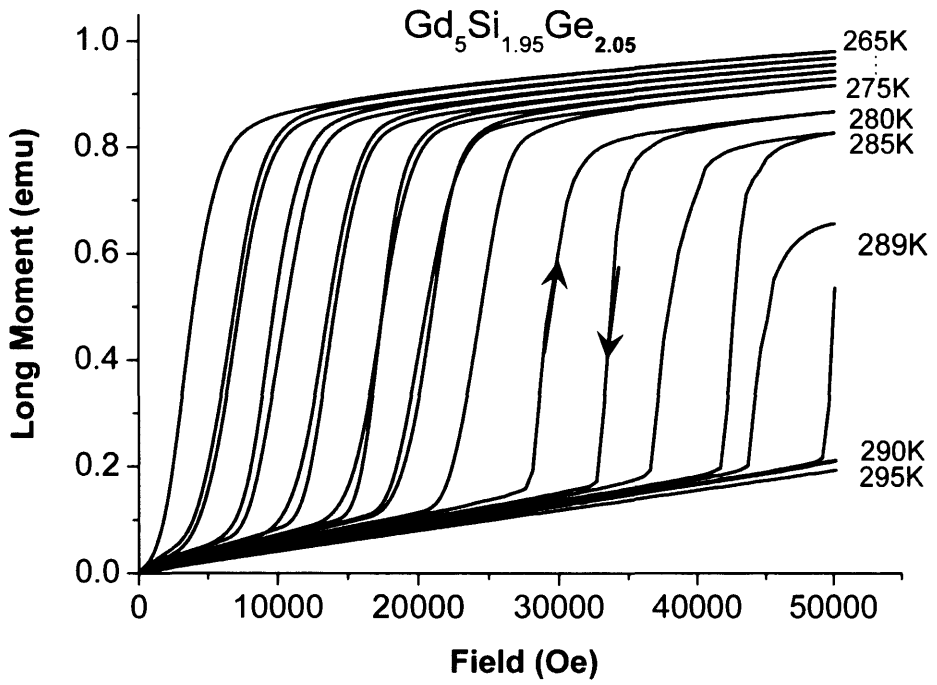

Fig. 2.10 Magnetic moment vs. magnetic field for various temperatures above the first order phase transition temperature showing the field induced phase transition for a single crystal $Gd_5Si_{1.95}Ge_{2.05}$.

It is also possible to shift the transition temperature of the $Gd_5(Si_xGe_{1-x})_4$ system by varying the applied magnetic field for compositions $x<0.575$. Fig. 2.11 shows measurement of magnetic moment vs. temperature for various applied magnetic fields. The inset figure of Fig. 2.11 is measurement of magnetic moment vs. temperature showing the first order phase transition temperature of 263 K at an applied field of 100 Oe for a single crystal $Gd_5Si_{1.95}Ge_{2.05}$ which was determined using inflection point on the curve. Similar measurement was also carried out on a single crystal $Gd_5Si_{1.8}Ge_{2.2}$ sample shown in Fig. 2.13. The inset figure is the measurement of magnetic moment vs. temperature showing the first order phase transition temperature of 238 K. It can be noted from Fig 2.11 and 2.13 that the rate of increase in the transition temperature is constant which is illustrated in Fig. 2.12 for the single crystal $Gd_5Si_{1.95}Ge_{2.05}$ ($x=0.475$)and in Fig. 2.14 for the single crystal $Gd_5Si_{1.8}Ge_{2.2}$ ($x=0.45$) sample. In all the figures when long moment is used as a parameter, it implies longitudinal moment measured with respect to the equipment.

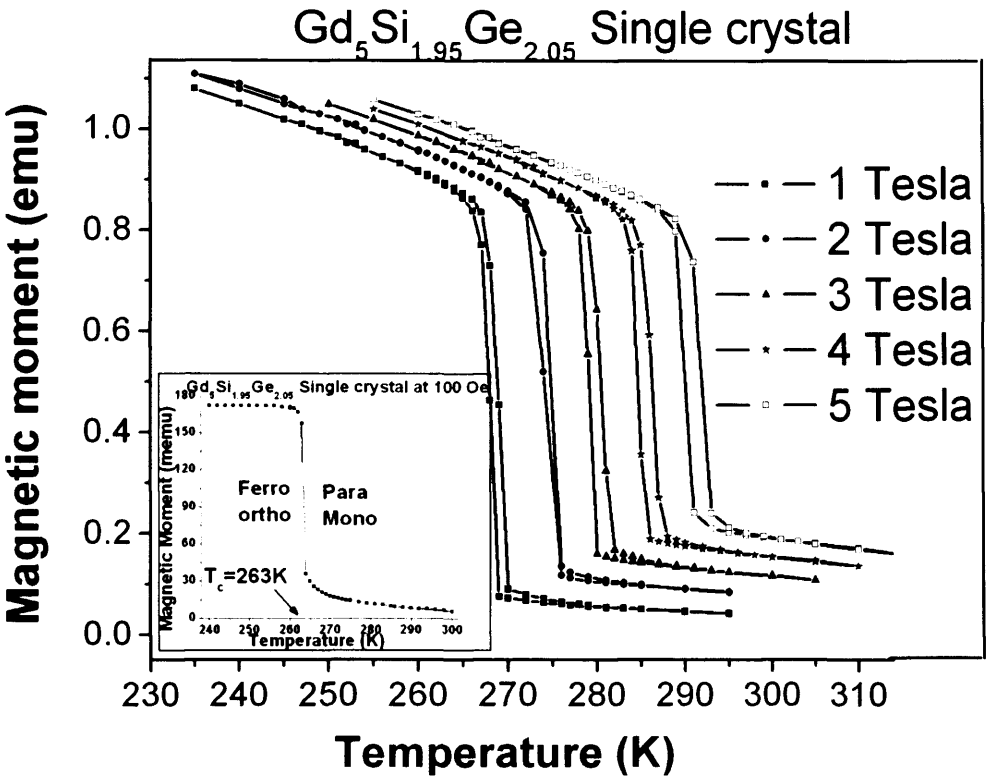

Fig. 2.11 Measurement of magnetic moment vs. temperature for various applied magnetic fields for the single crystal $Gd_5Si_{1.95}Ge_{2.05}$ (x=0.475). Inset is the transition temperature at an applied field of 100 Oe.

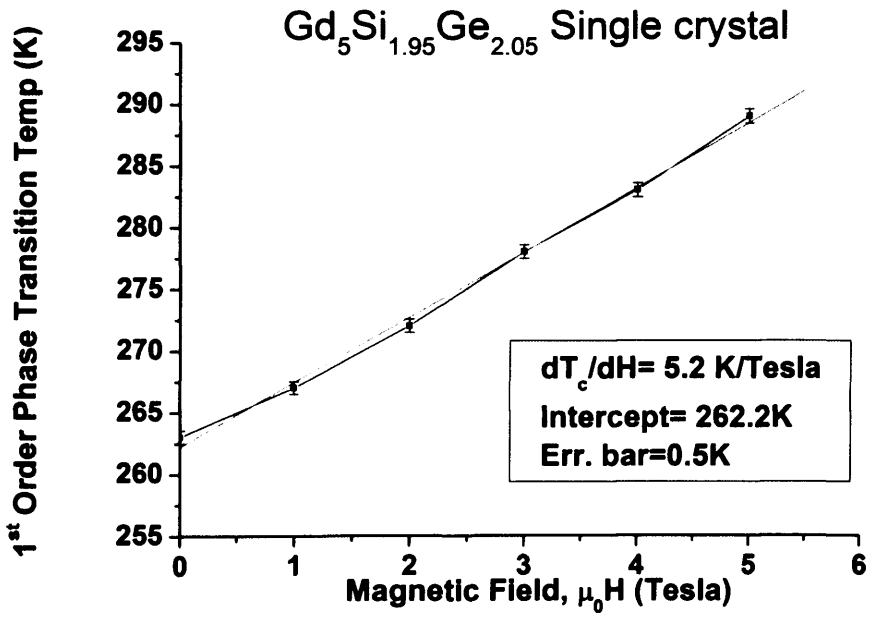

Fig 2.12 Field induced first order phase transition temperature as a function of applied magnetic field for the single crystal $Gd_5Si_{1.95}Ge_{2.05}$ (x=0.475) sample showing a constant rate of 5.25 K/Tesla.

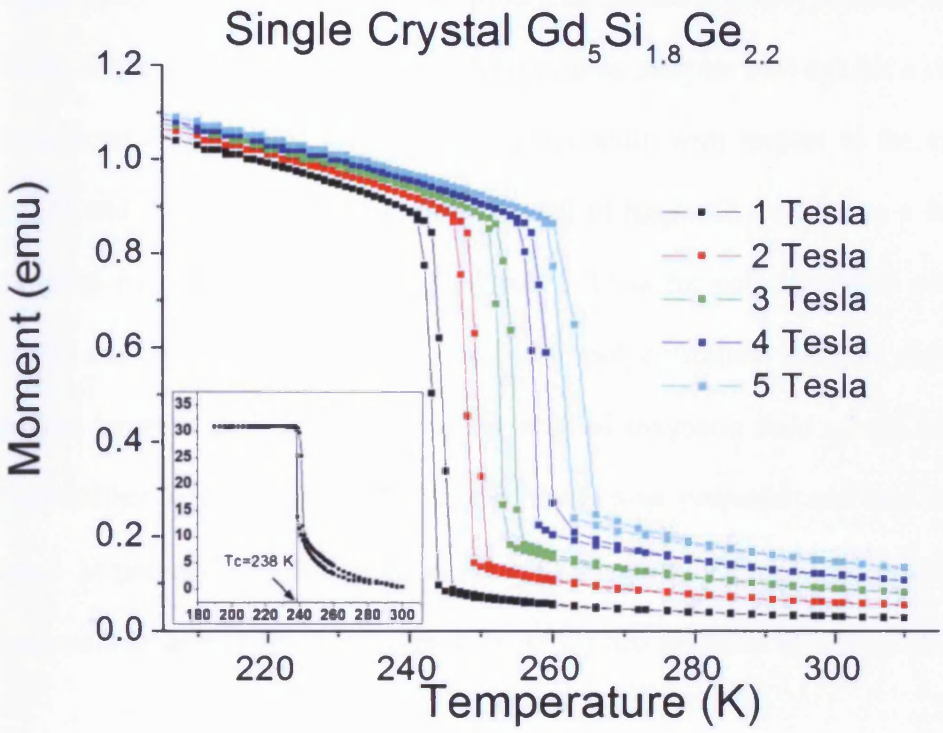

Fig. 2.13 Measurement of magnetic moment vs. temperature for various magnetic fields for the single crystal $Gd_5Si_{1.8}Ge_{2.2}$ (x=0.45). Inset is the transition temperature at an applied field of 100Oe.

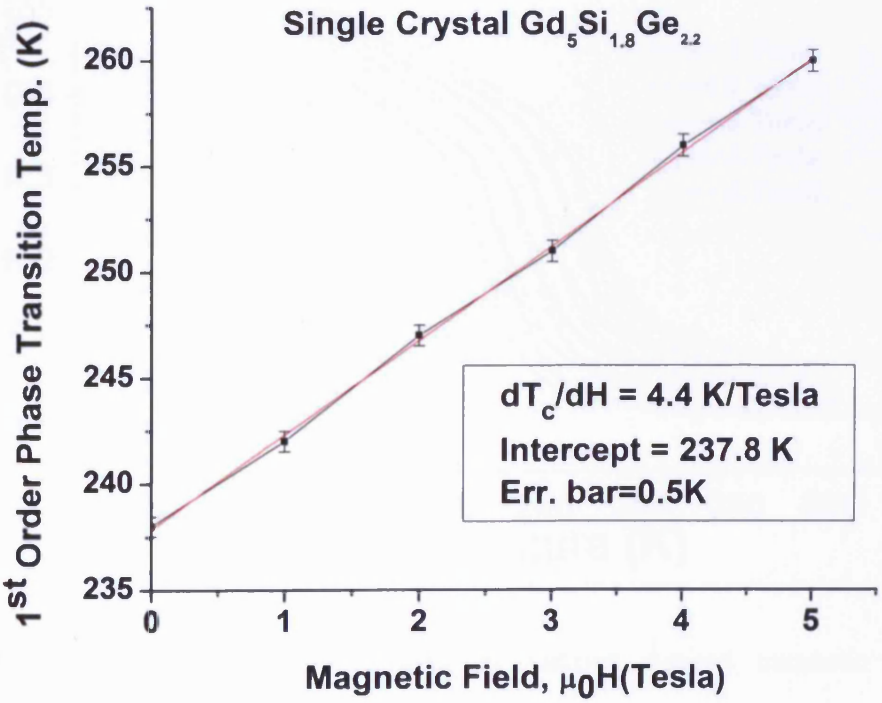

Fig 2.14 Field induced first order phase transition temperature as a function of applied magnetic field for the single crystal $Gd_5Si_{1.8}Ge_{2.2}$ (x=0.45) sample showing a constant rate of 4.46 K/Tesla.

The field induced first order phase transition temperature in polycrystalline samples is not as abrupt as in the single crystal samples. The polycrystalline samples also exhibit a constant increase in the field induced first order phase transition temperature with respect to the applied magnetic field. Fig. 2.15 and Fig. 2.16 shows the measurement of magnetic moment as a function of temperature for applied magnetic fields of 1, 2, 3, 4 and 5 Tesla for polycrystalline samples of $Gd_5Si_{1.8}Ge_{2.2}$ (x=0.45) and $Gd_5Si_{2.09}Ge_{1.91}$(x=0.52). Both the polycrystalline samples show a rate of change of transition temperature with respect to the applied magnetic field nearly equal to 5 K/Tesla. The polycrystalline sample of $Gd_5Si_{1.8}Ge_{2.2}$ (x=0.45) was prepared and heat treated at the Material Science Department of Birmingham University using commercial grade gadolinium and the polycrystalline sample of $Gd_5Si_{2.09}Ge_{1.91}$ (x=0.52) was prepared at Ames Laboratory, DOE, US.

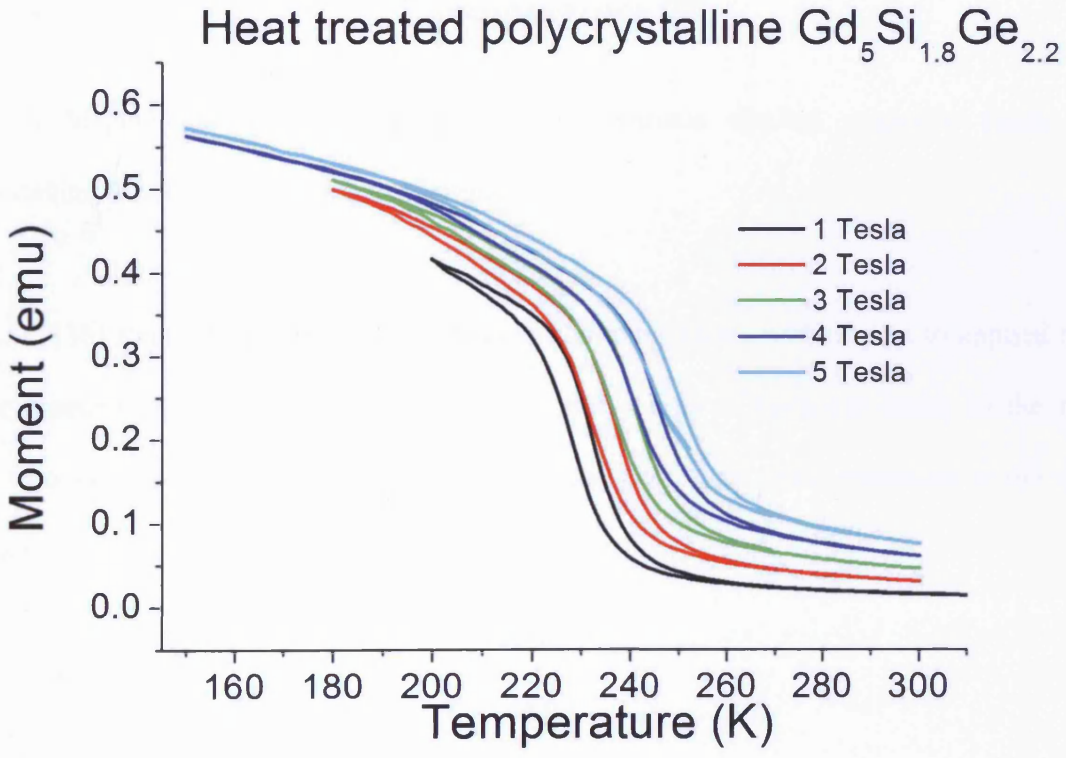

Fig. 2.15 Magnetic moment vs. temperature at various applied magnetic fields for the polycrystalline $Gd_5Si_{1.8}Ge_{2.2}$ (x=0.45) sample.

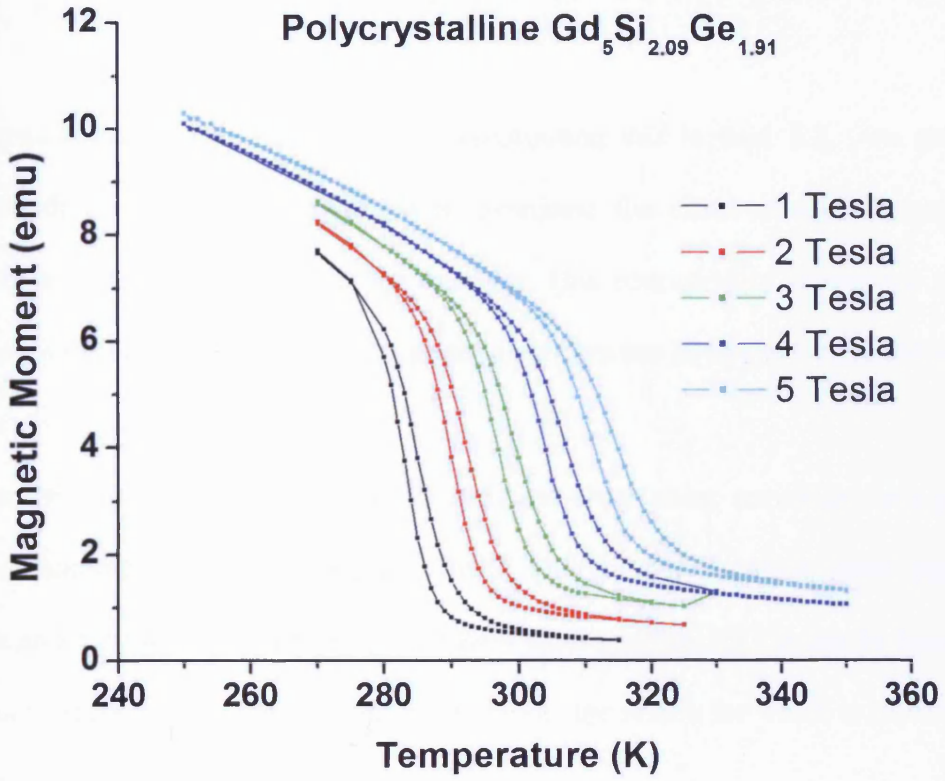

Fig. 2.16 Magnetic moment vs. temperature at various applied magnetic fields for the polycrystalline $Gd_5Si_{2.09}Ge_{1.91}$ (x=0.52) sample.

Han *et. al.* [36] found the rate of change of transition temperature with respect to applied magnetic field or magnetic induction by equating the thermal energy of each Gd atoms to the magnetic energy to overcome the thermal energy to induce the first order phase transition at the transition temperature:

$$\frac{n}{2}k_B\Delta T = m\Delta B \tag{2.2}$$

where n is number of degrees of freedom, k_B is the Boltzmann constant ($1.38\text{x}10^{-23}$ JK^{-1}), and m is the magnetic moment of Gd atom (7.9 $\mu_B = 7.3\text{x}10^{-23}$ $A.m^2$). Therefore,

$$\frac{\Delta T}{\Delta B} = \frac{2m}{nk_B} = \frac{10.6}{n} KT^{-1} \qquad (2.2)$$

From our measurements $(\Delta T/\Delta B)_{measured} \approx 5$, substituting this in Eqn. 2.2, we get $n \approx 2$. This suggests that the thermal energy required to overcome the effect of applied magnetic field is equivalent to a system with 2 degrees of freedom. This restriction of movement along one axis might be due to the existence of strong covalent bonds between Si-Si and Ge-Ge atoms.

Casanova *et. al.*[37] measured the field induced first order phase transition for a polycrystalline $Gd_5Si_{1.9}Ge_{2.1}$ sample for various applied fields and plotted the first order phase transition temperature as a function of applied magnetic field shown in Fig. 2.17. It can be seen that the error bars are much higher at higher applied magnetic fields; the reason for which is explained in Section 3.5 and page 3.26.

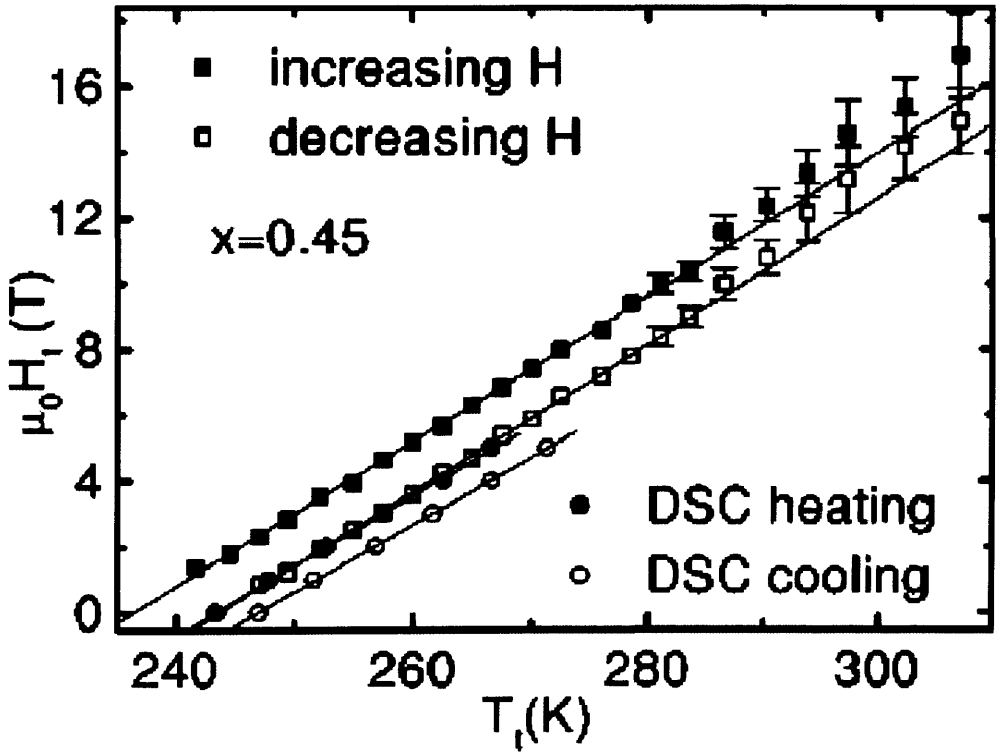

Fig. 2.17 Field induced first order phase transition temperature for a polycrystalline $Gd_5Si_{1.9}Ge_{2.1}$ (x=0.47) sample at various applied magnetic fields up to 16 Tesla. [37]

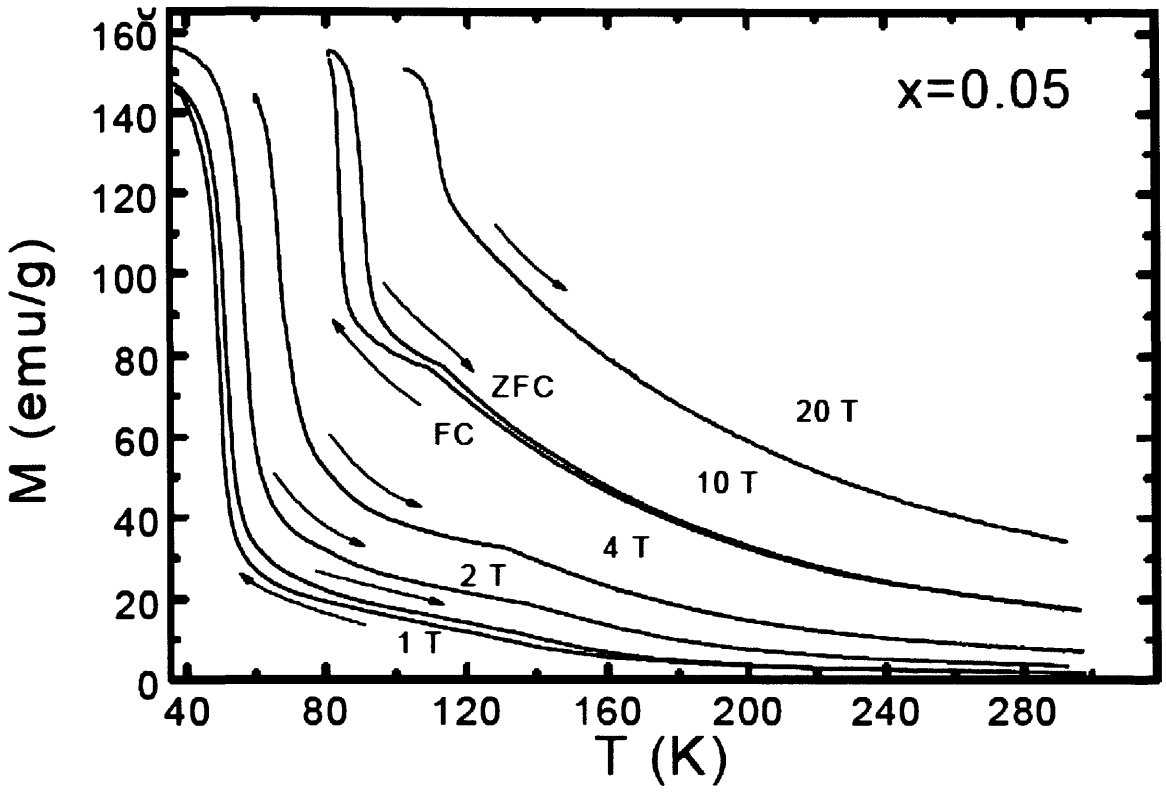

Fig. 2.18 Magnetic moment as a function of temperature for a polycrystalline $Gd_5Si_{0.2}Ge_{3.8}$ (x=0.05) sample at various applied fields up to 20 Tesla [38].

$Gd_5(Si_xGe_{1-x})_4$ with composition $x<0.25$ exhibits a phase transition from ferromagnetic to antiferromagnetic phase at the first order phase transition temperature and from antiferromagnetic to paramagnetic phase at the Neel temperature. The first order phase transition temperature shows a similar rate of increase with respect to the applied magnetic field. The Neel temperature shows an inverse trend i.e. the Neel temperature decreases with increase in applied magnetic field and disappears at very high magnetic fields of the order of 20 Tesla as shown in Fig. 2.18 for a polycrystalline $Gd_5Si_{0.2}Ge_{3.8}$ (x=0.05) sample [38].

The disappearance of the second order phase transition from paramagnetic to antiferromagnetic phase is because of the overlapping of the first order antiferromagnetic to ferromagnetic and second

order paramagnetic to antiferromagnetic transitions which indicates that the second order phase transition at the Neel temperature decreases with the increase in the temperature.

$Gd_5(Si_xGe_{1-x})_4$ at the composition $x > 0.575$ does not exhibit any field induced phase transition as the transition is second order. Fig. 2.19 shows measurement of magnetic moment as a function of temperature for applied magnetic fields of 1, 2 and 3 Tesla. The inset shows the second order phase transition temperature of 307 K at an applied field of 100 Oe but, the transition at higher applied magnetic fields starts to broaden and it is not possible to accurately measure the transition temperature (see further discussion in Chapter 3, Section 3.5).

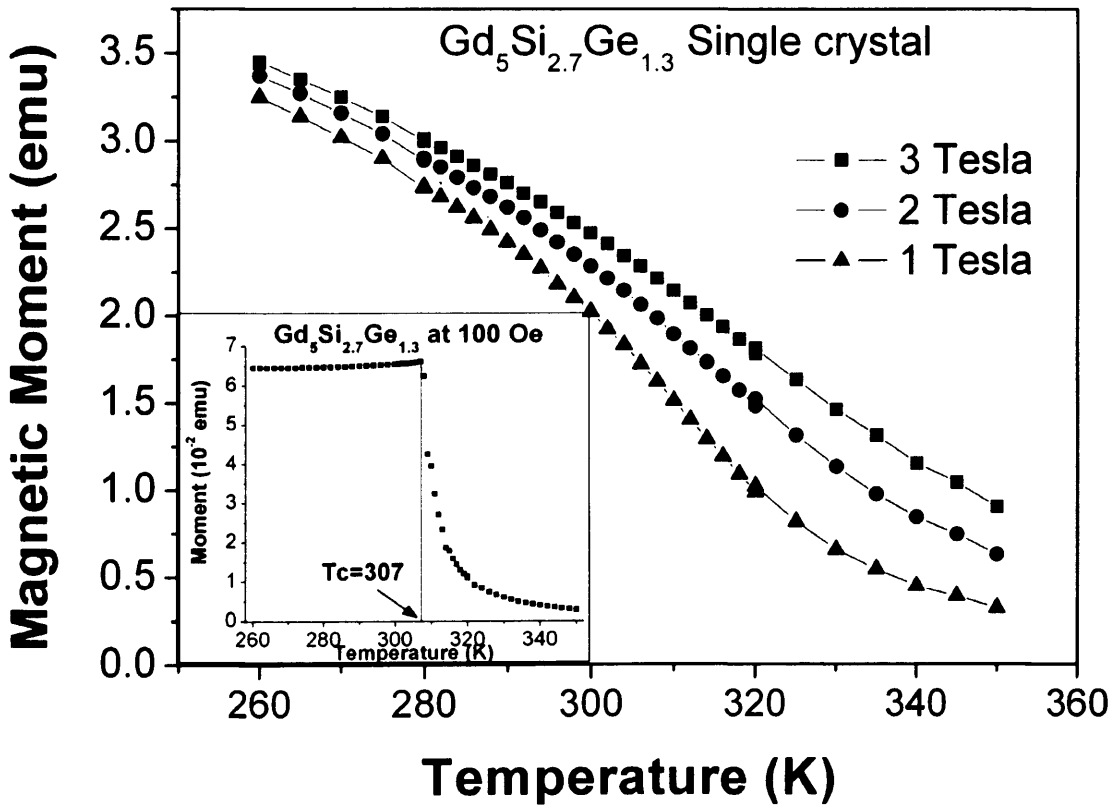

Fig. 2.19 Magnetic moment vs. temperature at various applied magnetic fields for the single crystal $Gd_5Si_{2.7}Ge_{1.3}$ (x=0.67). Inset is the second order phase transition temperature at an applied field of 100 Oe.

2.8 Summary

A literature review of magnetic-structural phase diagram, crystal structure and Widmanstatten lines of $Gd_5(Si_xGe_{1-x})_4$ was carried out with description of the different regions of the phase diagram. The field induced phase transition in $Gd_5(Si_xGe_{1-x})_4$ was observed in several compositions in magnetic moment vs. magnetic field measurements and the rate of change of the first order phase transition temperature with respect to the applied magnetic field was determined to be approximately 5 K/Tesla.

References

[1] F. Holtzberg, R. J. Gambino and T. R. McGuire, "*New ferromagnetic 5:4 compounds in the rare earth silicon and germanium systems*", J. Phys. Chem. Solids, **28**, pp. 2283-2289, (1967).

[2] G. S. Smith, A. G. Tharp, and Q. Johnson, "*Rare earth-germanium and -silicon compounds at 5:4 and 5:3 compositions*", Acta Crystallogr., **22**, pp. 940 (1967).

[3] G. S. Smith, Q. Johnson, and A. G. Tharp, "*Crystal structure of Sm_5Ge_4*", Acta Crystallogr., **22**, pp. 269 (1967).

[4] V. K. Pecharsky and K. Gschneidner Jr., "*Giant Magnetocaloric Effect in $Gd_5(Si_2Ge_2)$*", Phys. Rev. Lett., **78**, pp. 4494-4497, (1997).

[5] V. K. Pecharsky and K. Gschneidner Jr., "*Tunable magnetic regenerator alloys with a giant magnetocaloric effect for magnetic refrigeration from ~ 20 to ~ 290 K*", App. Phys. Lett., **70**, pp. 3299-3301, (1997).

[6] V. K. Pecharsky and K. A. Gschneidner, Jr., "*Phase relationships and crystallography in the pseudobinary system Gd_5Si_4-Gd_5Ge_4*", J. Alloys Comp., **260**, pp. 98 (1997).

[7] V. K. Pecharsky and K. A. Gschneidner, Jr., "*Effect of alloying on the giant magnetocaloric effect of $Gd_5(Si_2Ge_2)$*", J. Magn. Magn. Mater., **167**, pp. L179 (1997).

[8] K.A. Gschneidner and V.K. Pecharsky, "*Thirty years of near room temperature magnetic cooling: Where we are today and future prospects*", Int. J. Refrig., **31**, pp. 945-961, (2008).

[9] A. O. Pecharsky, K. A. Gschneidner, Jr., V. K. Pecharsky and C. E. Schindler, "*The room temperature metastable/stable phase relationships in the pseudo-binary Gd_5Si_4–Gd_5Ge_4 system.*", J. Alloys. Comp., **338**, pp.126-135, (2002).

[10] V. K. Pecharsky, G. D. Samolyuk, V. P. Antropov, A. O. Pecharsky, and K.A. Gschneidner, Jr., "*The effect of varying the crystal structure on the magnetism, electronic structure and thermodynamics in the $Gd_5(Si_xGe_{1-x})_4$ system near $x=0.5$*", J. Solid. State. Chem., **171**, pp. 57-68, (2003).

[11] K. A. Gschneidner Jr., V. K. Pecharsky and A. O. Tsokol, "*Recent developments in magnetocaloric materials*", Rep. Prog. Phys., **68**, pp. 1479–1539, (2005).

[12] A. O. Pecharsky, V. K. Pecharsky and K. A. Gschneidner, "*The giant magnetocaloric effect of optimally prepared $Gd_5Si_2Ge_2$*", J. Appl. Phys., **93**, pp. 4722-4724, (2003).

[13] M. Han, D. C. Jiles, J. E. Snyder, T. A. Lograsso, and D. L. Schlagel, *"Angular Dependence of the Unusual First-Order Transition Temperature in Single-Crystal"* IEEE Trans. Magn., **39**, pp. 3151-3153, (2003).

[14] C. Magen, L. Morellon, P. A. Algarabel, M. R. Ibarra, Z. Arnold, J. Kamarad, T. A. Lograsso, D. L. Schlagel, V. K. Pecharsky, A. O. Tsokol, and K. A. Gschneidner, Jr "*Hydrostatic pressure control of the magnetostructural phase transition in $Gd_5Si_2Ge_2$ single crystals*", Phys. Rev. B, **72**, pp. 024416, (2005).

[15] L. Morellon, J. Stankiewicz, B. García-Landa, P. A. Algarabel, and M. R. Ibarra, "*Giant magnetoresistance near the magnetostructural transition in* $Gd_5(Si_{1.8}Ge_{2.2})$", Appl. Phys. Lett., **73**, pp. 3462-3464, (1998).

[16] D. W. Lu, X. N. Xu, H. B. Wu, , X . Jin, "*A permanent-magnet magneto-refrigerator study using Gd/Gd-Si-Ge/Gd-Si-Ge-Ga alloys*" Egolf, P.W. (Ed.), Proceedings of the First International Conference on Magnetic Refrigeration at Room Temperature, Montreux, Switzerland, International Institute of Refrigeration, Paris, pp. 291–296, (2005).

[17] C. Zimm, A. Jastrab, A. Sternberg, V. K. Pecharsky, K. Gscheidner, Jr., M. Osborne and I. Anderson, Adv. Cryog. Eng., **43**, pp. 1759, (1998).

[18] A. E. Clark, in *Handbook on the Physics and Chemistry of Rare Earths*, edited by K. A. Gschneidner, Jr. and L. R. Eyring, North-Holland, Amsterdam, Vol. 2, Chap. 15, (1979).

[19] N. Nersessian, S. Wing Or, G. P. Carman, S. K. McCall, W. Choe, H. B. Radousky, M. W. McElfresh, V. K. Pecharsky and A. O. Pecharsky "$Gd_5Si_2Ge_2$ *composite for magnetostrictive actuator applications*", Appl. Phys. Lett., **84** , pp.4801-4803, (2004).

[20] D. L. Schlagel, Ames Laboratory, US Department of Energy, Private communication, (2008).

[21] K. A. Gschneidner, Jr. and V. K. Pecharsky, "*Magnetocaloric Materials*", Annu. Rev. Mater. Sci., 30, pp. 387–429, (2000).

[22] V. K. Pecharsky and K. A. Gschneidner, Jr., "*$Gd_5(Si_xGe_{1-x})_4$: An extremum material*", Adv. Mater., **13**, pp. 683-686, (2001).

[23] W. Choe, V. K. Pecharsky, A. O. Pecharsky, K. A. Gschneidner, Jr., V. G.Young, Jr., and G. J. Miller, "*Making and Breaking Covalent Bonds across the Magnetic Transition in the Giant Magnetocaloric Material $Gd_5(Si_2Ge_2)$*", Phys. Rev. Lett., **84**, pp. 4617, (2000).

[24] G. H. Rao, "*Correlation between crystal structure and magnetic properties of $Gd_5(Si_xGe_{1-x})_4$ compounds*", J. Phys.: Condens. Matter, **12**, L93, (2000).

[25] J. Szade, G. Skorek, and A. Winiarski, "*Surface structure of $Gd_5(Si,Ge)_4$ crystals*", J. Cryst. Growth, **205**, pp. 289–293 (1999).

[26] J.S. Meyers, L. S. Chumbley, F. Laabs, and A. O. Pecharsky, "*Determination of phases in as prepared $Gd_5(Si_xGe_{1-x})_4$, where $x \cong 1/2$*", Scripta. Mater., **47**, pp. 509–514, (2002).

[27] O. Ugurlu, L.S. Chumbley, D.L. Schlagel and T.A. Lograsso, "*Characterization of an Atypical Widmansta¨tten structure in $Gd_5Si_2Ge_2$ alloys*", Acta. Mater., **53**, pp. 3525–3533, (2005).

[28] B. Podmiljšak, P. J. McGuiness, I. Škulj, G. Dražič and S. Kobe, "*A microstructural investigation of $Gd_5(Si_xGe_{1-x})$ alloys produced by the arc-melting technique*", Second IIF-IIR International Conference on Magnetic Refrigeration at Room Temperature, Portoroz, Slovenia, 11-13 April 2007.

[29] O. Ugurlu, L.S. Chumbley, D.L. Schlagel and T.A. Lograsso, "*Orientation and formation of atypical Widmanstaetten plates in the $Gd_5(Si_xGe_{1-x})_4$ system*", Acta. Mater., **54**, pp. 1211–1219, (2006).

[30] O. Ugurlu, L.S. Chumbley, D.L. Schlagel, T.A. Lograsso, and A. O. Tsokol, "*Identification of thin plates seen in $R_5(Si_xGe_{1-x})_4$ alloys, where R is Gd, Tb, Dy, and Er*", Scripta. Mater., **53**, pp. 373–377, (2005).

[31] P. Ehrenfest, Acad. Sci., Amesterdam Mitt. Kammerligh Onnes Inst., Leiden, **36**, 153 Supl. 75b, (1933).

[32] M. Hillert, "*Phase Equilibria, Phase Diagrams and Phase Transformations Their Thermodynamics Basics*", Cambridge University Press, pp. 323, (1998).

[33] H. G. Lee, "*Chemical Thermodynamics for Metals and Materials*", Imperial College Press, (1999).

[34] M. E. Fine, "*Introduction to phase transformations in condensed systems*", Macmillan, New York, (1965).

[35] A. K. Jena and M. C. Chaturvedi, "*Phase transformation in materials*", Prentice Hall, (1992).

[36] M. Han, J. A. Paulsen, J. E. Snyder, D. C. Jiles, T. A. Lograsso, and D. L. Schlagel, "*Thermal Expansion of Single-Crystal $Gd_5(Si_{1.95}Ge_{2.05})$ Showing Unusual First-Order Transformation*", IEEE. Trans. Magn., **38**, pp. 3252, (2002).

[37] F. Casanova, X. Battle and A. Labarta, "*Scaling of the entropy change at the magnetoelastic transition in $Gd_5(Si_xGe_{1-x})_4$*", Phys. Rev. B, **66**, pp. 212402, (2002).

[38] F. Casanova, "*Magnetocaloric effect in $Gd_5(Si_xGe_{1-x})_4$ alloys*", PhD Thesis, Universitat de Barcelona, Departament de Física Fonamental, Spain, (2003).

Chapter 3: Phase Transition in $Gd_5(Si_xGe_{1-x})_4$

3.1 Introduction

$Gd_5(Si_xGe_{1-x})_4$ exhibits extreme and unusual properties at the first order phase transition temperature as discussed in earlier Chapter. In this chapter, the first order and second order phase transitions in $Gd_5(Si_xGe_{1-x})_4$ will be discussed in detail. The magnetic phase diagram of $Gd_5(Si_xGe_{1-x})_4$ is shown in Fig. 3.1 [1, 2, 3] where transition temperature as a function of composition is plotted indicating different phase transitions. Crystal structures at all the magnetic phases have also been labelled. The whole phase diagram can be divided into three main regions. The dotted lines parallel to the y-axis indicate the boundaries of the mixed phase regions. There is very little research carried out in these mixed phase regions as the mixed phase compositions do not have a clear transition temperature and exhibit lower magnetic properties such as magnetostriction, magnetocaloric effect, etc.

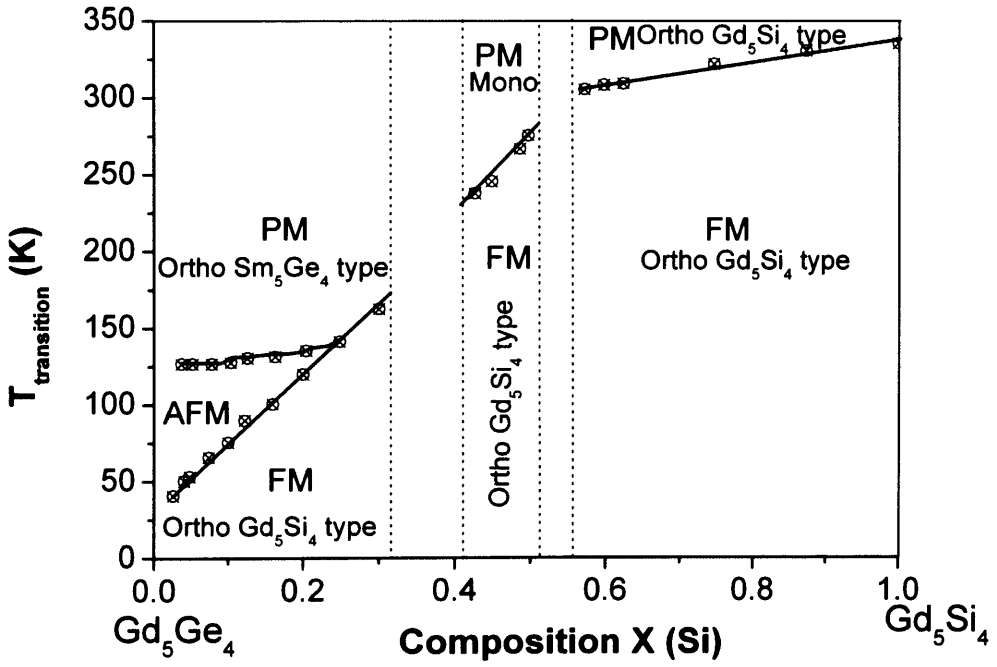

Fig. 3.1 Magnetic phase diagram for $Gd_5(Si_xGe_{1-x})_4$ system with crystal structures labelled [1, 2, 3].

3.2 First Order Phase Transition in $Gd_5(Si_xGe_{1-x})_4$

$Gd_5(Si_xGe_{1-x})_4$ exhibits the first order phase transition for the composition $x < 0.51$ [3, 4]. The first order magnetic phase transition is accompanied by a structural phase transition from a high

temperature monoclinic to low temperature orthorhombic crystal structure for the composition $0.4< x < 0.51$. The transition temperature of the composition $0.4< x < 0.51$ falls close to room temperature, hence it is a widely researched region of the phase diagram. The structural phase for transition compositions $x < 0.51$ is accompanied by a large volume change in the crystal which results in extreme change in various magnetic properties of the material [5]. Fig. 3.2 shows measurement of magnetic moment as a function of temperature at an applied magnetic field of 100 Oe (8kA/m) of the single crystal $Gd_5Si_{1.95}Ge_{2.05}$ (x=0.475). The measurement was carried out on Quantum Design's Magnetic Properties Measurement System (MPMS) which is commonly known as a Super Conduction Quantum Interference (SQUID) magnetometer. It can be seen that there is a sudden change in the magnetic moment at 263 K which is the first order magnetic-structural phase transition temperature of $Gd_5Si_{1.95}Ge_{2.05}$ in agreement with the phase diagram. The first order magnetic-structural phase transition in $Gd_5(Si_xGe_{1-x})_4$ is accompanied by hysteresis in cooling and heating curves in magnetic moment vs. temperature measurements as shown in Fig. 3.3. Hysteresis in the measurement should not be confused with thermal lag. The cooling and heating rate was maintained at 5K/min. A time interval of 60sec was introduced before measuring the magnetic moment at every point. This procedure was employed for all the measurements which was sufficient to remove any thermal gradient between the sample and the thermocouple. This can be

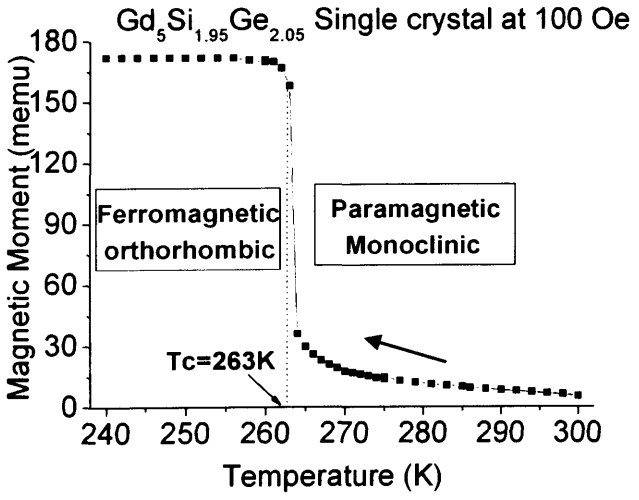

Fig. 3.2 Magnetic moment vs. temperature measurement on the single crystal $Gd_5Si_{1.95}Ge_{2.05}$ (x=0.475) at an applied magnetic field of 100 Oe (8kA/m).

observed in the measurement of M vs. T for the second order transition compositions which do not show any thermal hysteresis as shown in Fig. 3.7.

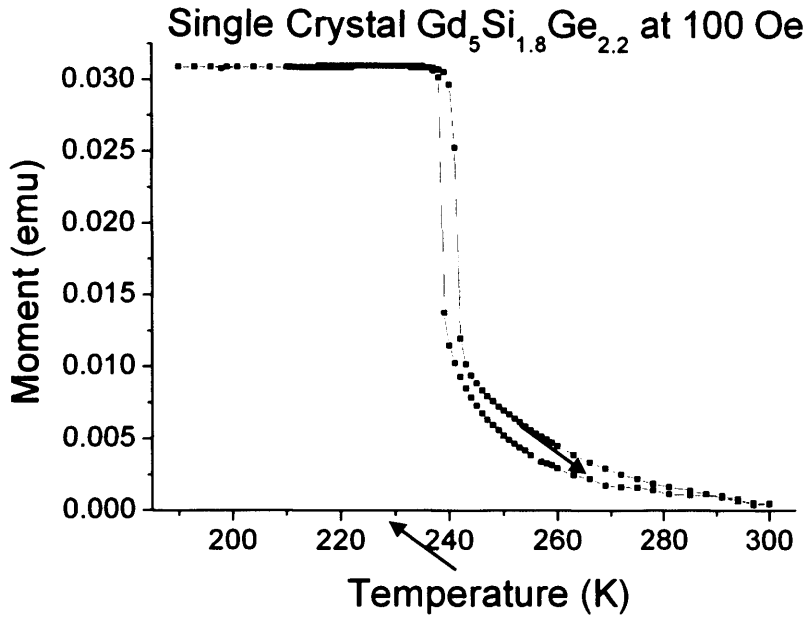

Fig. 3.3 Magnetic moment as a function of temperature on a single crystal $Gd_5Si_{1.8}Ge_{2.2}$ (x=0.45) at an applied magnetic field of 100 Oe (8kA/m).

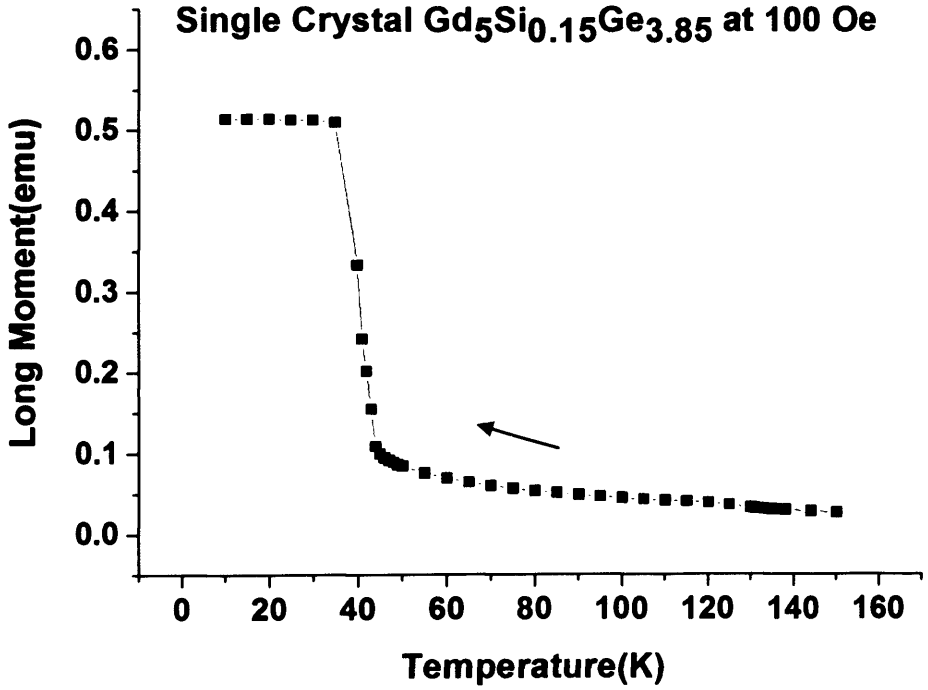

Fig. 3.4 Magnetic moment as a function of temperature for a single crystal $Gd_5Si_{0.15}Ge_{3.85}$ (x=0.035) at an applied magnetic field of 100 Oe (8kA/m).

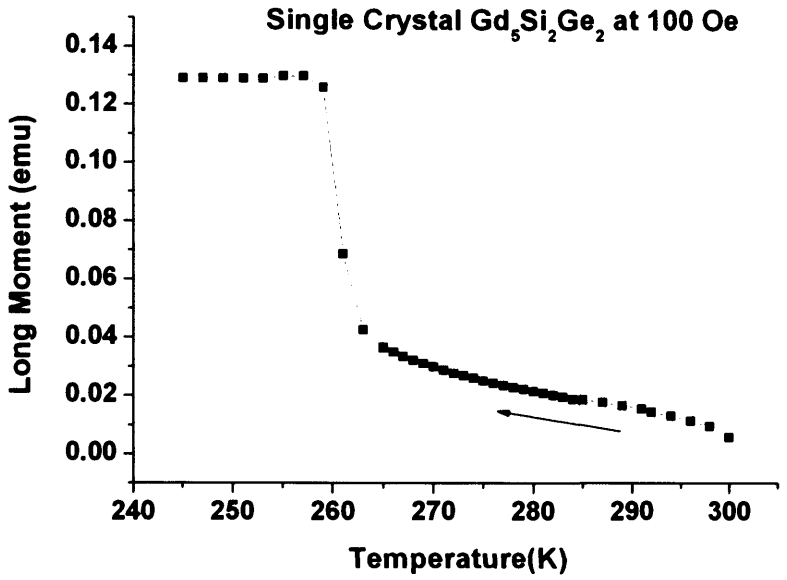

Fig. 3.5 Magnetic moment as a function of temperature for a single crystal $Gd_5Si_2Ge_2$ (x=0.5) at an applied magnetic field of 100 Oe (8kA/m).

Magnetic moment vs. temperature at an applied field of 100 Oe (8kA/m) for single crystal $Gd_5Si_{1.95}Ge_{2.05}$, $Gd_5Si_{1.8}Ge_{2.2}$, $Gd_5Si_{0.15}Ge_{3.85}$, and $Gd_5Si_2Ge_2$ showed a sharp transition indicating the first order magnetic-structural phase transition at 263 K, 240 K, 40 K and 263 K as shown in Fig. 3.2, 3.3, 3.4, and 3.5 respectively. The transition temperatures were measured for cooling curves and were in general agreement with the previously reported work in references [3, 4, 5].

Magnetic moment vs. temperature measurements on polycrystalline samples also exhibited the first order magnetic-structural phase transition but the transition was not as sharp as in the single crystal samples. The hysteresis between the heating and the cooling curves was higher than some single crystal samples. Fig. 3.6 shows the measurement of magnetic moment vs. temperature on the polycrystalline $Gd_5Si_{2.09}Ge_{1.91}$ (x=0.52) sample at an applied magnetic field of 100 Oe (8kA/m). The first order magnetic-structural phase transition temperature of the sample occurs at 280 K. There is an indication of the existence of small amount of secondary phase in the measurement taken close to 300 K.

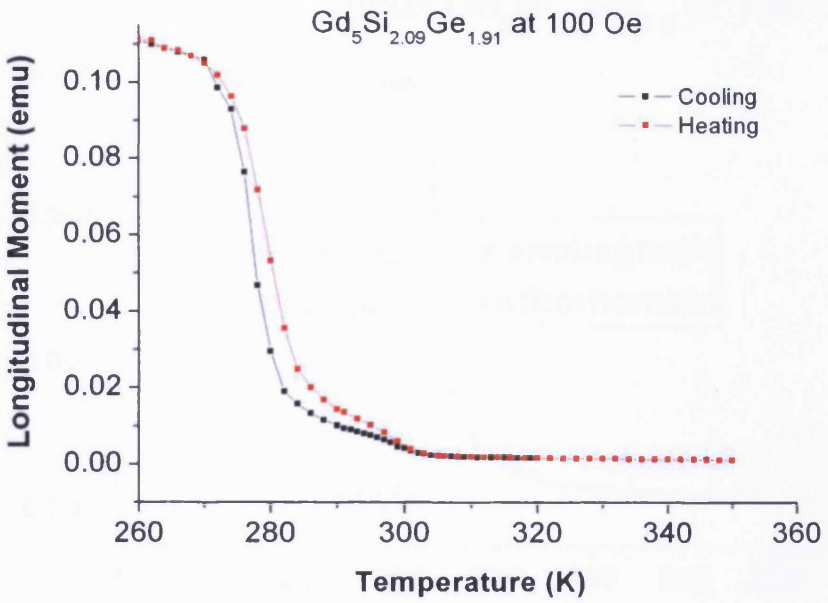

Fig. 3.6 Magnetic moment as a function of temperature of a polycrystalline $Gd_5Si_{2.09}Ge_{1.91}$ (x=0.52) sample at an applied magnetic field of 100 Oe (8kA/m).

3.3 Second Order Phase Transition in $Gd_5(Si_xGe_{1-x})_4$

$Gd_5(Si_xGe_{1-x})_4$ exhibits a second order phase transition for the composition $x > 0.51$ [2, 3, 4]. In this phase transition, a high temperature paramagnetic-orthorhombic phase transforms to a low temperature ferromagnetic-orthorhombic phase. Since there is only a magnetic phase transition, there is no volume change in the crystal structure; hence the second order phase transition does not exhibit extreme change in the magnetic properties. The second order phase transition is not hysteretic. Fig. 3.7 and Fig. 3.8 show the measurement of magnetic moment as a function of temperature at an applied magnetic field of 100 Oe (8kA/m) on a single crystal $Gd_5Si_{2.2}Ge_{1.8}$ and $Gd_5Si_{2.7}Ge_{1.3}$ samples respectively. It can be seen that the magnetic moment change is gradual over a wider temperature change and with no hysteresis indicating that the phase transition is a second order phase transition. The transition temperature show in Fig. 3.7 and Fig. 3.8 were determined by inflection point method. A more advanced and accurate method known as Arrott plot method is described in the next section.

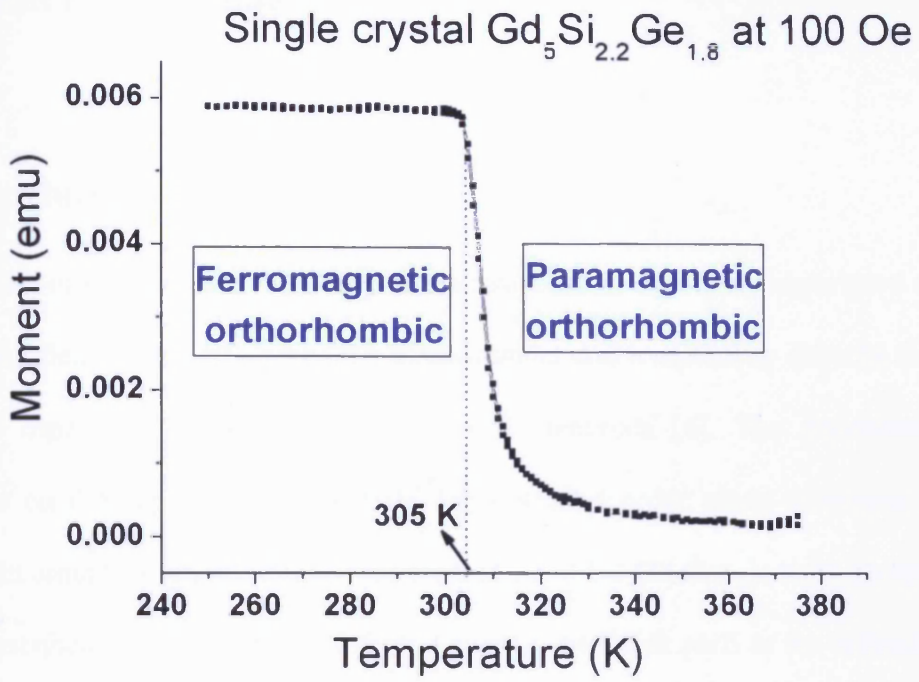

Fig. 3.7 Magnetic moment vs. temperature at an applied magnetic field of 100 Oe (8kA/m) on a single crystal $Gd_5Si_{2.2}Ge_{1.8}$ (x=0.54) sample showing a second order phase transition (Curie) temperature of 305 K.

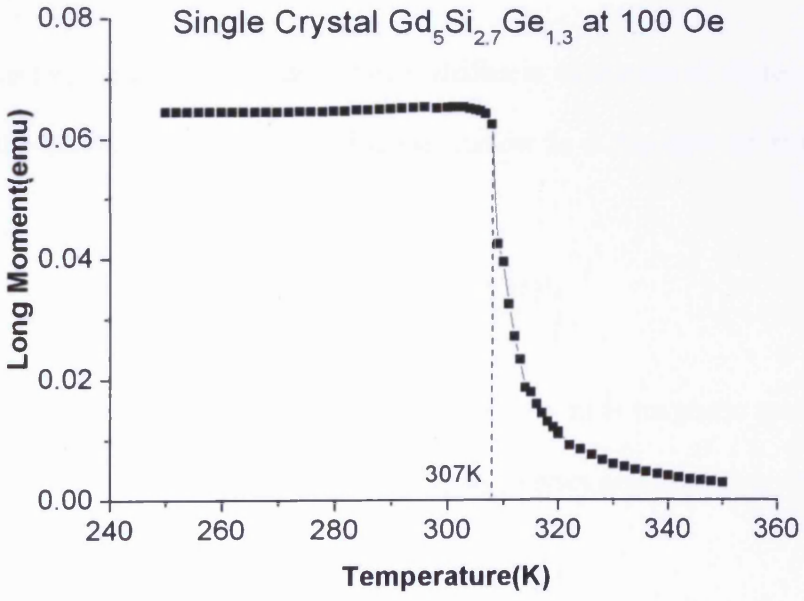

Fig. 3.8 Magnetic moment vs. temperature at an applied magnetic field of 100 Oe (8kA/m) on a single crystal $Gd_5Si_{2.7}Ge_{1.3}$ (x=0.675) sample showing a second order phase transition (Curie) temperature of 307 K.

3.4 Arrott Plot Technique

3.4.1 Introduction

Determination of Curie temperature by plotting magnetic moment vs. temperature curves requires a small applied field, which influences the measurement and temporarily disturbs the temperature of the sample especially for highly magnetocaloric materials [6]. The dependence of transition temperature on the applied magnetic field for a second order phase transition is shown in the Fig. 2.17. In order to study the transition temperature of $Gd_5(Si_xGe_{1-x})_4$ more accurately a variety of methods described in the literature were investigated. Methods such as the inflection point method and the line projection method give different second order phase transition (Curie) temperatures at different applied fields [7]. It is also difficult to maintain temperature equilibrium between the inside of the sample and the temperature sensor due to magnetocaloric effects. The Arrott plot technique was therefore used in order to determine the Curie temperature for a magnetocaloric samples.

The Arrott plot technique is based on the Weiss-Brillouin treatment of molecular field theory [8]. Eq. (3.1) gives the proposed equation for magnetization as a function of both applied field and temperature [9]:

$$M = M_0 \tanh\left(\frac{m(H + NM)}{kT}\right) \tag{3.1}$$

where M_0 is the spontaneous magnetisation at absolute zero, m is magnetic moment per atom and N is the molecular field constant. Rewriting Eqn. (3.1) as a series and assuming M/M_0 to be very small near the Curie temperature we get:

$$\frac{mH}{kT} + N\frac{mM}{kT} = \frac{M}{M_0} + \frac{1}{3}\left(\frac{M}{M_0}\right)^3 + \frac{1}{5}\left(\frac{M}{M_0}\right)^5 + \ldots, \tag{3.2}$$

ignoring higher order terms in M/M_0 and rewriting Eqn. (3.2) we get:

$$\frac{1}{\chi} = \left(\frac{kT}{mM_0}\right) - N. \tag{3.3}$$

At the Curie temperature, $1/\chi=0$, so Eqn. (3.3) can be written as

$$T_c = \left(\frac{mN}{k}\right) M_0 \tag{3.4}$$

Substituting Eqn. 3.4 in Eqn. 3.3

$$\frac{mH}{kT_c} = \frac{1}{3}\left(\frac{M}{M_0}\right)^3 + \frac{1}{5}\left(\frac{M}{M_0}\right)^5 + ... \tag{3.5}$$

The above equation can be rewritten for conditions above and below the Curie temperature as [10]:

$$\frac{mH}{kT} = \varepsilon\frac{M}{M_0} + \frac{1}{3}\left(\frac{M}{M_0}\right)^3 + \frac{1}{5}\left(\frac{M}{M_0}\right)^5 + ..., \tag{3.6}$$

where $\varepsilon = \dfrac{T - T_c}{T}$.

Considering terms only up to third order and introducing the critical exponents γ and β into Eqn. 3.6 to accommodate for deviations from the mean field approximation and also to accommodate for both polycrystalline and single crystal samples [11] we get:

$$\left(\frac{H}{M}\right)^{1/\gamma} = \frac{T - T_c}{T_1} + \left(\frac{M}{M_1}\right)^{1/\beta} \tag{3.7}$$

where M_1 and T_1 are new constants with $M_1=(3M_0^3m/k)^{\beta}$ and $T_1=k/M_0mT$.

Eq. 3.7 is used to identify the values of the critical exponents γ and β under which isothermal *M-H* curves are straight and parallel lines. When this is done, the isotherm which passes through the origin of the plot of $\left(\frac{H}{M}\right)^{1/\gamma}$ versus $M^{1/\beta}$ represents the Curie temperature. For the best estimation of Curie temperature, isothermal *M-H* measurements close to the Curie temperature should be used.

3.4.2 Estimation of Second Order Phase Transition in $Gd_5(Si_xGe_{1-x})_4$ for (x>0.51) using Arrott Plot technique

In order to make Arrott plots for determining the second order transition temperature of the single crystal $Gd_5Si_{2.7}Ge_{1.3}$ (x=0.675) sample, isothermal M vs. H measurements were carried out at various temperatures close to the second order phase transition temperature on the MPMS as shown in Fig. 3.9. Plots of $\left(\frac{H}{M}\right)^{1/\gamma}$ vs. $M^{1/\beta}$ were drawn over the temperature range of 295 K to 322 K as shown in Fig. 3.10. The values for γ and β needed to obtain straight lines were found to be 1.13 and 0.45 respectively. The error bar in the estimation is about ±05. It can be seen from Fig. 3.8 that isotherms above the calculated second order phase transition (Curie) temperature are curved downwards at the end and are converging to the origin, while the isotherms below the calculated Curie point are curved upwards at the ends and are converging to the origin. The isotherm at the second order phase transition (Curie) temperature should not have its end curved as it should be a straight line passing through the origin. Thus, the second order phase transition (Curie) temperature was determined from Fig. 3.10 to be 305 K.

Similarly the second order phase transition temperatures were determined using Arrott plots for the single crystal $Gd_5Si_{2.2}Ge_{1.8}$ (x=0.54) sample. Fig. 3.11 shows the M vs. H measurements at various temperatures close to the second order phase transition temperature. It is worth noting that there is no hysteresis in all the isotherms confirming that the composition exhibits a pure second order phase transition. $\left(\frac{H}{M}\right)^{1/\gamma}$ vs. $M^{1/\beta}$ was plotted iterating the values of γ and β until the plots are straight lines. Fig. 3.12 shows the Arrott plots for the values of $\gamma = 1.15$ and $\beta = 0.54$ with an error of ±05. The isotherm that passes through the origin is 304 K hence, the second order phase transition temperature of the single crystal $Gd_5Si_{2.2}Ge_{1.8}$ sample is 304 K.

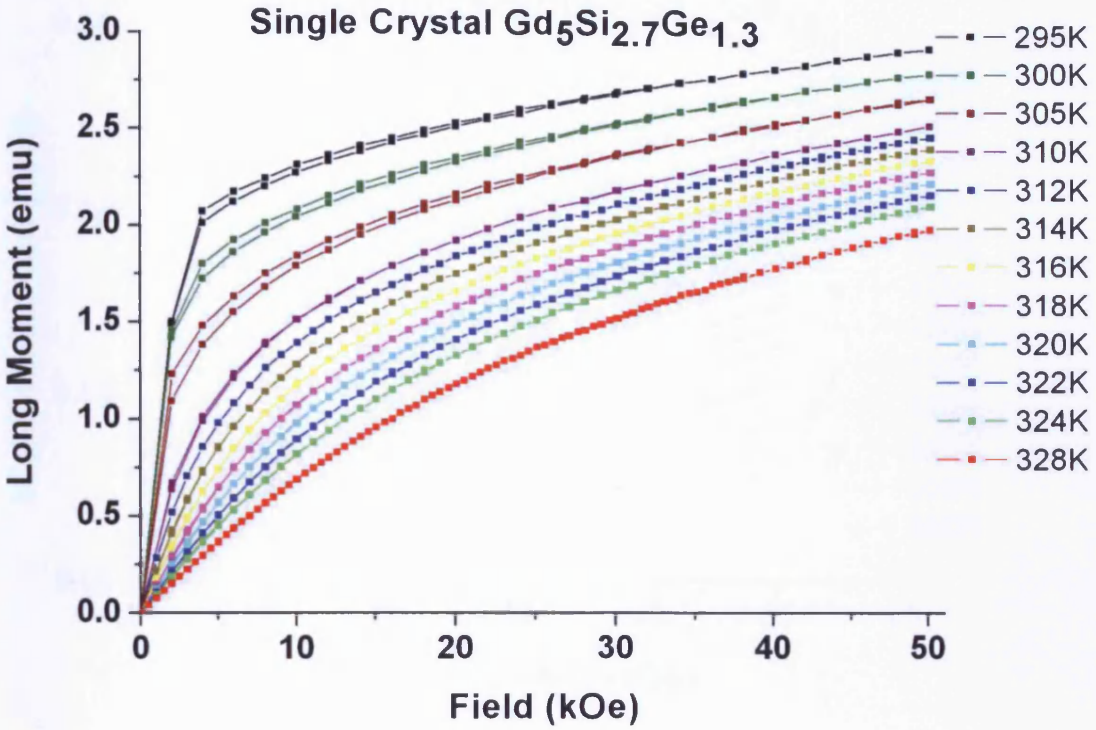

Fig. 3.9 Magnetic moment as a function of magnetic field at various temperatures on a single crystal $Gd_5Si_{2.7}Ge_{1.3}$ sample

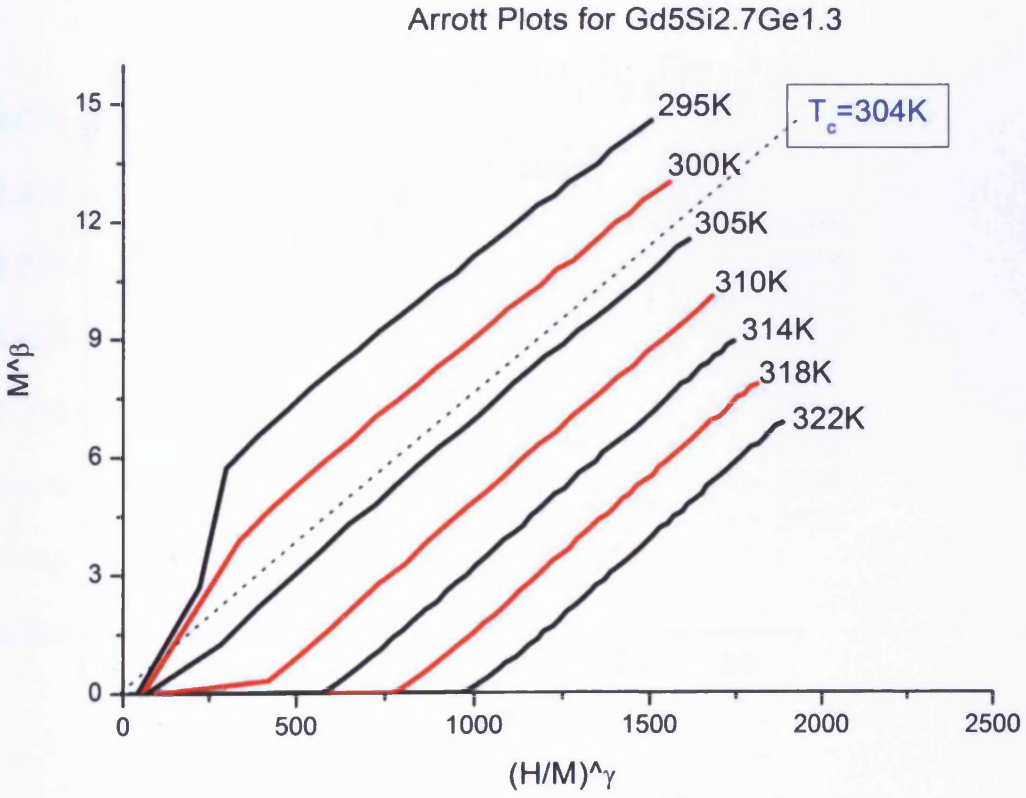

Fig.3.10 Arrott plots for single crystal $Gd_5Si_{2.7}Ge_{1.3}$ sample with the best values of the critical exponents $\beta = 0.45$ and $\gamma = 1.13$ with an error of ±05.

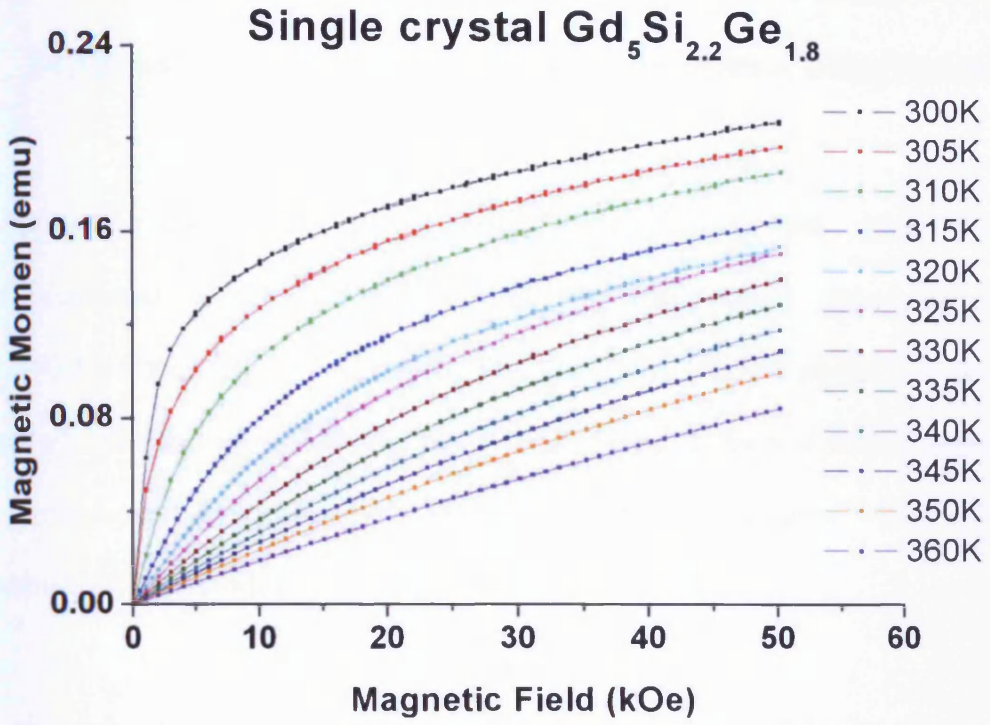

Fig. 3.11 Magnetic moment as a function of magnetic field for various temperatures on a single crystal $Gd_5Si_{2.2}Ge_{1.8}$ (x=0.54) sample.

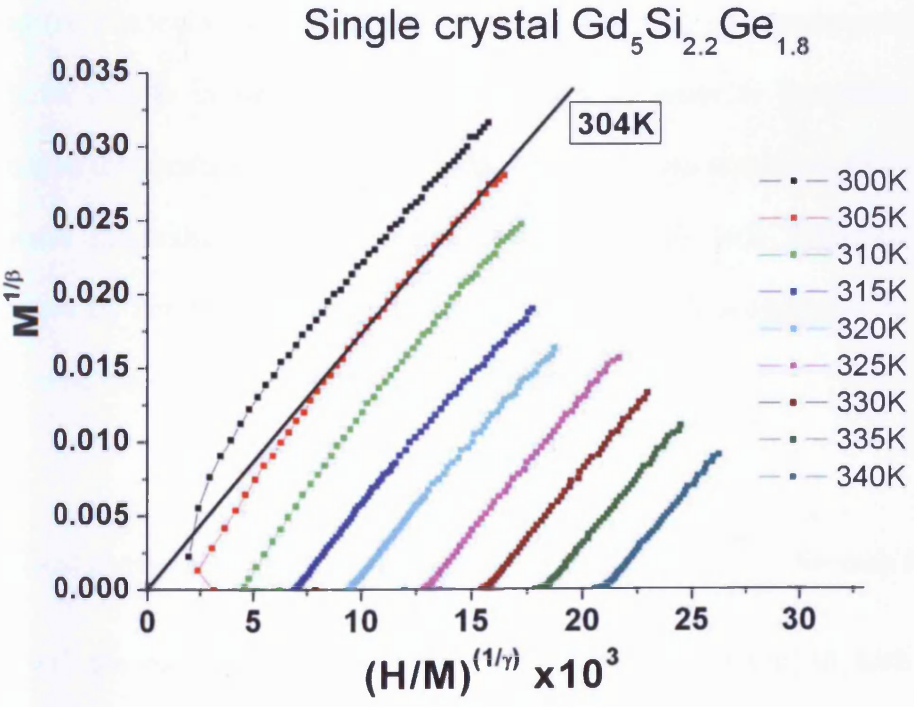

Fig.3.12 Arrott plots for single crystal $Gd_5Si_{2.2}Ge_{1.8}$ (x=0.54) sample with the second order phase transition temperature of 304 K.

3.4.3 Estimation of Second Order Phase Transition Temperature when it is Suppressed by the First Order Phase Transition Using Arrott Plots

$Gd_5(Si_xGe_{1-x})_4$ exhibits a first order magnetic-structural phase transition from ferromagnetic/orthorhombic phase to paramagnetic/monoclinic phase for the composition $0.4< x < 0.51$. If the first order structural phase transition from orthorhombic to monoclinic could be suppressed, then the orthorhombic phase would eventually show a second order phase transition from ferromagnetic to paramagnetic phase at a higher temperature, which would be the Curie temperature of the orthorhombic phase.

It is not possible however to directly measure this second order phase transition temperature since the first order structural phase transition occurs at a lower temperature thereby obscuring the second order transition. In this section the second order phase transition temperature of the orthorhombic phase (i.e. the temperature at which it would transform from ferromagnetic to paramagnetic if there were no change in structure) was determined. In order to determine the second order phase transition temperature of the orthorhombic phase we use the Arrott plot technique. This technique connects magnetisation and magnetic field with the Curie temperature through the equation proposed by Arrott as shown in Eqn. 3.7. In order for this technique to work, the measurements have to be made near to the critical temperature.

As stated above for the correct γ and β, a plot of $M^{\frac{1}{\beta}}$ vs. $\left(\frac{H}{M}\right)^{\frac{1}{\gamma}}$ for each MH isotherm is a straight line and the plots for all of the M-H isotherms are parallel to each other. For an ordinary ferromagnetic material, i.e. one which exhibits a second order transition from the paramagnetic to the ferromagnetic state, the isotherm that passes through the origin of the Arrott plot corresponds to the transition temperature.

In order to use this technique for our samples, only the ferromagnetic parts of the M-H isotherms (i.e. where the sample is in the orthorhombic phase) should be used. For our samples, only the isotherms below 275 K in case of the single crystal $Gd_5Si_{1.95}Ge_{2.05}$ (x=0.475) sample were used to construct the Arrott plots. This is because for higher temperatures the useful ferromagnetic part of the curves is small due to the limit of the available magnetic field (see Fig. 3.13).

The Arrott plot for the $Gd_5Si_{1.95}Ge_{2.05}$ (x=0.475) sample is shown in Fig. 3.14. It was found that the selected (ferromagnetic) parts of the isotherms were straight lines and were parallel to each other for $1/\gamma = 0.75$ and $1/\beta = 2.5$ with an error of ±05. It is noticeable that the ends of the straight sections of these isotherms have curvature going down out of the ferromagnetic region as shown in Fig. 3.14. Projecting the parallel isotherms to higher temperatures, we constructed an isotherm which is parallel to them and passes through the origin. The distance of this isotherm from the others was measured and the second order transition temperature of the orthorhombic phase was thus determined to be 296 K for $Gd_5Si_{1.95}Ge_{2.05}$ (x=0.475).

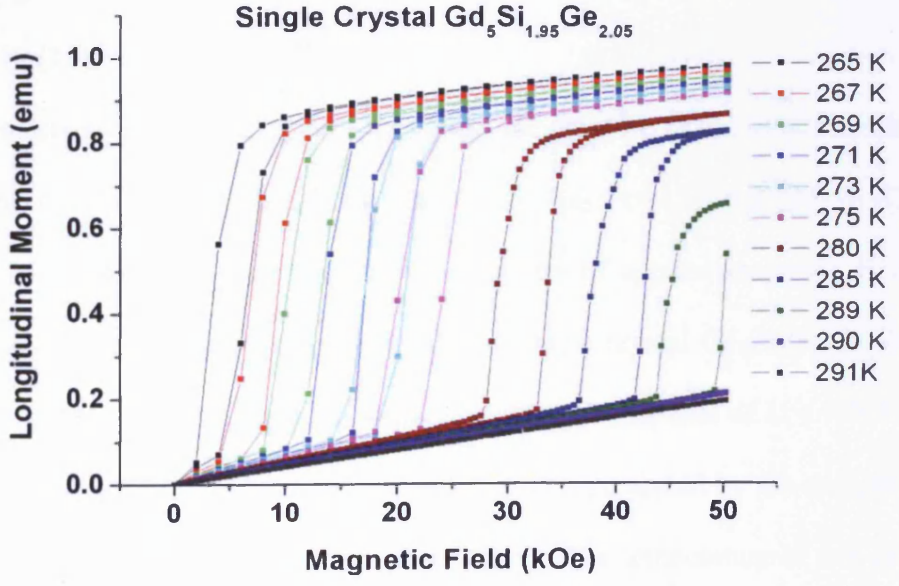

Fig. 3.13 Magnetic moment as a function of magnetic field at various temperatures above and below the first order phase transition temperature for single crystal $Gd_5Si_{1.95}Ge_{2.05}$(x=0.475) sample.

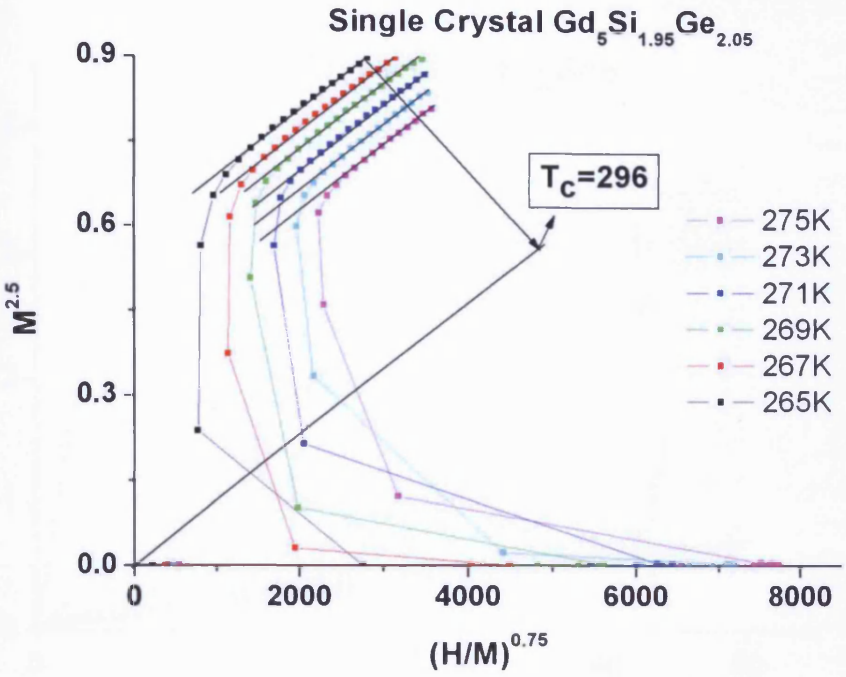

Fig. 3.14 Arrott plots for single crystal $Gd_5Si_{1.95}Ge_{2.05}$ (x=0.475) sample with the projected second order phase transition temperature of the orthorhombic phase which was found to be 296 K.

When the estimated second order phase transition temperature of the orthorhombic phase is plotted on the phase diagram it falls on the projected second order phase transition temperature line as shown in Fig. 3.19 [11].

Similarly the projected second order phase transition temperature of the orthorhombic phase was determined using Arrott plots for single crystal $Gd_5Si_2Ge_2$ (x=0.5) and $Gd_5Si_{1.8}Ge_{2.2}$ (x=0.45) samples. Fig. 3.15 shows magnetic moment as a function of applied magnetic field for various temperatures close to the transition temperature of the single crystal $Gd_5Si_2Ge_2$ (x=0.5). Fig. 3.16 shows the Arrott plots for the same sample with the critical coefficients of $1/\gamma = 0.9$ and $1/\beta = 2.2$ with an error of ±05. The ferromagnetic parts of the curves represented by the straight parallel lines are projected to the line where it passes through the origin. The temperature of this isotherm which passes through the origin was estimated to be 301 K for the single crystal $Gd_5Si_2Ge_2$ (x=0.5). It was then plotted on the phase diagram as shown in Fig. 3.19. It can be seen that the temperature falls on the projected line

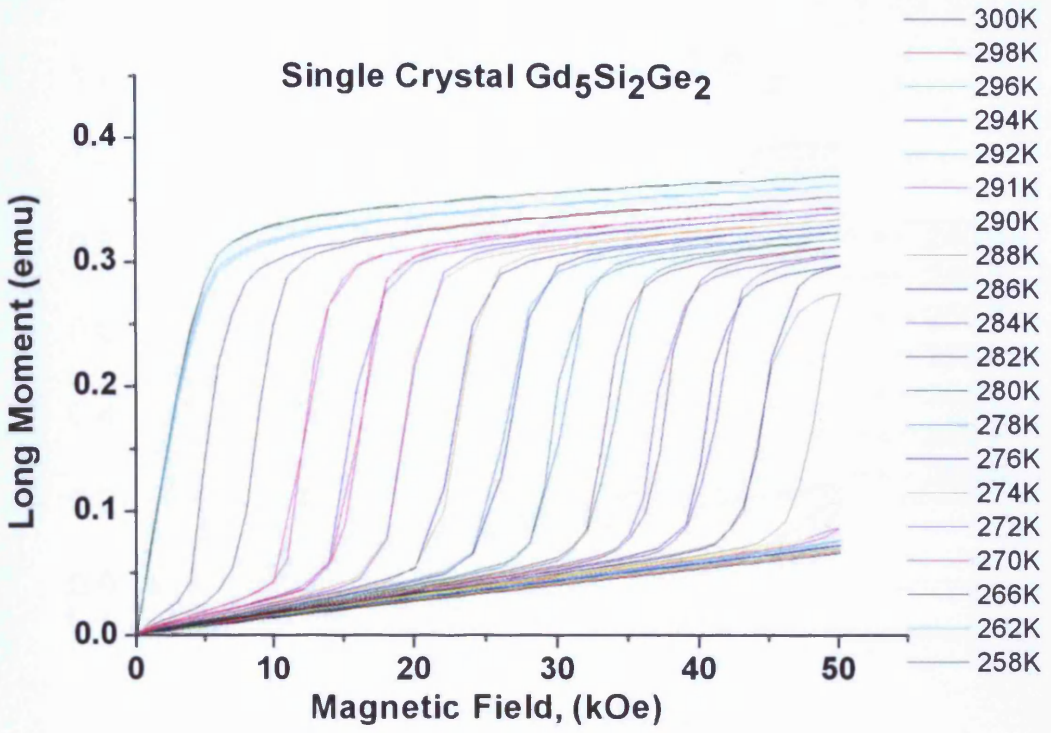

Fig. 3.15 Magnetic moment as a function of magnetic field at various temperatures above and below the first order phase transition temperature for single crystal $Gd_5Si_2Ge_2$ (x=0.5)sample.

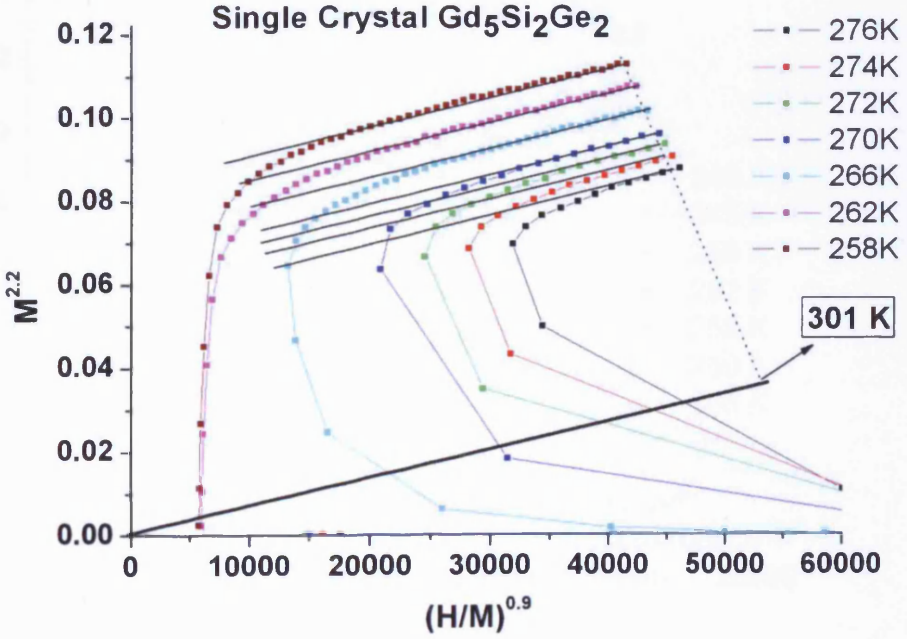

Fig. 3.16 Arrott plots for single crystal $Gd_5Si_2Ge_2$ (x=0.5) sample showing the projected second order phase transition temperature of the orthorhombic phase which was found to be 301 K.

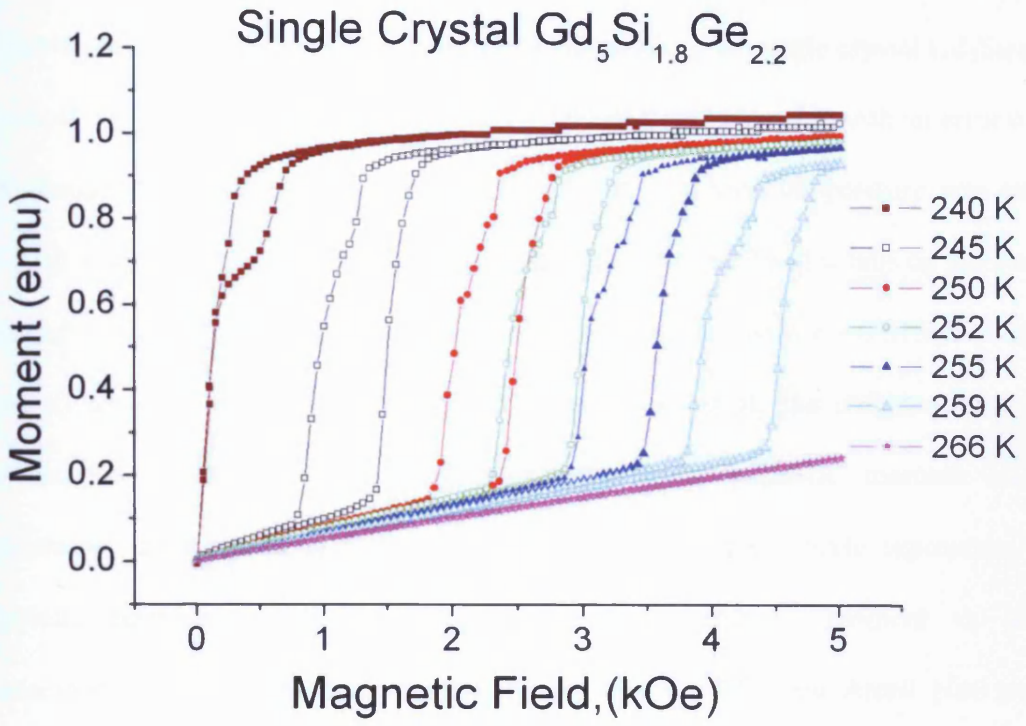

Fig. 3.17 Magnetic moment as a function of magnetic field at various temperatures above and below the first order phase transition temperature for single crystal $Gd_5Si_{1.8}Ge_{2.2}$ (x=0.45) sample.

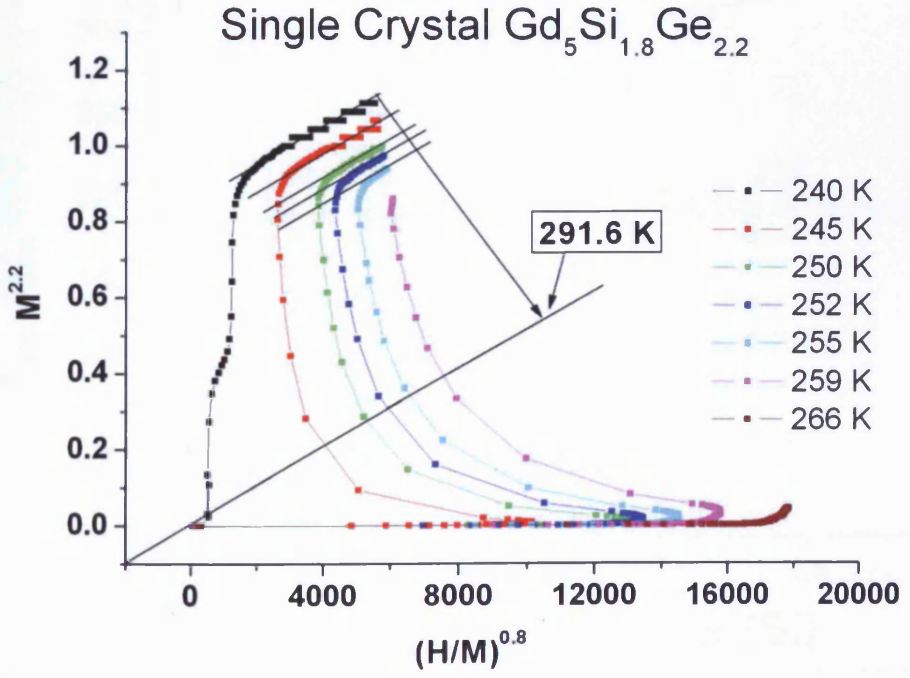

Fig. 3.18 Arrott plots for single crystal $Gd_5Si_{1.8}Ge_{2.2}$ (x=0.45) sample with the projected second order phase transition temperature of the orthorhombic phase which was found to be 291.6 K.

from the region where there exists a second order phase transition temperature. Fig. 3.17 shows the M-H curves and Fig. 3.18 shows corresponding Arrott plots for single crystal $Gd_5Si_{1.8}Ge_{2.2}$ sample. The critical coefficients were determined to be $1/\gamma = 0.8$ and $1/\beta = 2.2$ with an error of ±05 in order to get straight parallel lines. The second order phase transition temperature was estimated to be 291.6 K. It is plotted on the phase diagram as shown in Fig. 3.19 and it falls on the projected line of the second order phase transition temperature from the region with $x > 0.575$. The modified phase diagram (Fig. 3.19) shows two transition temperatures for all the compositions. The red stars represents the transition temperature determined from magnetic moment vs. temperature measurements using the inflection point method and the blue circle represents the transition temperature determined from the Arrott plots using magnetic moment vs. magnetic field measurements. In the region with composition $0.41 < x < 0.51$, the Arrott plot method and the inflection point method (using

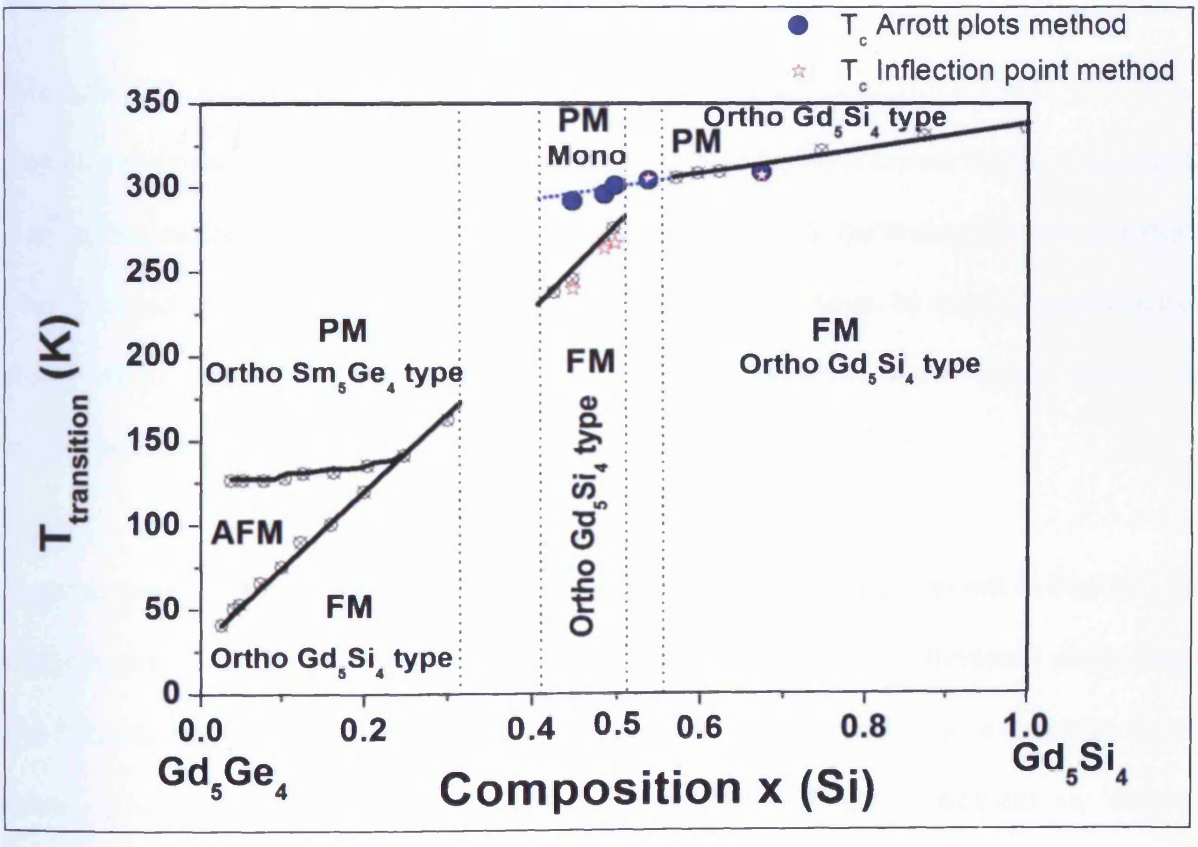

Fig. 3.19 Modified Phase diagram with the estimated second order phase transition temperatures from Arrott plots (star) and first order phase transition temperature for various samples (blue circle)

magnetic moment vs. temperature) of transition temperature measurements show different temperatures because Arrott plot method always give the second order phase transition while inflection method shows first order phase transition temperature for that composition.

For composition $0.51 < x < 1$, both Arrott plot and the inflection point method give the same transition temperature as the Arrott plot method always shows the second order phase transition temperature and the inflection point method gives second order phase transition temperature for this composition.

3.4.4 Estimation of Second Order Phase Transition Temperature in the Mixed Phase Region ($0.31<x<0.41$) Using Arrott Plots

$Gd_5(Si_xGe_{1-x})_4$ exhibits a mixed phase region for the composition $0.31 < x < 0.41$ [12]. Fig. 3.20 shows the magnetic moment as a function of temperature of a single crystal $Gd_5Si_{1.5}Ge_{2.5}$ (x=0.375) at an applied magnetic field of 100 Oe. The transition observed in the measurement is not sharp like other first order phase transitions of single crystal samples. This might be due to the presence of two phases whose transition temperatures are close to each other which might appear in the measurement as a continuous single transition.

Magnetic moment vs. magnetic field measurements on the same sample shown in Fig. 3.21 exhibit a large hysteresis confirming that the transition is a first order magnetic-structural phase transition. The first order phase transition is not sharp unlike other single crystal first order phase transitions instead, it has occurred on a wide field range similar to magnetic moment vs. temperature measurement indicating the presence of a secondary phase in the sample.

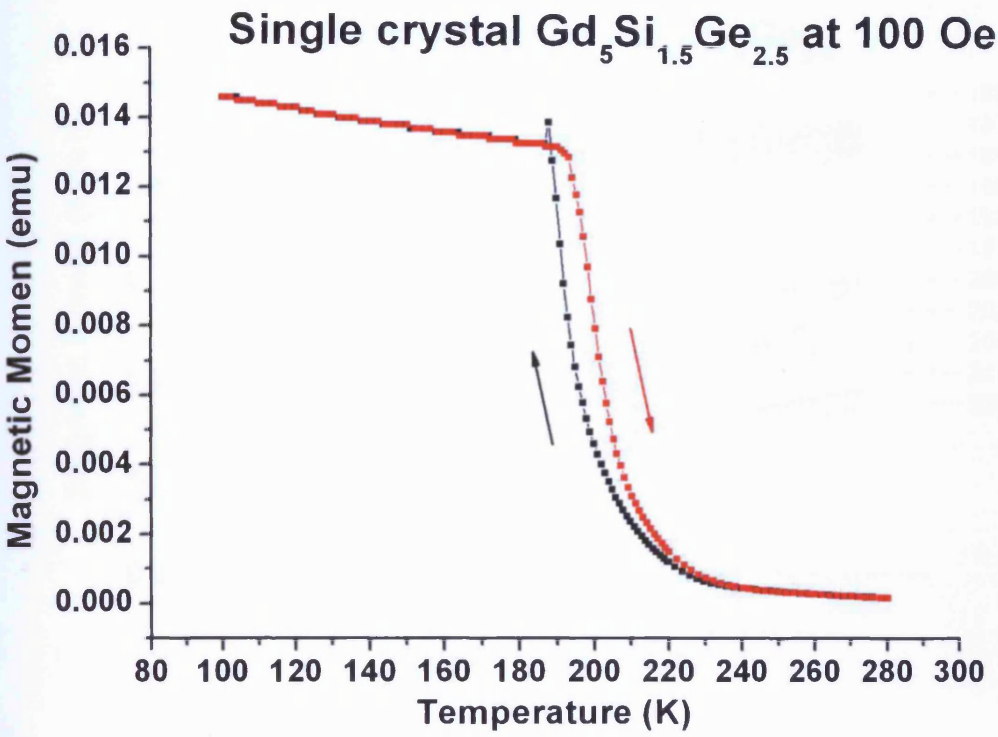

Fig. 3.20 Magnetic moment as a function of temperature of a single crystal $Gd_5Si_{1.5}Ge_{2.5}$ (x=0.375) sample at an applied magnetic field of 100 Oe (8 kA/m). Hysteresis indicates that the transition is first order transition.

The Arrott plots were drawn from $M^{1/\beta}$ and $(H/M)^{1/\gamma}$ isotherms for critical coefficients of $1/\gamma = 0.85$ and $1/\beta = 1.85$ with an error of ±05 as shown in Fig. 3.24. It can be seen in the Arrott plots that there are two set of parallel lines with different slopes. The top set represents the ferromagnetic part of the orthorhombic phase. Using these lines second order phase transition temperature of the orthorhombic phase was projected and was estimated to be about 300 K. From the modified phase diagram shown in Fig. 3.20, the projected second order phase transition temperature of the orthorhombic phase for the composition $Gd_5Si_{1.5}Ge_{2.5}$ (x=0.375) is 290 K. The Arrott plot estimation of the second order phase transition temperature of 300 K is 10 K higher which might be due to the fact that the isotherms used for the estimation are far from the actual transition temperature.

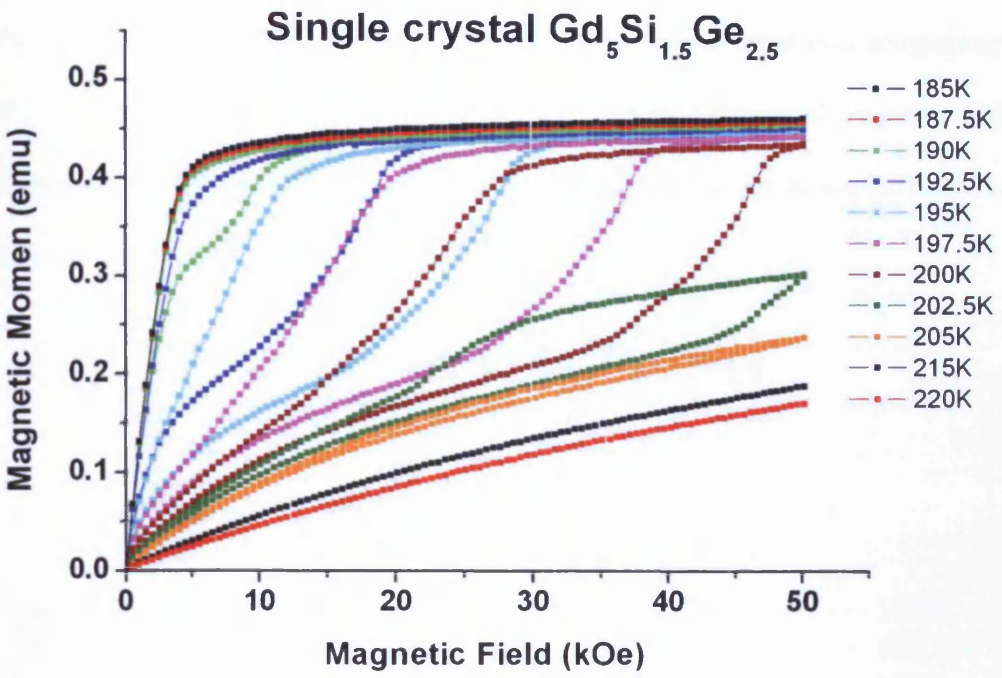

Fig. 3.21 Magnetic moment vs. magnetic field for various temperatures close to the first order phase transition for a single crystal $Gd_5Si_{1.5}Ge_{2.5}$ (x=0.375) sample showing large amount of hysteresis.

The second set of parallel lines in the Arrott plots represent the ferromagnetic part of the second phase in the mixed phase alloy. This second phase shows a phase transition similar to a second order phase transition as shown in Fig. 3.10 and 3.12. Since it shows a second order phase transition, one of the isotherms passes through the origin and there is no need for projecting to estimate the transition temperature. The isotherm that passes through the origin is 197.5 K hence it is the second order phase transition of the second phase of the single crystal $Gd_5Si_{1.5}Ge_{2.5}$ (x=0.375) alloy.

Since the second phase exhibits a second order phase transition with a transition temperature of 197.5 K and the Arrott plots shows isotherms that show the transformation from ferromagnetic orthorhombic to this second phase it gives an indication that the second phase in the mixed phase is actually the monoclinic phase. Since the second order phase transition temperature of the monoclinic phase is higher than its first order phase transition from the orthorhombic phase to the

monoclinic phase for this composition, we can see the presence of a second order phase transition in the Arrott plots. Unlike the projection of the second order phase transition temperature of the orthorhombic phase in the phase diagram, it is not possible to estimate the second order phase transition temperature of the monoclinic phase from the phase diagram to support the Arrott plot technique applied to monoclinic phase.

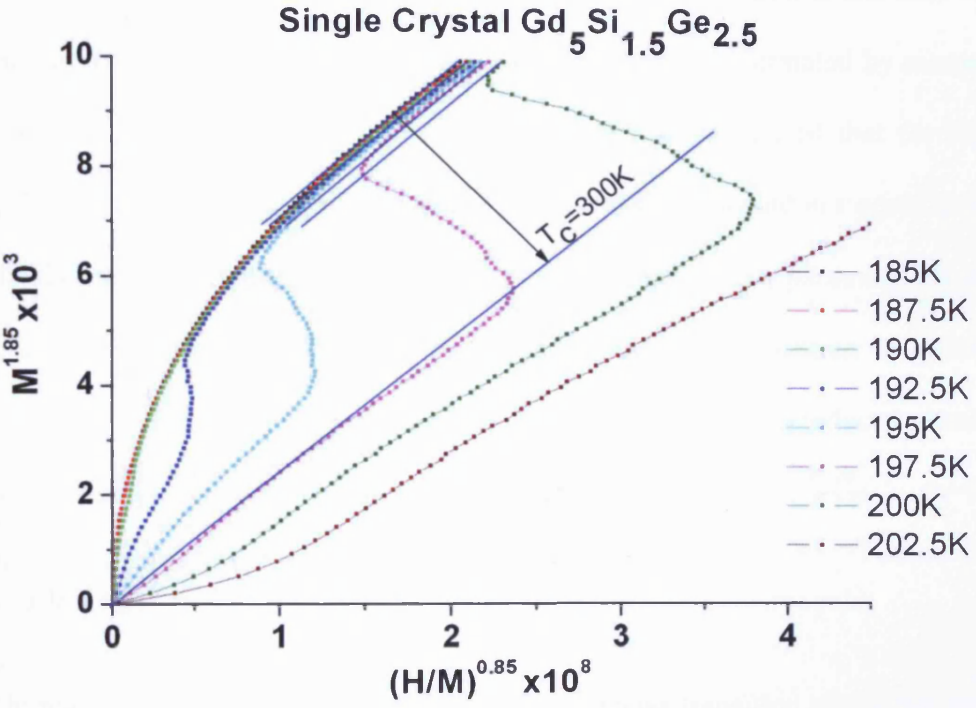

Fig. 3.22 Magnetic moment vs. magnetic field for various temperatures close to the first order phase transition for a single crystal $Gd_5Si_{1.5}Ge_{2.5}$ (x=0.375) sample showing large amount of hysteresis.

3.5 Verification of Arrott Plot Technique on the First Order Phase Transition Using Field Induced Phase Transition at High Magnetic Fields

For composition $0.41 < x < 0.51$ of $Gd_5(Si_xGe_{1-x})_4$, if the thermodynamic temperature T is higher than the first order transition temperature (T_{FO}), the field induced first order phase transition will occur under a sufficiently high magnetic field. This is discussed in detail in the Field Induced Phase Transition section (2.7) of Chapter 2. The magnetic field needed to induce the field induced first

order phase transition increases with thermodynamic temperature T. The converse effect is also true; in magnetic moment vs. temperature measurement for different isomagnetic fields the transition temperature T_{FO} increases with the increase in the applied magnetic field with a rate of typically 5 K/Tesla [13].

It is reasonable to expect that the orthorhombic phase has a second order Curie temperature (T_C^*) as well. However this temperature T_C^* cannot be directly measured as the first order phase transition occurs at lower temperatures, $T_{FO} < T_C^*$ but it still can be estimated by means of Arrott plot techniques as shown in Fig. 3.14, 3.16 and 3.18. It was hypothesized that for high enough temperatures, $T > T_C^*$, the field induced first order phase transition would not occur even for very high applied fields because the orthorhombic phase would already be in a paramagnetic state at that temperature [11]. The temperatures T above the second order phase transition temperature of the orthorhombic phase, $T > T_C^*$, where it would be paramagnetic and no field induced phase transition exists was determined for to be $T_C^* = 296$ K for single crystal $Gd_5Si_{1.95}Ge_{2.05}$ (x=0.475) and $T_C^* = 301$ K for the single crystal $Gd_5Si_2Ge_2$ (x=0.5) [11].

To prove the hypothesis of non existence of field induced phase transition above the second order phase transition temperature, T_C^*, we need to measure M vs. H isotherm at temperatures above 296 K and 301 K for the single crystal $Gd_5Si_{1.95}Ge_{2.05}$ (x=0.475) and $Gd_5Si_2Ge_2$ (x=0.5) samples respectively. As discussed earlier, the field required to induce the phase transition above the temperatures of 296 K and 301 K is more than 5 Tesla. The MPMS at Wolfson Centre for Magnetics has a maximum magnetic field range of 5 Tesla hence these measurements were carried out at the University of Sheffield in 9 Tesla range Vibrating Sample Magnetometer (VSM) provided by Oxford Instruments. Fig. 3.23 shows the magnetic moment as a function of magnetic field at 296 K and 300 K for the single crystal $Gd_5Si_{1.95}Ge_{2.05}$ (x=0.475). It is clearly seen that a field induced first order phase transition occurred even at temperatures higher than $T_C^* = 296$ K for single crystal $Gd_5Si_{1.95}Ge_{2.05}$. The same is observed for the single crystal $Gd_5Si_2Ge_2$ (x=0.5) sample

(see Fig. 3.24), which exhibits the field induced first order phase transition above the second order phase transition temperature, T_C^* = 301 K of the orthorhombic phase[14].

Occurrence of a field induced first order phase transition at temperatures above the second order phase transition temperature of the orthorhombic phase at a high magnetic field can possibly be explained by the fact that the transition of the underlying orthorhombic phase from ferromagnetic to paramagnetic is not distinct and it spreads over a wide range of higher temperatures. The broadening of the transition to a wider range of temperatures is clearly seen in Fig. 2. 17 which shows the measurement of magnetic moment vs. temperature for single crystal $Gd_5Si_{2.7}Ge_{1.3}$ (x=0.675) at high applied magnetic field strengths. At temperatures higher than the second order phase transition temperature, T_C and at high magnetic fields (9 Tesla) the magnetic moment is large even for the paramagnetic phase of the orthorhombic structure. Such a large magnetic moment of the orthorhombic phase makes the transition from monoclinic to orthorhombic transition appear as a field induced first order magnetic-structural phase transition.

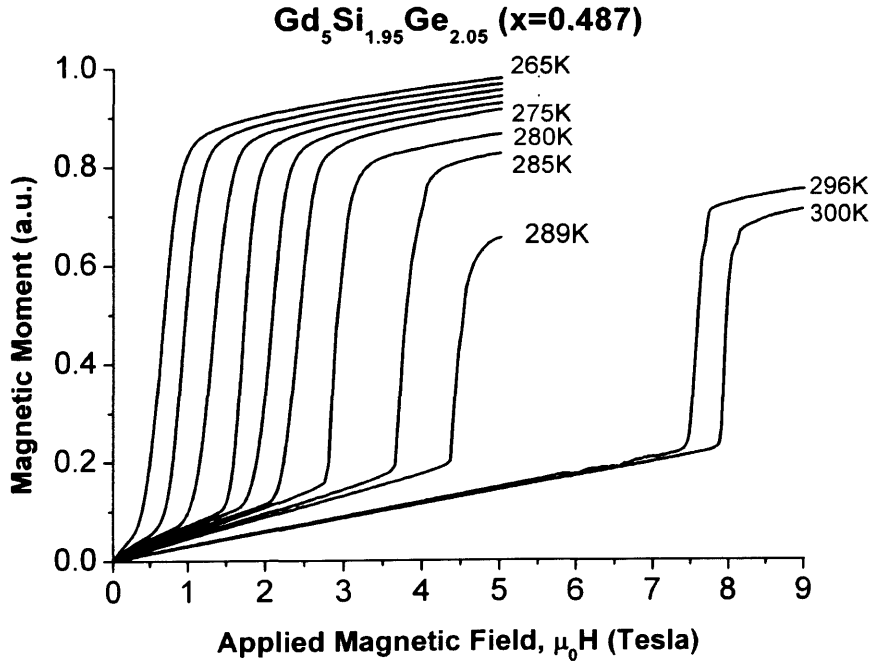

Fig. 3.23 Magnetic moment as a function of magnetic field for the single crystal $Gd_5Si_{1.95}Ge_{2.05}$ (x=0.475) at temperatures above and below the second order phase transition temperature of the orthorhombic phase.

Observation of a field induced first order phase transition temperature at high magnetic fields of up to 16 Tesla has been reported by Casanova *et al.* [15], but it was not compared to the projected second order phase transition temperature of the orthorhombic phase. It can also be seen from their paper that the error bars increased at higher magnetic fields in the transition field vs. transition temperature graphs. It can be suggested that this is due to the broadening of the transition of the underlying orthorhombic phase at high magnetic fields. The magnetization vs. temperature characteristics of the underlying orthorhombic phase of $Gd_5Si_{1.95}Ge_{2.05}$ and $Gd_5Si_2Ge_2$ should be quite similar to those we measured for orthorhombic $Gd_5Si_{2.7}Ge_{1.3}$ (x=0.675) as shown in Fig.2.17.

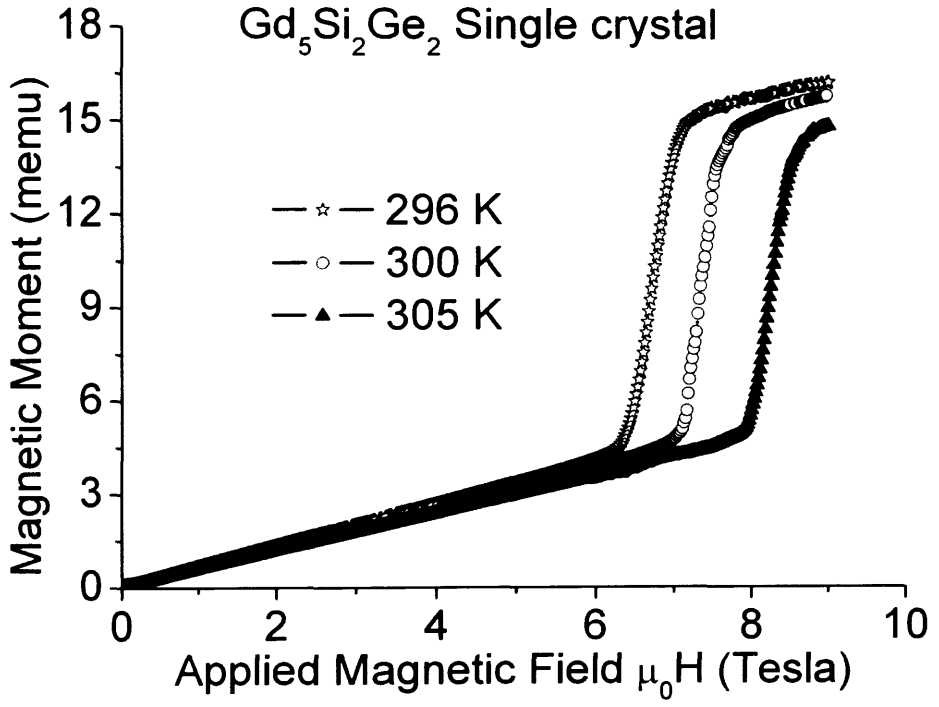

Fig. 3.24 Magnetic moment as a function of magnetic field for the single crystal $Gd_5Si_2Ge_2$ (x=0.5) at temperatures near the second order phase transition temperature of the orthorhombic phase.

The rate of change of transition temperature with respect to field (5 K/Tesla) can be lowered by applying external compressive pressure. According to the work reported by Megan *et al.* [16], this rate decreases with increase in the isobaric compressive pressure on the sample. With the application of compressive pressure they have obtained a field induced first order phase transition at

temperatures above the second order phase transition temperature of the orthorhombic phase. This can be explained with the observation of a non-zero compressive isobaric pressure-induced magnetization of the ferromagnetic orthorhombic phase after the transition which is 25% less than the magnetization for the same isotherm after the transition under zero compressive pressure. This is an indicative of an incomplete magnetic phase transformation of the underlying orthorhombic phase.

3.6 Summary

A literature review of the first order and the second order phase transition was carried out. The first order and second order phase transition temperatures for various compositions of $Gd_5(Si_xGe_{1-x})_4$ were measured. Various methods of transition temperature measurements were compared and the Arrott plot technique was determined to be a suitable method for these materials. An improved technique based on Arrott plots was developed to estimate the second order phase transition temperature when it is suppressed by the first order phase transition. This technique was also extended to estimate the transition temperature of mixed phase alloys. Field induced phase transition at high temperature using high magnetic field measurements up to 9 Tesla were carried out on two compositions $Gd_5(Si_xGe_{1-x})_4$ of (x=0.5 and x=0.475) to validate the Arrott plot technique.

References

[1] A. O. Pecharsky, K. A. Gschneidner, Jr, V. K. Pecharsky and C. E. Schindler, "*The room temperature metastable/stable phase relationships in the pseudo-binary Gd_5Si_4–Gd_5Ge_4 system.*", J. Alloys. Comp., **338**, pp.126-135, (2002).

[2] F. Holtzberg, R.J. Gambino and T.R. McGuire "*New ferromagnetic 5 : 4 compounds in the rare earth silicon and germanium systems*", J. Phys. Chem. Solids, **28**, pp. 2283-2289, (1967).

[3] V. K. Pecharsky and K. A. Gschneidner. Jr., "*Phase relationships and crystallography in the pseudobmary system Gd_5Si_4---Gd_5Ge_4*", J. Alloys. Comp., **260**, pp. 98-106, (1997).

[4] V.K. Pecharsky, G.D. Samolyuk, V.P. Antropov, A.O. Pecharsky, and K.A. Gschneidner, Jr.,"*The effect of varying the crystal structure on the magnetism, electronic structure and thermodynamics in the $Gd_5(Si_xGe_{1-x})_4$ system near $x=0.5$*", J. Solid. State. Chem., **171**, pp. 57-68, (2003).

[5] V. K. Pecharsky and K. A. Gschneidner. Jr. "*$Gd_5(Si_xGe_{1-x})_4$: An Extremum Material*", Adv. Mater., **13**, pp. 683-686, (2001).

[6] S. Yu. Dan'kov, A. M. Tishin, V. K. Pecharsky and K. A. Gschneidner, Jr., "*Experimental device for studying the magnetocaloric effect in pulse magnetic fields*", Rev. Sci. Instrum., **68**, pp. 2432-2436, (1997).

[7] R. L. Hadimani, M. Melikhov, J. E. Snyder and D. C. Jiles, "*Determination of Curie temperature by Arrott plot technique in $Gd_5(Si_xGe_{1-x})_4$ for $x>0.575$*", J. Magn. Magn. Mater., **320**, pp. e696-e698, (2008).

[8] A. Arrott, "*Criterion for Ferromagnetism from Observations of Magnetic Isotherms*", Phys. Rev., **108,** pp. 1394-1396, (1957).

[9] S. Chikazumi, "*Physics of Ferromagnetism*", New York: Oxford Science Publications pp.118-119, (1997).

[10] A. Arrott and J. E. Noakes, "*Approximate Equation of State for Nickel near its Critical Temperature*", Phys. Rev. Lett., **19,** pp. 786-788, (1967).

[11] R. L. Hadimani, M. Melikhov, J. E. Snyder and D. C. Jiles, "*Estimation of second order phase transition temperature of the orthorhombic phase of $Gd_5(Si_xGe_{1-x})_4$ using Arrott plots*", J. Appl. Phys., **103**, pp. 033906, (2008).

[12] K. A. Gschneidner Jr., V. K. Pecharsky, and A. O. Tsokol, "*Recent developments in magnetocaloric materials*", Rep. Prog. Phys., **68,** pp.1479–1539, (2005).

[13] M. Han, J. A. Paulsen, J. E. Snyder, D. C. Jiles, T. A. Lograsso, and D. L. Schlagel, "*Thermal Expansion of Single-Crystal $Gd_5(Si_{1.95}Ge_{2.05})$ Showing Unusual First-Order Transformation*", IEEE Trans. Magn, **38**, pp. 3252-3254, (2002).

[14] R. L. Hadimani, M. Melikhov, J. E. Snyder and D. C. Jiles, "*Field induced structural phase transition at temperatures above the Curie point in* $Gd_5(Si_xGe_{1-x})_4$", J. Appl. Phys. **105**, pp. 07A927-3, (2009).

[15] F. Casanova, X. Battle and A. Labarta, "*Scaling of the entropy change at the magnetoelastic transition in* $Gd_5(Si_xGe_{1-x})_4$", Phys. Rev. B, **66**, pp. 212402, (2002).

[16] C. Megan, L. Morellon, P. A. Algarabel, M. R. Ibarra, Z. Arnold, J. Kamarad, T. A. Lograsso, D. L. Schlagel, V. K. Pecharsky, A. O. Tsokol and K. A. Gschneidner, Jr., "*Hydrostatic pressure control of the magnetostructural phase transition in* $Gd_5Si_2Ge_2$ *single crystals*", Phys. Rev. B, **72**, pp. 024416, (2005).

Chapter 4: Giant Magnetocaloric Effect in $Gd_5(Si_xGe_{1-x})_4$

4.1 Introduction

4.1.1 Magnetocaloric Effect

The magnetocaloric effect is the adiabatic change in temperature of a magnetic material when an external magnetic field is applied. Most ferromagnetic materials exhibit magnetocaloric effect but with a small adiabatic temperature change. It was first discovered by Warburg in 1881 in iron [1, 2]. He noted that heat was either absorbed or rejected when magnetic field was changed. Under adiabatic conditions there was a temperature change in the system. This effect has been extensively used in very low temperature cooling below mK instead of dilution refrigerators which can not go below mK. Paramagnetic salts are used in magnetic cooling below mK hence the process is sometimes called paramagnetic cooling. Langevin was the first to demonstrate a temperature change in paramagnetic materials due to change in magnetisation in 1905 [3]. Later Debye and Giauque proposed magnetic refrigeration utilising the temperature change in paramagnetic salts to obtain low temperatures by adiabatic demagnetisation now widely used as paramagnetic cooling [1, 4].

Magnetic refrigerators work in an analogous cycle to that of a normal liquid-vapour cycle refrigerator. Magnetic field (H) is used to change the temperature of a refrigeration material in the magnetic refrigerator instead of pressure (P) in the liquid-vapour refrigerators. Rotary compressors are normally used to pressurise the refrigeration material in the liquid-vapour refrigerators which are not efficient devices. Figure 4.1 shows the comparison of magnetic and liquid-vapour cycle refrigeration. The magnetocaloric material (refrigeration material) has a positive magnetocaloric effect in this case i.e. the temperature of the magnetocaloric material increases upon application of an external magnetic field in an adiabatic condition similar to the vapour-liquid cycle. The heat generated in the adiabatic magnetisation process is then removed either by natural convection of air

or a forced convection of any fluid reducing the temperature of the magnetocaloric material. Once the magnetocaloric material is at room temperature under an

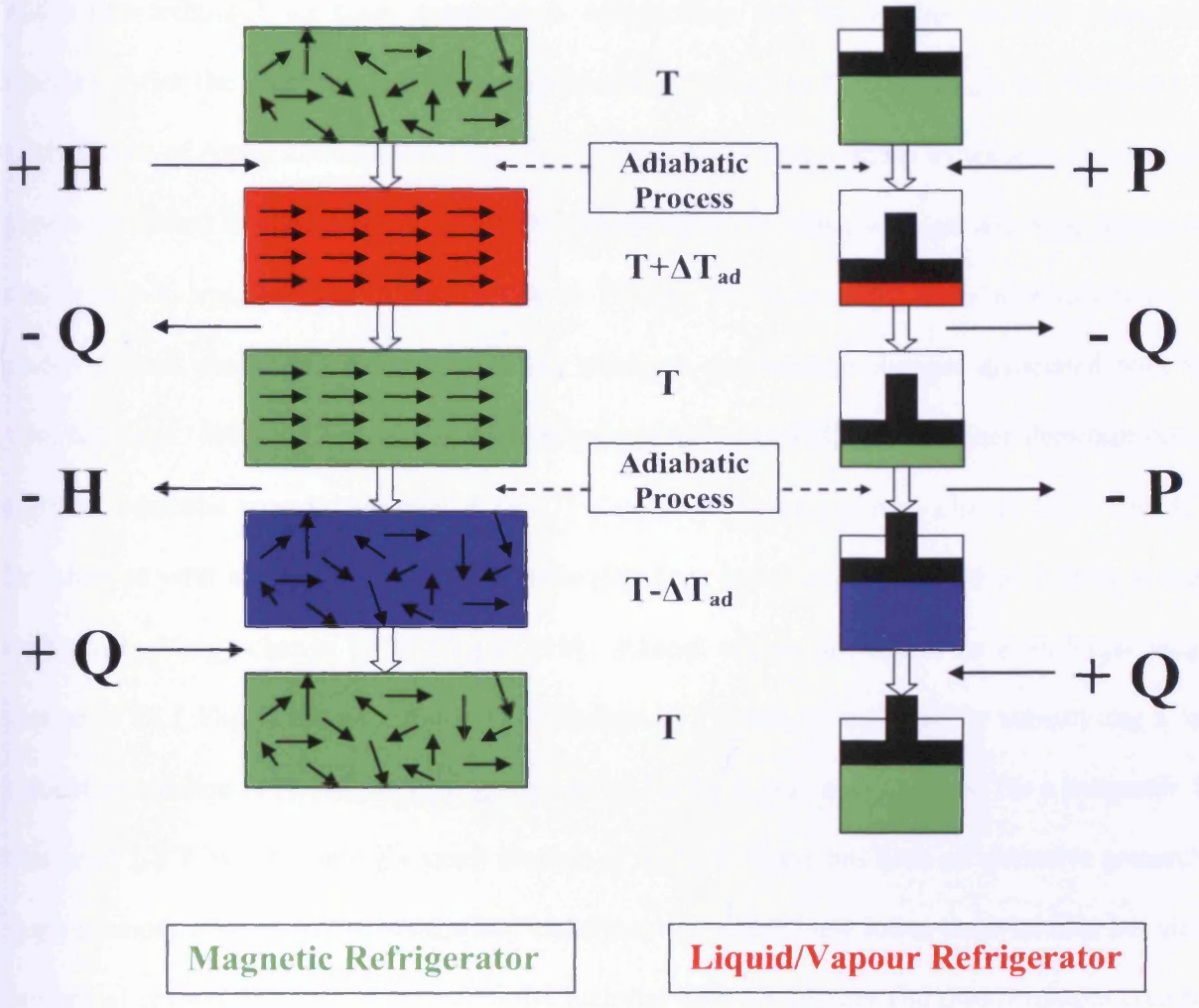

Fig. 4.1 Comparison of magnetic and liquid-vapour cycle refrigeration [6].

applied magnetic field, the external applied magnetic field is removed adiabatically, and the temperature of the magnetocaloric material decreases. This low temperature can be used to extract the heat from the environment that needs to be cooled.

4.1.2 Magnetocaloric Refrigeration

Magnetic refrigeration has been widely used in very low temperature regions. It was not possible to utilise this technique for room temperature refrigeration due the smaller adiabatic temperature changes. After the discovery of giant magnetocaloric effect in $Gd_5(Si_xGe_{1-x})_4$ by Pecharsky and Gschneidner of Ames Laboratory in the US [7], there has a been a sharp increase in the number of papers published in magnetocaloric effect. Magnetocaloric effect with an adiabatic temperature change of 2 K was observed in neodymium in 1990 by Zimm *et al.* [8]. Similar observations were made on other pure rare earth elements but adiabatic temperature changes associated with them were not large. With the giant magnetocaloric material of $Gd_5Si_2Ge_2$, it has been demonstrated that a greater adiabatic temperature change of 17° C or an isothermal entropy change of 36 J/kg K can be achieved with a magnetic field of 5 Tesla [9]. At a lower magnetic field of 2 Tesla it has an isothermal entropy change of 18 J/kg K [10]. Recent studies show that an even larger entropy change of 25.1 J/kg K for a magnetic field change of 2 T can be achieved by substituting a small amount of terbium [11]. An entropy change of 16.7 J/kg K was also obtained for a magnetic field change of 1.8 T by substituting a small amount of tin [12]. There has been an extensive research on shape memory alloys such as Ni_2MnGa, FeMnPAs, etc. which have lower material cost but similar isothermal entropy [13, 14]. A list of all the material with advantages and disadvantages compared to elemental gadolinium has been published by Gschneidner [15]. It can be seen from the table that the raw material cost of nickel and manganese based shape memory alloys are lower than the elemental gadolinium.

There are various attempts by various research groups to find a material with even higher adiabatic temperature change but have not been successful so far. One such group; Kumar *et al.* [16] tried by combining rare earth based materials and the shape memory alloys where in they synthesised and

characterised $Gd_{1-x}Sm_xMn_2Si_2$ but, the adiabatic ΔT obtained was much lower than that of the materials exhibiting highest magnetocaloric effect.

Table 4.1 List of magnetocaloric materials with advantages and disadvantages compared to elemental gadolinium. [15]

Factor	Gd	Gd_5T_4	$RMnO_3$	LaFeSi	MnAs	FeMnPAs	Ni_2MnGa
Raw material costs	0	–	++	++	++	++	+
Preparation	0	–	– –	–	– –	– –	– –
Vapor pressure	0	0	0	0	– –	– – –	0
Fabrication (sheet)	0	–	–	–	–	–	–
≥1 kg production	0	0	?	0	?	?	?
MCE, ΔS_m	0	++	–	+	+	+	+
MCE, ΔT_{ad}	0	+	–	–	–	0	–
Refrigeration capacity	0	+	?	+	?	+	?
Hysteresis	0	– –	0	–	–	–	– –
Time dependence of ΔT_{ad}	0	–	?	–	?	?	?
Environmental concerns	0	0	0	0	– –	–	0
Corrosion	0	++	?	–	?	?	0
Friability	0	–	?	–	?	–	–

Elemental Gd is taken as the baseline.

The search for new magnetocaloric materials with higher magnetocaloric effect (both ΔS and ΔT), cheaper raw material, low hysteresis, higher refrigeration capacity, low corrosion, etc. is continuing with the anticipation that in few years from now there will be much better magnetocaloric materials available.

4.2 Magnetic Refrigerator

The research on room temperature magnetic refrigerator development (meaning the system development side) has not kept its pace with the research on room temperature magnetocaloric materials. There has been no magnetic refrigerator built with newer bulk material such as Ni_2MnGa, FeMnPAs or $Gd_5(Si_xGe_{1-x})_4$ so far. There are about 15-20 near room temperature magnetic refrigerators built so far compared to thousands of publications on room temperature magnetocaloric materials. Table 4.2 shows some of the latest room temperature magnetic refrigerators built in different universities and laboratories with ΔT Max, type, magnetocaloric

material used, etc. As it can be seen from Table 4.2 the type of the magnetic refrigerator can be a rotary or reciprocating. In the following section different designs of magnetic refrigerators have been discussed.

Table 4.2 List of near room temperature magnetic refrigerators built in different universities and laboratories from 2004 to 2007 [15].

Name	Location	Announcement date	Type	Max. cooling power (W)	Max. ΔT (K)	Max. magnetic field[a] (kOe)	Regenerator material	Reference
Univ. Quebec, Trois Rivieres	Trois Rivieres, Quebec, Canada	Feb. 2004	Reciprocating	2	14	20 (S)	Gd-R alloys[b]	Richard et al. (2004)
George Washington Univ.	Ashburn, Virginia, USA	June 2005	Reciprocating	?	5	20 (P)	Gd pwdr.	Shir et al. (2005)
Nanjing Univ.	Nanjing, China	Sept. 27, 2005	Reciprocating	40	25	14 (H)	Gd pwdr. $Gd_5(Si,Ge)_4$ pwdr.	Lu et al. (2005)
Tokyo Inst. Tech.	Yokohama, Japan	Sept. 27, 2005	Rotary	60	4	7.7 (P)	Gd-R alloys[b]	Okamura et al. (2006)
Univ. Victoria	Victoria, Canada	Sept. 27, 2005	Reciprocating	?	50	20 (S)	Gd-R alloys[b]	Rowe et al. (2005)
Astronautics	Madison, Wisconsin, USA	Sept. 27, 2005	Rotary	50	25	15 (P)	Gd, Gd alloys[b] $La(Fe,Si)_{13}H_x$	Zimm et al. (2006)
Sichuan Univ.	Chengdu, China	April 11, 2007	Rotary	40	11.5	15 (P)	Gd particles	Chen et al. (2007)
Astronautics	Madison, Wisconsin, USA	April 12, 2007	Rotating magnet	220	11	14 (H)	Gd plates	Zimm et al. (2007)
Sichuan Univ.	Chengdu, China	April 12, 2007	Rotary	?	6.2	7.8 (P)	Gd sheets in water	Tang et al. (2007)
Univ. Victoria	Victoria, British Columbia, Canada	April 13, 2007	Rotary	?	13	14 (H)	Gd particles	Tura and Rowe (2007)
Chelyabinsk State Univ.	Chelyabinsk, Russia	April 13, 2007	Rotary	?	?	9 (P)	Gd and Heusler alloy	Buchelnikov et al. (2007)
Tokyo Inst. Tech.	Yokohama, Japan	April 13, 2007	Rotary	540	7.5	11 (P)	Gd spheres	Okamura et al. (2007)
Univ. Ljubljana	Ljubljana, Slovenia	April 13, 2007	Rotary	?	?	9.7 (P)	Various	Poredos and Sarlah (2007)

a Magnetic field source: S = superconducting magnet; P = permanent magnet; H = Halbach magnet.
b Layered bed.

There are mainly two types of magnetic refrigeration systems; active magnetic refrigeration (AMR) and Carnot magnetic refrigeration (CMR). A typical schematic diagram of an active magnetic refrigerator (AMR) is shown in Fig. 4.2. It uses pumps to circulate the fluid to the hot and cold heat exchangers. There are various designs of room temperature magnetic refrigerators based on the magnetic field source, magnetocaloric material used, and design of heat/cold exchangers. Depending on the magnetic field source, magnetic refrigerators can be classified as rotating table, reciprocating and pulsed field magnetic refrigerators.

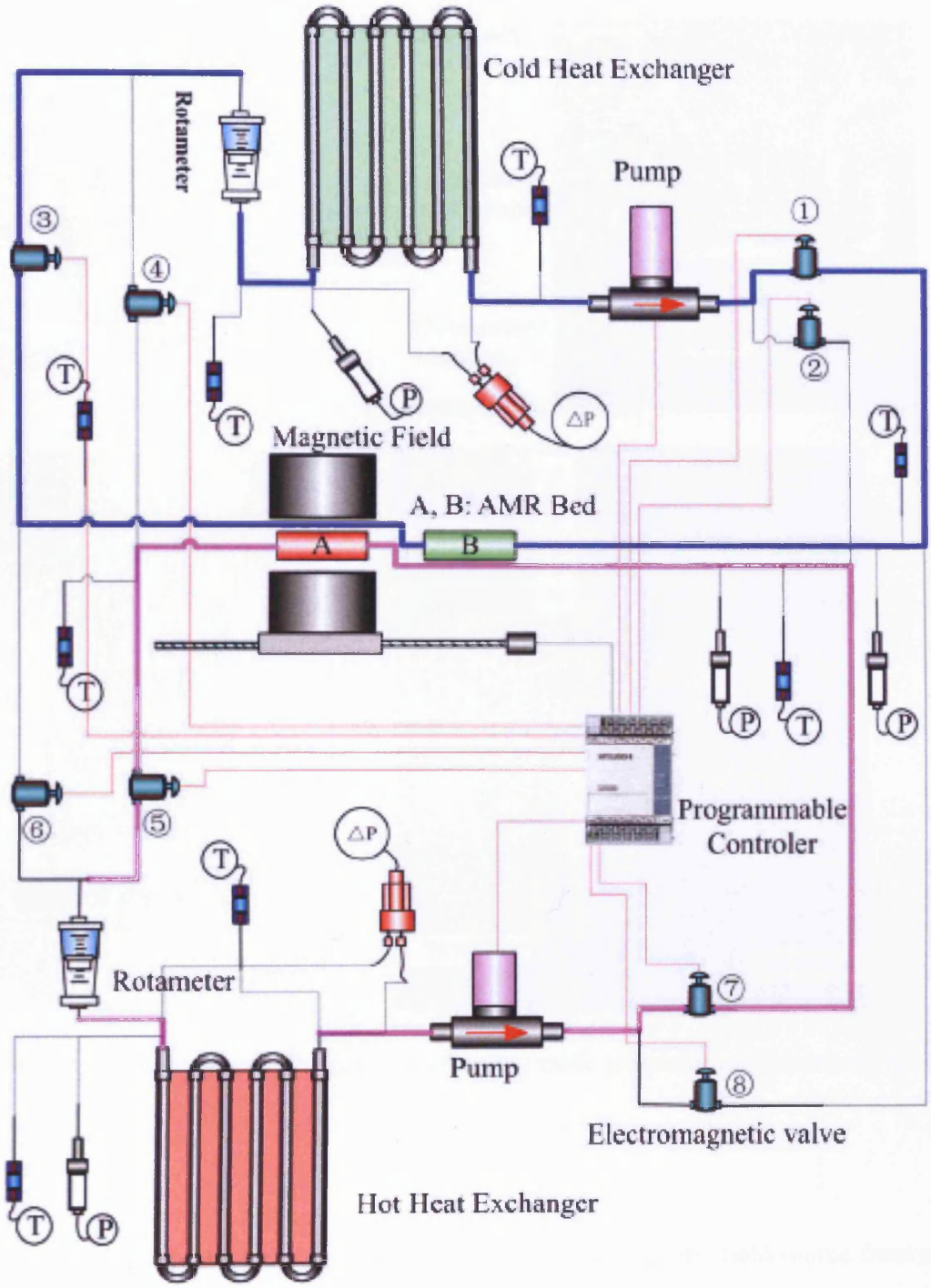

Fig. 4.2 Schematic diagram of an active magnetic refrigerator (AMR) where it uses two separate pumps to circulate the fluid to the hot and cold heat exchangers [17].

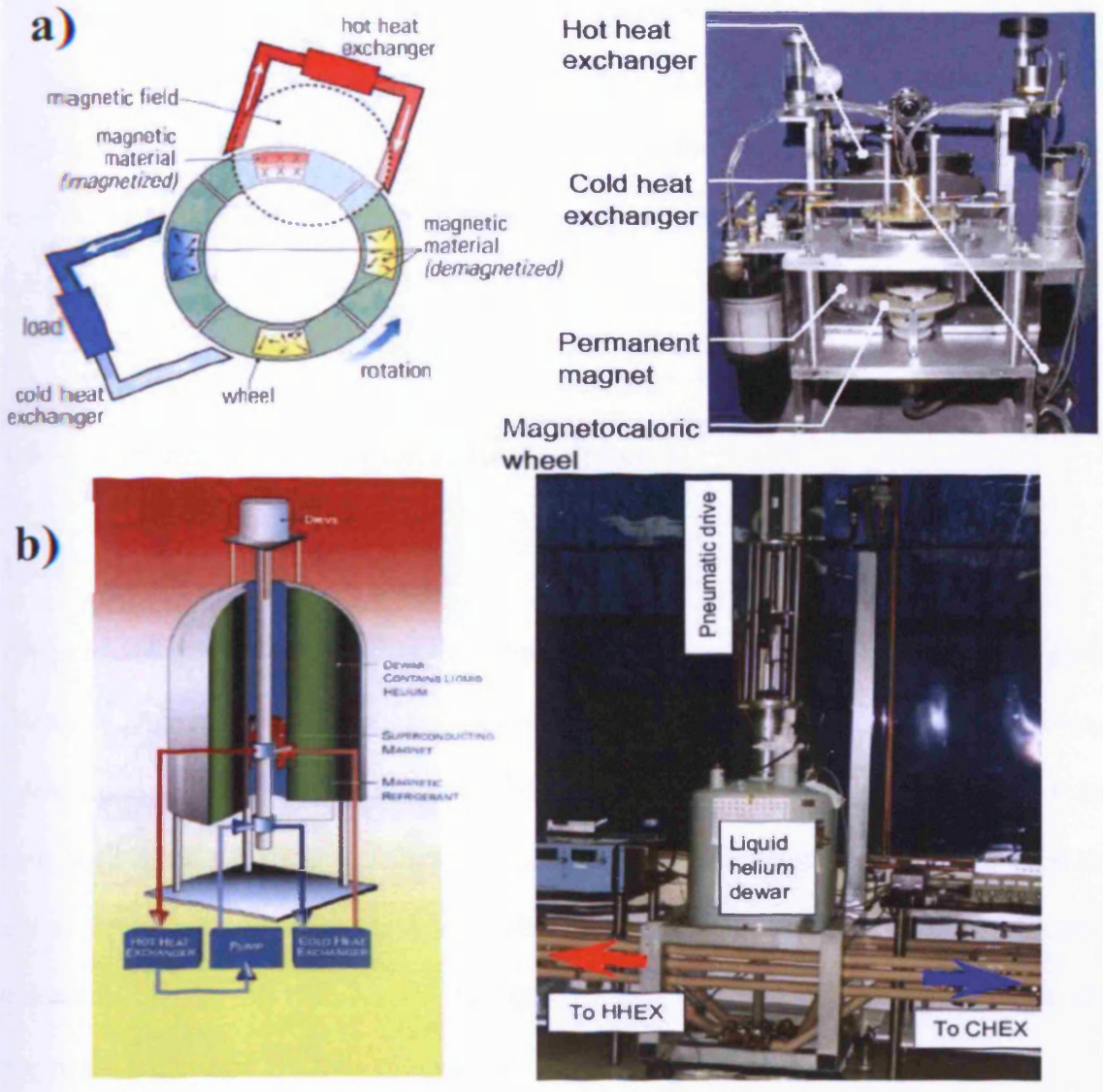

Fig. 4.3 Schematic diagram and images of a) rotating table magnetic refrigerator b) reciprocating magnetic refrigerator [15]

Fig. 4.3 a) shows a rotating table magnetic refrigerator with a magnetic field source from a Halbach permanent magnet. With Halbach permanent magnet array, flux densities of 2 Tesla can be achieved. There has been some work on improving the maximum flux density to 3 Tesla in a special geometric arrangement [18]. The table is made from a magnetocaloric material and rotates passing through the permanent magnets. The temperature of the magnetocaloric material rises when it reaches the magnetic field and water is circulated to cool the material. When the magnetocaloric material comes out of the magnetic field it cools down below room temperature. Fig. 4.3. b) shows

a reciprocating magnetic refrigerator where a superconducting magnet is used as a source of magnetic field and the magnetocaloric material reciprocates (moves forward and backward alternatively) through the magnetic field produced by the superconducting magnet which is housed in a liquid helium dewar. Any benign circulating fluid such as water or alcohol can be circulated through the hot and cold heat exchangers.

4.3 Estimation of Magnetocaloric Effect

4.3.1 Magnetocaloric Theory

When a magnetic field larger than the saturation magnetic field H_s is applied on a magnetic material, spins are aligned in the direction of applied field. In an adiabatic condition the entropy, S of the entire material is constant at constant temperature T, pressure, P and magnetic field, H as shown in Eqn. 4.1. When the spins are aligned, the entropy of the material decreases, to keep the material under the same energy state the thermal energy (atoms/molecule/particle vibration) increases which results in rise in the temperature T. Total entropy of the whole material can be divided into magnetic, lattice and electron components.

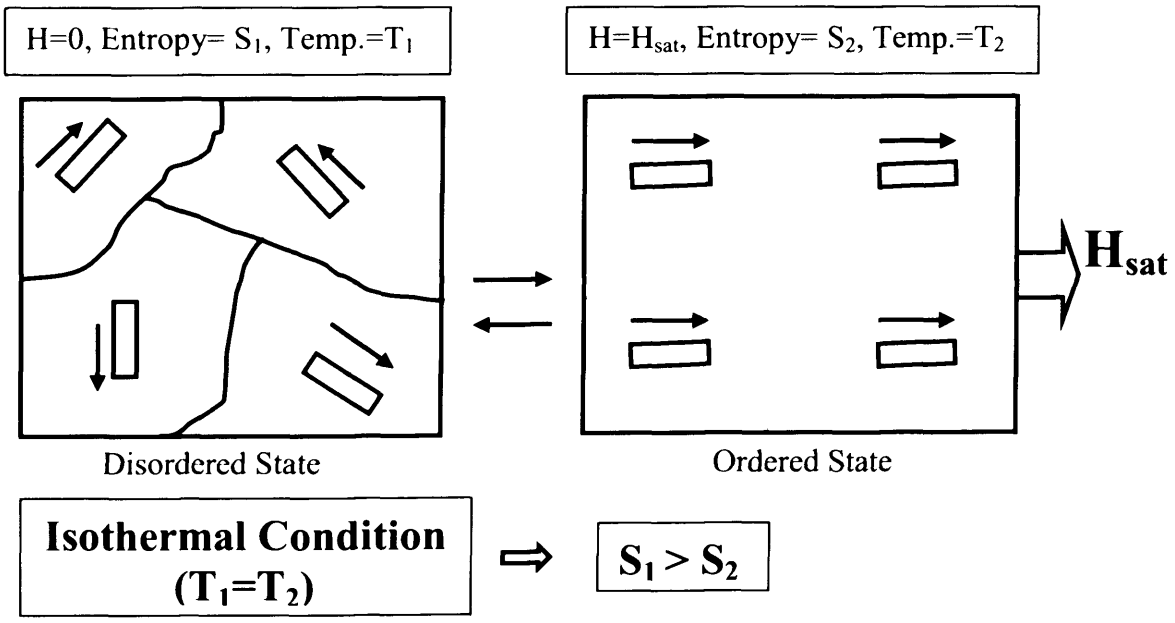

Fig. 4.4 Application of magnetic field under isothermal conditions

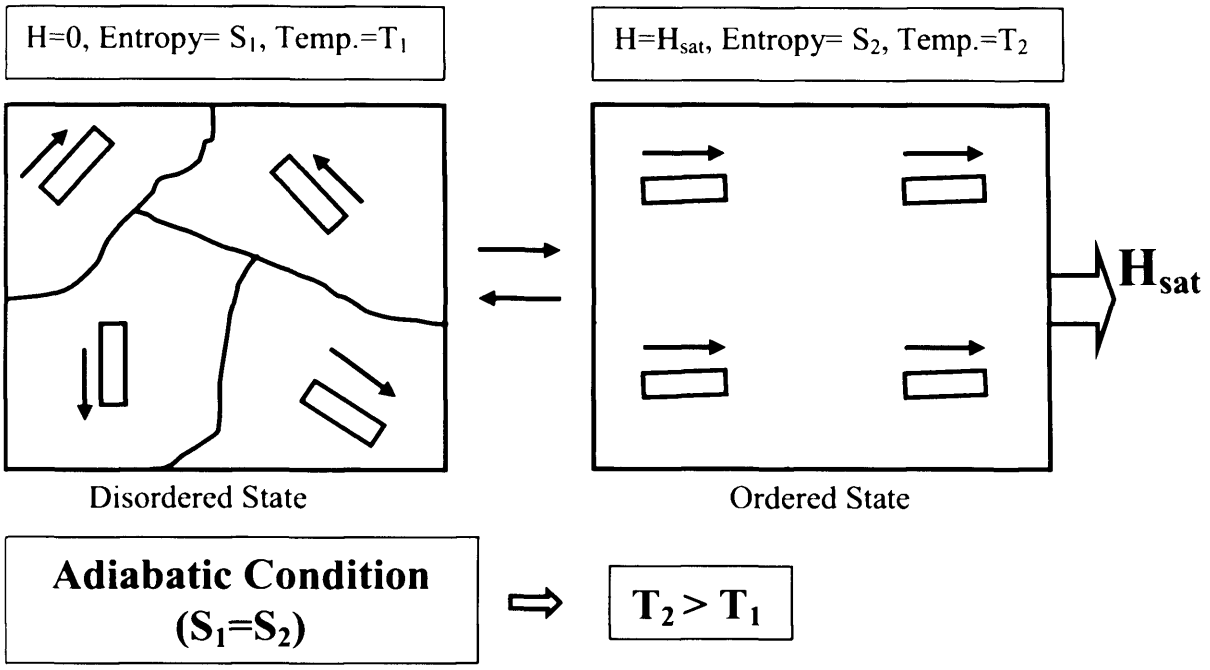

Fig. 4.5 Application of magnetic field under different conditions

$$S(T,H) = S_{magnetic}(T,H) + S_{lattice}(T) + S_{electronic}(T) \tag{4.1}$$

where S is entropy, T is temperature, H is magnetic field.

Fig. 4.6 shows entropy as a function of temperature for two different magnetic fields applied on a magnetocaloric material. The dotted line represents the electronic and lattice component and solid lines represent the total entropy and dashed lines represent the magnetic part of the entropy. It can be seen that for an adiabatic condition (constant S_0) the temperature of the higher magnetic field is higher than the temperature of the lower magnetic field indicating a positive magnetocaloric effect. The difference in the temperatures is ΔT_{ad}. For an isothermal condition (constant temperature T_0) the entropy at higher magnetic field is lower than the entropy at lower magnetic field. The difference in the entropy is ΔS_M.

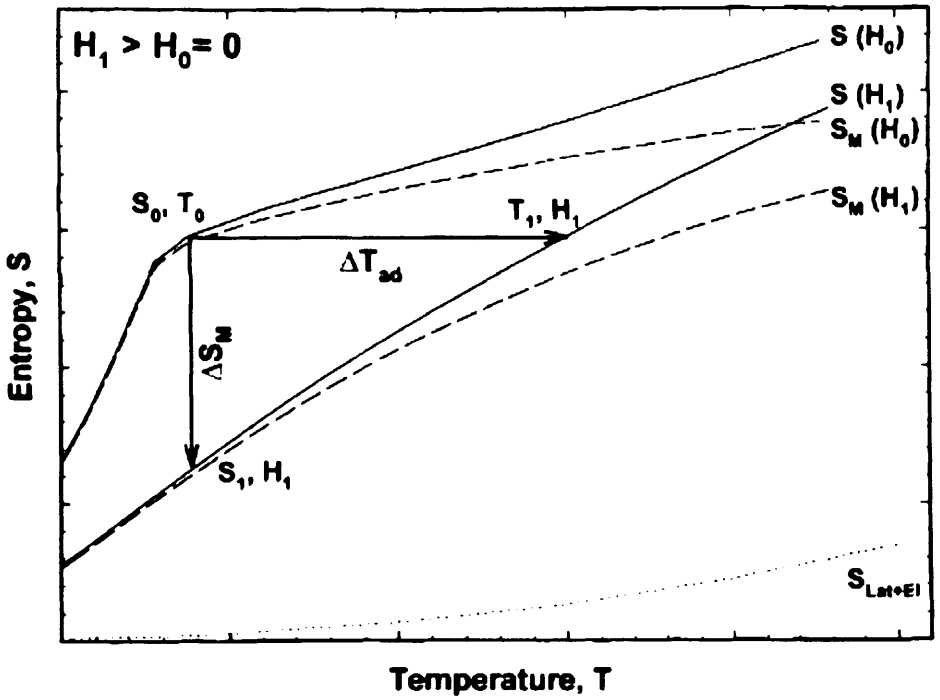

Fig 4.6 S-T curves for two magnetic fields on a magnetic material showing magnetic component in dashed line, lattice and Electronic component in dotted line and total in solid line [19].

The relation between ΔT_{ad}, ΔS_M, magnetisation and magnetic field is given by Maxwell's relations as shown in Eqn. 4.2 [19]:

$$\left(\frac{\partial S(T,H)}{\partial H}\right)_T = \mu_0\left(\frac{\partial M(T,H)}{\partial T}\right)_H \tag{4.2}$$

For an isothermal and isobaric process and integrating the above equation becomes [19]:

$$\Delta S_M(T,\Delta H) = \mu_0 \int_{H_1}^{H_2}\left(\frac{\partial M(T,H)}{\partial T}\right)_H dH \tag{4.3}$$

The infinitesimal temperature change dT for an adiabatic and isobaric process can be given by the equation [19]:

$$dT = -\left(\frac{T}{C(T,H)}\right)_H\left(\frac{\partial M(T,H)}{\partial T}\right)_H dH \tag{4.4}$$

Integrating the above equation we get

$$\Delta T_{ad}(T,\Delta H) = -\int_{H_1}^{H_2}\left(\frac{T}{C(T,H)}\right)_H\left(\frac{\partial M(T,H)}{\partial T}\right)_H dH \qquad (4.5)$$

where ΔT_{ad} is the adiabatic temperature change and C is heat capacity at constant pressure.

4.3.2 Estimation of Magnetocaloric Effect

There are two ways of estimating magnetocaloric effect: the direct and indirect methods. In thedirect method the temperature of the samples is measured directly by a contact or non-contact means. The accuracy of the measurement depends on the thermometry and ability to apply a sudden magnetic field. The insulation of the sample to achieve adiabatic condition is also critical. The accuracies of these measurements have been reported to be 5-10% [15, 20]. With direct method adiabatic temperature change ΔT_{ad} is the only parameter that can be determined. In the indirect method of measuring heat capacity at different applied field we can calculate adiabatic temperature change ΔT_{ad} and entropy change ΔS_M or we can determine entropy change using measurement of isothermal M-H curves which has been described in the following section in detail.

4.3.3 Estimation of Entropy Change Using M-H Curves

Adiabatic entropy change can be calculated from M-H curves using the integrated Maxwell's relation which is shown in Eqn. 4.3 [19]. It can be transformed into a numerical integral form using a numerical method such as the trapezoidal rule as shown below [21, 22].

$$\Delta S_M(T)_{\Delta H} = \mu_0 \frac{\delta H}{2\delta T}\left(\delta M_1 + 2\sum_{k-2}^{n-1}\delta M_K + \delta M_n\right) \qquad (4.6)$$

The above equation gives an adiabatic entropy change for an average temperature change T_{av} which is difference between two isothermal temperatures at which M-H curves are plotted ($T_{av} = (T_u +$

$T_l)/2$) and in a magnetic field change of $\Delta H = H_F - H_I$ where H_F is final field and H_I is initial field. $\delta T = T_u - T_l$, $\delta H = \Delta H/(n-1)$ and $\delta M_k = [M(T_u)_k - M(T_l)_k]$. The resultant adiabatic temperature change ΔS_M can be plotted against temperature for various magnetic field changes. Fig 4.7 shows a plot of ΔS_M vs. temperature for gadolinium metal with an applied field up to 5 Tesla [21].

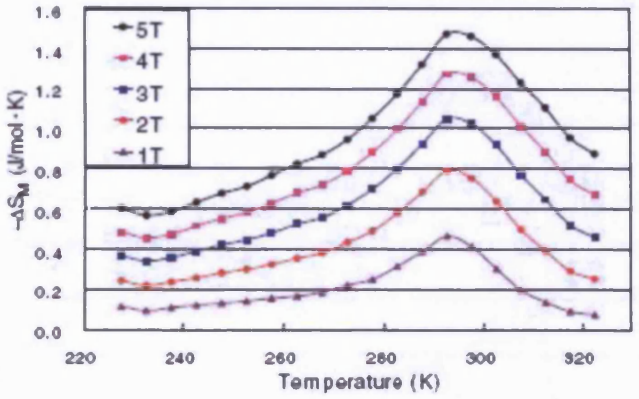

Fig. 4.7 Adiabatic entropy change calculated numerically integrating Maxwell's relation using M vs.H isotherms of a polycrystalline gadolinium sample [21].

4.3.4 Estimation of Isothermal Entropy Change and Adiabatic Temperature Change Using Heat Capacity Data

Isothermal entropy change can be determined by heat capacity measurements using the equations below. Entropy at zero applied field is determined followed by entropy at an applied field H:

$$S(T)_{H=0} = \int_0^T \frac{C(T)_H}{T} dT + S_0 \tag{4.7}$$

$$S(T)_{H\neq 0} = \int_0^T \frac{C(T)_H}{T} dT + S_{0,H} \tag{4.8}$$

where S_0 is entropy at 0 K and S_{0H} is entropy at 0 K and H field. In a condensed system $S_0 = S_{0H}$ [23]. Since we know entropy at any temperature at a given magnetic field $S(T)_H$, both $\Delta S_m(T, \Delta H)$ and $\Delta T_{ada}(T, \Delta H)$ can be determined [24]. Fig 4.8 a) shows heat capacity measurement on a polycrystalline gadolinium sample. It can be seen that there is a sudden jump in the heat capacity at the Curie temperature of the sample at 293 K. Fig 4.8 b) shows the calculated adiabatic temperature change from the heat capacity measurements in the range of 285 to 293 K which is near its Curie Temperature [21].

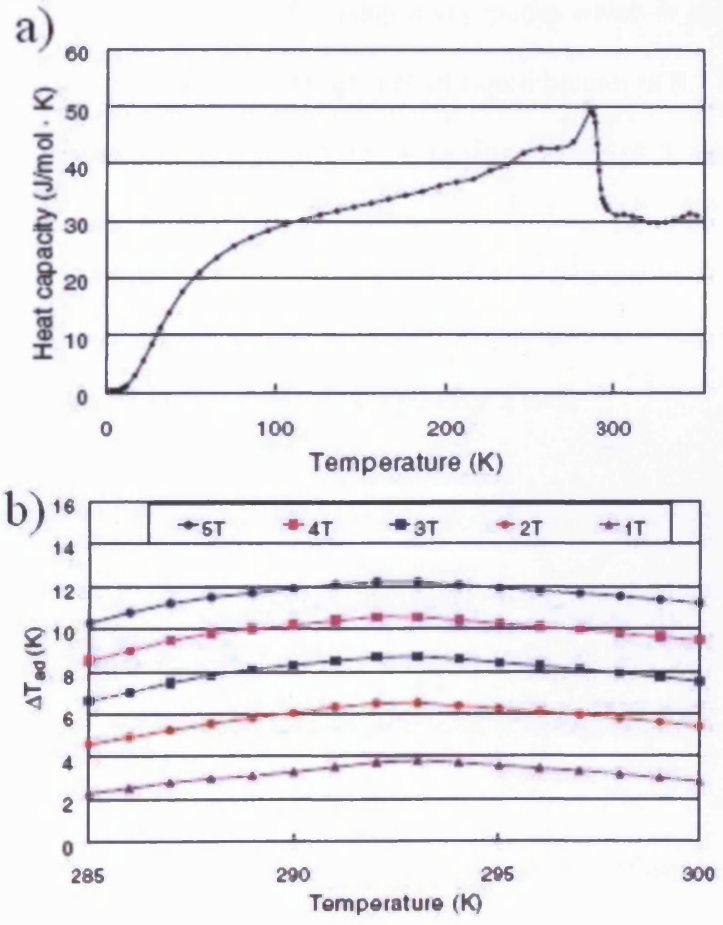

Fig 4.8 a) Heat capacity vs. temperature and b) adiabatic temperature calculated from the heat capacity data of a polycrystalline gadolinium [21].

4.4 Heat Capacity Measurements on PPMS

4.4.1 Overview of PPMS

Physical Properties Measurement System (PPMS) can perform various physical properties measurement such as heat capacity, resistivity, etc. vs. magnetic field and temperature. It is developed by Quantum Design, USA. The PPMS used in the Wolfson Centre for Magnetics has a magnetic field range of 7 Tesla, temperature range of 1.9 to 400 K and vacuum of 10^{-8} Torr can be achieved in the sample chamber which is necessary for heat capacity measurement. Such a high vacuum (10^{-8} Torr) is achieved in the PPMS using a cryopump which is also used in obtaining a temperature of 1.9 K which is below the temperature of liquid helium of 4.2 K. PPMS has 3 active channels though which it can take 3 simultaneous measurements of 3 samples. For a detailed description of the system see reference [25].

4.4.2 Measurement on Standard Heat Capacity Puck

Heat capacity of a material is the amount of heat required to raise the temperature of that material by 1° C. In order to measure the heat capacity, the PPMS inputs a certain amount of heat using the platform heating coil in a high vacuum to avoid all the modes of heat transfer processes. It then measures rise in the temperature of the sample using two platform resistive thermometers. PPMS uses a cryopump to obtain a high vacuum of the order of 10^{-8} Torr. Fig. 4.9 shows the construction of a heat capacity puck. The sample is mounted on a suspended platform in a heat capacity puck using Apiezon grease. The suspension is made of thin wires of platinum gold alloy so that it offers good electrical and poor thermal conduction as shown in Fig. 4.10. It can be noted that the platform is suspended from the printed circuit board which is electrically connected to the pins at the bottom on the puck. The heat capacity puck has a metallic cover to shield the sample from any radiation noise. Heat capacity is measured for the puck alone and the data is saved as addendum data after

which the heat capacity is recorded by mounting the sample on the platform using Apiezon grease. Heat capacity of the sample is calculated by subtracting the addendum data from the total heat capacity data. Heat capacity is measured first for zero field and then for various applied fields. For a detailed description on the measurement technique, see reference [26].

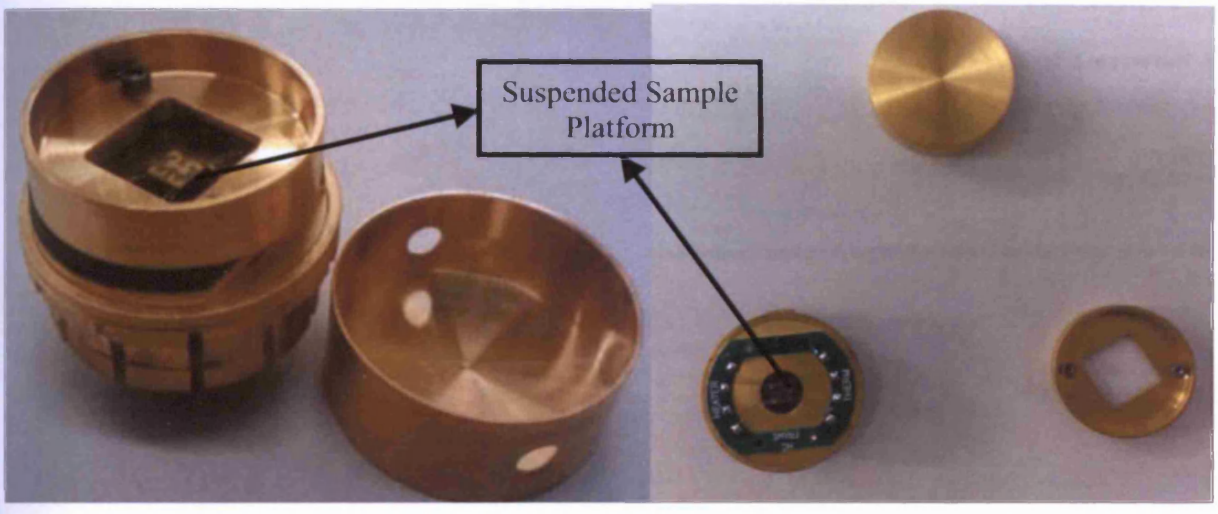

Fig. 4.9 Heat capacity pucks showing a suspended platform and the shield.

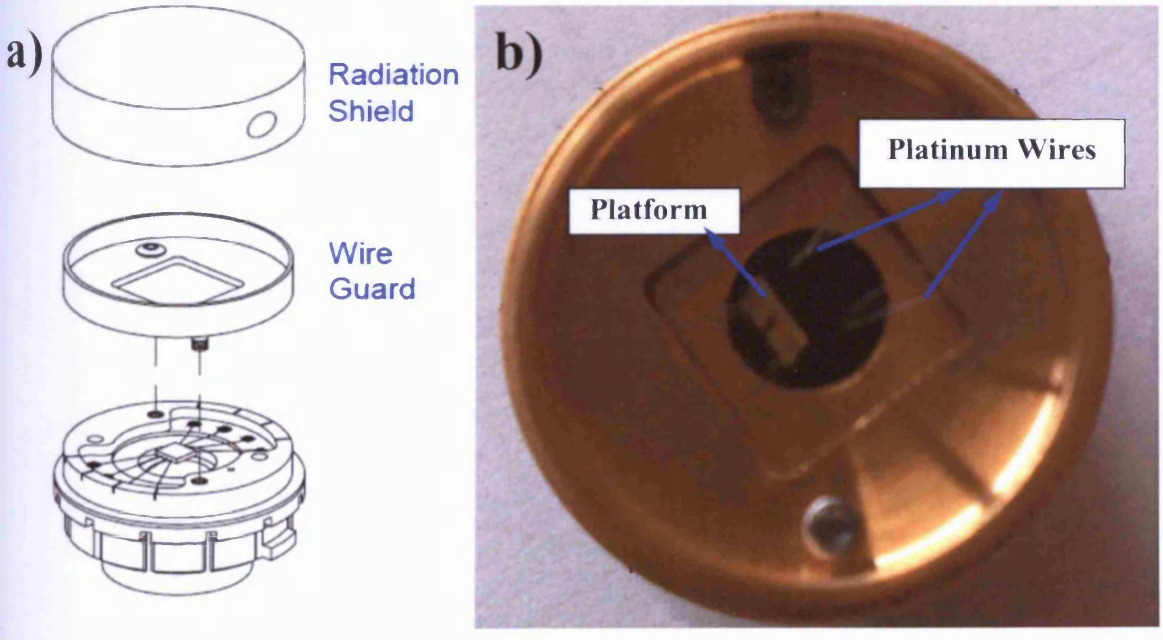

Fig. 4.10 a) Schematic diagram showing assembly of heat capacity puck b) heat capacity puck showing the platform snapped from suspended platinum-gold wires.

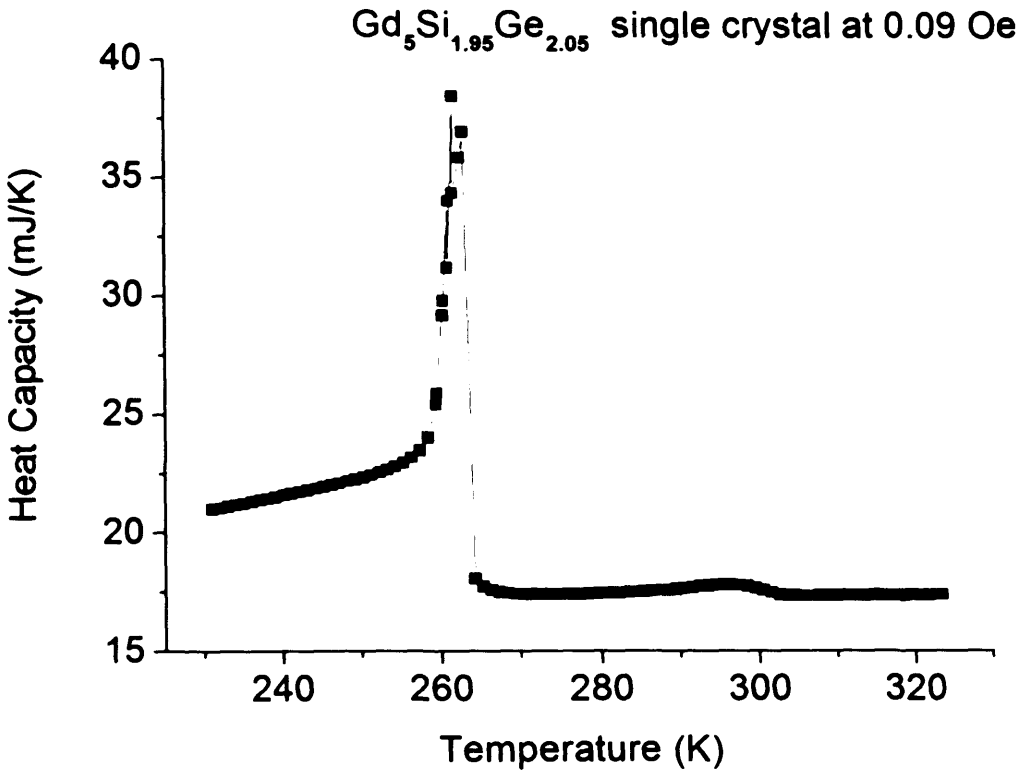

Fig. 4.11 Heat capacity vs. Temperature for a single crystal $Gd_5Si_{1.95}Ge_{2.05}$ sample at an applied magnetic field of 0.09 Oe

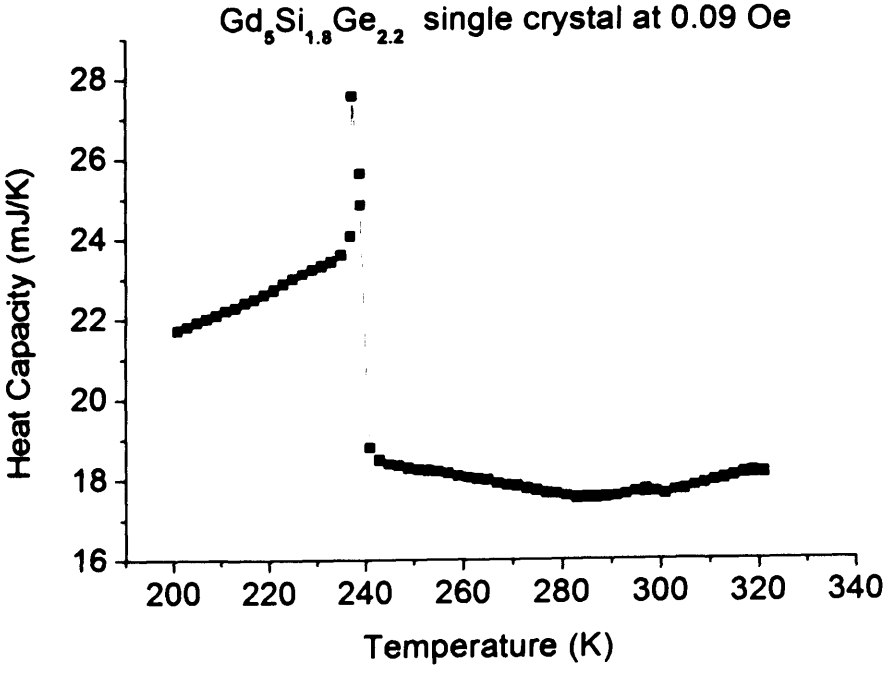

Fig 4.12 Heat capacity as a function of temperature at zero field for single crystal $Gd_5Si_{1.8}Ge_{2.2}$

For more accurate heat capacity data the sample has to be larger so that the measured heat capacity is much larger than the error in the system. To obtain an accurate adiabatic temperature change or isothermal entropy change, the magnetocaloric effect has to be larger which is obtained by applying large magnetic fields [27]. Fig 4.11 and 4.12 shows heat capacity as a function of temperature at an applied magnetic field of 0.09 Oe on a single crystal $Gd_5Si_{1.95}Ge_{2.05}$ (0.475) and $Gd_5Si_{1.8}Ge_{2.2}$ (0.45) respectively. Note that, at the first order phase transition temperature of 263 K there is a sudden change in the heat capacity of the sample. This sudden change increases with increase in the applied magnetic field.

4.4.3 New Design of Heat Capacity Puck

If there is a gradient in the applied magnetic field inside the sample chamber then the sample experiences a force equal to the product of gradient field and magnetic moment of the sample. If the sample is anisotropic and not oriented with its easy axis to the applied magnetic field then the sample experiences a rotational torque whose magnitude is equal to the product of anisotropic field and magnetic moment of the sample. In both the cases the mass/size of the sample and the applied magnetic field play an important role in determining the amount of force exerted by the sample on the suspended platform. For materials with high magnetic moment the mass of the sample needs to be smaller for safe operation of the heat capacity puck for a given magnetic field. Otherwise the exerted force due to the field gradient or due to shape/magnetocrystalline anisotropy can be so large that the platinum-gold wires can break from the printed circuit board and let the sample to drop into the cryostat of PPMS. There is a trade off between the size of the sample, amount of magnetic field and the accuracy of the heat capacity measurements. Since $Gd_5(Si_xGe_{1-x})_4$ posses high magnetic moment and exhibits high anisotropy even at smaller fields, it is extremely difficult to hold the sample stationary on the sample platform and measure heat capacity at high magnetic fields. Measurement of heat capacity of 80 mg of single crystal sample of $Gd_5Si_{1.95}Si_{2.05}$ at high magnetic

fields have resulted in breaking of sample platform. Fig. 4.10 shows a heat capacity puck with snapped off platinum wires due to the large force exertion on the platform. Design of a new improved puck described below was completed only at the end of this project hence the heat capacity measurement at high magnetic fields are not successfully completed.

The maximum mass of the sample that can be placed on the suspended platform at the maximum magnetic field applied can be calculated from the field gradient by equating this force to the ultimate tensile strength of the gold-platinum wire and by taking the maximum possible magnetic moment per gram. It was calculated to be 4 mm cube for a NdFeB sample at an applied field of 9 Tesla [27].

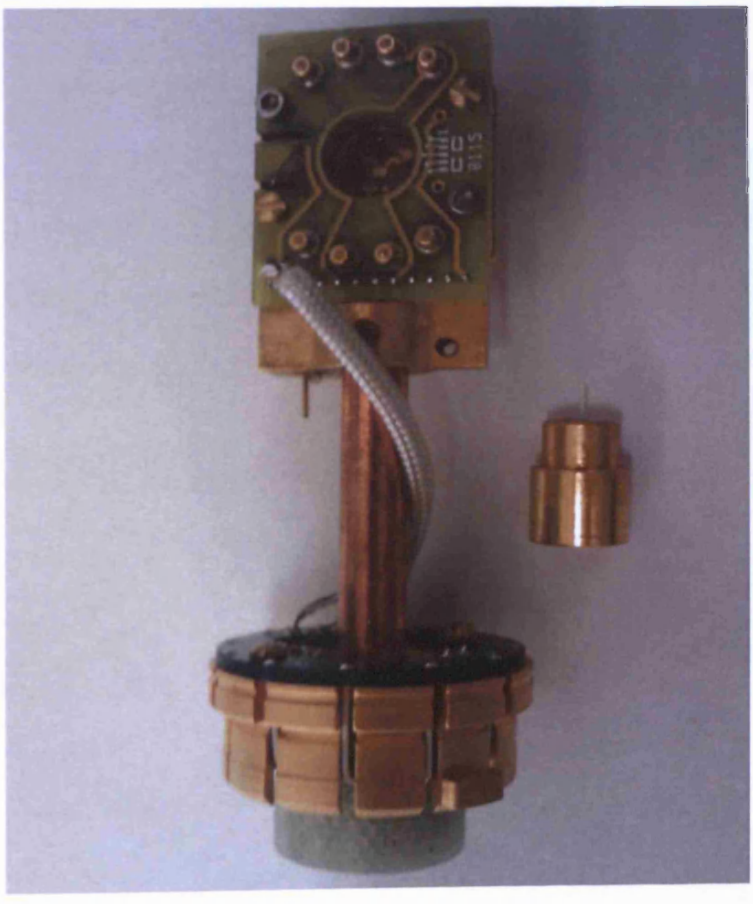

Fig. 4.13 New design of the heat capacity puck taking into account of field gradient and ease with which the sample can be mounted with its easy axis aligned with the field direction.

In order to overcome this problem the heat capacity puck was redesigned such that the field gradient is zero and the sample is supported additionally. Fig. 4.13 shows the new design of the heat capacity puck where the suspended platform has been raised above the puck into more uniform field thus minimising the field gradient. There is also an additional support which covers the top portion of the puck thus shielding any radiation noise and holds the sample in place with the help of a thin non electrical and thermal conducting plastic extension on the cover. This new design of the puck also helps the user to orient the sample's easy axis in the direction of the magnetic field.

4.5 Summary

A detailed literature review of magnetocaloric effect and magnetic refrigeration was carried out. Different designs of magnetic refrigeration and different methods of measuring magnetocaloric effect were discussed. Heat capacity measurements at zero applied magnetic field were carried out on a standard heat capacity puck using PPMS. Problems in the design of heat capacity puck were discussed and the design modification for the puck was recommended.

References

[1] A. M. Tishin and Y. I. Spichkin, "The magnetocaloric effect and its applications", Institute of Physics Publishing, Bristol, pp. 1, 2, (2003).

[2] E. Warburg, Ann. Phys., **13**, pp. 141, (1881).

[3] P. Langevin, Ann. Chem. Phys., **5**, pp. 70, (1905).

[4] P. Debye, Ann. Physik, **81**, pp. 1154, (1926).

[5] W. F. Giauque, J. Amer. Chem. Soc. **49**, pp. 1864, (1927).

[6] Wikipedia, "*Magnetocaloric Effect*", http://en.wikipedia.org/wiki/Magnetic_refrigeration, (16-10-2009).

[7] V. K. Pecharsky and K. A. Gschneidner, Jr., "*Tunable magnetic regenerator alloys with a giant magnetocaloric effect for magnetic refrigeration from ~ 20 to ~ 290 K*", Appl. Phys. Lett., **70**, pp. 3299, (1997).

[8] C.B. Zimm, P.M. Ratzmann, J.A. Barclay, G.F. Green and J.N. Chafe, "*The magnetocaloric effect in neodymium*"Adv. Cryog. Eng. **36**, pp. 763, (1990).

[9] A.O. Pecharsky, V.K. Pecharsky and K.A. Gschneidner, "*The giant magnetocaloric effect of optimally prepared $Gd_5Si_2Ge_2$*", J. Appl. Phys., **93**, pp.4722, (2003).

[10] O. Tegus, E. Bruck ck, K. H. J. Buschow and F. R. de Boer, "*Transition-metal-based magnetic refrigerants for room-temperature applications*", Nature, **415**, pp. 150-152, (2002).

[11] J. Q. Deng, Y. H. Zhuang, J. Q. Li, and K. W. Zhou, "*Magnetic phase transition and magnetocaloric effect in* $(Gd_{1-x}Tb_x)_5Si_{1.72}Ge_{2.28}$ *compounds*," J. Alloys Comp., **428**, pp. 28–33, (2006).

[12] T. Zhang, Y. Chen, Y. Tang, and M. Tu, "*Structural and magnetic characterization of* $Gd_5Si_{3.5-x}Ge_xSn_{0.5}$ *alloys*", J. Alloys Comp., **422**, pp. 25–27, (2006).

[13] X. Zhou, W. Li, H. P. Kunkel and G.Williams, "*A criterion for enhancing the giant magnetocaloric effect: (Ni–Mn–Ga)—a promising new system for magnetic refrigeration*", J. Phys.: Condens. Matter, **16,** pp. 39-44, (2004).

[14] F. Albertini, J. Kamarád, Z. Arnold, L. Pareti, E. Villa and L. Righi, "*Pressure effects on the magnetocaloric properties of Ni-rich and Mn-rich* Ni_2MnGa *alloys*", J. Magn. Magn. Mater., **316**, pp. 364-367, (2007).

[15] K.A. Gschneidner and V.K. Pecharsky, "*Thirty years of near room temperature magnetic cooling: Where we are today and future prospects*", Int. J. Refrig., **31**, pp. 945-961, (2008).

[16] P. Kumar, N. K. Singh, K. G. Suresh, A. K. Nigam, S. K. Malik, "*Heat capacity and magnetocaloric effect in polycrystalline* $Gd_{1-x}Sm_xMn_2Si_2$", J. Magn. Magn. Mater., **319**, pp. 1-4, (2007).

[17] Z.G. Zheng, H.Y. Yu, X.C. Zhong, D.C. Zeng, Z.W. Liu, "*Design and performance study of the active magnetic refrigerator for room-temperature application*", Int. J. Refrig, **32**, pp. 78-86, (2009).

[18] S. J. Lee and D. C. Jiles, "*Geometrical Enhancements to Permanent Magnet Flux Sources: Application to Energy Efficient Magnetocaloric Refrigeration Systems*", IEEE Trans. Magn., **35**, pp. 3105-3107, (2000).

[19] V. K. Pecharsky and K. A. Gschneidner Jr., "*Magnetocaloric effect and magnetic refrigeration*", J. Magn. Magn. Mater., **200**, pp. 44-56, (1999).

[20] S. Yu. Dan'kov, A. M. Tishin, V. K. Pecharsky, K. A. Gschneidner Jr., "*Experimental device for studying the magnetocaloric effect in pulse magnetic fields*", Rev. Sci. Instrum., **68**, pp. 2432-2437, (1997).

[21] J. S. Lee, "*Evaluation of the magnetocaloric effect from magnetisation and heat capacity data*", Phys. Stat. Sol. (b), **241**, pp. 1765-1768, (2004).

[22] V. K. Percharsky and K. A Gschneidner Jr., "*Magnetocaloric effect from indirect measurements, Magnetization and Heat Capacity*", *J. Appl. Phy.*, **86**, pp.566, (1999).

[23] M. W. Zemansky, "*Heat and Thermodynamics*", 6th ed., McGraw-Hill, New York, (1981).

[24] V. K. Pecharsky and K. A. Gschneidner, Jr., "*Magnetic Refrigerator Materials: Properties and Application*", Adv. Cryog. Eng., **42A**, pp. 423 (1996).

[25] Quantum Design, "*PPMS brochure*", pp. 1-8, http://www.qdusa.com/products/ppms.html , retrieved, October 2009.

[26] Quantum Design, "*PPMS-Advanced Heat Capacity with Helium 3*", retrieved, October 2009 http://www.qdusa.com/pdf/brochures/heat.pdf.

[27] N. Dilley, Quantum Design, "Private Email communication", (October 2008).

Chapter 5: Magnetostriction in $Gd_5(Si_xGe_{1-x})_4$

5.1 Introduction

Magnetostriction is a change in the dimension of a magnetic material during the magnetisation process. It is of the order of 10^{-4} to 10^{-6} for steels and it is denoted by λ and measured in parts per million (ppm). It can be measured with various techniques, the most popular being with the resistive strain gauges. Dependence of magnetostriction, λ on the angle between magnetic field and magnetostriction axis in isotropic materials is given by Eqn. 5.1 and Fig. 5.1 [1] shows a plot of magnetostriction, $\Delta l/l$ vs. magnetic field, H.

$$\frac{\Delta l}{l} = e\cos^2\theta \tag{5.1}$$

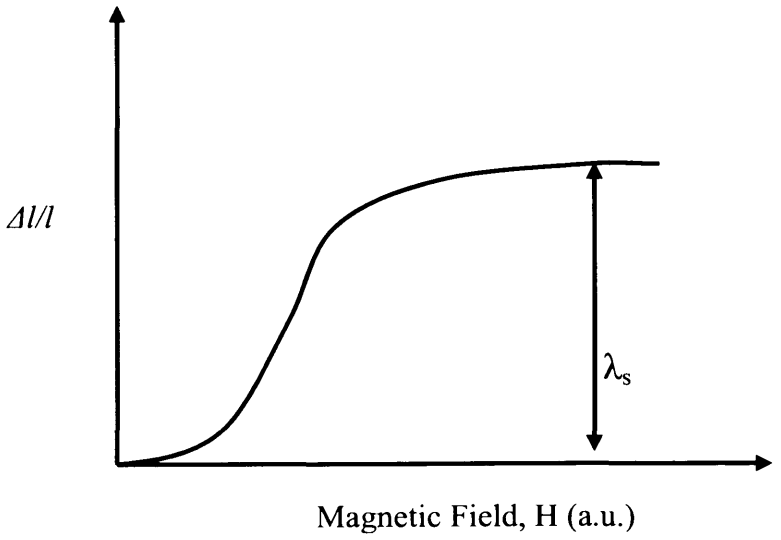

Fig. 5.1 Dependence of magnetostriction, λ on the applied magnetic field, H for positive magnetostrictive materials. Note that saturation magnetostriction λ_s, is at higher magnetic fields.

The change in the dimension of the magnetic material during magnetostriction is due to the alignment of magnetic moments in the domains to the direction of applied magnetic field resulting in increase or decrease of the dimension of the ferromagnetic material as shown in Fig. 5.2 [2].

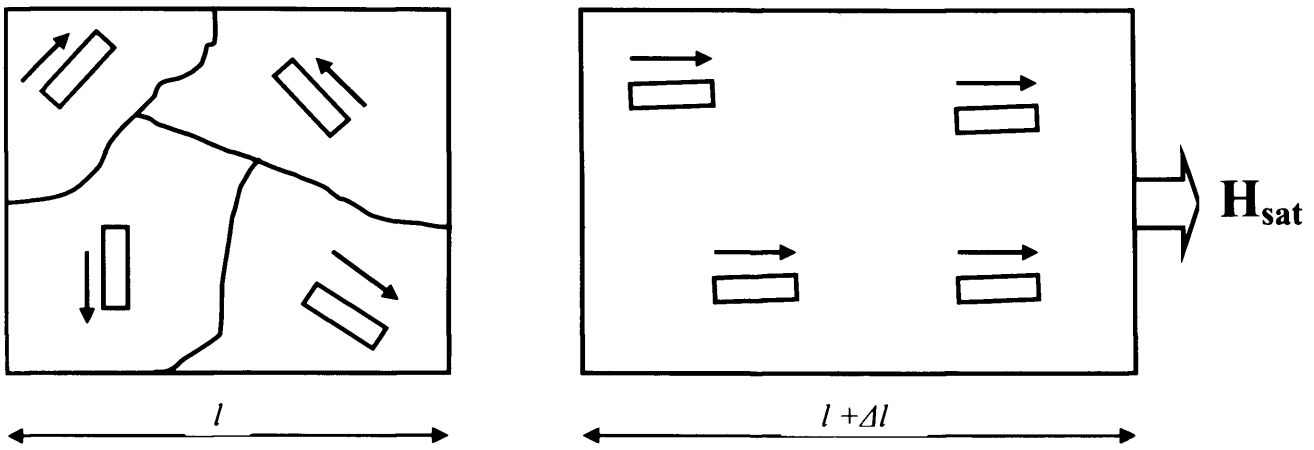

Fig. 5.2 Alignment of magnetic moments in the domains with the direction of magnetic field resulting in change in the dimension of the magnetic material.

Magnetostriction can be classified into two types, spontaneous magnetostriction, λ_0 which is due to the change in the dimension of the material arising from the phase transition from paramagnetic to ferromagnetic phase and saturation magnetisation, λ_s which is due to the change in the dimension of the material arising from magnetising the material to its saturation field. The relation between e, λ_0 and λ_s is given by $e = \lambda_0 + \lambda_s$.

Saturation magnetostriction λ_s in terms of complete magnetostriction is given by

$$\lambda_s = \frac{2}{3}e \text{ and } \lambda_0 = \frac{1}{3}e \tag{5.2}$$

In general magnetostriction is measured along the direction of the applied magnetic field. If the axis of measurement of magnetostriction makes an angle θ with the axis of applied magnetic field, saturation magnetostriction, λ_s can be determined by the Eqn. (5.3) for isotropic materials [2].

$$\lambda_s(\theta) = \frac{3}{2}\lambda_s\left(\cos^2\theta - \frac{1}{3}\right) \tag{5.3}$$

The above equation is not applicable to anisotropic materials. Saturation magnetostriction, λ_s as a function of orientation with the direction of applied field for a simple cubic material can be given by the Eqn. (5.4) [2]

$$\lambda_s = \frac{3}{2}\lambda_{100}\left(\alpha_1^2\beta_1^2 + \alpha_2^2\beta_2^2 + \alpha_3^2\beta_3^2 - \frac{1}{3}\right) + 3\lambda_{111}(\alpha_1\alpha_2\beta_1\beta_2 + \alpha_2\alpha_3\beta_2\beta_3 + \alpha_3\alpha_1\beta_3\beta_1) \quad (5.4)$$

where α_1,α_2 and α_3 are the direction cosines of magnetisation β_1,β_2 and β_3 are the direction cosines of magnetostriction measurement. When the axis of magnetostriction measurement and the axis of applied magnetic field are the same then Eqn. 5.4 reduces to

$$\lambda_s = \lambda_{100} + 3(\lambda_{111} - \lambda_{100})(\alpha_1^2\alpha_2^2 + \alpha_2^2\alpha_3^2 + \alpha_3^2\alpha_1^2) \quad (5.5)$$

where λ_{100} and λ_{111} are magnetostriction values along 100 and 111 directions

For the polycrystalline cubic samples the above equation can be reduced to Eqn. (5.6) [2]

$$\lambda_s = \frac{2}{5}\lambda_{100} + \frac{3}{5}\lambda_{111} \quad (5.6)$$

For orthorhombic, monoclinic and hexagonal crystal lattices Eqn. 5.6 becomes more complicated.

5.2 Magnetostriction in $Gd_5(Si_xGe_{1-x})_4$ Samples

As stated in previous chapters, $Gd_5(Si_xGe_{1-x})_4$ exhibits a colossal magnetostriction or a thermally induced strain close to its first order phase transition temperature. This magnetostriction/thermally induced strain occurs due to the change in volume of the crystal structure from monoclinic to orthorhombic. This colossal magnetostriction/ thermally induced strain can be used in various engineering applications such as sensors and actuators. As a part of this thesis magnetostriction or thermally induced strain has been studied by varying different properties such as applied magnetic field, temperature and composition of the material in the following sections.

5.2.1 Experimental Set-up

Magnetostriction was measured by mounting resistive strain gauges on the sample and measuring the change in the resistance of the strain gauges when the sample was subjected to a magnetic field. The non inductive strain gauges were procured from Vishay Micro-Measurements. These strain gauges were WK-06-031CF-350 series which have a temperature range of 4 K to 565 K. The strain gauge material was made out of a special alloy called 'modified Karma alloy' or 'K-alloy' which has self temperature compensation [3]. Strain gauges were bonded to the sample using M-bond 610 adhesive procured from Vishay Micro-Measurements. A Wheatstone bridge was configured with the 'strain gauge mounted' $Gd_5(Si_xGe_{1-x})_4$ sample, 'strain gauge mounted' copper sample and 2 high tolerance resistances of 350 Ω as four arms of the bridge (Fig. 5.4). The 'strain gauge mounted' copper sample was used as a temperature compensation for the $Gd_5(Si_xGe_{1-x})_4$ sample at temperatures other than room temperature. Two arms of the Wheatstone bridge consisting of 'strain gauge mounted' $Gd_5(Si_xGe_{1-x})_4$ sample and 'strain gauge mounted' copper sample were glued with varnish on a puck with the strain gauge axis aligned normal to the puck plane. The puck is inserted in the cryostat where the required temperature and magnetic field were established. The other two arms of the Wheatstone bridge consisting of two 350 Ω resistors are placed outside the cryostat at room temperature.

5.2.1.1 Strain Gauge Set-up

Strain gauges are bonded to the sample with the M-bond by avoiding any air bubbles being trapped in between the strain gauge and the sample. M-bond 610 is an epoxy resin and it has a wide temperature range of 4 K to 530 K [4]. The bonded samples needed to be cured at 350 K for a minimum of 4 hours for optimal operation of the strain gauges. The strain gauge was aligned to the direction of magnetic field and the active area of the strain gauge was bonded in the middle of the

sample to get the highest magnetostriction. Care was taken to isolate strain gauge leads from shorting with the sample especially when the samples were large.

5.2.1.2 Wheatstone Bridge Set-up

A Wheatstone full bridge was build by connecting two standard resistors of 350 Ω as two arms of the bridge and 'strain gauge mounted' $Gd_5(Si_xGe_{1-x})_4$ sample and copper samples as the other 2 arms of the bridge as shown in Fig. 5.4. The potential difference between point A and point B on the circuit is measured which is directly proportional to the change in the resistance of the strain gauge mounted on the $Gd_5(Si_xGe_{1-x})_4$ sample.

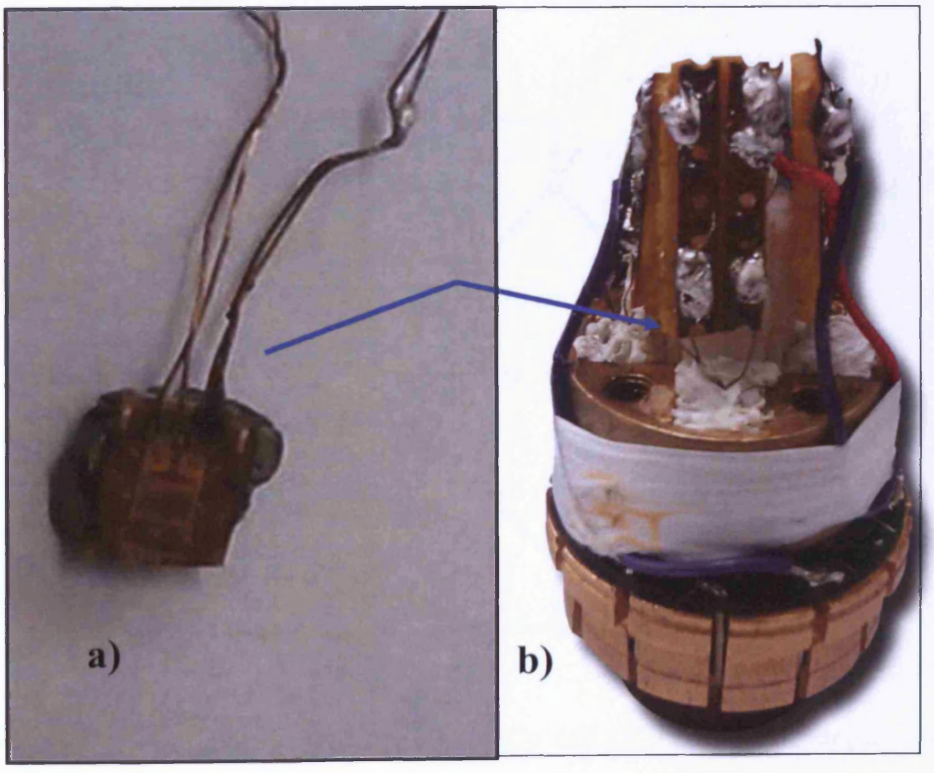

Fig. 5.3 Photograph of a (a) strain gauge bonded onto a polycrystalline $Gd_5Si_{2.09}Ge_{1.91}$ (x=0.52) sample and (b) the puck that connects to the electrical contacts in the PPMS cryostat.

a)

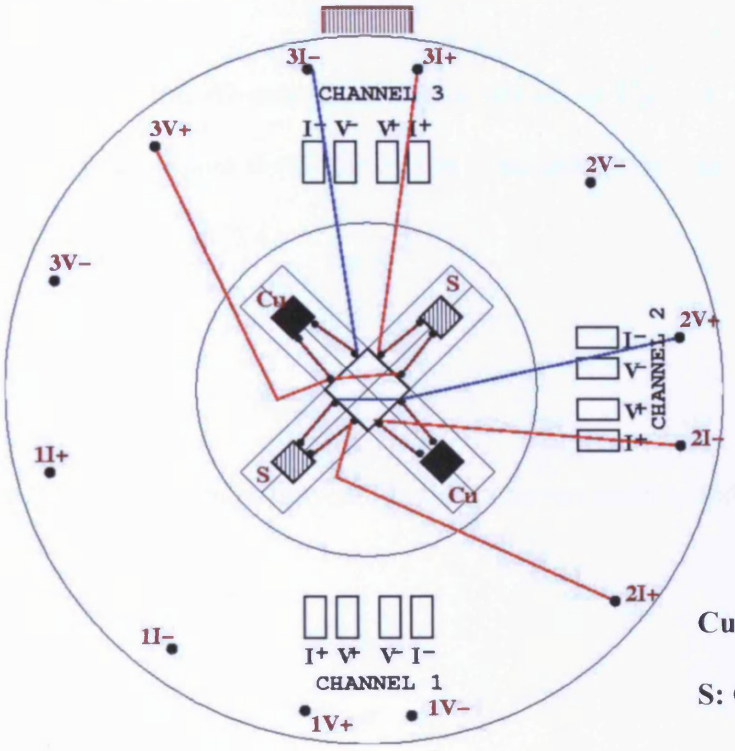

Cu: copper sample

S: $Gd_5(Si_xGe_{1-x})_4$

b)

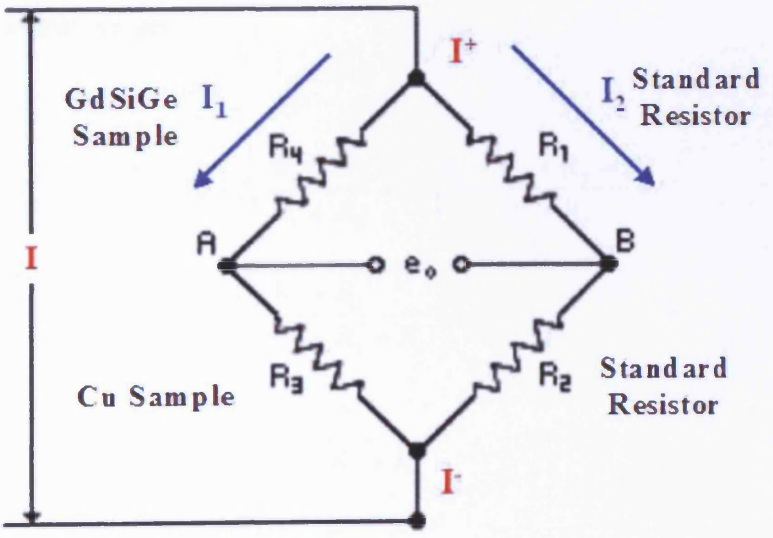

Fig. 5.4 a) Lay out of the puck designed to house Cu and $Gd_5(Si_xGe_{1-x})_4$ samples and electrically connect them to the Wheatstone bridge (drawing by Naresh Ranvah). Wheatstone bridge configuration showing the 'strain gauge mounted' $Gd_5(Si_xGe_{1-x})_4$ and copper sample and the standard resistors.

A constant current is passed to the Wheatstone bridge as shown in Fig. 5.4. PPMS measures the potential difference, e_0 at A and B and divides it by the constant current I to obtain the resistance change in the sample as shown in Eqn. 5.6.

$$R_{PPMS} = \frac{e_0}{I} \tag{5.6}$$

as it can be seen in the Wheatstone bridge current I divides into two parts I_1 and I_2

$$I = I_1 + I_2$$

$$\frac{I_1}{I_2} = \frac{R_1 + R_2}{R_3 + R_4}$$

$$I_2 = I_1 \frac{R_3 + R_4}{R_1 + R_2}$$

substituting I_1 and I_2 in I term we get

$$I = I_1 + I_2 = I_1 + I_1 \frac{R_3 + R_4}{R_1 + R_2} = I_1 \frac{R_1 + R_2 + R_3 + R_4}{R_1 + R_2}$$

hence,
$$I_1 = \frac{R_1 + R_2}{R_1 + R_2 + R_3 + R_4} I \tag{5.7}$$

similarly,
$$I_2 = \frac{R_3 + R_4}{R_1 + R_2 + R_3 + R_4} I \tag{5.8}$$

$$e_0 = E_A - E_B$$

where E_A and E_B are voltages at A and B

$$= I_1 R_4 - I_2 R_1$$

substituting I_1 and I_2 in the equation above

$$e_0 = \left[\frac{(R_1 + R_2)R_4}{R_1 + R_2 + R_3 + R_4} - \frac{(R_3 + R_4)R_1}{R_1 + R_2 + R_3 + R_4} \right] I \tag{5.9}$$

substituting Eqn. 5.9 in Eqn. 5.6, we get:

$$\frac{e_0}{I} = \frac{(R_1 + R_2)R_4 - (R_3 + R_4)R_1}{R_1 + R_2 + R_3 + R_4}$$

$$\frac{e_0}{I} = \frac{R_2R_4 - R_3R_1}{R_1 + R_2 + R_3 + R_4} \tag{5.10}$$

At room temperature resistances of strain gauge on R_3 and R_4 and standard resistances R_1 and R_2 are equal to same value (350 Ω) and therefore e_0=0. When temperature or magnetic field is changed inside the cryostat, resistances R_3 and R_4 will change to $R_3+\Delta R_3$ and $R_4+\Delta R_4$, respectively. Substituting the new values in Eqn. 5.10 we get

$$\frac{e_0}{I} = \frac{R[(R + \Delta R_3) - (R + \Delta R_4)]}{4R + \Delta R_3 + \Delta R_4}$$

$$\frac{R(\Delta R_3 - \Delta R_4)}{4R + \Delta R_3 + \Delta R_4}$$

$$\approx \frac{R(\Delta R_3 - \Delta R_4)}{4R}$$

$$\frac{e_0}{I} = \frac{(\Delta R_3 - \Delta R_4)}{4}$$

$$\frac{e_0}{I} = \frac{(\Delta R_{Copper} - \Delta R_{Gd_5(Si_xGe_{1-x})_4})}{4} \tag{5.11}$$

Since copper is a non-magnetic material, magnetostriction of copper is zero and hence the resistance change of the strain gauge is only due to the temperature change. This is assumed to be equal to the resistance change in the strain gauge mounted on the $Gd_5(Si_xGe_{1-x})_4$ sample due to the

temperature change (coefficient of thermal expansion of copper is considered equal to the coefficient of thermal expansion of $Gd_5(Si_xGe_{1-x})_4$ which is $17x10^{-6}/K$ [5]).

$$(\Delta R_{Gd_5(Si_xGe_{1-x})_4} - \Delta R_{Copper})_{magnetic} = (\Delta R_{Gd_5(Si_xGe_{1-x})_4})_{magnetic}$$

$$\frac{e_0}{I} = \frac{\Delta R_{Gd_5(Si_xGe_{1-x})_4}}{4} \tag{5.12}$$

Since gauge factor of a strain gauge is given by

$$F_G = \frac{\Delta R_{Gd_5(Si_xGe_{1-x})_4}/R}{\varepsilon_{Gd_5(Si_xGe_{1-x})_4}}$$

Substituting the above equation in Eqn. 5.12 we get

$$\varepsilon_{Gd_5(Si_xGe_{1-x})_4} = \frac{e_0}{I} \times \frac{4}{F_G R} \tag{5.13}$$

In our case resistance of the strain gauge R is 350 Ω and gauge factor F_G is 2.02

$$Magnetostriction = PPMS_{output} \times \frac{4}{2.02 \times 350}$$

This formula is used to convert the change in the resistance to the magnetostriction.

5.2.1.3 Physical Properties Measurement System (PPMS) Set-up

PPMS supplied by Quantum Design measures resistance of samples by passing a known constant current, measuring the voltage across the sample and calculating the resistance using V/I formula [6]. The pins have been configured such that PPMS passes the known constant current to Wheatstone bridge at one pair of the arms and measures voltage at the other pair of arms as shown in Fig. 5.4. Magnetic field and temperature changes are established in the cryostat as shown in Fig. 5.5. The cabinet houses temperature controller and power supply for the magnet and other electronics. The measurements are carried out at a low pressure of about 4 torr [6]. A special puck

was built to house 2 pairs of $Gd_5(Si_xGe_{1-x})_4$ samples and 2 copper samples as "dummies" for temperature compensation to enable the PPMS make measurements on 2 samples simultaneously. PPMS has 3 channels for measuring resistance of the samples. Each pair of a $Gd_5(Si_xGe_{1-x})_4$ and copper sample utilise one channel of the PPMS.

Fig. 5.5 Physical Properties Measurement System (PPMS) at Wolfson Centre. Cryostat contains a sample chamber which controls temperature, pressure and magnetic field.

5.2.2 Magnetostriction in Ferromagnetic $Gd_5(Si_xGe_{1-x})_4$

$Gd_5Si_{2.09}Ge_{1.91}$ (x=0.52) exhibits a first order magnetic-structural phase transition at 283 K [7] and it is ferromagnetic at 220 K. Magnetostriction was measured at 220 K on the polycrystalline $Gd_5Si_{2.09}Ge_{1.91}$ (x=0.52) sample and the magnetostriction loops resembled the classical butterfly loops in ferromagnetic materials as shown in Fig. 5.6. The maximum magnetostriction of 65 ppm at an applied field of 3 Tesla (0.23 MA/m) was observed as shown in Fig. 5.6. This saturation magnetostriction is 150 times smaller than the peak strain obtained during the field induced or

temperature induced first order magnetic-structural phase transition of single crystal samples [8], hence these measurements are not carried out by other researchers. It can be seen from the figure that the magnetostriction was not completely saturated at 3 Tesla field. The saturation magnetostriction might be higher than 65 ppm at a field higher than 3 Tesla.

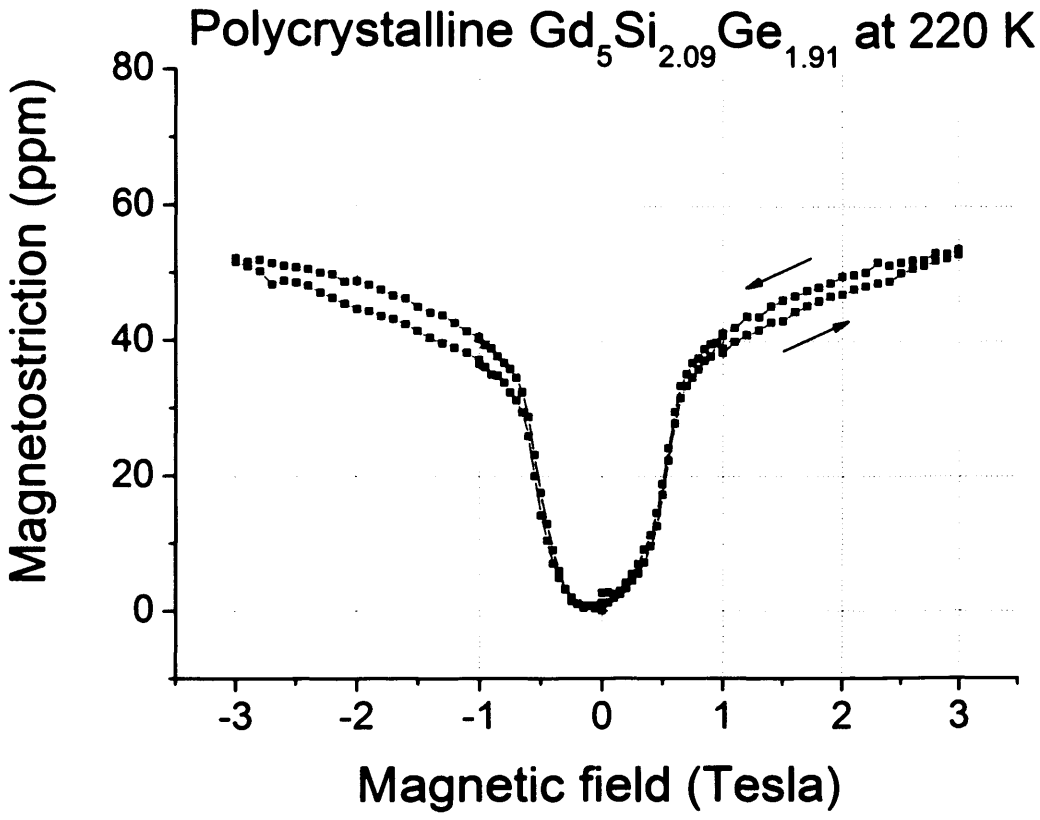

Fig. 5.6 Magnetostriction measurement on a polycrystalline $Gd_5Si_{2.09}Ge_{1.91}$ (x=0.52) at 220 K when the sample is in ferromagnetic phase.

5.2.3 Magnetostriction in $Gd_5(Si_xGe_{1-x})_4$ Due to the First Order Phase Transition

$Gd_5(Si_xGe_{1-x})_4$ has a complex phase diagram shown in Fig. 2.3. It exhibits a field or temperature induced first order phase transition for compositions $0<x<0.57$ [9]. The transition temperature is close to room temperature for the composition $0.31<x<0.57$ [9]. For the composition $0<x<0.31$ [10], the alloy exhibits ferromagnetic, antiferromagnetic and paramagnetic phases at different

temperatures making it a complicated system, hence the magnetostriction measurements are carried out close to $0.31<x<0.57$. Single crystal samples exhibit highest magnetostriction along the 'a' axis which is of the order of 10,000 ppm at the first order phase transition as shown in the Fig. 5.7 in which a single crystal $Gd_5Si_{1.95}Ge_{2.05}$ (x=0.487) sample was used in the measurement [11]. Maximum strain at the first order phase transition that was measured along 'b' and 'c' axis and was of the order of 2000 ppm [12, 13].

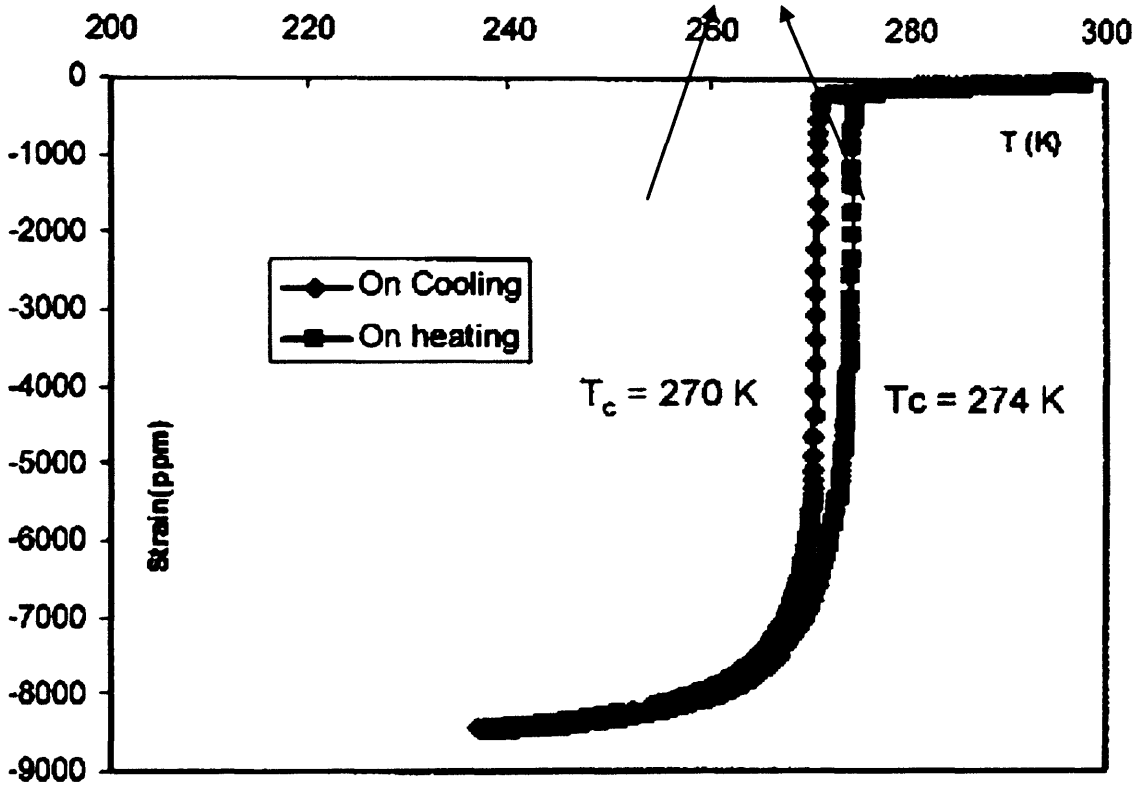

Fig. 5.7 Magnetostriction/thermally induced strain vs. temperature for the single crystal $Gd_5Si_{1.95}Ge_{2.05}$ (x=0.487) sample when the strain was measured on 'a' axis [11].

A single crystal $Gd_5Si_2Ge_2$ (x=0.5) sample was used to measure the strain as a function of temperature on 'ab' plane at an applied field of 0.08 Oe (6.4 A/m). The strain gauge was installed close to the 'a' axis making an angle of about 20°. Strain obtained at the first order phase transition was of the order of 6000 ppm which is less than the highest magnetostriction of 10,000 ppm when

measured exactly on 'a' axis (Fig. 5.8). The same sample was used to measure magnetostriction at various temperatures in the magnetic field range of 0 to 7 Tesla. Fig. 5.9 shows strain vs. magnetic field measurement at temperatures in the range of 285 to 300 K. The field induced first order phase transition was observed for all the isotherms above the transition temperature of $Gd_5Si_2Ge_2$ (x=0.5) sample which is ≈270 K [14, 15, 16]. Magnetostriction exhibited at the field induced first order phase transition decreased with the increase in the transition temperature of the sample. It can be seen from Fig 5.9 that the field required to induce the first order phase transition increases by about 1 Tesla for every 5 K increase in the temperature above the transition temperature. i.e. the field required to induce the first order phase transition for 285 K is 3 Tesla and the field required to induce the first order phase transition at 300 K is 6 Tesla making a rate of ≈5 K/Tesla which is in agreement with the previous observations [17, 18]. Highest magnetostriction measured for 285 K isotherm is higher than the highest magnetostriction measured for the isotherm 300 K.

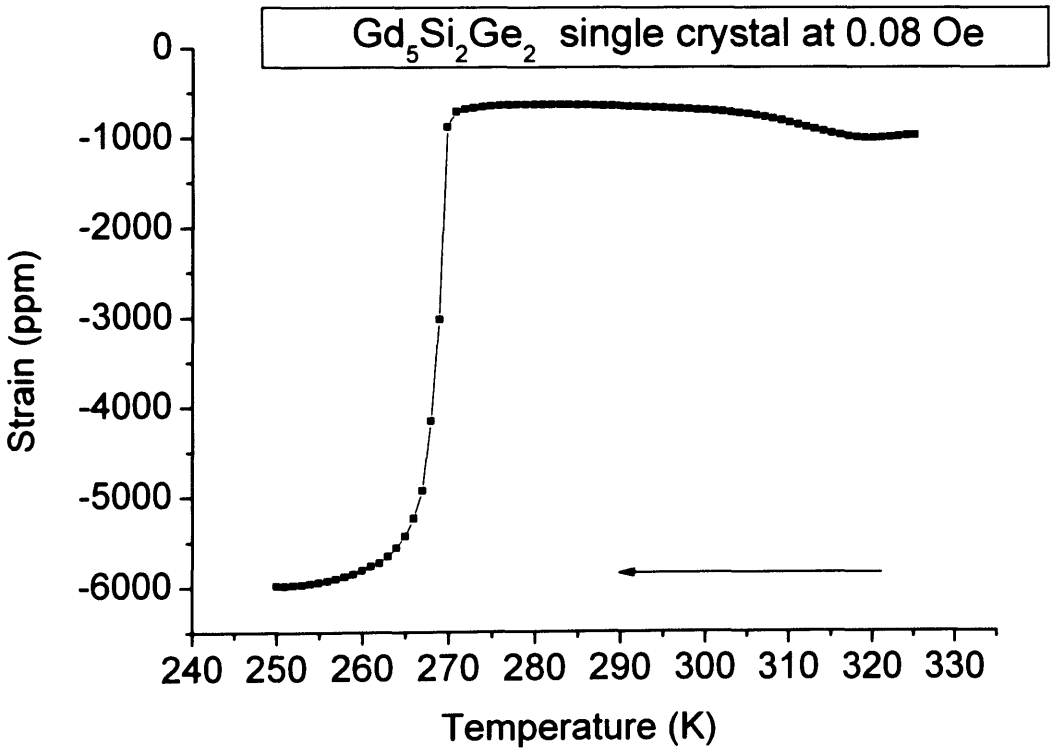

Fig. 5.8 Strain as a function of temperature for a single crystal $Gd_5Si_2Ge_2$ (x=0.5) sample measured at angle of 20° to the 'a' axis with a small applied field of 0.08 Oe (0.6 A/m).

Magnetostriction was also measured for polycrystalline $Gd_5Si_{2.09}Ge_{1.91}$ (x=0.52) sample. It was observed that the highest strain measured for the polycrystalline sample was of the order of 2500 ppm. The strain recorded was negative for both strain vs. temperature and strain vs. magnetic field measurements. These measurements are in agreement with the previous report by Han *et. al.* [19]. Fig. 5.10 shows the first order phase transition at 285 K at which a strain of about 2100 ppm was measured and Fig 5.11 shows the magnetostriction measurement at the field induced first order phase transition for various constant temperatures.

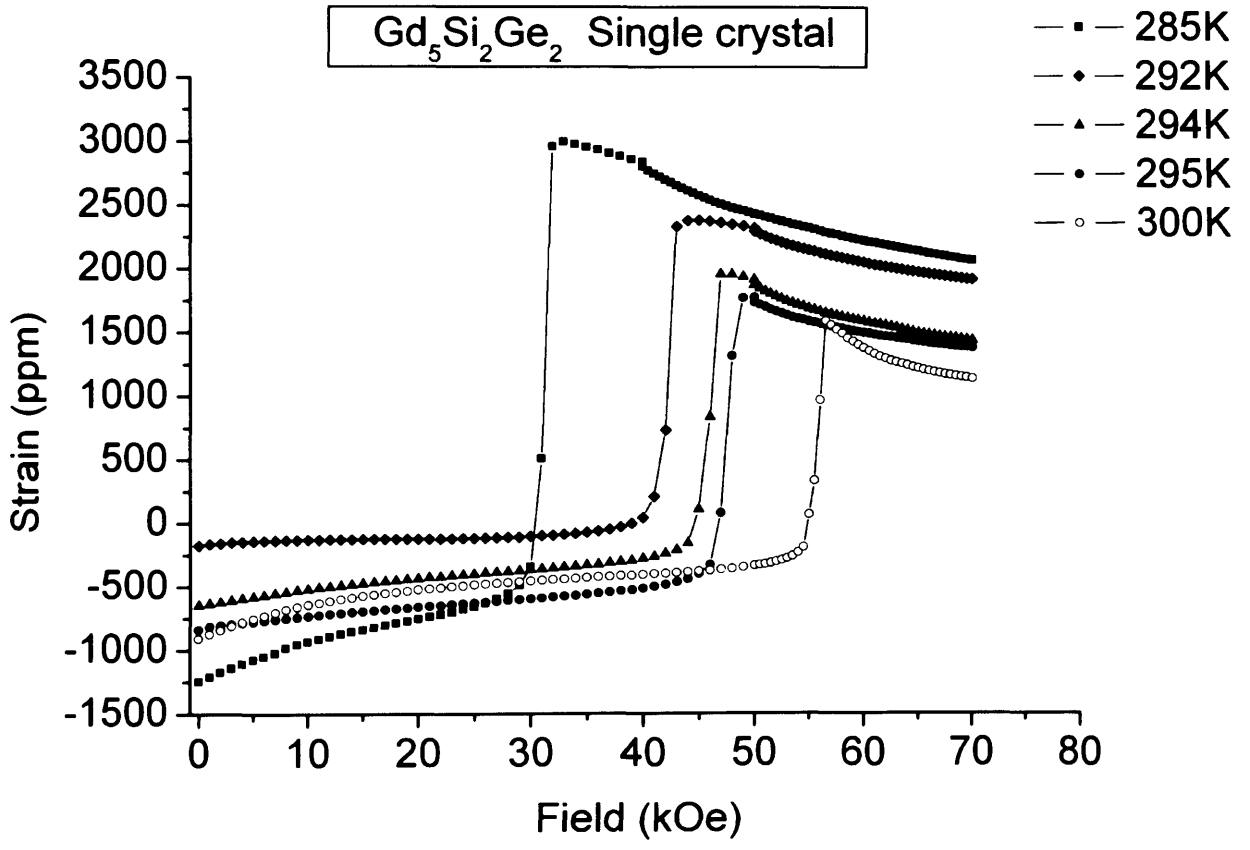

Fig. 5.9 Strain as a function of magnetic field applied for a single crystal $Gd_5Si_2Ge_2$ (x=0.5)sample, measured at angle of 20° to the 'a' axis for various temperatures above the transition temperature of 270 K.

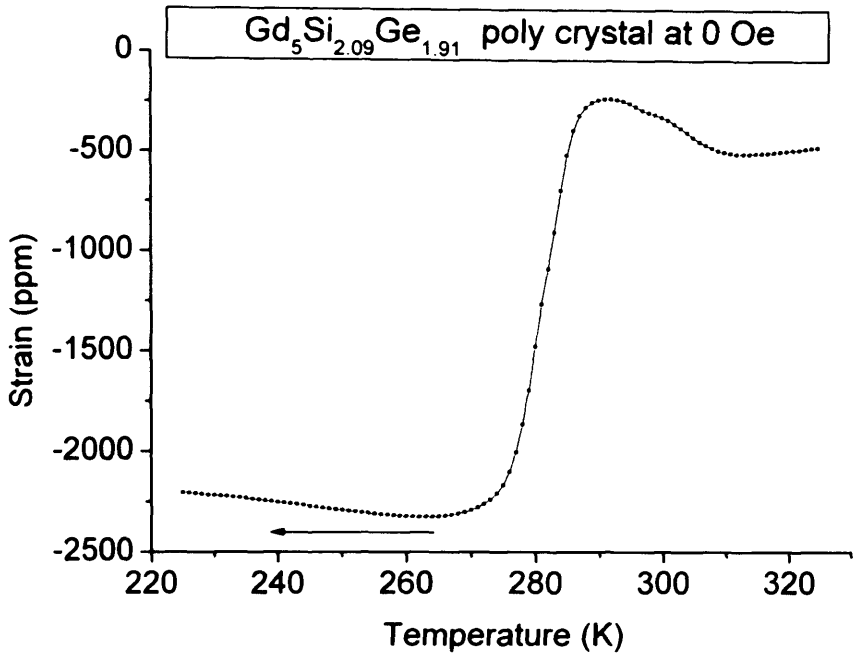

Fig. 5.10 Strain as a function of temperature for a polycrystalline $Gd_5Si_{2.09}Ge_{1.91}$ (x=0.52) sample measured at an applied field of 0 Oe. This composition similar to Fig. 5.11 has a secondary phase which can be seen in the measurement

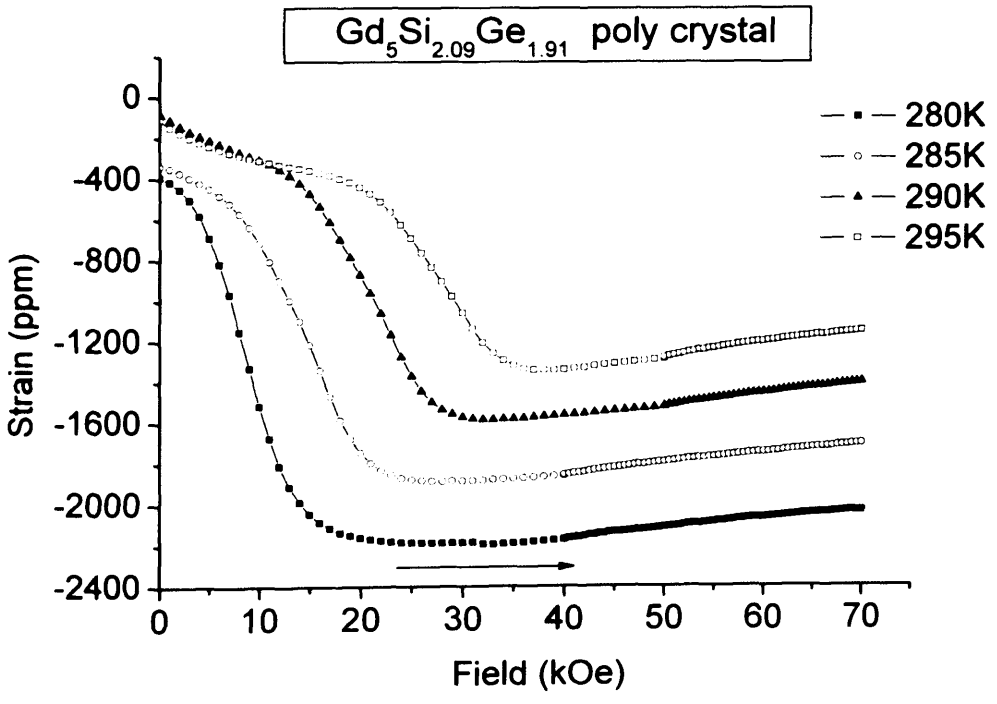

Fig. 5.11 Strain as a function of magnetic field applied for a polycrystalline $Gd_5Si_{2.09}Ge_{1.91}$ (x=0.52) sample measured at various temperatures close to the transition temperature of 285 K.

It can also be seen in Fig. 5.11 that the rate of change of transition field with respect to the isothermal temperature is about 5 K/Tesla. Magnetostriction measured at 280 K is about 2000 ppm and reduces with the isothermal temperature similar to the single crystal $Gd_5Si_2Ge_2$ (x=0.5) sample. The first order phase transition of this composition is 282 K which is close to room temperature of 295 K. By reducing the sample temperature by 10-15 K from room temperature, a giant magnetostriction thermally induced strain can be obtained for the composition $Gd_5Si_{2.09}Ge_{1.91}$(x=0.52).

5.3 Fine Structure Observation in Magnetostriction Measurements of $Gd_5Si_{1.95}Ge_{2.05}$

A series of magnetostrictive strain measurements was carried out as a function of magnetic field strength at different temperatures and as a function of temperature at different magnetic field for single and polycrystalline $Gd_5Si_{1.95}Ge_{2.05}$ (x=0.487) samples. For the first time the observation of fine structure in the variation of strain with magnetic field near the first order phase transition temperature was reported. This fine structure was observed only for the single crystal and polycrystalline samples of $Gd_5Si_{1.95}Ge_{2.05}$ (x=0.487) but not for $Gd_5Si_2Ge_2$ (x=0.5) and $Gd_5Si_{2.09}Ge_{1.91}$ (x=0.52) samples.

5.3.1 Fine Structure Observation in Magnetostriction Measurements of the Single Crystal $Gd_5Si_{1.95}Ge_{2.05}$

Magnetostrictive strain as a function of magnetic field strength was measured using the PPMS (Fig. 5.12) for single crystal $Gd_5Si_{1.95}Ge_{2.05}$ (x=0.487) sample at 275 K, which is below the first order phase transition temperature for this composition. The magnetic field strength was varied

from 0 Oe to 70 kOe (5.6×10^6 A/m), 70 kOe to -70 kOe, -70 kOe to 70 kOe and 70 kOe to 0 kOe. In all these parts of measurements there was a sudden increase in the magnetostrictive strain just before the onset of the first order phase transition. Fig. 5.13 shows the magnetostrictive strain as a

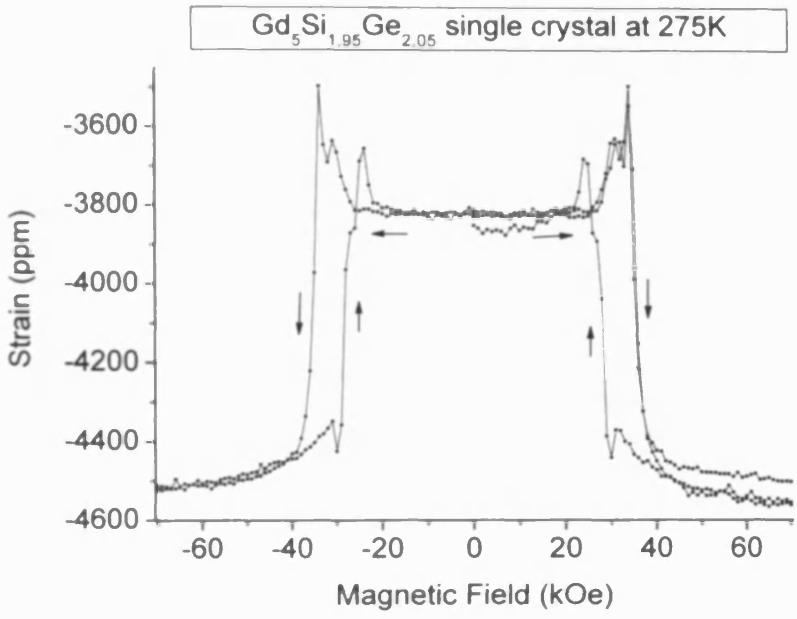

Fig. 5.12 Magnetostrictive strain as a function of magnetic field strength for single crystal $Gd_5Si_{1.95}Ge_{2.05}$ (x=0.487) sample at 275 K showing a sudden increase in the strain near the field induced first order phase transition.

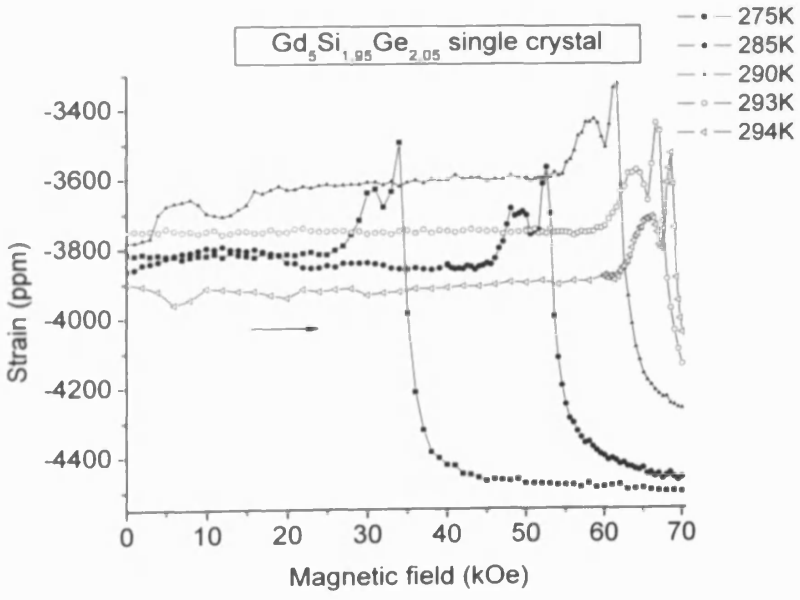

Fig. 5.13. Magnetostrictive strain as a function of magnetic field strength for single crystal $Gd_5Si_{1.95}Ge_{2.05}$ (x=0.487) sample for temperatures ranging from 275 K to 294 K.

function of magnetic field strength for various temperatures for single crystal $Gd_5Si_{1.95}Ge_{2.05}$ (x=0.487) sample above its transition temperature. Note the sudden increase in the magnetostrictive strain of the order of 200-300 ppm just near the field induced first order phase transition temperature. There is a change in the transition temperature of the order of 5-6 K per Tesla of applied magnetic field for the single crystal $Gd_5Si_{1.95}Ge_{2.05}$ (x=0.487) confirming the previous work reported by Han, *et.al* [19]. Fig. 5.14 shows magnetostrictive strain as a function of temperature at a magnetic field strength of 300 Oe for single crystal $Gd_5Si_{1.95}Ge_{2.05}$ (x=0.487). It shows a sudden increase in the strain of the order of 200-300 ppm close to its critical temperature. Both the sudden change and the step change at the transition now have the opposite sign, may be due to the anisotropy of strain change at the transition.

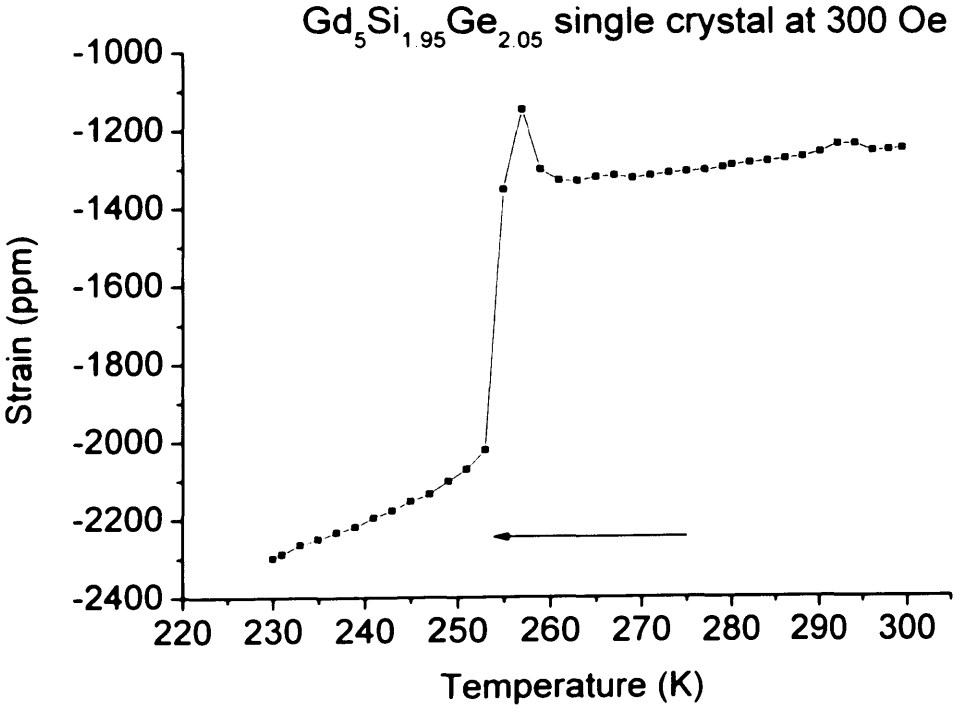

Fig. 5.14 Magnetostrictive strain as a function of temperature for single crystal $Gd_5Si_{1.95}Ge_{2.05}$ (x=0.487) sample with an applied magnetic field of 300 Oe (2.4 kA/m). Note a sudden increase in the strain of the order of 200ppm near the field induced first order phase transition.

5.3.2 Fine Structure Observation in Magnetostriction Measurements of the Polycrystalline $Gd_5Si_{1.95}Ge_{2.05}$

Fig. 5.15 shows magnetostrictive strain as a function of magnetic field strength at various temperatures for a polycrystalline $Gd_5Si_{1.95}Ge_{2.05}$ (x=0.487) sample. For the polycrystalline sample the sudden increase in the strain is of the order of 40 ppm which is not as high as single crystal sample. Fig. 5.8 and Fig. 5.9 show magnetostrictive strain as a function of temperature and as a function of magnetic field strength for different temperatures for a single crystal $Gd_5Si_2Ge_2$ (x=0.5) sample. Fig. 5.10 and Fig. 5.11 show magnetostrictive strain as a function of temperature and as a function of magnetic field strength for different temperatures for a polycrystalline $Gd_5Si_{2.09}Ge_{1.91}$ (x=0.52) sample. It can be seen from Fig. 5.8-5.11 that unlike the $Gd_5Si_{1.95}Ge_{2.05}$ (x=0.487) single crystal (Fig. 5.12, Fig. 5.13 and Fig. 5.14) and polycrystalline sample (Fig. 5.15) in these measurements there is no sudden increase in the strain close to the transition temperature.

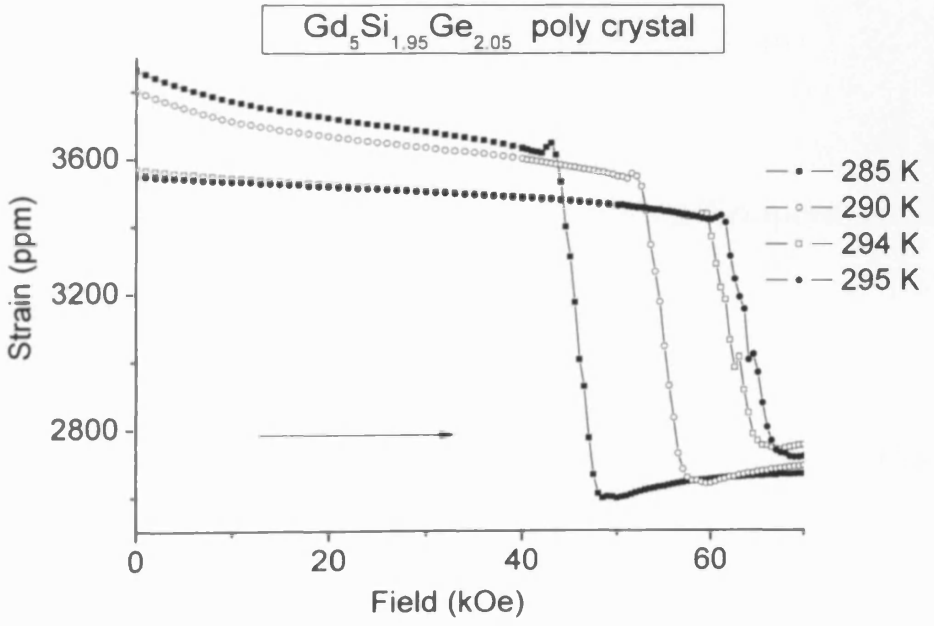

Fig. 5.15 Magnetostrictive strain as a function of magnetic field strength for poly crystal $Gd_5Si_{1.95}Ge_{2.05}$ sample for temperatures ranging from 285 K to 295 K showing a strain change of the order of 40 ppm close to the transition.

Of the four samples measured, the anomaly in the magnetostrictive strain curves was observed only for the composition $Gd_5Si_{1.95}Ge_{2.05}$ (x=0.487) in both single crystal and polycrystalline samples. The anomaly was observed both for magnetostrictive strain versus magnetic field strength and magnetostrictive strain versus temperature measurements, indicating that it is likely not the result of an experimental error in one type of measurement. However this anomaly was not observed when single crystal $Gd_5Si_2Ge_2$ (x=0.5) and polycrystalline $Gd_5Si_{2.09}Ge_{1.91}$ (x=0.522) samples were measured for both kinds of measurements: magnetostrictive strain as a function of magnetic field strength and magnetostrictive strain as a function of temperature using the same measurement equipment. This indicates that there is a fine structure in the magnetostrictive curve for the composition $Gd_5Si_{1.95}Ge_{2.05}$ (x=0.487) near its first order phase transition temperature.

It can be suggested that this fine structure observation in magnetostriction curve for $Gd_5Si_{1.95}Ge_{2.05}$ (x=0.487) sample could be indicative of differences in switching field strengths for different regions of the material which could be due to the presence of two phases.

5.4 Exhibition of Giant Magnetostriction by Varying Temperature Using a Peltier Cell

As mentioned in previous sections that $Gd_5(Si_xGe_{1-x})_4$ exhibits a colossal strain change of the order of 10,000 ppm near its coupled first-order magnetic-structural phase transition. This transition occurs near room temperature for the composition $0.4 \leq x \leq 0.5$. This room temperature colossal strain change can be utilised for both magnetic sensor and actuator applications [20]. Terfenol D is currently the most widely used magnetostriction actuator material as it exhibits 2000 linear and 0 volumetric magnetostriction [21] but $Gd_5(Si_xGe_{1-x})_4$ has potential to be a better actuator material with even larger magnetostriction of 10,000 ppm. There are few attempts reported in the literature

to utilize $Gd_5(Si_xGe_{1-x})_4$ for sensor and actuator applications due to the bulky apparatus required to produce a high magnetic field to induce a first order phase transition and the appearance of eddy currents at higher frequencies [22].

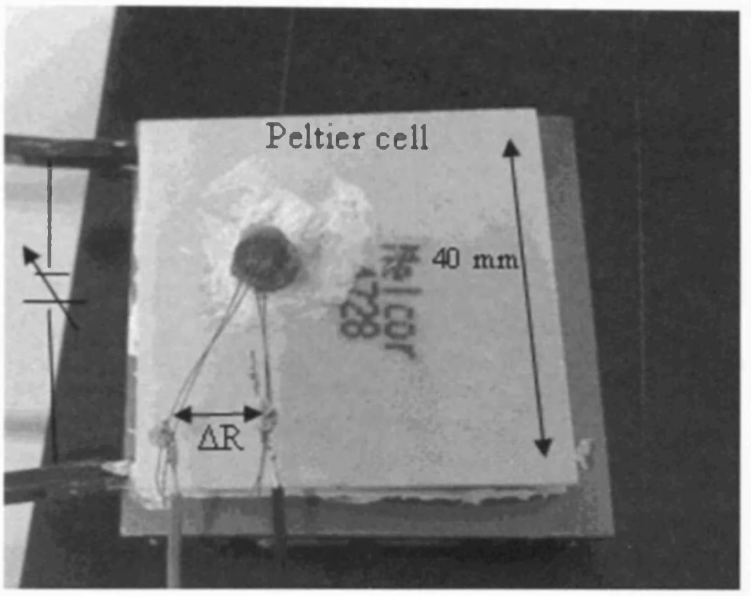

Fig. 5.16 Polycrystalline $Gd_5Si_{2.09}Ge_{1.91}$ sample mounted on the Peltier cell with heat sink compound when the temperature of the sample was reduced it exhibited a strain change of 1813 ppm.

A recent work reported by Nersessian *et.al* [22] overcame the eddy currents by utilising the composite of ball milled $Gd_5Si_2Ge_2$ (x=0.5) particles in a resin matrix but the maximum strain obtained was 1300 ppm. we present for the first time a strain change of the order of 1813 ppm in polycrystalline $Gd_5Si_{2.09}Ge_{1.91}$ (x=0.52) sample obtained by varying the temperature using a Peltier cell.

A strain change of 1813 ppm was achieved in polycrystalline $Gd_5Si_{2.09}Ge_{1.91}$ (x=0.52) sample by varying the temperature of the sample from the room temperature to 268 K using a Peltier cell. A strain gauge was mounted on the polycrystalline sample and allowed to cure for 3 hours at 353 K.

The stain gauge mounted sample was then mounted on a Melcore Peltier cell of dimension 40×40 mm as shown in Fig. 5.16. A heat sink compound was used to mount the sample on the Peltier cell which also acted as a good thermal conductor between the sample and the Peltier cell. A voltage of 5 V and a current of 3.8 A corresponding to 19 W was applied on the Peltier cell to attain a temperature of 268 K from the room temperature. The change in the resistance of the strain gauge was allowed to reach the equilibrium and then was measured using a multimeter. The corresponding strain in the sample was calculated. The resistance change was measured to be 1.3 Ω corresponding to a strain in the sample of 1813 ppm for several measurements on the same sample. The time to attain this strain change varied depending on the environmental conditions ranging from 15 to 30 seconds. This demonstrates a strain change of the order of 1813 ppm at nearly zero field can be achieved in $Gd_5Si_{2.09}Ge_{1.91}$ (x 0.52) using a Peltier cell [23].

5.5 Summary

Fundamentals of magnetostriction were explained and a literature review on magnetostriction in $Gd_5(Si_xGe_{1-x})_4$ was carried out Magnetostriction measurements were carried out on $Gd_5(Si_xGe_{1-x})_4$ for various compositions. Fine structure was observed in the magnetostriction measurement in single crystal and polycrystalline $Gd_5Si_{1.95}Ge_{2.05}$ samples but not on other compositions which might be due to the presence of secondary phase. It was demonstrated that a giant magnetostriction of the order of 1813 ppm could be obtained by varying the temperature using a Peltier cell and removing the requirement of bulky equipment such as Physical Properties Measurement System (PPMS).

References

[1] S. Chikazumi, Physics of Ferromagnetism, Oxford Science Publications, pp.249, (1997)

[2] D.C. Jiles, Introduction to Magnetism and Magnetic Materials, Chapman and Hall, pp. 126, (1998).

[3] Vishya Micro Measurements, "*Strain Gauge Selection: Criteria, Procedures, Recommendations*", Tech Note TN-505-4, pp.50, (2007)

[4] Vishya Micro Measurements, "*Strain Gage Adhesives and Cements*", Document Number: 11009, pp. 2, (2007)

[5] Hyperphysics, "Thermal Coefficient Expansions at 20 C" http://hyperphysics.phy-astr.gsu.edu/hbase/tables/thexp.html#c1, Retrieved , April 2010.

[6] Quantum Design, "*Hardware and Options Manual*", Resistivity Option User Manual, Part Number 1076-100A, pp.1-2, (2005)

[7] R. L. Hadimani, Y. Melikhov, J. E. Snyder, D. C. Jiles, "*Fine structure observation in magnetostriction near the critical temperature in* $Gd_5Si_{1.95}Ge_{2.05}$", International Magnetic Conference (INTERMAG), Madrid, Spain, **HG-11**, (2008)

[8] L. Morellon, J. Blasco, P. A. Algarabel, and M. R. Ibarra, "*Nature of the first-order antiferromagnetic-ferromagnetic transition in the Ge-rich magnetocaloric compounds* $Gd_5(Si_xGe_{1-x})_4$", Phys. Rev. B, **62**, pp. 1022-1026, (2000)

[9] V. K. Pecharsky and K. A. Gschneidner, Jr., "*$Gd_5(Si_xGe_{1-x})_4$: An Extremum Material*", Adv. Mater., **13**, pp. 683-686, (2001)

[10] A. O. Pecharsky, K. A. Gschneidner, Jr., V. K. Pecharsky and C. E. Schindler, "*The room temperature metastable/stable phase relationships in the pseudo-binary Gd_5Si_4–Gd_5Ge_4 system*" , J. Alloys. Comp., **338**, pp. 126-135, (2002)

[11] M. Han, "*Critical behavior of thermal expansion and magnetostriction in the vicinity of the first order transition at the Curie point of $Gd_5(Si_xGe_{1-x})_4$*" PhD Thesis, Iowa State University, Ames, U.S.A., pp. 91-115, (2004).

[12] L. Morellon, P.A. Algarabel, M. R. Ibarra, J. Blasco and B.Garcia-Landa, "*Magnetic-field-induced structural phase transition in $Gd_5(Si_{1.8}Ge_{2.2})$* ", Phys. Rev. B, **58**, pp.R14 721-R14724, (1998).

[13] M. Han, D. C. Jiles, J. E. Snyder, T. A. Lograsso, and D. L. Schlagel, "*Giant magnetostriction behaviour at the Curie temperature of single crystal $Gd_5(Si_{0.5}Ge_{0.5})_4$*", J. App. Phys, **95**, pp. 6945-6947, (2004).

[14] A. O. Pecharsky, K. A. Gschneidner, Jr. and V. K. Pecharsky, "*The giant magnetocaloric effect of optimally prepared $Gd_5Si_2Ge_2$*", J. App. Phys., **93**, pp. 4722-4728, (2003)

[15] B. Podmiljšak, I. Škulj, B. Markoli, P.J. McGuiness, S. Kobe, "*Microstructural changes in Fe-doped $Gd_5Si_2Ge_2$*", J. Magn. Magn. Mater, **321**, pp. 300-304, (2008)

[16] B. Podmiljšak, I. Škulj, B. Markoli, P.J. McGuiness, S. Kobe, "*Microstructural Changes and Hysteresis Losses in Fe-Doped $Gd_5Si_2Ge_2$*" IEEE Trans. Magn., **44**, pp. 4529-4532, (2008)

[17] M. Han, J. A. Paulsen, J. E. Snyder, D. C. Jiles, T. A. Lograsso, and D. L. Schlagel, "*Thermal Expansion of Single-Crystal $Gd_5(Si_{1.95}Ge_{2.05})$ Showing Unusual First-Order Transformation*", IEEE Trans. Magn., **38**, pp. 3252-3254, (2002)

[18] L. Morellon, J. Stankiewicz, B. García-Landa, P. A. Algarabel, and M. R. Ibarra, "*Giant magnetoresistance near the magnetostructural transition in $Gd_5.Si_{1.8}Ge_{2.2}$*", App. Phys. Lett., **73**, pp. 3462-3464, (1998)

[19] M. Han, D. C. Jiles, J. E. Snyder, C.C. H. Lo, J. S. Leib, J. A. Paulsen, and A. O. Pecharsky, "*Thermal expansion studies on the unusual first order transition of $Gd_5Si_{2.09}Ge_{1.91}$: effects of purity of Gd*", J. App. Phys, **93**, pp. 8486-8488, (2003)

[20] D. C. Jiles and C. C. H. Lo, "*The role of new materials in the development of magnetic sensors and actuators*", Sens. Act. A, **106**, pp. 3-7, (2003)

[21] A. E. Clark, in *Handbook on the Physics and Chemistry of Rare Earths*, edited by K. A. Gschneidner, Jr. and L. R. Eyring, North-Holland, Amsterdam, Vol. 2, Chap. 15, (1979)

[22] N. Nersessian, S. Wing Or, G. P. Carman, S. K. McCall, W. Choe, H. B. Radousky, Mike W. McElfresh, V. K. Pecharsky and A. O. Pecharsky "*$Gd_5Si_2Ge_2$ composite for magnetostrictive actuator applications*", App. Phys. Lett., **84** , pp.4801-4803, (2004)

[23] R. L. Hadimani, P. A. Bartlett, Y. Melikhov, J. E. Snyder, D. C. Jiles, "*Field and temperature induced colossal strain in Gd5(SixGe1-x)4*", J. Magn. Magn. Mater, Submitted, (2009)

Chapter 6: Magnetoresistance in $Gd_5(Si_xGe_{1-x})_4$

6.1 Introduction

The effect of change in the resistance of a material due to the application of a magnetic field is called magnetoresistance. This change in resistance is usually small (≈1-2%) for most of the materials and considerably large for strong ferromagnetic materials such as nickel, iron and rare earth materials with layered structuring. Resistance of most of the materials increases when the magnetic field is applied perpendicular to the direction of the electric current. The amount of increase in the resistivity of the material due to the application of magnetic field is in some simplified cases given by Eqn.6.1 [1].

$$\rho_{mag} = \rho_0 \frac{e^2 B^2}{m^2} \tau \tag{6.1}$$

where τ is the mean free time of the collision between the electrons, e is charge of the electron, B is magnetic induction and m is magnetic moment of an electron.

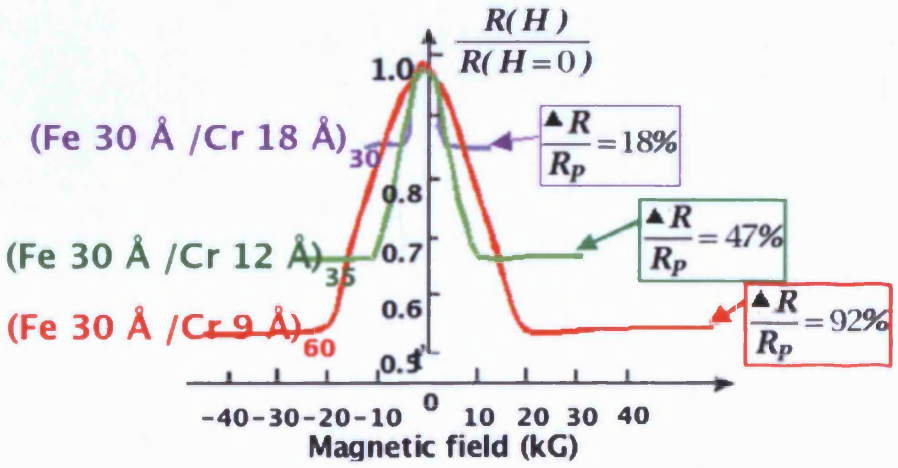

Fig 6.1 Giant magnetoresistance in iron and chromium thin films stacked together [2, 3, 4] which is due to the spin dependent scattering phenomenon unlike in $Gd_5(Si_xGe_{1-x})_4$ system

In thin films and multi layers the magnetoresistance can be larger. For example constructing multilayer of magnetic materials separated by a non magnetic material and controlling the direction

of magnetisation of these magnetic layers individually can be used in building a "spin valve". This device shows a large change in the resistance when a magnetic field is applied and can switch from high resistance state to low resistance state. Disc drive read heads use this concept to sense the magnetisation in the discs in the form of data. Fig. 6.1 shows the so called giant magnetoresistance effect in iron and chromium layers stacked together.

Large changes in the resistivity can also be observed in some bulk magnetic materials at the phase transition. The giant magnetoresistance in iron and chromium multilayered thin films structure is due to the spin dependent scattering phenomenon unlike in $Gd_5(Si_xGe_{1-x})_4$ system. The resistivity of the $Gd_5(Si_xGe_{1-x})_4$ material is higher in the paramagnetic/monoclinic state and is lower when the material undergoes the first order phase transition to the orthorhombic/ferromagnetic state at lower temperatures for the composition $0.41<x<0.52$ [5]. The strain induced in the sample due to the first order phase transition is large, of the order of 10,000 ppm (1%) [6] which can also induce various defects such as dislocations [7] and in extreme cases micro-cracks [8, 9,10]. The strain induced dislocations and micro-cracks as obstacles in the path of the electron movement in the material which increase the resistivity of the samples irreversibly [11, 12]. This effect can be observed in various measurements on both polycrystalline and single crystal samples. The irreversible increase in the resistivity is linear with the number of thermal cycles through the first order phase transition.

However when kept at room temperature over a long period of time of few years the sample showed a recovery (decrease) in the irreversibly increased resistivity [13]. We predict that the recovery in the resistivity occurs when the dislocations that are trapped in the local energy minima escape from them. When these escaped dislocations meet opposite vector dislocations they annihilate resulting in the decrease in dislocation density thus reducing the scattering of electrons and hence the resistivity of the sample. A model based on the above theory was developed using Matthiessen's rule and a modified Arrhenius equation. This model was experimentally verified by thermally

cycling a single crystal $Gd_5Si_{1.5}Ge_{2.5}$ (x=0.375) and polycrystalline $Gd_5Si_{2.09}Ge_{1.91}$ (x=0.52) samples several times and then holding them at higher temperature in-situ over a period of few days instead of years. Resistivity recovery was observed and measured and the parameters were extracted by solving the model equations which were then used to calculate the recovery time for different holding temperatures.

6.2 Resistivity Measurements

As discussed in the previous chapters $Gd_5(Si_xGe_{1-x})_4$ exhibits a giant magnetoresistance close the first order phase transition temperature. This resistance change in the material at the phase transition close to room temperature can be used for sensors or actuators hence, it is important to study the magnetoresistance behaviour of this material for various compositions, temperatures and applied magnetic fields.

6.2.1 Experimental Details

All the measurements were carried out in a Quantum Design Physical Properties Measurement System (PPMS). Fig.6.2. shows the schematic diagram of the connections for resistance measurements and Fig.6.3 shows the photograph of a polycrystalline $Gd_5Si_{2.09}Ge_{1.91}$ (x=0.52) mounted on the puck which goes into the PPMS. The connections on the sample are in a 4 point "inline" configuration as shown in Fig.6.3. Connectors were attached to the disc using conducting glue called "silverdag" whose maximum serviceable temperature is 105° C [14]. The conducting glue was cured for 2-3 hours at room temperature.

6.2.2 Four Point Inline Method

Four point inline method is widely used method for its simplicity and ease with which resistivity can be measured. A constant current was applied at the end pair of connectors and the voltage was

measured at the inner pair of connectors. This method was chosen to keep the measurement technique consistent with the other groups that have carried out resistivity measurements [8-12]. Resistance was calculated from the measured voltage and the known constant current. Resistivity was then measured using Eqn. (6.2).

$$R = \frac{V}{I}; \qquad \rho = \frac{R \times Area}{Length} \tag{6.2}$$

The above procedure was repeated again with reverse polarity and the average of the 2 resistivity is calculated to avoid any thermoelectric voltages produced during the measurement. This widely used technique to remove thermoelectric voltages while measuring resistivity.

A nickel sample with a dimension of 5mm×5mm×5mm was measured using the 4 point inline method and the resistivity at 300 K was determined to be 9×10^{-8} Ωm. The temperature coefficient of resistance in the range of 290-310 K was determined to be 5×10^{-3} K^{-1}. These results were in agreement with the literature values [15].

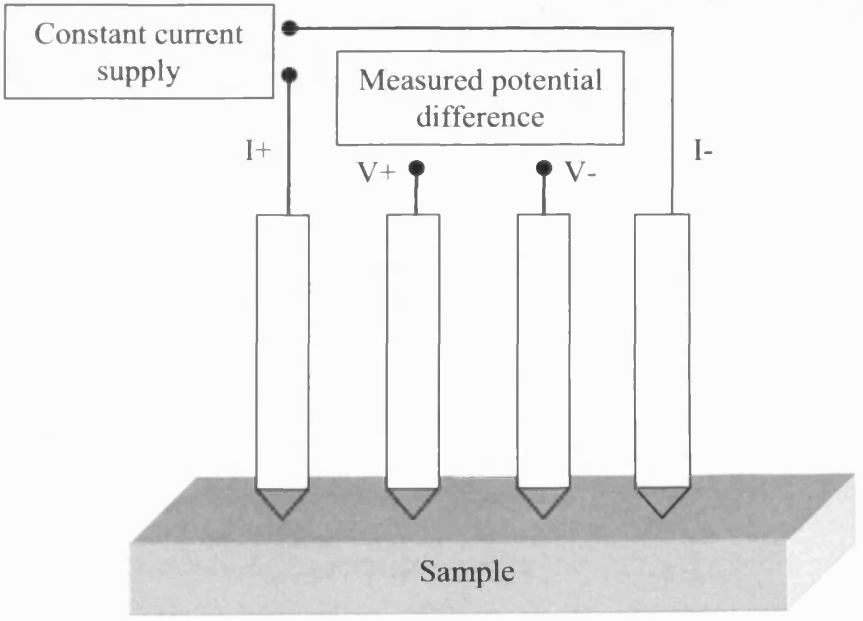

Fig. 6.2 Inline Four Point Method

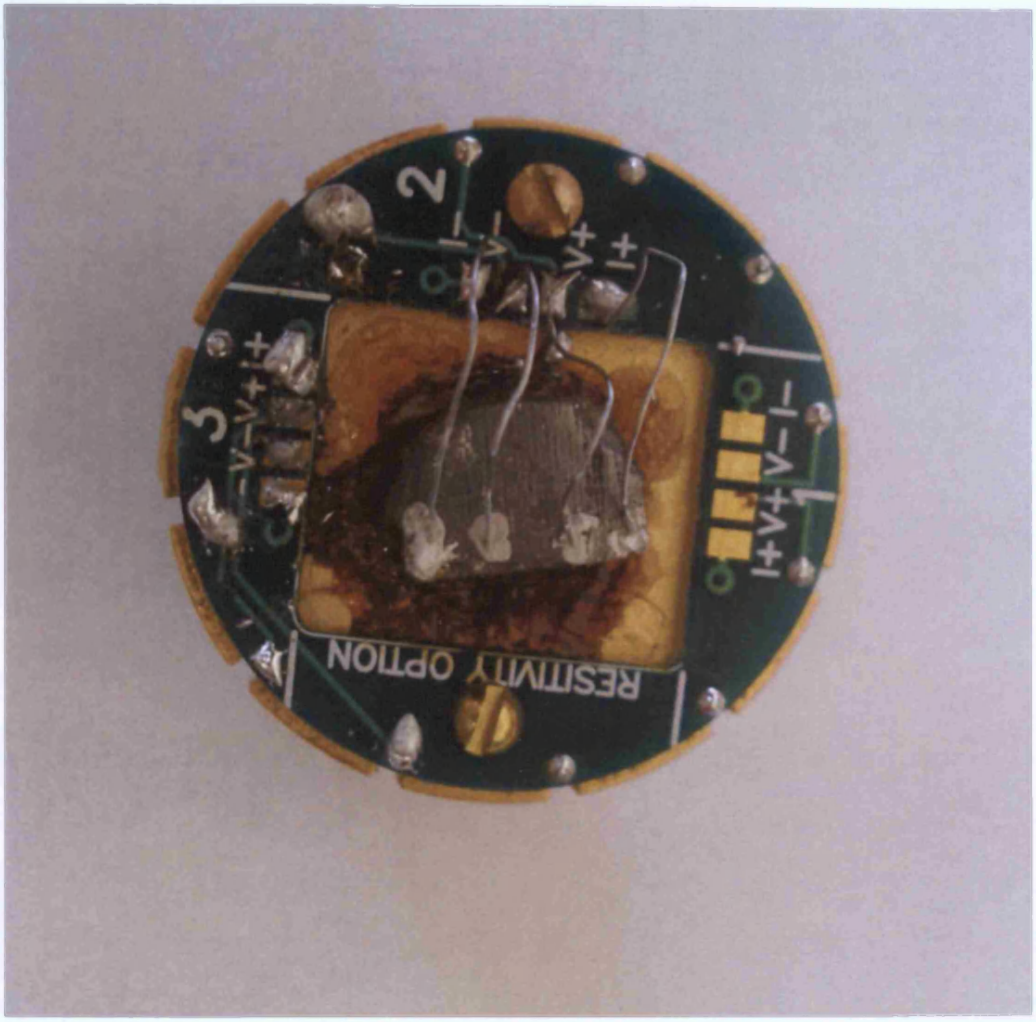

Fig.6.3 Photographic image of polycrystalline $Gd_5Si_{2.09}Ge_{1.91}$ mounted on the puck.

6.2.4 Resistivity vs. Temperature Measurements Showing Irreversible Resistivity

Fig.6.4 shows the resistivity as a function of temperature measurement on a single crystal $Gd_5Si_{1.8}Ge_{2.2}$ (x=0.45) sample at 0 applied magnetic field. The sample was cut in the form of a disc with 'b' axis of the crystal structure as the principal axis of the disc and having dimensions of 5mm diameter and 2.5mm thickness. There is a sudden change in the resistivity of the sample at 240 K. This is the first order magnetic-structural phase transition temperature at which the high

temperature paramagnetic monoclinic phase transforms into the low temperature ferromagnetic orthorhombic phase. This is in agreement with the measured variation in magnetic moment as function of temperature shown in Fig.6.4 inset. The sudden change in the resistivity for both cooling and heating curve is always increasing and is irreversible. The abrupt change in the resistivity is similar to magnetic moment vs. temperature measurement.

Fig. 6.5 shows resistivity as a function of temperature measurement for a polycrystalline $Gd_5Si_{2.09}Ge_{1.91}$ (x=0.52) sample at 0 applied magnetic field. The sample was cut with dimensions of 5mm×3.5mm×3mm. There is a sudden change in the resistivity at the first order phase transition temperature of 283 K. The resistivity change is increasing for both cooling and heating curves showing the irreversibility in the resistivity change at the transition. In both cases this is due to the combination dislocations and micro-cracks.

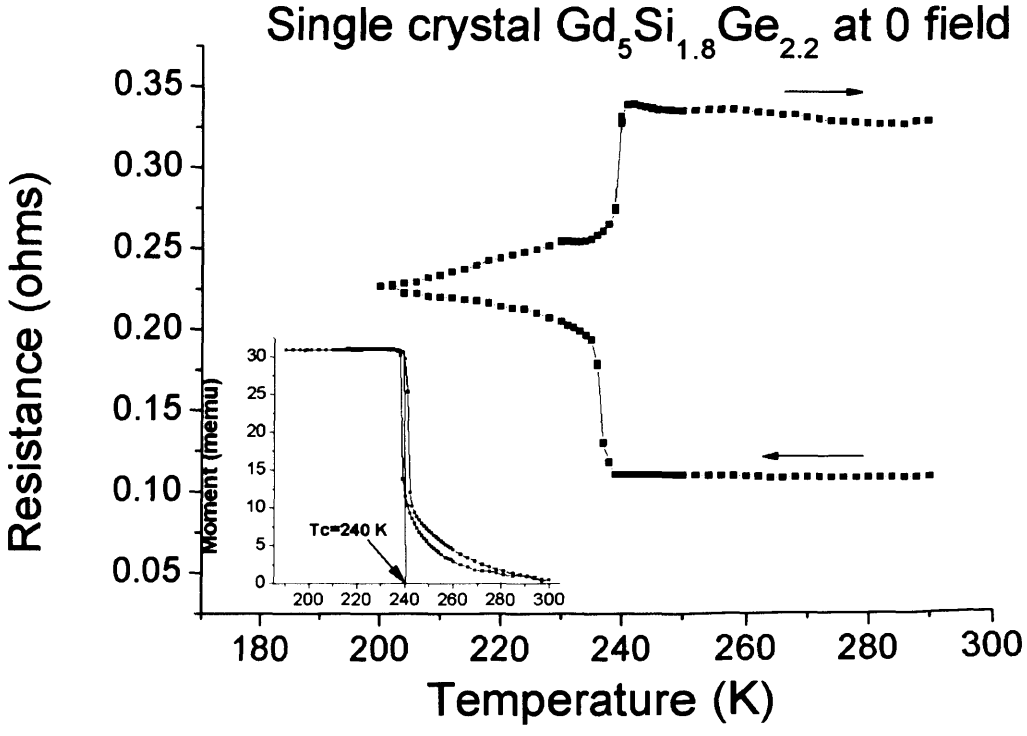

Fig. 6.4 Resistivity vs. Temperature measurement on a single crystal $Gd_5Si_{1.8}Ge_{2.2}$ sample for heating and cooling curves. Inset is the first order phase transition temperature measurement.

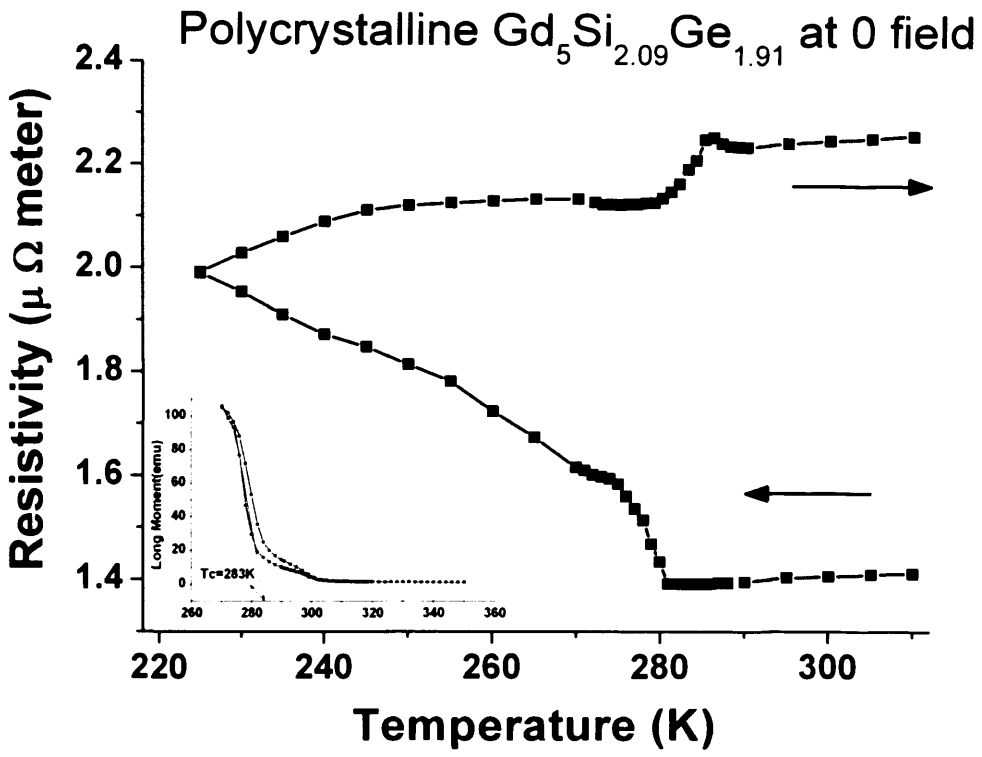

Fig. 6.5 Resistivity as a function of temperature at 0 applied field for the polycrystalline $Gd_5Si_{2.09}Ge_{1.91}$ (x=0.52) sample. Inset is the first order phase transition temperature measurement.

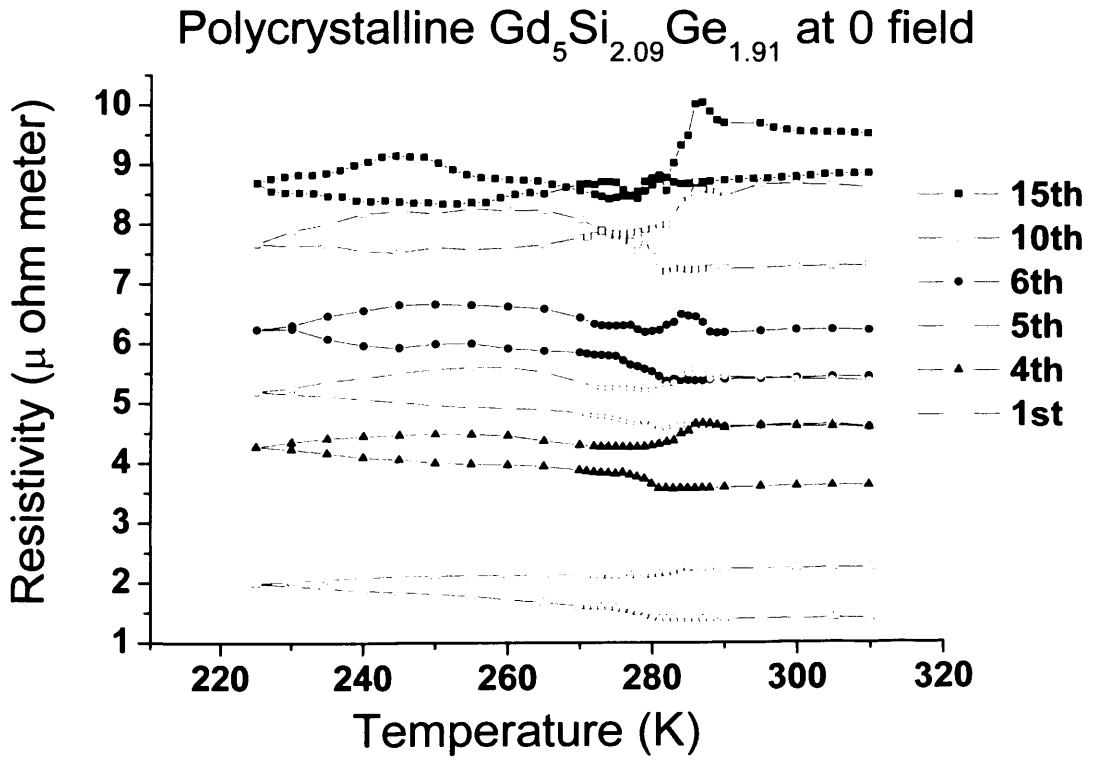

Fig. 6.6 Resistivity as a function of temperature for 15 thermal cycles through first order phase transition temperature for the polycrystalline $Gd_5Si_{2.09}Ge_{1.91}$ (x=0.52) sample.

The sample was cycled through the first order magnetic-structural phase transition temperature 15 times and was found that an irreversible change in the resistivity occurs every time the sample passes though the phase transition. The measurement becomes noisy at higher number of cycles which might be due to the development of dislocations and disappearance of dislocations due to the coalescence of dislocations. Fig. 6.6 shows the irreversible change in the resistivity for 15 thermal cycles passing through the first order phase transition temperature of 283 K. When the resistivity as a function of number of cycles at 310 K is plotted, a straight line for initial cycles can be observed for initial cycles and tends to saturate at higher number of cycles as shown in Fig. 6.7.

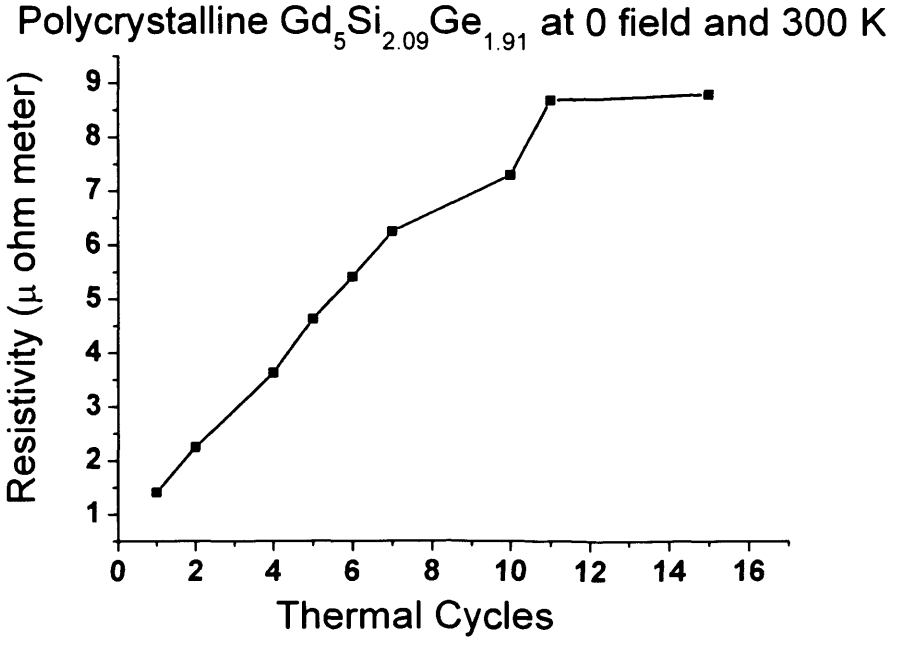

Fig. 6.7 Resistivity of heating curve as a function of thermal cycles at 310 K.

Resistivity measurements were also carried on a single crystal $Gd_5Si_{2.09}Ge_{1.91}$ (x=0.52) sample. The sample was cut with dimensions of 4.4mm×3.78 mm×2.91 mm. The connectors were on the 'bc' plane aligned along 'c' axis. Fig. 6.8 shows the measurement of resistivity as a function of temperature through the first order phase transition temperature of 200 K at 0 applied field. The first cycle shows the increase in the resistivity at the first order phase transition for both heating and cooling curves but this trend changes for subsequent cycles with a decrease in the resistivity for cooling and an increase in the resistivity for heating cycles.

At every phase transition there is a certain amount of irreversible increase in the resistivity. The sample was thermally cycled through the first order phase transition temperature 20 times. Fig. 6.9 shows 20 cycles of cooling curves from 230 K to 150 K. Measurement was noisy at higher cycles. The resistivity of the sample showed a trend to saturate in the last few cycles. The resistivity at the 20^{th} cycle was slightly lower than the resistivity of 19^{th} cycle which might fall within the error bars of the measurement.

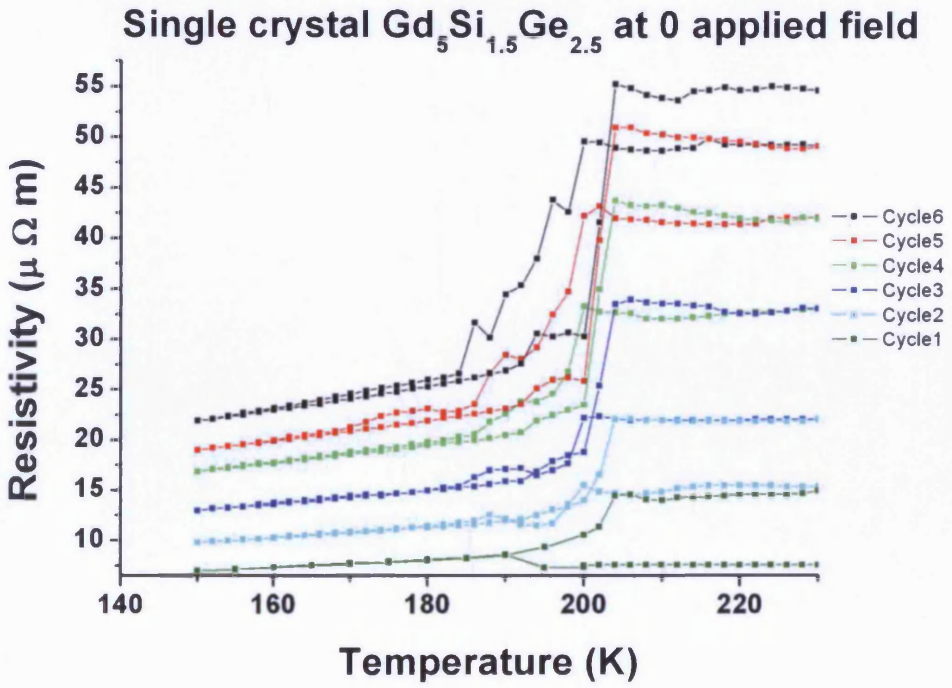

Fig. 6.8 Resistivity vs. temperature of single crystal $Gd_5Si_{1.5}Ge_{2.5}$ (x=0.375) at zero applied field. Note that the cooling curve of first cycle shows an increase in the resistivity unlike subsequent cooling curves.

When the resistivity of single crystal $Gd_5Si_{1.5}Ge_{2.5}$ (x=0.375) was plotted against the number of thermal cycles through the first order magnetic-structural phase transition a linear dependence was observed for the first few cycles and then it shows a trend to saturate at higher cycles as shown in Fig. 6.10 which is similar to the polycrystalline $Gd_5Si_{2.09}Ge_{1.09}$ (x=0.52) sample shown in Fig. 6.7

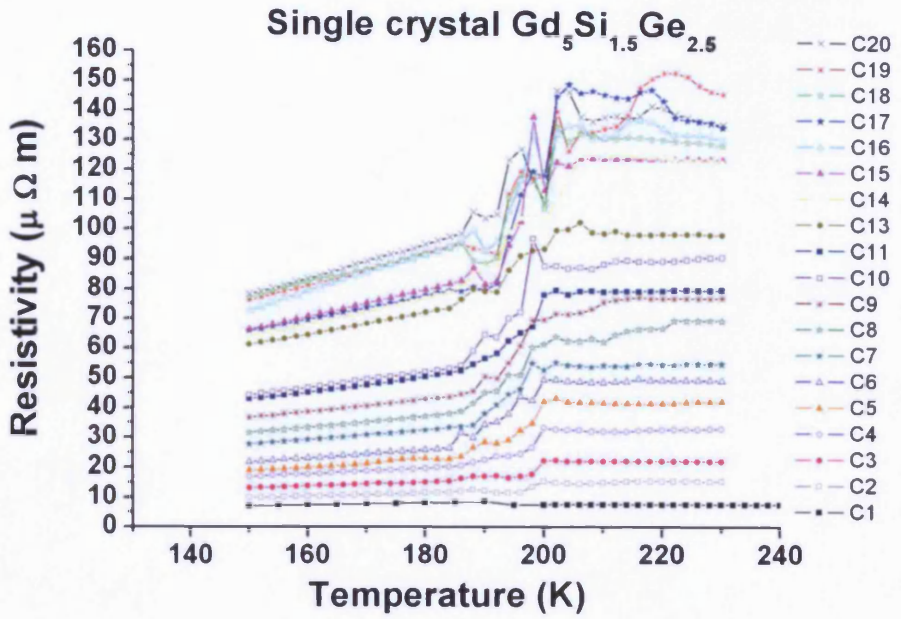

Fig. 6.9 Resistivity vs. temperature of single crystal $Gd_5Si_{1.5}Ge_{2.5}$ (x=0.375) at 0 applied field up to 20 cycles

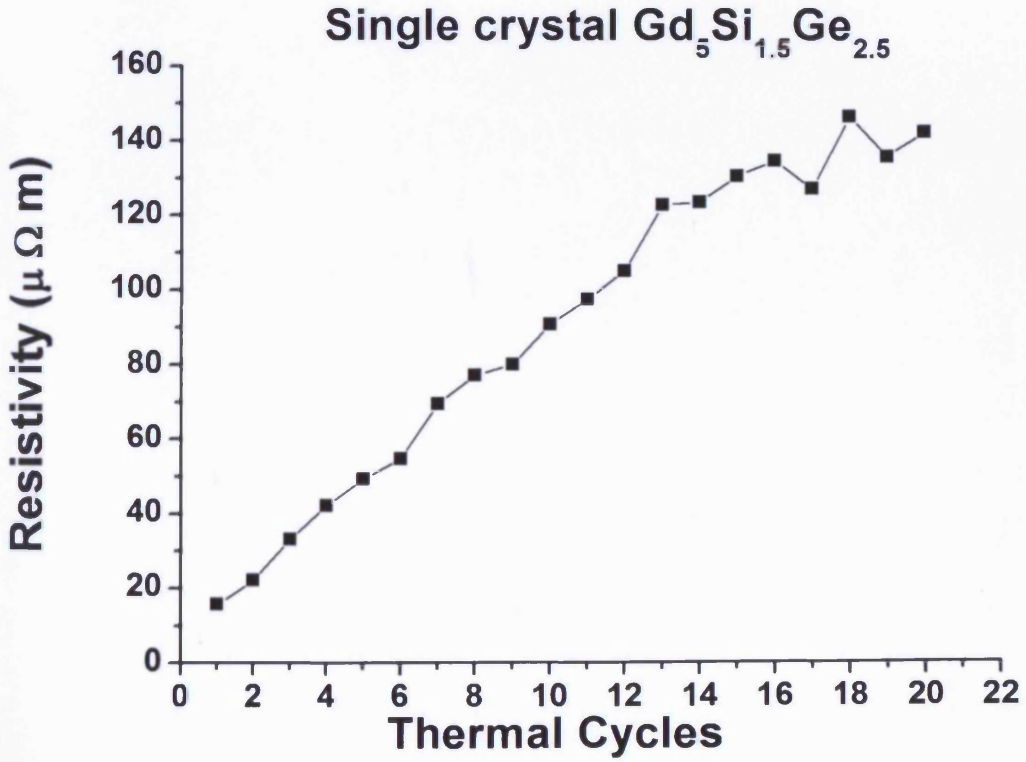

Fig.6.10 Resistivity of single crystal $Gd_5Si_{1.5}Ge_{2.5}$ (x=0.375) vs. number of thermal cycles through the first order phase transition temperature.

6.2.5 Resistivity vs. Magnetic Field Measurement

Resistivity was also measured for the polycrystalline $Gd_5Si_{2.09}Ge_{1.09}$ when the sample was held at 290 K and the first order phase transition was induced by the application of magnetic field. Fig. 6.11 shows the measurement for forward and reverse sweep of the magnetic fields. An irreversible increase in the resistivity can be seen even in these measurements. The inset figure is magnetic moment vs. magnetic field ($\mu_0 H$) measurement showing the field induced first order magnetic-structural phase transition between 1.5 to 2.5 kOe on a polycrystalline $Gd_5Si_{2.09}Ge_{1.09}$ (x=0.52) sample which is in agreement with the ρ vs. $\mu_0 H$ measurement on a polycrystalline sample with the same composition.

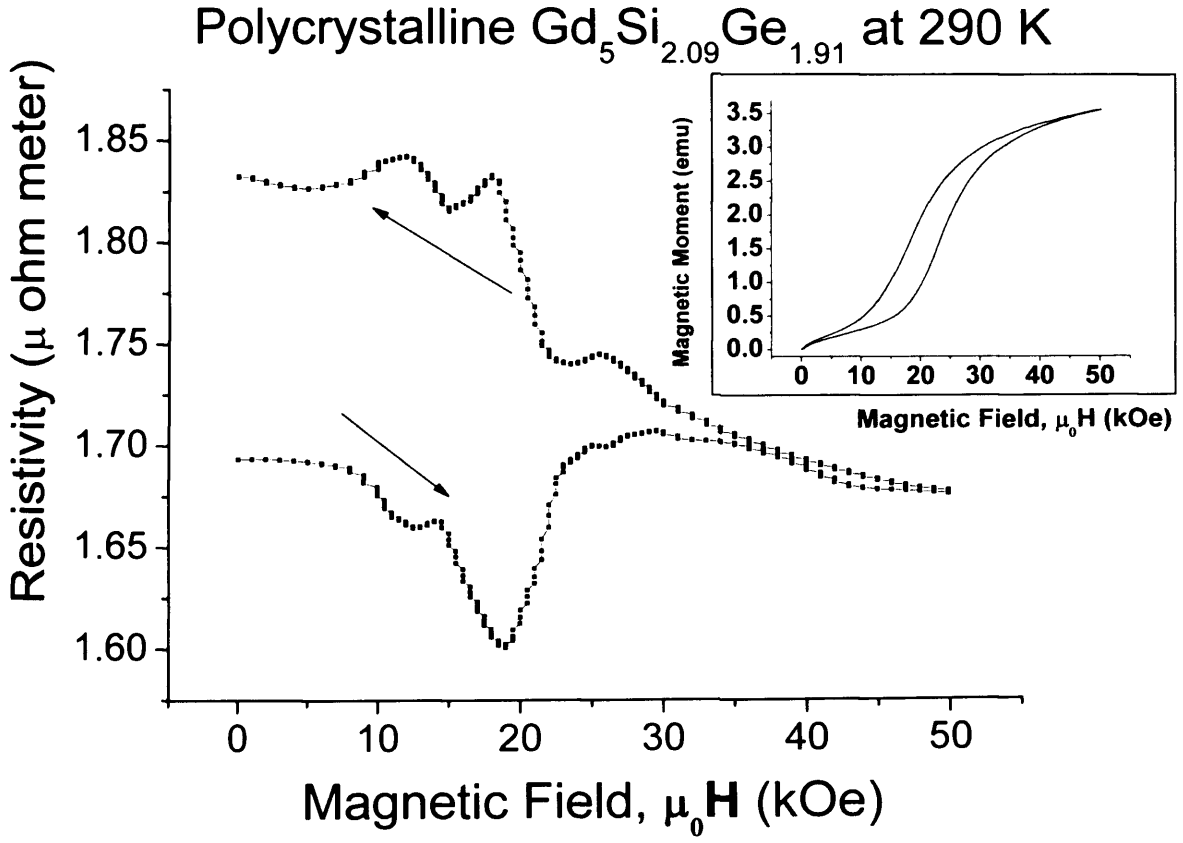

Fig. 6.11 Resistivity vs. magnetic field measurement at 290 K on a polycrystalline $Gd_5Si_{2.09}Ge_{1.09}$ (x=0.52) sample. Inset is the magnetic moment vs. magnetic field measurement showing the field induce phase transition at 290 K.

6.3 Irreversible Change in Coercivity Due to Thermal Cycling

Irreversible change in the resistivity was observed in single crystal and polycrystalline samples in both resistivity vs. magnetic field and resistivity vs. temperature measurements. Other properties such as coercevity and saturation magnetisation behaviour when cycled through the first order phase transition were not reported before in the literature. In this measurement a single crystal $Gd_5Si_{1.8}Ge_{2.2}$ (x=0.45) sample was thermally cycled from room temperature to a lower temperature below the sample's first order structural-magnetic phase transition (240 K) and hysteresis loops were plotted at a lower temperature when the sample is in ferromagnetic phase. Fig. 6.12 shows the hysteresis loops taken at 220 K after every thermal cycle from 300 K to 220 K for 15 times. Since the coercivity of the sample is very low the hysteresis loops are overlapping on each other.

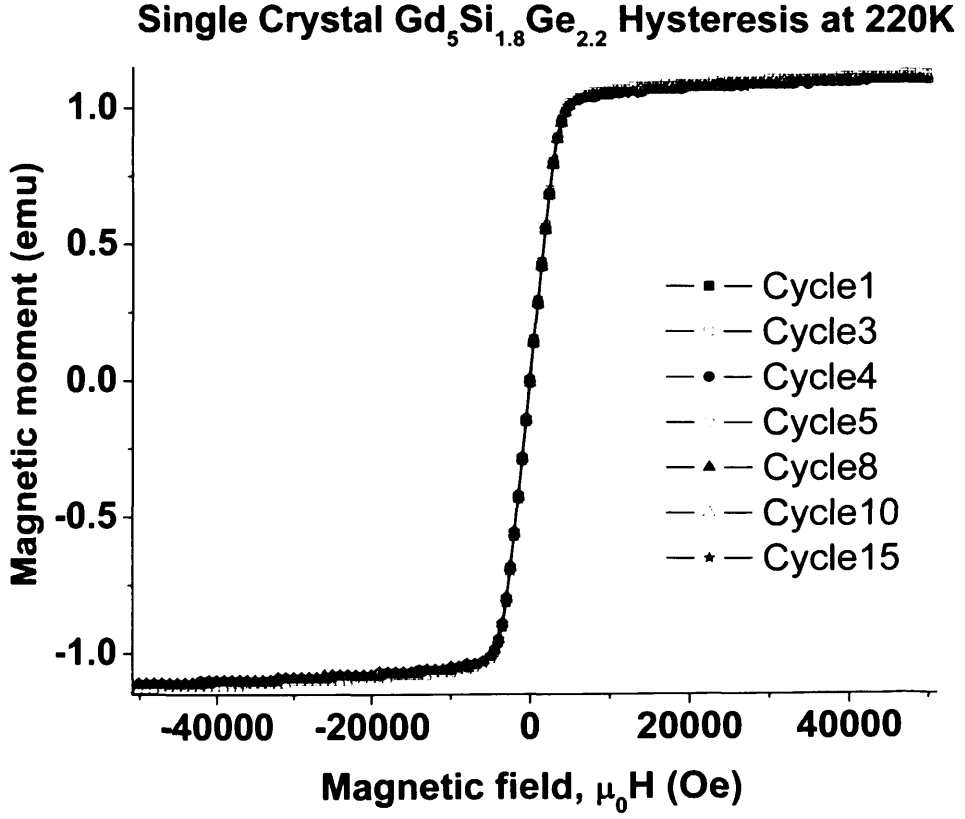

Fig. 6.12 Hysteresis loops at 220 K of single crystal $Gd_5Si_{1.8}Ge_{2.2}$ (x=0.45) measured after each thermal cycle through the first order phase transition temperature.

When the area close to the origin in the plot is magnified, the difference in coercivity of different cycles can be seen. Fig.6.13 shows a magnified region of Fig. 6.12 close to the origin. It can be seen that coercivity of cycles 1, 2 and 3 do not change and coercivity of cycle 4 is higher than the coercivity of cycle 3 by 15 Oe. Coercivity of cycle 5, 6, 7, 8, 9 and 10 is higher than cycle 4 by 15 Oe. This confirms that there is an irreversible change in the coercivity when the single crystal $Gd_5Si_{1.8}Ge_{2.2}$ (x=0.45) sample is cycled through the first order magnetic-structural phase transition. When the sample is cycled through the first order phase transition, dislocations may develop due to high strain at the first order phase transition. These dislocations act as pinning sites in the domain motion. These pinning sites are responsible for the observed irreversible change in the coercivity. The saturation magnetisation did not show any significant changes for different cycles.

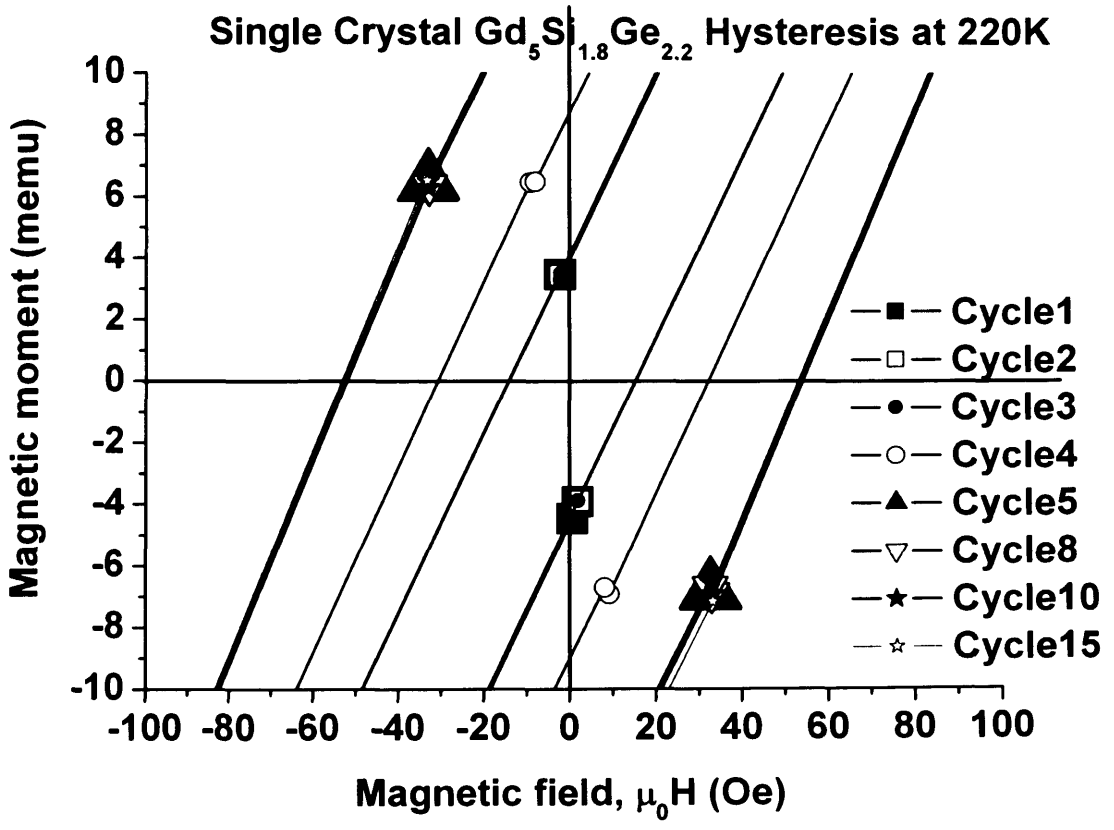

Fig. 6.13 Magnified region of Fig. 6.12 showing irreversible change in the coercivity of the single crystal $Gd_5Si_{1.8}Ge_{2.2}$ (x=0.45) sample for various thermal cycles through the first order phase transition temperature.

6.4 Recovery of Irreversible Resistivity Kept at Room Temperature

After discussing with various researchers about the irreversible increase in the resistivity of $Gd_5(SixGe_{1-x})_4$, we came across one interesting observation by Zou of the Ames Laboratory, USA, in which the sample had been passed through the thermally induced first order phase transition 30 times and an irreversible increase in the resistivity had been observed as shown in Fig.6.14, Red solid circles represent the thermal cycle 1 and hollow red circle represent the thermal cycle 30. The sample had been kept with all the leads connected to sample for about 2.5 years at room temperature. When resistivity of the sample was measured after 2.5 years it was noticed that there was a recovery in the resistivity that had increased irreversible before, Green lines in Fig. 6.14 shows the measurements carried out after 2.5 years.

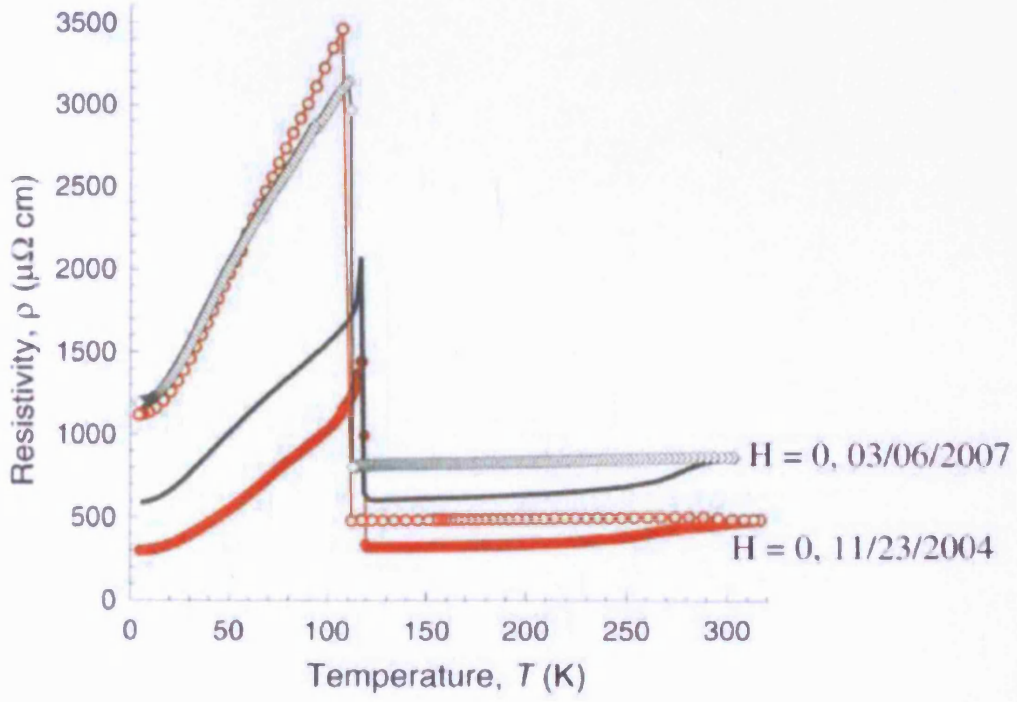

Fig. 6.14 Resistivity vs. temperature for a single crystal $Gd_5(Si_xGe_{1-x})_4$ sample with the composition $0<x<0.31$ measured at two time intervals in a span of 2.5 years [13].

A model explaining the recovery in resistivity when kept at longer periods was developed based on a combination of Matthiessen's rule and modified Arrhenius equation as part of the research in this thesis. The developed model was experimentally verified by passing the $Gd_5(Si_xGe_{1-x})_4$ samples through the temperature induced first order phase transition in order to obtain irreversible change in the resistivity and holding the sample at an elevated temperature for a certain period of time.

6.5 Thermodynamic Theory of Resistivity Recovery

In order to explain the behaviour of resistivity in $Gd_5(Si_xGe_{1-x})_4$ we start from an assumption known as Matthiessen's rule [11,19, 20] in which the various contributions to resistivity can be added. The contributions to resistivity are separated into 3 different terms as shown in Eqn. (6.6).

$$\rho = \rho_{Lattice} + \rho_{Dislocations} + \rho_{Microstructure} \tag{6.6}$$

The strain dependent component of resistivity $\rho_{Dislocations}$ can be rewritten in terms of the number density N of dislocations:

$$\rho_{Dislocations} = kN \tag{6.7}$$

where k is proportionality constant

so the total resistance becomes:

$$\rho = \rho_{Lattice} + kN + \rho_{Microstructure} \tag{6.8}$$

We assume that the dislocations in the material, which are created by the generation of stress in the material through magnetostriction, are metastable, being trapped in localized potential wells, and that they can escape from the traps by thermal activation.

Although in practice there will be a range of depths of these localized potential wells, for the purposes of a theoretical analysis we take a typical depth of potential well as representative of the

naterial. If the depth of the potential well is ΔE, the probability of a dislocation overcoming the barrier of the potential well is, according to statistical thermodynamics [19], proportional to

$$\exp\left(\frac{-\Delta E}{k_B T}\right)$$

where T is the thermodynamic temperature and k_B is Boltzmann's constant.

The probability, P of a single dislocation being thermally activated and escaping the potential well in unit time can be expressed in terms of a frequency s which can be thought of as the rate at which the dislocations attempt to escape the potential well

$$P = s.\exp\left(\frac{-\Delta E}{k_B T}\right) \tag{6.9}$$

The rate of dislocations escaping the potential well, per unit volume per unit time, is then the product of this probability P for the typical single dislocation and the number of dislocations per unit volume N remaining:

$$\frac{dN}{dt} = -NP \tag{6.10}$$

The remaining dislocation density N (ie. the original dislocation density minus the number per unit volume escaping over a given time interval t), is obtained by integration of Eqn.(6.10)

$$\int_0^t -\frac{1}{N}\frac{dN}{dt} = \int_0^t P dt \tag{6.11}$$

$$-\log_e\left(\frac{N}{N_0}\right)=\int_0^t P\,dt \tag{6.12}$$

The number density of dislocations N remaining after a time t is therefore given by

$$N = N_0 \exp(-Pt) \tag{6.13}$$

where N_0 is initial dislocation density.

Substituting for the probability P the expression for N becomes

$$N = N_0 \exp\left(-s.\exp\left(\frac{-\Delta E}{k_B T}\right)t\right) \tag{6.14}$$

This is analogous to the Randall-Wilkins equation for electron trapping [19].

Combining both Matthiessen's rule for resistivity and the above equation for the number of dislocations per unit volume N remaining, the dependence of resistivity on temperature and time becomes

$$\rho = \rho_{lattice} + kN_0 \exp\left(-s.\exp\left(\frac{-\Delta E}{k_B T}\right)t\right) + \rho_{Microstructure} \tag{6.15}$$

From Zou's (Fig.6.14) data it is known that the resistivity of the sample before the stress cycling was $\rho = \rho_{lattice}$ = 300 μΩ cm and that after stress cycling it was ρ = 1200 μΩ cm and after 2.5 years at 300K it had recovered to ρ = 600 μΩ cm. This allows us to make some estimates of the parameters in the equation that will result in this behaviour, although we do not yet have enough data to obtain unambiguous values of these parameters. After 30 cycles resistivity had increased to ρ = 1200 μΩ cm (corresponding to holding time t=0, and holding temperature T=300 K). After leaving the material for a "holding time" t = 833 days at T=300 K, the resistivity had recovered to ρ = 600 μΩ cm.

The coefficients kN_0, s and ΔE were estimated by trial and error to see whether the equation could give a plausible variation of resistivity with time and temperature. Graphs were plotted for various different holding times and temperatures, and the results are shown in the following Fig. 6.15.

We observe from the Fig.6.15, which represents solutions to the theoretical equation, the sensitivity of the recovery of the resistivity to the holding temperature.

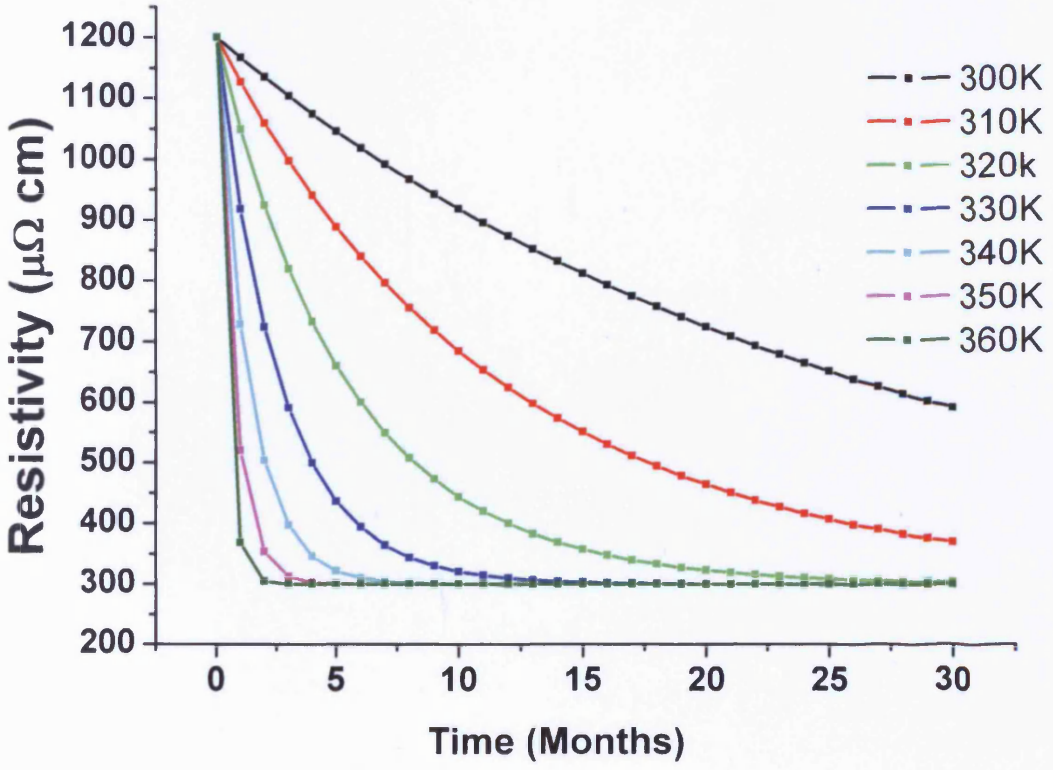

Fig. 6.15 Solution to the proposed thermodynamic equation using Matthiessen's rule and modified Arrhenius equation. Where the parameters are: ΔE is $1.5x10^{-19}$, s is $1.5x\ 10^3$, $\rho_{lattice}$ is 300 μΩcm.

The equation with the estimated coefficients is

$$\rho = 300 + 900\exp\left(-1.5\times10^{3}\times Time\times\exp\left(\frac{-1.5\times10^{-19}}{k_B\times Temperature}\right)\right)+\rho_{Microstructure} \quad (6.16)$$

(kN_0 → N_0; $\rho_{Lattice}$ → 300; ΔE → -1.5×10^{-19}; s → -1.5×10^{3})

Typically $N_0 \approx 10^8$ m^{-2} and $k=10^{-6}$ μΩm [21].

so that at time $t = \infty$ the resistivity will have completely recovered to $\rho = \rho_{Lattice} + \rho_{Microstructure}$.

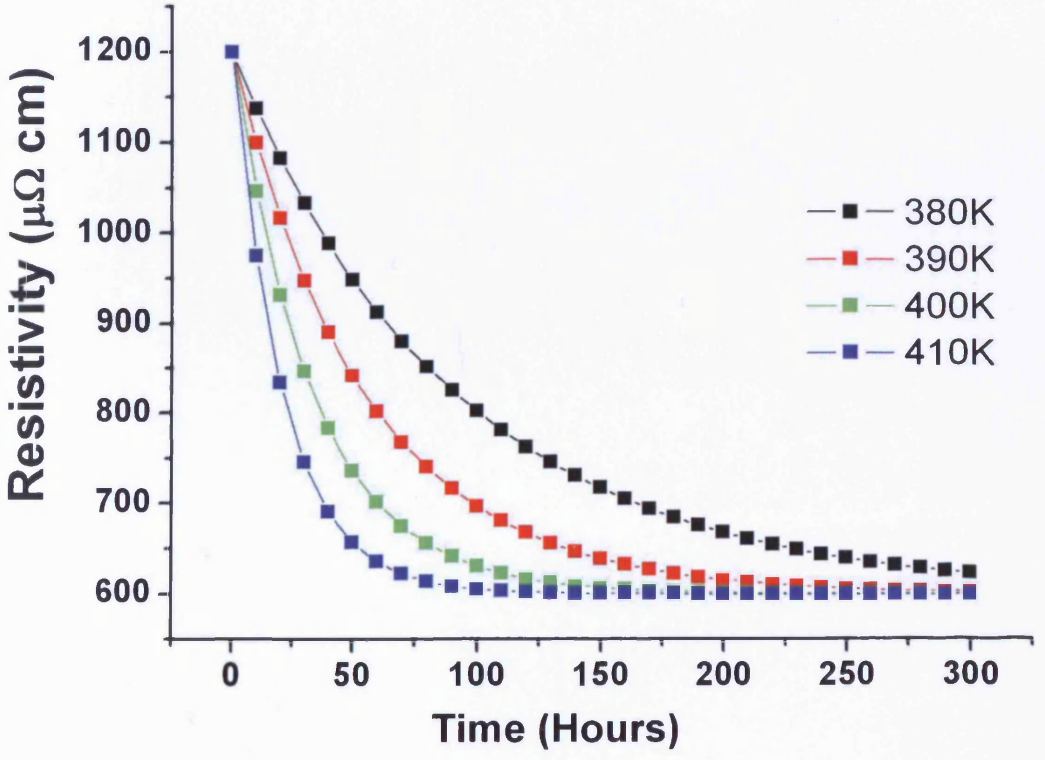

Fig. 6.16 Solution to our thermodynamic equation (Eqn. (6.16)) for smaller time intervals in hour and at higher holding temperatures.

There are other possibilities to consider in this theoretical approach. In particular if the stress cycling does cause micro-cracking (which is not recoverable by thermal processes short of melting) then the final value of ρ (as t tends to infinity) will have an offset from its initial pre-stressed value. The offset will then represent an irrecoverable component of resistivity. The same recovery equation can be applied in this situation, the difference being that the recovery does not apply to the whole of kN_0 but instead to the fraction ($kN_0 - \rho_{crack}$), and in this case in the limit as t tends to infinity ρ will tend to ρ_{crack}.

Fig.6.18 shows the solution to our equation based on Matthiessen's rule and Randall-Wilkins equation for time intervals in hours and at elevated holding temperatures of 380 to 410 K. It can be noted that at a holding temperature of 400 K, we can achieve a complete recovery in 150 hours (6 days).

6.6 Experimental Validation of Thermodynamic Theory of Resistivity Recovery

A single crystal $Gd_5Si_{1.5}Ge_{2.5}$ (x=0.375) sample was first thermally cycled through its first order magnetic-structural phase transition for 20 times to obtain an irreversible change in the resistivity as shown in Fig. 6.9. The sample was then held at an elevated temperature of 345 K for more than 50 hours in situ and resistivity was recorded every minute. It can be seen in the Fig. 6.17 that the resistivity was reduced to 50 μΩm after 45 hours and showed a trend to stabilise. The total reduction in the resistivity was about 110 μΩm from 160 μΩm which is about 65% recovery. All the parameters in the model equation (Eqn. 6.14) were determined for the single crystal $Gd_5Si_{1.5}Ge_{2.5}$ (x=0.375) sample.

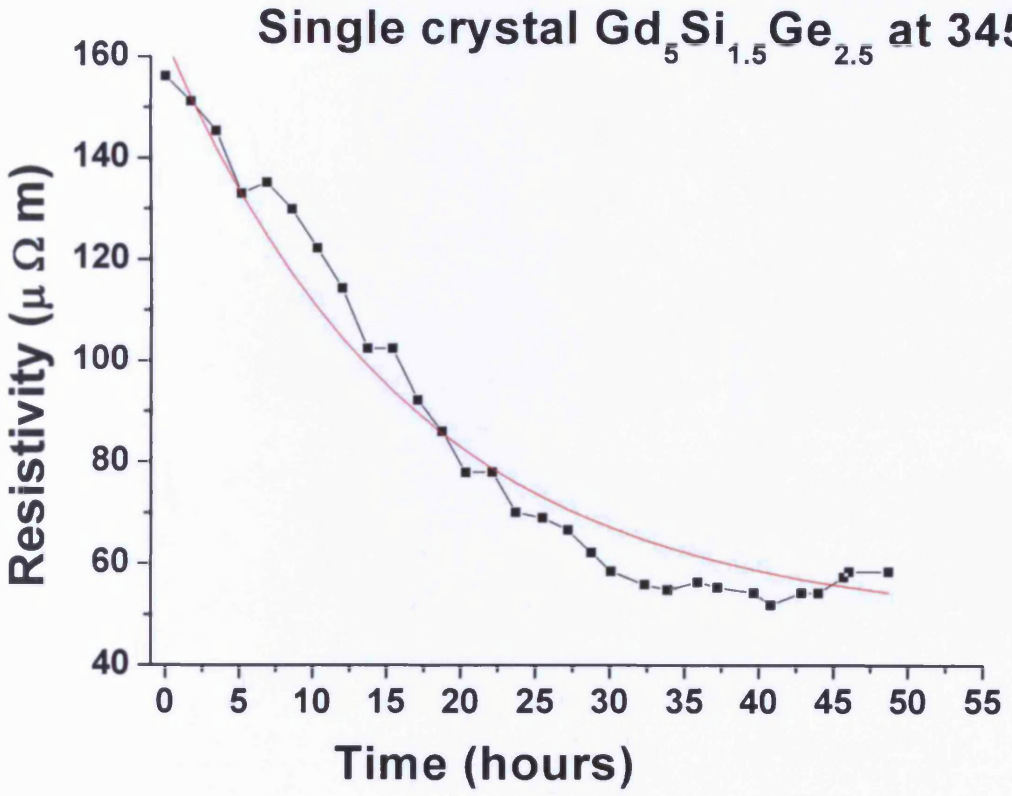

Fig. 6.17 Recovery in resistivity of the single crystal $Gd_5Si_{1.5}Ge_{2.5}$ (x=0.375) sample when held at 345 K after cycling the sample through the first order phase transition for 20 times. Values of model parameters of Eqn. (6.16) obtained by least squares fitting are $s = 0.26 \times 10^6\ s^{-1}$, $\Delta E = 1.1 \times 10^{-19}$ J

The Arrhenius constant and the energy barrier of the dislocations were determined to be $s = 0.26 \times 10^6 s^{-1}$ and 1.11×10^{-19} J respectively. The lattice component of the resistivity $\rho_{lattice}$ was assumed to be the initial resistivity of the sample which is 5 μΩm (Fig.6.8) and this component will not change upon thermal cycling of the sample through the first order magnetic-structural phase transition. The microstructure component of the resistivity $\rho_{Microstructure}$ was determined from the measurement to be 50 μΩm (Fig. 6.17).

Resistivity recovery measurements were also carried on polycrystalline $Gd_5Si_{2.09}Ge_{1.91}$ (x=0.52) sample. Similar to the previous measurement first the sample was cycled through the first order magnetic-structural phase transition for 20 times and then the sample was held at an elevated

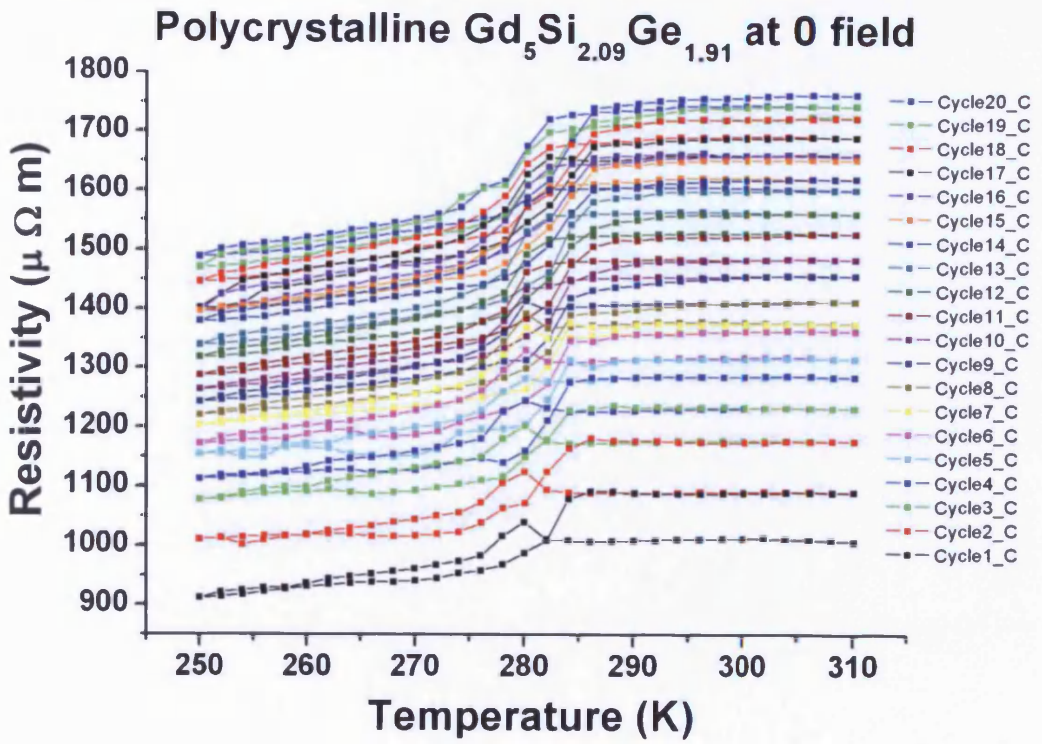

Fig. 6.18 Resistivity vs. Temperature for a polycrystalline $Gd_5Si_{2.09}Ge_{1.91}$ (x=0.52) sample at 0 field when cycled through the first order phase transition 20 times.

temperature of 360 K. Fig. 6.19 shows the thermal cycling of the sample through the first order phase transition temperature at 0 applied magnetic field. Resistivity was increased from 900 μΩm to 1800 μΩm in 20 thermal cycles. After the thermal cycling of the sample through the first order phase transition, temperature of the sample space was increased to 360 K and resistivity was recorded at every minute for more than 25 hours. Fig. 6.19 shows the measurement of resistivity vs. time of polycrystalline $Gd_5Si_{2.09}Ge_{1.91}$ (x=0.52) sample held at 360 K. Resistivity at 360 K was 1975 μΩm and started to fall with the time. After 25 hours, resistivity of the sample was about 1500 μΩm and stabilised at this value. The percentage recovery in the resistivity for this polycrystalline $Gd_5Si_{2.09}Ge_{1.91}$ sample was about 50%. All the parameters in the model equation (Eqn. 6.16) were determined for the polycrystalline $Gd_5Si_{2.09}Ge_{1.91}$ sample. The Arrhenius constant and the barrier energy of the dislocations were determined to be s $=0.08\times10^{6}\ s^{-1}$ and $\Delta E = 1.05\times10^{-19}$ J respectively.

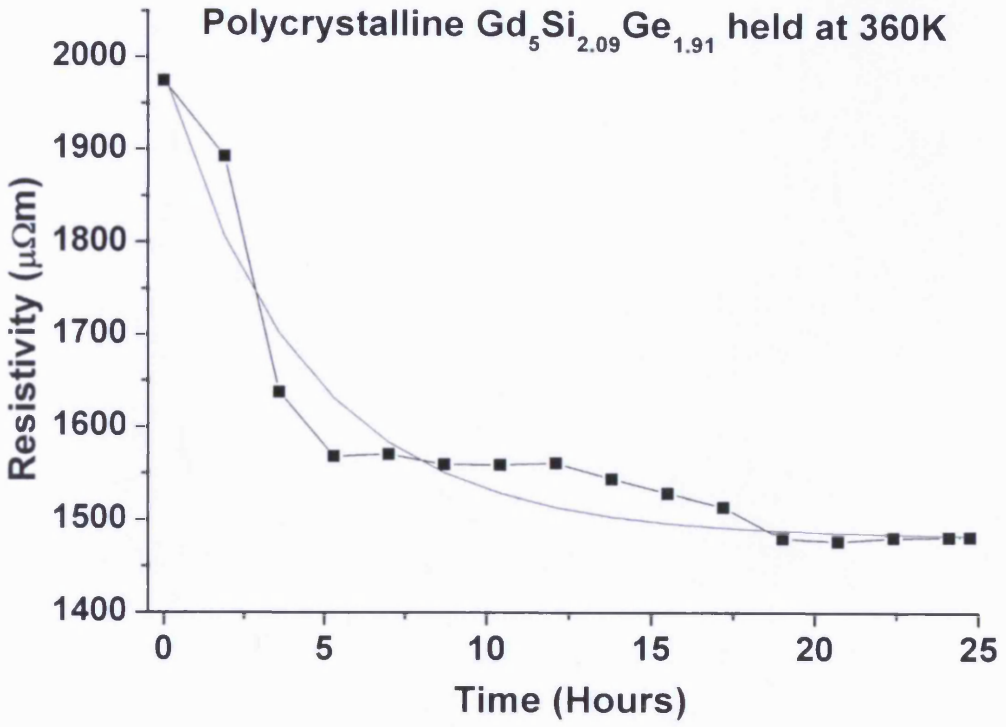

Fig. 6.19 Resistivity vs. time for a polycrystalline $Gd_5Si_{2.09}Ge_{1.91}$ (x=0.52) sample held at 360 K after cycling the sample through the first order phase transition for 20 times. The parameters of Eqn.(6.16) obtained by least square fit are $s = 0.08 \times 10^6 s^{-1}$ and $\Delta E = 1.04 \times 10^{-19}$ J

The lattice component of the resistivity $\rho_{lattice}$ was assumed to be the initial resistivity of the sample which is 900 μΩm (Fig.6.18) and this component will not change upon thermal cycling of the sample through the first order magnetic-structural phase transition. The microstructure component of the resistivity $\rho_{Microstructure}$ was determined from the measurement to be 600 μΩm (Fig. 6.19). The dislocation component of the resistivity $\rho_{Lattice}$ which was recovered was determined to be 500 μΩm which is 25% of the resistivity before the recovery.

Irreversible increase in the resistivity of other materials exhibiting the first order phase transition was recently reported in $Tb_5Si_2Ge_2$ by Zou. *et. al.* [22]. The samples were cycled through the first order phase transition several times and were kept at room temperature for 21 months. The resistivity recovery was observed when the sample's resistivity was measured. This phenomenon might also exist in other materials which exhibit first order phase transition such as shape memory alloys and $R_5(Si_xGe_{1-x})_4$ where R is Dy, Eu and Sm.

6.7 Summary

Fundamentals of magnetoresistance including in thin films was explained and a literature review on magnetoresistance in $Gd_5(Si_xGe_{1-x})_4$ was carried out. Magnetoresistance was measured for various compositions and an irreversible increase in resistivity was observed which depended linearly on the number of thermal cycles passing through the first order phase transition temperature. The irreversibly increased resistivity was recovered by holding the samples at high temperature for a long period of time up to 3 days. A theoretical model was developed to explain the recovery in the resistance and was experimentally verified.

References

[1] D. C. Jiles, Introduction to the Electronic Properties of Materials,pp.170, Nelson Thornes, (2001).

[2] G. Binasch, P. Grunberg, F. Sauerenbach and W. Zinn, "*Enhanced magnetoresistance in layered magnetic structures with antiferromagnetic interlayer exchange*", Phys. Rev. B, **39**, pp. 4828-4830, (1989).

[3] M. N. Baibich, J. M. Broto, A. Fert, F. Nguyen Van Dau, and F. Petroff, "*Giant magnetoresistance in Fe(001)/Cr(001) superlattices*", Phys. Rev. Lett., **61**, pp. 2472-2475, (1988).

[4] T. Valet and A. Fert, "*Theory of the perpendicular magnetoresistance in magnetic multilayers*", Phys. Rev. B, **48**, pp. 7099-7113, (1993).

[5] A. O. Pecharsky, K. A. Gschneidner, Jr., and V. K. Pecharsky, "*The giant magnetocaloric effect between 190 and 300 K in the $Gd_5Si_xGe_{4-x}$ alloys for $1.4 \leq x \leq 2.2$*" , J. Magn. Magn. Mater., **267**, pp. 60-68, (2003).

[6] M. Han, D. C. Jiles, J. E. Snyder, T. A. Lograsso, and D. L. Schlagel, *"Angular Dependence of the Unusual First-Order Transition Temperature in Single-Crystal"*, IEEE. Trans. Magn., **39**, pp. 3151-3153, (2003).

[7] R. L. Hadimani, Y. Melikhov, J.E. Snyder, D.C. Jiles, *"Anomalous Behavior in Electrical Transport Properties in Single-Crystal $Gd_5Si_{1.8}Ge_{2.2}$ and Polycrystalline $Gd_5Si_{2.09}Ge_{1.91}$ "* IEEE Trans. Magn., **45**, pp. 4368 - 4371, (2009).

[8] M. Manekar, R. Kaul, V. K. Pecharsky, K. A. Gschneidner Jr., M. K. Chattopadhyay, *"Training effects in Gd_5Si_4: role of microstructure"*, J. Phys.:Condens. Matter, **18**, pp. 6017-6032, (2006).

[9] L. Morellon, J. Stankiewicz, B. García-Landa, P. A. Algarabel, and M. R. Ibarra, *"Giant magnetoresistance near the magnetostructural transition in $Gd_5(Si_{1.8}Ge_{2.2})$"*, App. Phys. Lett., **73** , pp.3462-3464, (1998).

[10] E. M. Levin, V. K. Pecharsky and K. A. Gschneidner, Jr., *"Magnetic-field and temperature dependencies of the electrical resistance near the magnetic and crystallographic first-order phase transition of $Gd_5(Si_2Ge_2)$"*, Phys. Rev. B, **60**, pp. 7993-7997, (1999).

[11] R. Zurcher, M. Muller, F. Sachslehner, V. Groger and M. Zehetbauer, *"Dislocation resistivity in Cu: dependence of the deviations from Matthiessen's rule on temperature, dislocation density and impurity content"* J. Phys: Condens. Matter, **7**, pp. 3515-3528, (1995).

[12] J. B. Sousa , M. E. Braga, F. C. Correia, F. Carpinteiro, L. Morellon, P. A. Algarabel, and M. R. Ibarra, *"Anomalous behavior of the electrical resistivity in the giant magnetocaloric compound $Gd_5(Si_{0.1}Ge_{0.9})_4$"*, Phys. Rev. B., **67**, pp. 134416-8, (2003).

[13] M. Zou, *"Structural, magnetothermal, and magnetotransport properties of single crystal $Tb_5Si_{2.2}Ge_{1.8}$ and spontaneous generation of voltage in single crystal $Gd_5Si_2Ge_2$ and Gd"*, PhD Thesis, Iowa State University, Ames, USA, May (2009).

[14] Agar Scientific, "*Electrodag 1415 Technical Information Manual*", pp. 2, (2008).

[15] HyperPhysics, "Resistivity and Temperature Coefficients at 20°C", Retrieved, 17-09-2009, from http://hyperphysics.phy-astr.gsu.edu/hbase/Tables/rstiv.html#c1.

[16] L. J. Van der Pauw, "*A method of measuring specific resistivity and Hall Effect of discs of arbitrary shape*", Philips Research Reports, **13**, (1958).

[17] E. M. Levin, V. K. Pecharsky and K. A. Gschneidner, Jr., "*Spontaneous generation of voltage in $Gd_5(Si_xGe_{4-x})$ during a first-order phase transition induced by temperature or magnetic field*", Phys. Rev. B, **63**, pp. 174110-174116, (2001).

[18] M. Zou, H. Tang, D. L. Schlagel, T. A. Lograsso, V. K. Pecharsky and K. A. Gschneidner, Jr., "*Spontaneous generation of voltage in single-crystal $Gd_5Si_2Ge_2$ during magnetostructural phase transformations*", J. App. Phys. **99**, 08B304, (2006).

[19] D. C. Jiles, "*Introduction to the Electronic Properties of Materials*", pp.163, Nelson Thornes (2001).

[20] A. Matthiessen, Rep. Brit. Ass. **32**, 144 (1862).

[21] S. K. Khanna and K. G. Rajan, "*Growth of low dislocation density single crystals of nickel*", Bull. Mater. Sci., **8**, pp. 467-470, (1986).

[22] M. Zou, V. K. Pecharsky, K. A. Gschneidner, Jr., Y. Mudryk, D. L. Schlagel, and T. A. Lograsso, "*Electrical resistivity and magnetoresistance of single-crystal* $Tb_5Si_{2.2}Ge_{1.8}$", Phys. Rev. B, **80**, pp. 174411-7, (2009).

Chapter 7: Magnetocrystalline and Shape Anisotropy in $Gd_5(Si_xGe_{1-x})_4$

7.1 Introduction

Anisotropic materials are those materials which exhibit different properties when measured in different directions. With respect to magnetism we can state that the dependence of magnetic properties of magnetic materials along a preferred direction is called magnetic anisotropy. Magnetic anisotropy plays an important role in determination of various magnetic properties of materials. There are various forms of magnetic anisotropy. The main three kinds are: magnetocrystalline anisotropy, shape anisotropy and stress anisotropy. There are also other types of magnetic anisotropy such as magnetic annealing anisotropy and exchange anisotropy, which are used in special applications such as data recording using thin films.

7.1.1 Magnetocrystalline Anisotropy

Various magnetic materials show different magnetic properties when measured along different crystal axes, this effect is called magnetocrystalline anisotropy. Anisotropy energy can be defined as the energy required to deflect the magnetic moment from easy axis to hard axis in a single crystal magnetic material. Magnetocrystalline anisotropy is an intrinsic property of magnetic materials which results from interaction between spin and orbit known as spin-orbital coupling. The crystal axis which exhibits the highest magnetic moment at an applied field slightly smaller than saturation field is called the easy axis and the axis which exhibits lowest magnetic moment at that field is called the hard axis. Fig. 7.1 shows the hard and easy axes of a face centred cubic structure of nickel; the cubic diagonal axis [111] is the easy axis and the 'a' axis [100] is the hard axis. The diagonal of the sides [110] is an intermediate axis [1]. This crystal has more than one easy axis hence it does not have a uniaxial anisotropy. Other such examples of cubic crystals exhibiting polyaxial anisotropy are iron and magnetite. The materials which exhibit one easy axis in their crystal structure are called uniaxial anisotropic materials. Cobalt, Hematite, $Gd_5(Si_xGe_{1-x})_4$, all exhibit uniaxial magnetocrystalline anisotropy. Cobalt has a hexagonal crystal lattice and the easy axis is its 'c' axis

while all the base plane axes are hard axes. Fig. 7.2 shows M vs. H curves of cobalt on its hard and easy axes of its hexagonal crystal lattice. $Gd_5(Si_xGe_{1-x})_4$ has an orthorhombic crystal structure and has an easy axis along its 'b' axis which is discussed in detail in later sections.

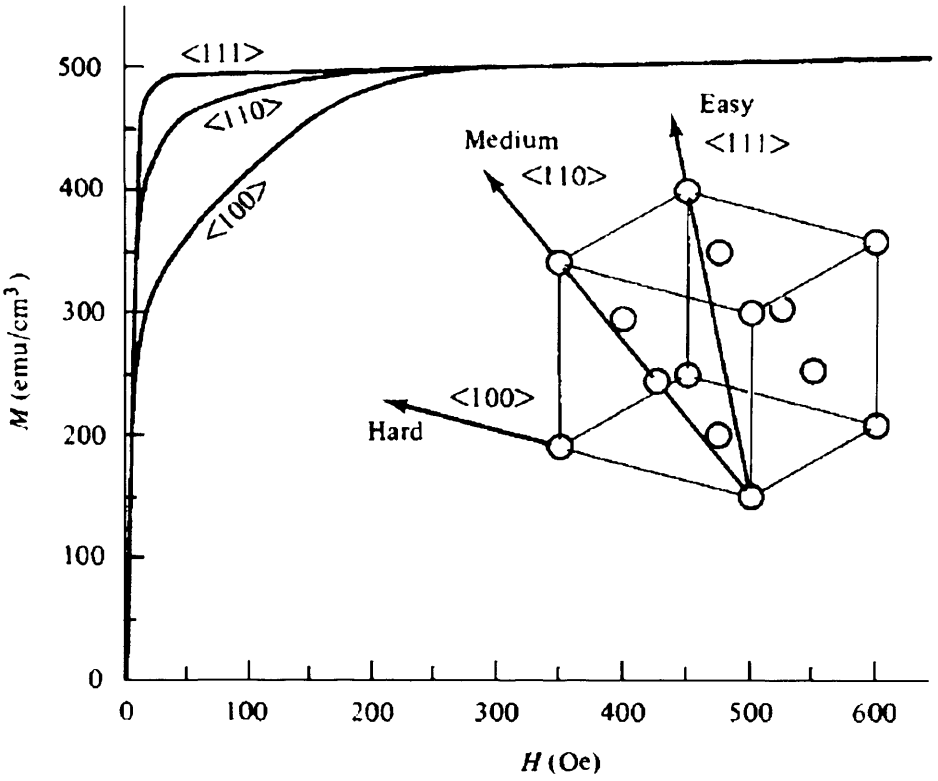

Fig. 7.1 M vs. H curves for nickel at various axes of its face centred cubic structure. Note that it has an easy axis at [111] and hard axis at [100] [1].

Crystal anisotropy energy can be expressed in terms of the cosines of angles between magnetisation M_s and the crystal axes [2].

$$E = K_0 + K_1(\alpha_1^2\alpha_2^2 + \alpha_2^2\alpha_3^2 + \alpha_3^2\alpha_1^2) + K_2(\alpha_1^2\alpha_2^2\alpha_3^2) + \ldots\ldots \quad (7.1)$$

where α_1, α_2 and α_3 are the angles between magnetisation and 'a', 'b' and 'c' axes of the crystal lattice.

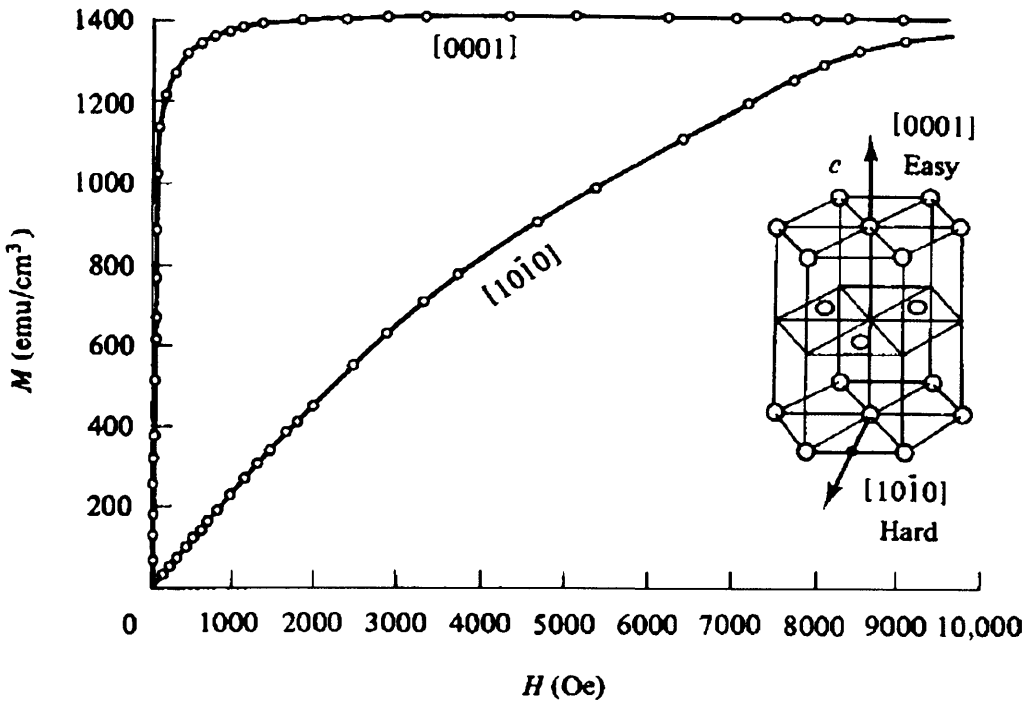

Fig. 7.2 M-H curves for cobalt on hard and easy axis of its hexagonal crystal lattice. Note the large difference in the initial permeability (slope) for easy and hard axis indicating high crystal anisotropy energy [1].

The expression for crystal anisotropy energy for a uniaxial anisotropy material is relatively simple as there is only one angle to be considered i.e. the angle between the easy axis and magnetisation.

$$E = K_0^{'} + K_1^{'} \cos^2\theta + K_2^{'} \cos^4\theta + \ldots\ldots \tag{7.2}$$

When cosθ is substituted with $(1\text{-}\sin^2\theta)^{0.5}$ and changing the constants in the above equation becomes [2]:

$$E = K_0 + K_1 \sin^2\theta + K_2 \sin^4\theta + \ldots\ldots \tag{7.3}$$

where K_0, K_1 and K_2 are anisotropic constants

when K_1 and K_2 are positive the axis making 0° is the easy axis, if K_1 and K_2 are negative then the easy axis makes 90° to the magnetisation.

7.1.2 Shape Anisotropy

Shape anisotropy is result of unequal demagnetising field along different directions. A shorter axis will have a higher demagnetising field than the larger axis hence the magnetisation is prefers to lie along a longer axis. A polycrystalline spherical magnetic sample will not have shape.

Shape anisotropy energy is given by the equation: [1]

$$E_{ShapeAnisotropy} = \frac{1}{2} M^2 N_c + \frac{1}{2}(N_a - N_c) M^2 \sin^2 \theta \tag{7.4}$$

where N_a and N_c are the demagnetising factors along the short and long axes of a geometry, respectively. Note that the above expression is similar to the uniaxial anisotropy expression in Eqn. 7.3. The shape anisotropy constant K_s is given by

$$K_S = \frac{1}{2}(N_a - N_c) M^2 \sin^2 \theta \tag{7.5}$$

When demagnetisation factors $N_a = N_c$, the shape anisotropy constant K_s is zero. A sphere has equal demagnetising factors along all axes hence the shape anisotropy constant K_s for a sphere is zero [1].

7.1.3 Stress Anisotropy

When stress is applied on a magnetised material it experiences a change in the magnetisation of the material (inverse magnetisation or Villari effect). A uniaxial stress can produce a unique easy axis of magnetisation if the stress is sufficient enough to overcome magnetocrystalline and shape anisotropy. Fig. 7.3 shows the magnetisation of Nickel at two applied stresses. Amount of magnetostriction of a single crystal material depends on the direction of magnetisation of the magnetic material. If additional strain is imposed by applying stress, the direction of magnetisation can be changed. The direction of magnetisation is now dependent on two factors, i.e.

magnetocrystalline anisotropy constant and mechanical stress σ. The energy expression for this combined effect is given by the equation below.

$$E = K_1(\alpha_1^2\alpha_2^2 + \alpha_2^2\alpha_3^2 + \alpha_3^2\alpha_1^2) - \frac{3}{2}\lambda_{100}\sigma(\alpha_1^2\gamma_1^2 + \alpha_2^2\gamma_2^2 + \alpha_3^2\gamma_3^2) - 3\lambda_{111}\sigma(\alpha_1\alpha_2\gamma_1\gamma_2 + \alpha_1\alpha_2\gamma_1\gamma_2 + \alpha_1\alpha_2\gamma_1\gamma_2) \quad (7.6)$$

where K_1 is the first anisotropy constant, α_1, α_2, α_3 are cosines of angles between magnetisation and 'a', 'b' and 'c' axes of the crystal lattice, γ_1, γ_2 and γ_3 are cosines of angles between the stress, σ and 'a', 'b' and 'c' axes of the crystal lattice.

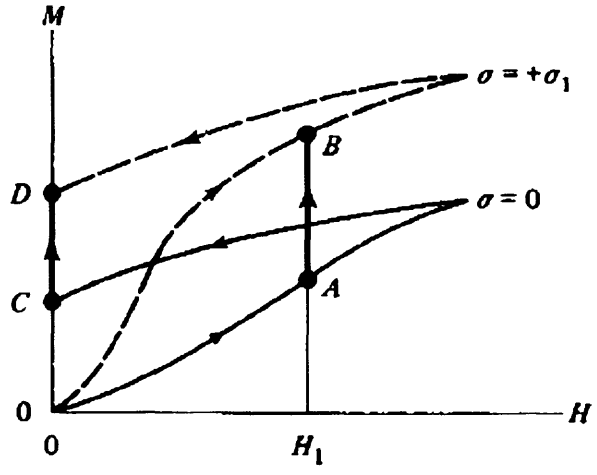

Fig.7.3 Change in the magnetisation of Nickel upon application of tensile stress. [1]

7.2 Magnetocrystalline Anisotropy in $Gd_5(Si_xGe_{1-x})_4$

$Gd_5(Si_xGe_{1-x})_4$ has orthorhombic crystal structure for all the compositions when the material is in ferromagnetic phase at lower temperatures as shown in Fig. 2. 9 [3]. At higher temperatures it is monoclinic for $0.41 \leq x \leq 0.57$, but orthorhombic for other compositions [4]. There are few publications in the literature on anisotropy study on $Gd_5(Si_xGe_{1-x})_4$. A previous anisotropy study carried out by Leib *et. al.* showed that $Gd_5Si_2Ge_2$ exhibits uniaxial anisotropy but this investigation was carried out by observation of MFM images and by measurement of hysteresis graphs along the

principal axes [100], [010] and [001] but not along [111] [5]. Measurement of magnetisation curves (M vs. H) along intermediate axes is important to determine if the material is uniaxial. Fig 7.4 (a), (b) and (c) shows hysteresis loop along 'a', 'b' and 'c' axis respectively. Based on the hysteresis loop measurements and MFM image observation it was concluded that 'b' is the easy axis and 'a' and 'c' are the hard axes; thus the orthorhombic crystal structure has a uniaxial anisotropy.

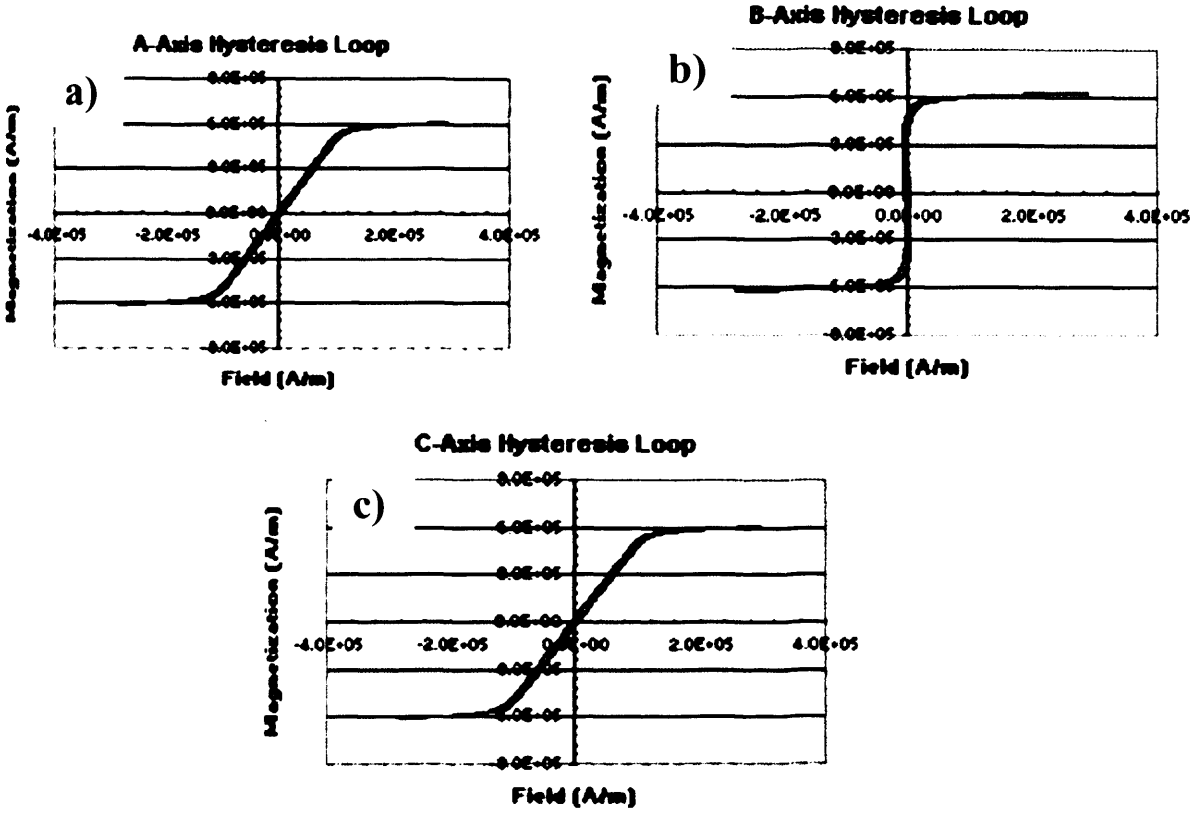

Fig 7.4 Hysteresis loop measurement on 'a', 'b' and 'c' axes of a single crystal $Gd_5Si_2Ge_2$ at 265 K when the sample is in ferromagnetic phase. [5]

MFM images of single crystal $Gd_5Si_2Ge_2$ at 260 K where taken on the principal axes; 'a', 'b' and 'c' as shown in Fig. 7.5 [5]. Rosette pattern in the MFM images is observed on the easy axis which can be seen in Fig 7.5 (b) and complete contrast of MFM image in Fig 7.5 (c) suggests that principal axis 'b' is the easy axis and 'c' is the hard axis. Fig 7.5 (a) has strip pattern in the MFM due to a significant angular change of 'b' axis with respect to 'ac' plane. To confirm this study magnetisation vs. angle of rotation and M vs. H measurements on single crystal $Gd_5Si_{2.7}Ge_{1.3}$ and

single crystal $Gd_5Si_{2.2}Ge_{1.8}$ samples were carried out in the present research and are discussed in detail in later sections.

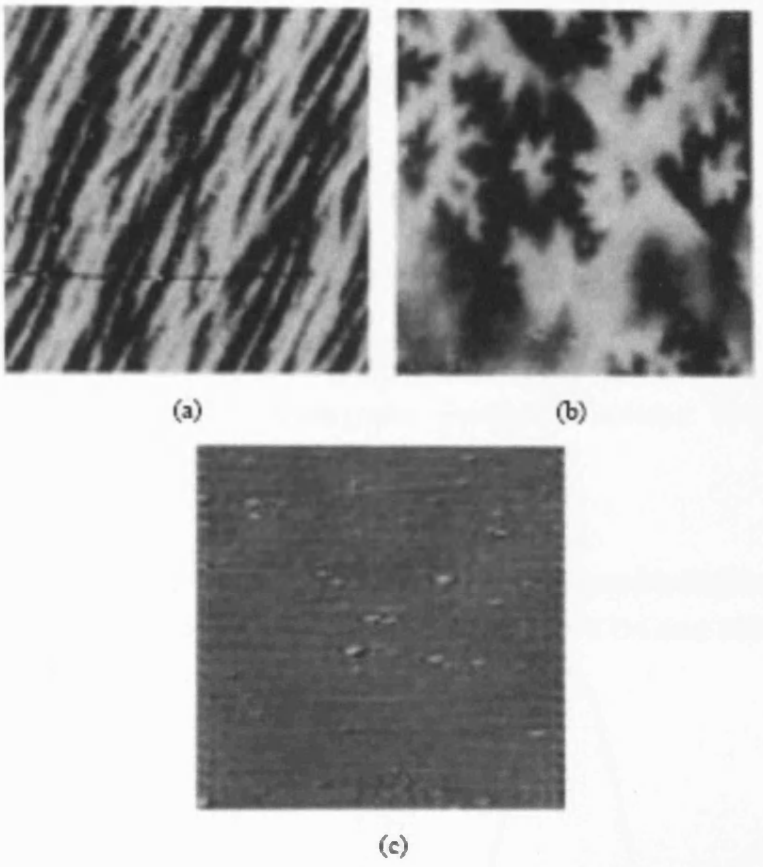

Fig 7.5 (a), (b) and (c) MFM images of a single crystal $Gd_5Si_2Ge_2$ at 260 K on principal axes 'a', 'b' and 'c' respectively when the sample is in ferromagnetic phase [5].

7.3 Determination of Magnetocrystalline Anisotropy of Single Crystal $Gd_5Si_{2.7}Ge_{1.3}$

Vibrating Sample Magnetometer (VSM) offers wide range of measurements from hysteresis loops to determination of anisotropy constants. The VSM (model 7410 by Lakeshore) used in the measurement below has high and low temperature capabilities using a thermostat and a furnace capability and can measure magnetic moment with an accuracy of 10^{-6} emu [6]. Magnetic moment as a function of the angle of rotation of sample and magnetic moment as a function of field was

measured to determine the magnetocrystalline anisotropy on single crystal $Gd_5Si_{2.7}Ge_{1.3}$ and single crystal $Gd_5Si_{2.2}Ge_{1.8}$ samples. It was seen from the measurements on single crystal $Gd_5Si_{2.2}Ge_{1.8}$ sample (Fig. 7.17- 7.19) that the shape anisotropy is more dominant than the magnetocrystalline anisotropy.

The single crystal $Gd_5Si_{2.7}Ge_{1.3}$ has a second order phase transition temperature of 310 K below which it is in ferromagnetic phase. A cubic sample with the side of 1.5×10^{-3} m was glued to the bottom of the sample holding rod with principal axis in line with the rod. The shape anisotropy in this sample was negligible compared to its magnetocrystalline anisotropy. The measurements were carried out at room temperature of 300 K ±1 K.

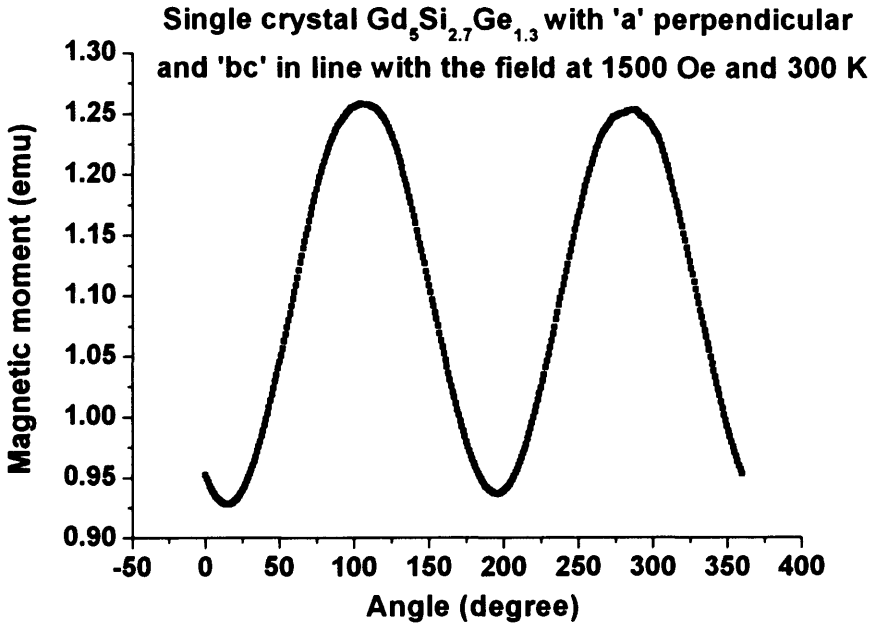

Fig 7.6 Magnetic moment vs. angle of rotation of 'bc' plane at an applied field of 1500 Oe ($1.2\text{x}10^5$ A/m) with axis 'c' being approximately at 0°. The ratio of magnetic moments m_b/m_c is 1.35.

Magnetic moment as a function of angle of rotation of single crystal $Gd_5Si_{2.7}Ge_{1.3}$ was measured as shown in Fig 7.6. Magnetic field of 1500 Oe was applied on the 'bc' plane of the

sample with axis 'c' in line with the field. This value for the field was chosen because the single crystal $Gd_5Si_{2.7}Ge_{1.3}$ starts to saturate close to this field at which the difference in the magnetic moment at different axes is the highest as shown in Fig. 7.7. The peak of the curve in Fig. 7.6 corresponds to axis 'b' and trough of the curve corresponds to axis 'c'. The ratio of magnetic moment at 'b' axis to the magnetic moment at 'c' axis is 1.35 which indicated that 'b' is easy compared to 'c'. Fig 7.7 shows M vs. H measurement of 'bc' plane of single crystal $Gd_5Si_{2.7}Ge_{1.3}$ for various angles of rotation of the plane. It can be seen that angles 0°, 180° and 360° curves have lower slope and low magnetic moment compared to 90° and 270° again confirming that 'b' axis is easy compared to 'c' axes.

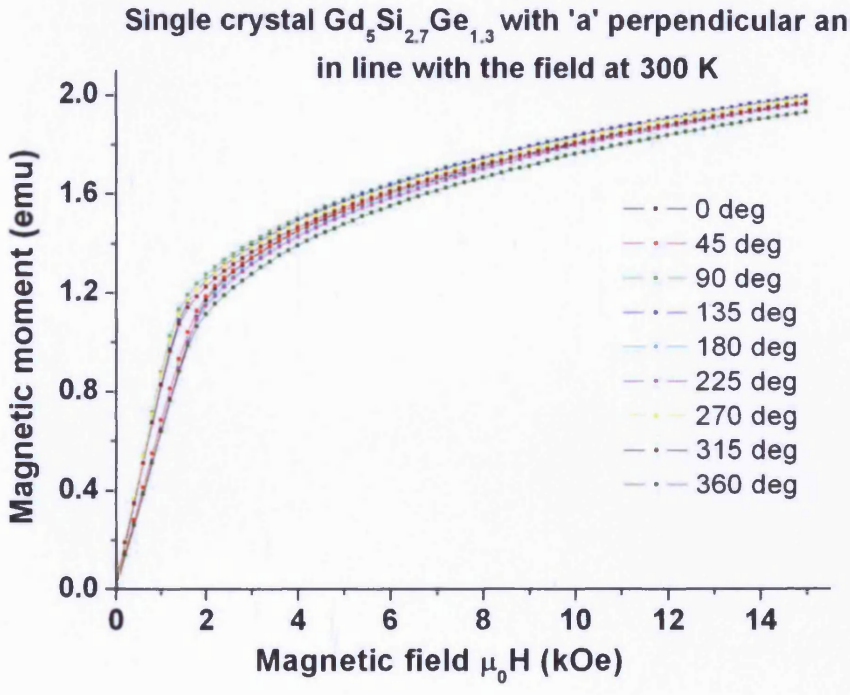

Fig. 7.7 Magnetic moment as a function of magnetic field on 'bc' axis of single crystal $Gd_5Si_{2.7}Ge_{1.3}$ for various rotation of the plane.

Magnetic moment as a function of angle of rotation of single crystal $Gd_5Si_{2.7}Ge_{1.3}$ was measured as shown in Fig 7.8 with a magnetic field of 1500 Oe applied on the 'ab' plane of the sample with axis 'a' in line with the field. It can be seen the peak of the curve corresponds to 'b' axis and trough of the curve corresponds to 'a' axis.

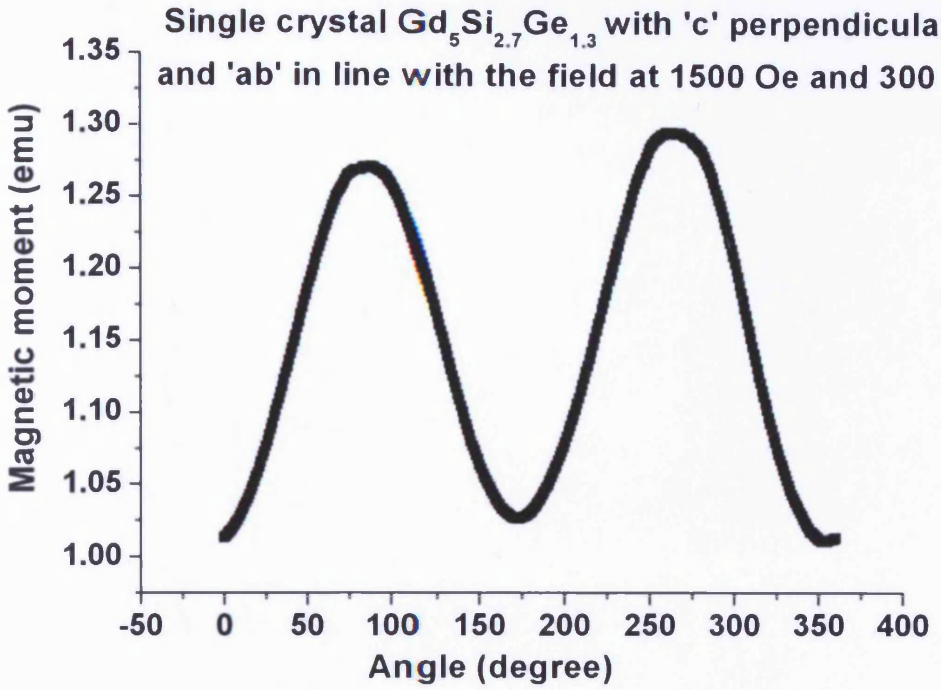

Fig. 7.8 Magnetic moment vs. angle of rotation of 'ab' plane of the single crystal $Gd_5Si_{2.7}Ge_{1.3}$ sample at 300 K with an applied field of 1500 Oe ($1.2x10^5$ A/m). The ratio of magnetic moments m_b/m_a is 1.28

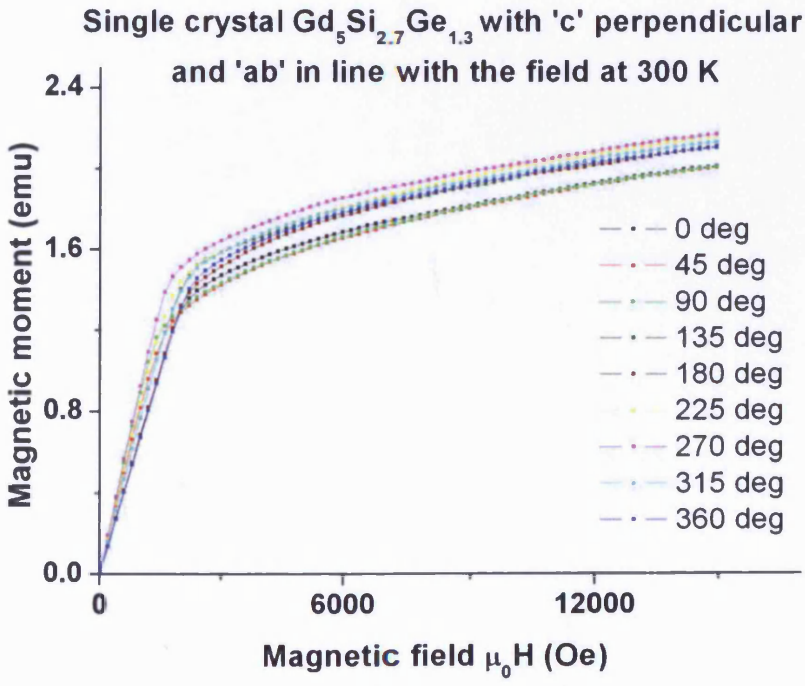

Fig. 7.9 Magnetic moment vs. magnetic field on 'ab' plane of the single crystal $Gd_5Si_{2.7}Ge_{1.3}$ sample at 300 K for various rotations of the plane starting with axis 'c' being approximately at 0°.

The ratio of magnetic moment at 'b' axis to the magnetic moment at 'a' axis is 1.28. Fig 7.9 shows M-H curves on 'ab' plane of single crystal $Gd_5Si_{2.7}Ge_{1.3}$ with 'a' axis in line with the field for various rotations of 'ab' plane. It can be seen in Fig. 7.9 that 0°, 180° and 360° have lower magnetic moment and lower susceptibility while 90° and 270° have higher magnetic moment and higher susceptibility indicating 'b' axis is the easy axis compared to 'a' axis.

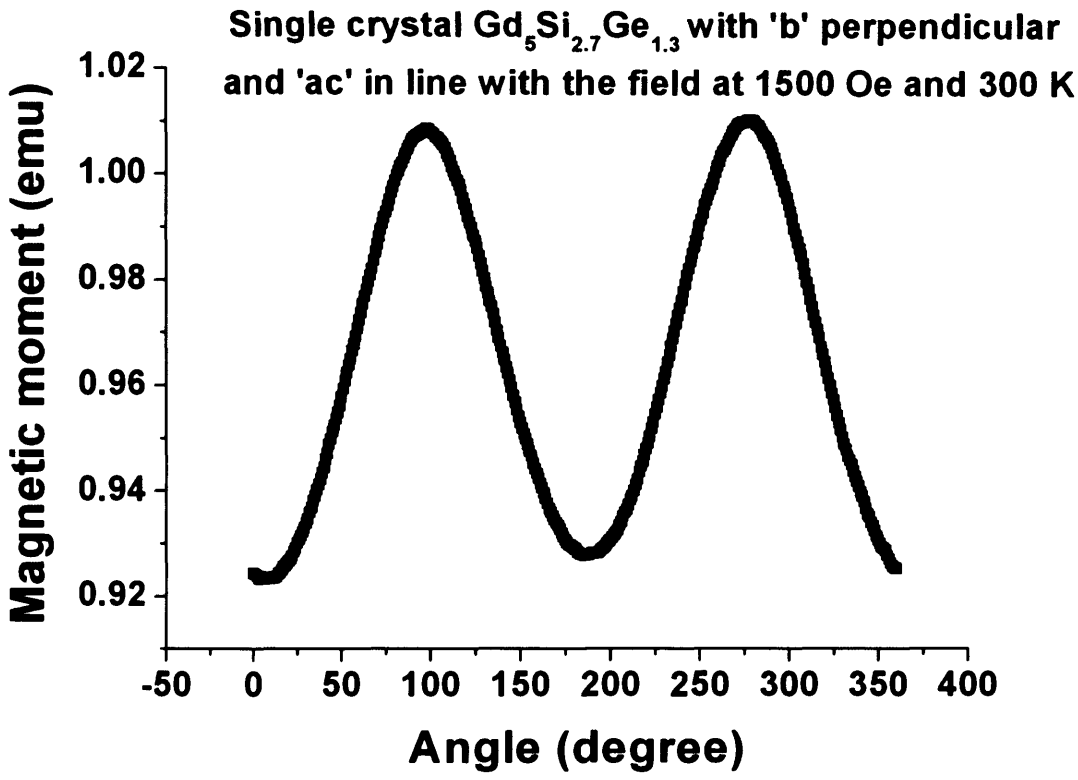

Fig. 7.10 Magnetic moment vs. angle of rotation on 'ac' plane of a single crystal $Gd_5Si_{2.7}Ge_{1.3}$ with 'c' axis inline with the field ('c'=0°). The ratio of magnetic moments m_a/m_c is 1.06

Similar measurements were carried out on 'ac' plane. It was noted that a small difference in the magnetic moment of 'a' and 'c' axes with a ratio of magnetic moment of 'a' to the magnetic moment of 'c' being 1.06 (Fig. 7.10) suggesting that both 'a' and 'c' axes are equally hard axes of the orthorhombic crystal structure. It can also be seen in the M vs. H measurements (Fig. 7.11) that for various orientations of the 'ac' plane the slope (susceptibility) and the magnetic moment are nearly same indicating that both 'a' and 'c' axes are hard axes.

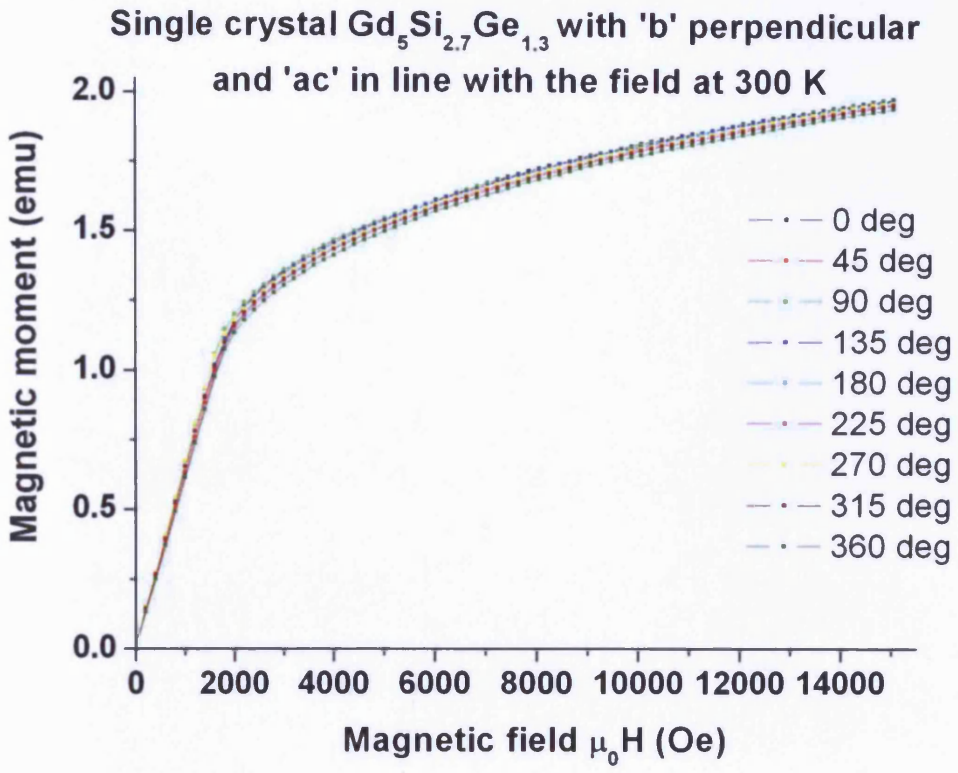

Fig. 7.11 M-H measurement on 'ac' plane of a single crystal $Gd_5Si_{2.7}Ge_{1.3}$ for various orientations at 300 K.

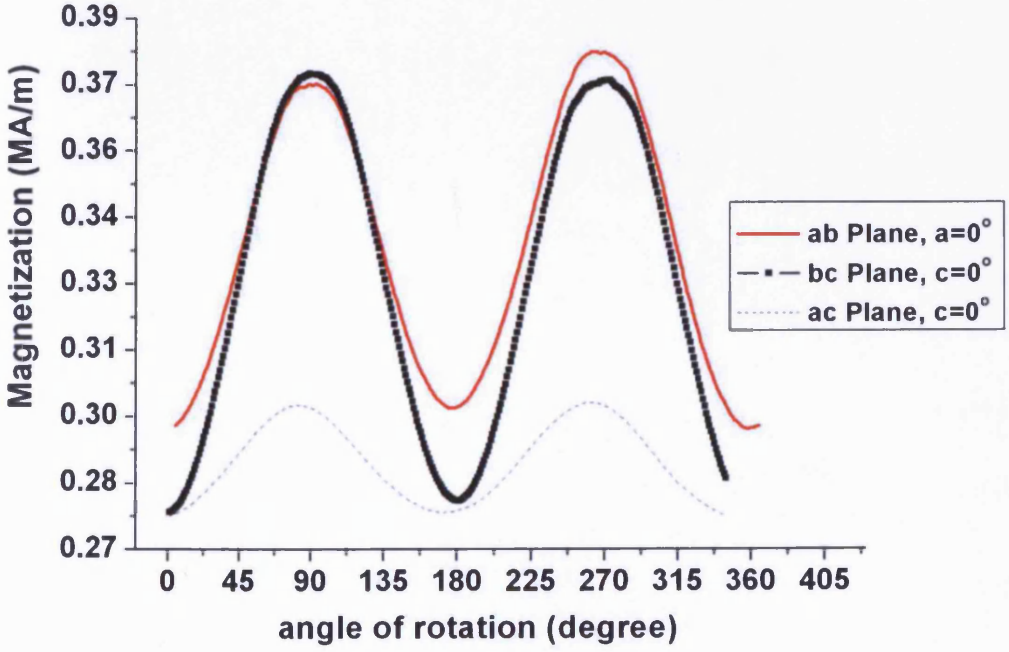

Fig. 7.12 Magnetic moment vs. angle of rotation on 'ab', 'bc' and 'ca' planes at an applied magnetic field of 1500 Oe ($1.2x10^5$ A/m)at 300 K.

When magnetic moment vs. angle of rotation measurements at 1500 Oe (1.2×10^5 A/m) on 'ab', 'bc' and 'ca' planes are plotted in a single graph (Fig. 7.12), it is clear that 'b' is the easy axis and 'a' and 'c' are the hard axes. The magnetic moment of 'a' is slightly higher than 'c' axis which might be due to some misalignment in the installation of the sample on the vibrating rod in the VSM. With these measurements it can be concluded that the orthorhombic structure in $Gd_5(Si_xGe_{1-x})_4$ has a uniaxial anisotropy without looking at measurements on other diagonal planes such as [111], [110], [101] and [011]. If any one of these diagonal planes were had higher susceptibility it would have been seen in the measurements on 'ab', 'bc' and 'ca' planes. Orthorhombic lattice may exhibit uniaxial anisotropy for all values of x at lower temperatures when the magnetic phase is ferromagnetic as all compositions have a common Gd_5Si_4 type orthorhombic structure in ferromagnetic phase.

Fig. 7.13 shows the measurement on 'bc' plane of single crystal $Gd_5Si_{2.7}Ge_{1.3}$ for various applied magnetic fields indicating that with an applied field of 1500 Oe (1.2×10^5 A/m) the difference in the magnetic moments of 'b' and 'c' axes is maximum confirming the selection of the applied field of 1500 Oe (1.2×10^5 A/m) for magnetic moment vs. angle of rotation measurements.

To determine the uniaxial anisotropy constant of the single crystal $Gd_5Si_{2.7}Ge_{1.3}$, anisotropy energy was calculated using the magnetic moment using the expression $E= \mu_0 MH$ for all the angles and was plotted against angle of rotation as shown in Fig. 7.14. It was then fitted to the uniaxial anisotropy energy expression which is shown in Eqn. 7.3. The curve was fitted up to second order terms and the higher order term were ignored. It was determined that the uniaxial magnetocrystalline anisotropy constant K_1 for a single crystal $Gd_5Si_{2.7}Ge_{1.3}$ at 300 K was 1.45×10^4 J/m^3 which is of the same order of magnitude compare with the previous report of magnetocrystalline anisotropy constant of single crystal $Gd_5Si_2Ge_2$ by Leib *et. al* [5].

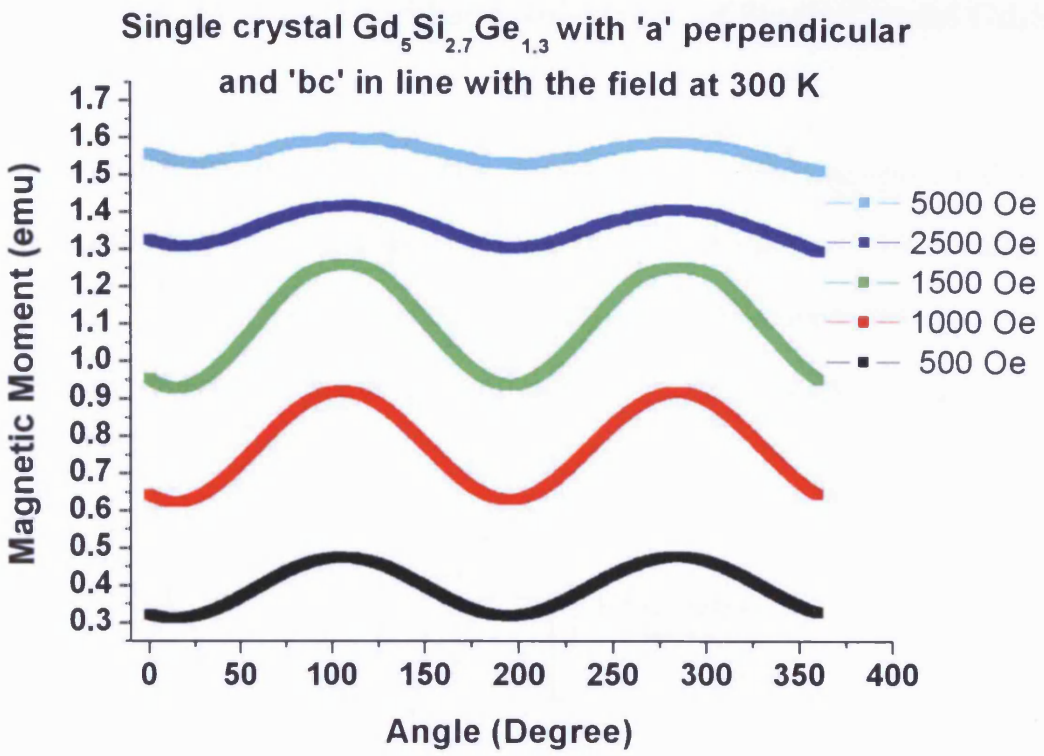

Fig. 7.13 Magnetic moment vs. angle of rotation on 'bc' plane with different applied magnetic fields at 300 K.

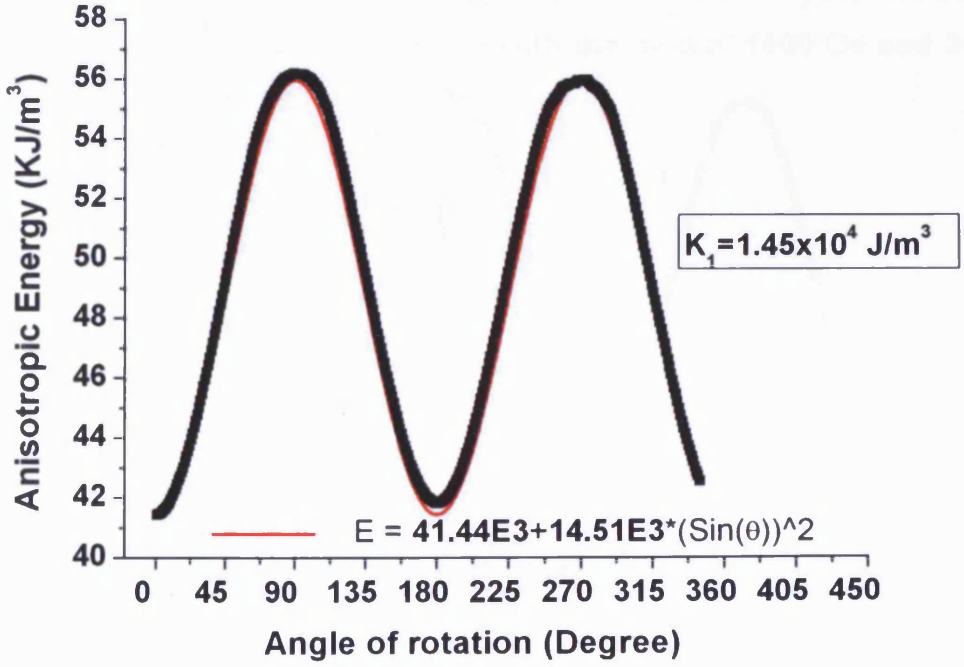

Fig. 7.14 Uniaxial magnetocrystalline anisotropy obtained by fitting the anisotropy energy equation to the magnetocrystalline anisotropy energy vs. angle of rotation curve on 'bc' plane.

7.4 Magnetocrystalline and Shape Anisotropy of Single Crystal $Gd_5Si_{2.2}Ge_{1.8}$

A single crystal $Gd_5Si_{2.2}Ge_{1.8}$ sample was also investigated for magnetocrystalline and shape anisotropy at 300 K. The sample has a phase transition temperature of 305 K at an applied field of 100 Oe (8×10^3 A/m). The sample was cut in a cuboid shape with dimensions 3.35 × 2.0 ×2.8 mm and was indexed with back scattered x-ray diffraction technique as shown in Fig 7.15.

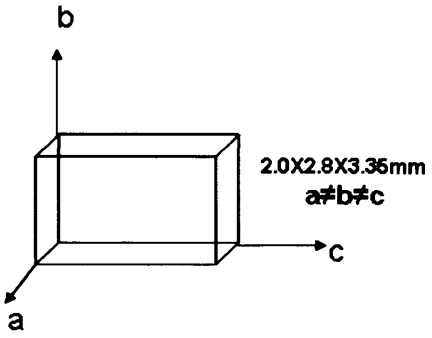

Fig. 7.15 Single crystal $Gd_5Si_{2.2}Ge_{1.8}$ sample shape, dimension and lattice orientation

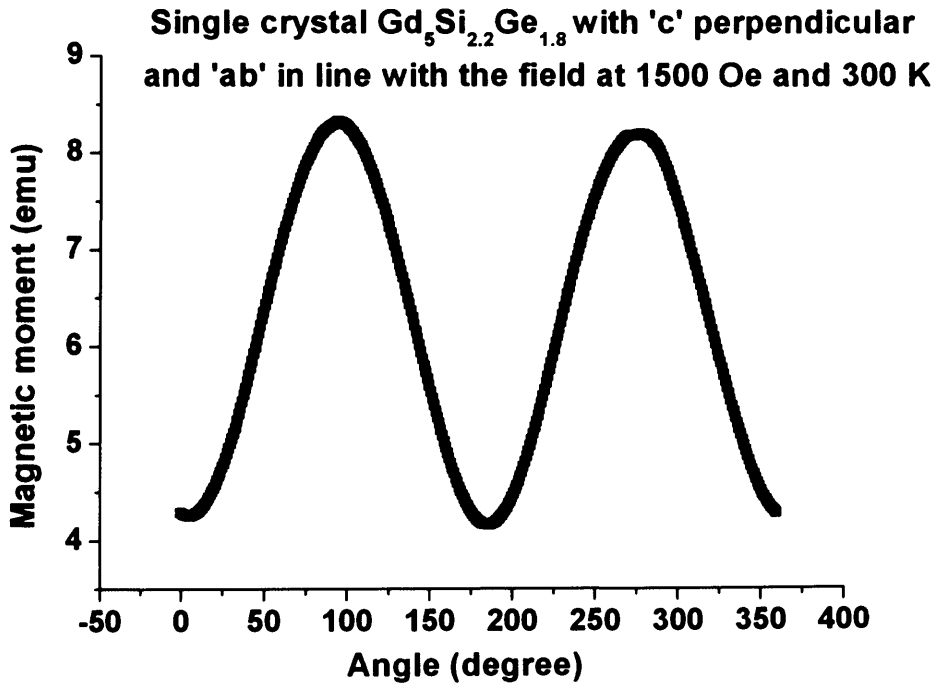

Fig. 7.16 Magnetic moment as a function of angle of rotation on 'ab' plane with 'a' =0° of the single crystal $Gd_5Si_{2.2}Ge_{1.8}$ sample at 300 K. The ratio of magnetic moment m_b/m_a= 1.95.

Magnetic moment as a function of angle of rotation of the sample and magnetic moment as a function of magnetic field measurements were also carried in the Vibration Sample Magnetometer (VSM). Fig. 7.16 shows the magnetic moment vs. angle of rotation at an applied field of 1500 Oe and 300 K. The ratio of magnetic moment of peak to trough (moment of the sample when 'a'=0° to the moment when 'b'=0°) was 1.95 indicating that 'b' is easy axis and 'a' is the hard axis.

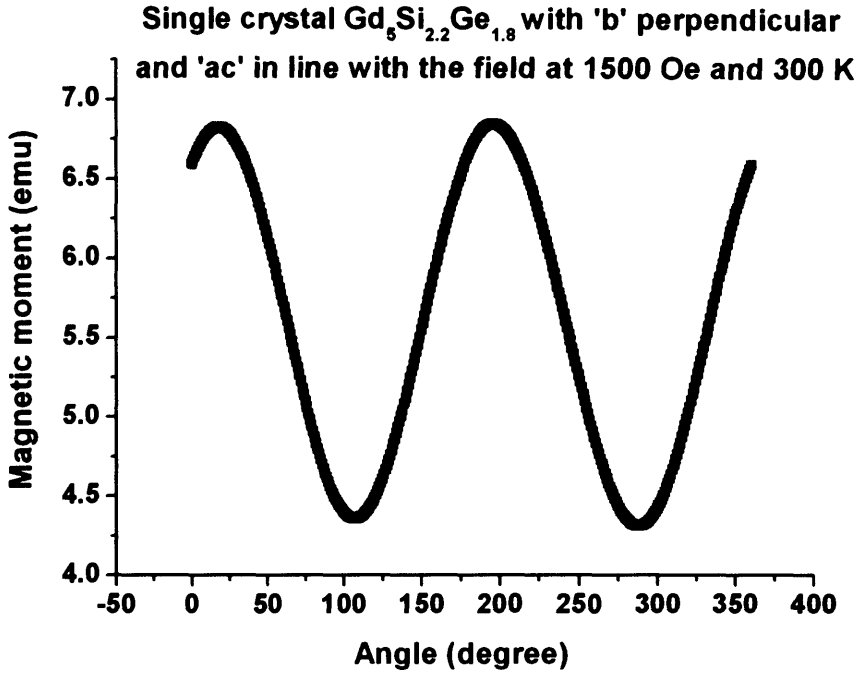

Fig. 7.17 Magnetic moment as a function of angle of rotation on 'ac' plane with 'c' ≈ 0° of the single crystal $Gd_5Si_{2.2}Ge_{1.8}$ sample at an applied field of 1500 Oe ($1.2x10^5$ A/m) and at 300 K. The ratio of magnetic moment m_c/m_a= 1.61.

Magnetic moment as a function of angle of rotation at 300 K with an applied field of 1500 Oe on the same single crystal $Gd_5Si_{2.2}Ge_{1.8}$ sample with 'ac' plane in line with the field was carried out as shown in Fig. 7.17. Same measurement was carried out when 'bc' plane was in line with the field shown in Fig. 7.18. The ratio of magnetic moment of peak to trough was calculated in both the cases. It was found that the ratio of magnetic moment of 'a' to 'c' axis was 1.61 whilst that of 'b' to 'c' was 1.28 which is also evident in Fig. 7.19. Magnetic moment of 'c' is still smaller than the moment of 'b' but ratio of 'c' to 'a' is larger than ratio of 'b' to 'c'.

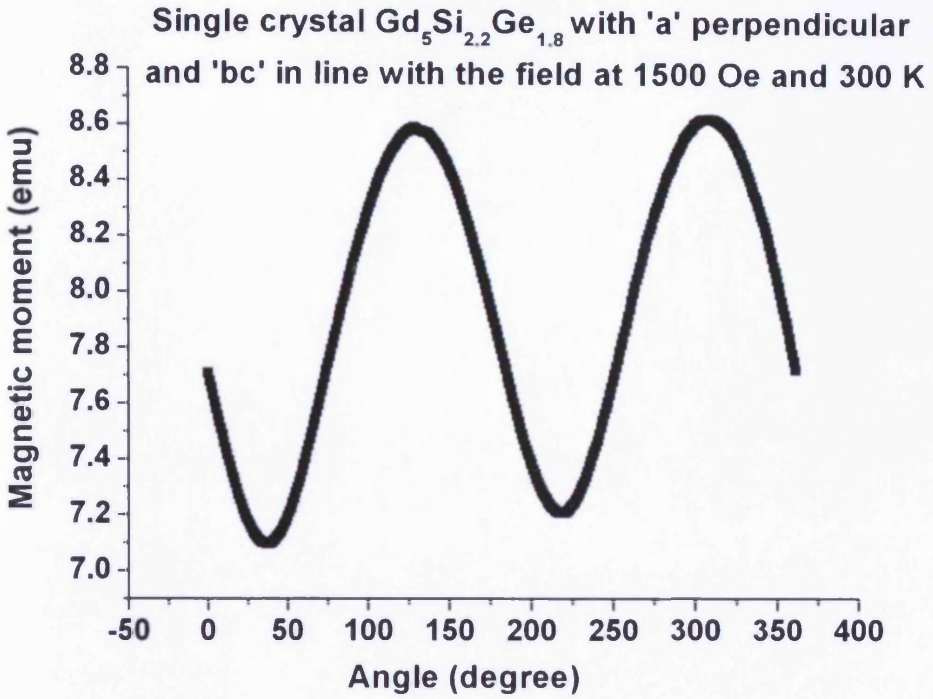

Fig. 7.18 Magnetic moment as a function of angle of rotation on 'bc' plane of the single crystal $Gd_5Si_{2.2}Ge_{1.8}$ sample at 300 K. The ratio of magnetic moment m_b/m_c= 1.28.

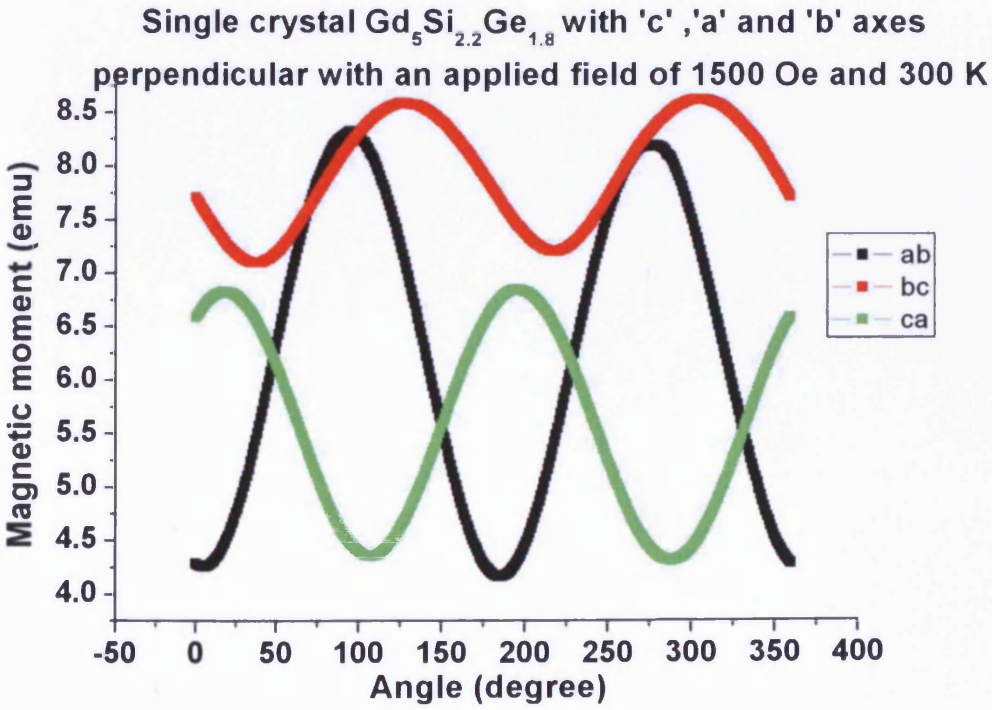

Fig. 7.19 Magnetic moment as a function of angle of rotation on 'ab', 'bc' and 'ca' planes of the single crystal $Gd_5Si_{2.2}Ge_{1.8}$ sample at an applied field of 1500 Oe ($1.2x10^5$ A/m) and at 300 K.

This in due to shape anisotropy in the sample. Since the shape of the sample is not a sphere, and the length of the sample representing 'c' axis is longer than the breadth and height of the sample it will exhibit a shape anisotropy. The shape anisotropy is smaller than the magnetocrystalline anisotropy hence we see that the magnetic moment of 'b' is still larger than 'c' axis. Fig. 7.20 shows the magnetic moment vs. angle of rotation for 'ab' plane at various applied magnetic fields and it can be seen that at 1500 Oe the difference in the moments between that planes is the largest.

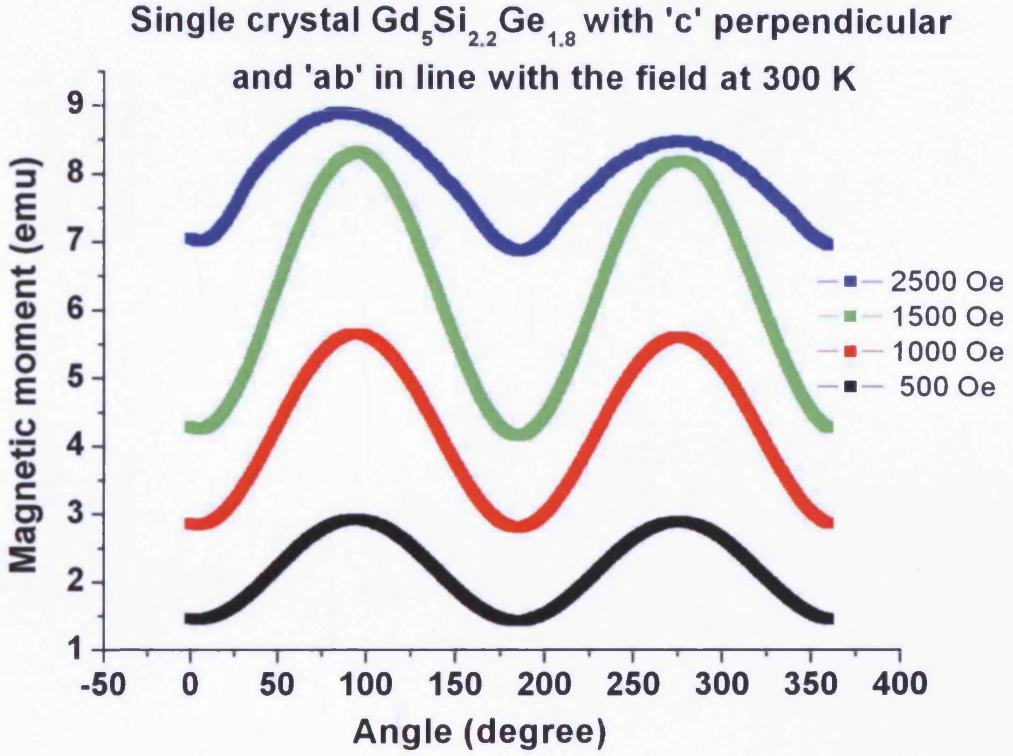

Fig. 7.20 Magnetic moment as a function of angle of rotation on 'ab' plane with 'a' =0° of the single crystal $Gd_5Si_{2.2}Ge_{1.8}$ sample at 300 K.

7.5 Dependence of Curie Temperature on Angle of Rotation of Samples

$Gd_5(Si_xGe_{1-x})_4$ exhibits uniaxial magnetocrystalline anisotropy with the anisotropy constant K_1 for a single crystal $Gd_5Si_{2.7}Ge_{1.3}$ at 300 K equal to 1.45×10^4 J/m^3 as discussed in the previous section

and the anisotropy constant K_1 for a single crystal $Gd_5Si_2Ge_2$ equal to 4×10^4 J/m^3 as shown by Leib *et. al.* [5]. It was important to investigate if the magnetocrystalline anisotropy influences the field induced first order phase transition temperature as the transition temperature of $Gd_5(Si_xGe_{1-x})_4$ varies with the amount of field applied on the sample. In fact if a sufficient field is applied it induces a field induced structural-magnetic phase transition. The transition temperature increases with increase in the applied magnetic field with a rate of 5 K/Tesla [7, 8, 9, 10].

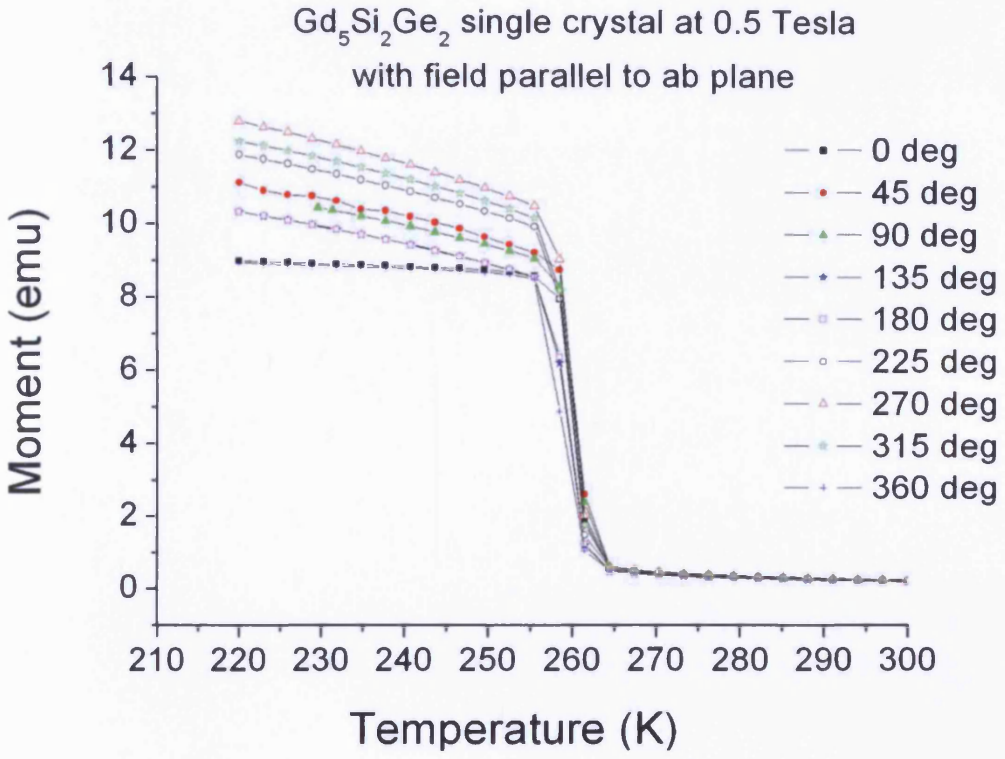

Fig. 7.21 Magnetic moment as a function of temperature measurement on a single crystal $Gd_5Si_2Ge_2$ sample with its 'ab' plane in line with the applied magnetic field of 0.5 Tesla for various orientations of the sample.

A single crystal $Gd_5Si_2Ge_2$ was cut in a disc shape with a diameter of 3×10^{-3} m and a height of 2×10^{-3} m. The 'c' axis was aligned perpendicular to the field and 'ab' plane in line with the field. The sample was glued with varnish to the Vibrating Sample Magnetometer's rod. A cryostat was installed to enable VSM to go to lower temperatures. Measurements of magnetic moment as a function of temperature were carried out for various sample rotations with the applied field of

0.5 Tesla as shown in Fig 7.21. It can be observed that there is no significant change in the first order phase transition temperature of the sample which occurs at 265 K as expected for this composition. The variation of magnetic moment at lower temperatures below 265 K is due to the magnetocrystalline/shape anisotropy of the sample. It is also seen in Fig. 7.21 that the 0 deg. and 180 deg. lines do not coincide which is due to a slight lilt on the samples face that is glued to the vibrating sample magnetometer rod.

Similar measurements were carried out on the same sample for various orientations with an applied field of 1 Tesla. Fig. 7.22 shows the measurement with a temperature range of 220 to 300 K. It can be seen from the figure that there is no significant change in the transition temperature (265 K) of the sample for different orientations of the sample with the field. It can also be noted that magnetisation of the ferromagnetic phase at low temperatures at an applied field of 0.5 Tesla shows higher variation for different orientations than when 1 Tesla field is applied.

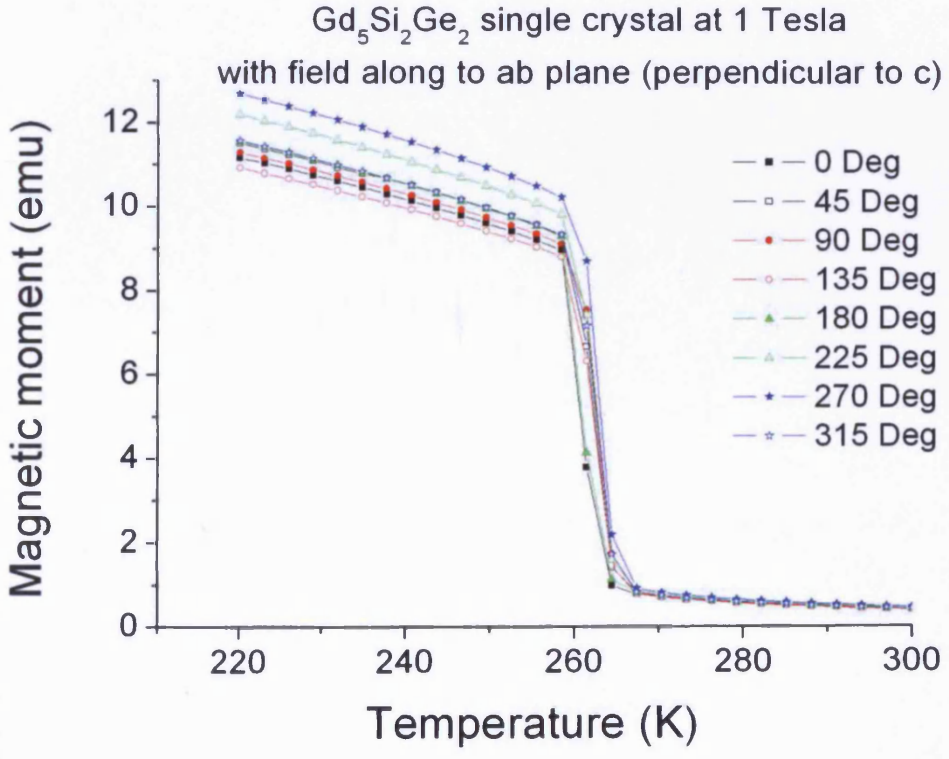

Fig. 7.22 Magnetic moment vs. temperature on a single crystal $Gd_5Si_2Ge_2$ with its 'ab' plane in line with the applied magnetic field of 1 Tesla for various orientations of the sample.

7.6 Summary

Various types of anisotropy were explained and a literature review on magnetocrystalline anisotropy in $Gd_5(Si_xGe_{1-x})_4$ was carried out. First order magnetocrystalline anisotropy constant K_1 easy and hard axes of the single crystal $Gd_5Si_{2.7}Ge_{1.3}$ sample were determined using magnetic moment as a function of angle of rotation of the sample at room temperature. Dependence of the first order phase transition temperature on the angle of rotation of the single crystal $Gd_5Si_2Ge_2$ sample was determined to be negligible.

References

[1] B. D. Cullity, Introduction to Magnetic Materials, Addison-Wesley Publishing Company, pp. 209, (1972).

[2] S. Chikazumi, Physics of Ferromagnetism, Oxford Science Publications, pp.250, (1997).

[3] Ya. Mudryk, Y. Lee, T. Vogt, K. A. Gschneidner, Jr., and V. K. Pecharsky, *"Polymorphism of $Gd_5Si_2Ge_2$: The equivalence of temperature, magnetic field, and chemical and hydrostatic pressures"*, Phys. Rev. B, **71**, pp. 174104, (2005).

[4] J. Leib, J. E. Snyder, T. A. Lograsso, D. Schlagel and D. C. Jiles, "*Dynamics of the magnetic field-induced first order magnetic-structural phase transformation of $Gd_5(Si_{0.5}Ge_{0.5})_4$*", J. App. Phys., **95**, pp. 6914-6915, (2004).

[5] J. S. Leib, C. C. H. Lo, J. E. Snyder, D. C. Jiles, V. K. Pecharsky, D. S. Schlagel, and T. A. Lograsso, "*Magnetic Force Microscopy Characterization of Unusual Magnetic Coupling in an Extraordinarily Responsive Magnetic Material*", IEEE Trans Magn, **38**, pp. 2447-2449, (2002).

[6] Lakeshore Ltd., Model 7400 VSM Hardware Reference Manual, Revision 1.0, **P/N 119-603,** September (2006).

[7] C. Magen, L. Morellon, P. A. Algarabel, M. R. Ibarra, Z. Arnold, J. Kamarad, T. A. Lograsso, D. L. Schlage V. K. Pecharsky, A. O. Tsokol, and K. A. Gschneidner, Jr.,

"*Hydrostatic pressure control of the magnetostructural phase transition in $Gd_5Si_2Ge_2$ single crystals*" Phys. Rev. B, **72**, pp. 024416, (2005).

[8] E. M. Levin, V. K. Pecharsky, K. A. Gschneidner Jr. and P. Tomlinson, "*Magnetic field and temperature-induced first-order transition in $Gd_5(Si_{1.5}Ge_{2.5})$: a study of the electrical resistance behaviour*". J. Magn. Magn. Mater, **210**, pp. 181-188, (2000).

[9] H. Tang, V. K. Pecharsky, G. D. Samolyuk, M. Zou, K. A. Gschneidner, Jr., V. P. Antropov, D. L. Schlagel, and T. A. Lograsso, "*Anisotropy of the Magnetoresistance in $Gd_5Si_2Ge_2$*" Phys. Rev. Lett., **93**, pp. 237203, (2004).

[10] E. M. Levin, V. K. Pecharsky and K. A. Gschneidner Jr. "*Transformations in the $Gd_5(Si_{1.95}Ge_{2.05})$ alloy induced by the temperature and magnetic-field cycling through the first-order magnetic-martensitic phase transition*" Phys. Rev. B, **63**, pp. 064426, (2001).

Chapter 8: Conclusions and Future Work

8.1 Conclusions

First order and second order phase transitions, magnetoresistance, magnetostriction and magnetocrystalline anisotropy of $Gd_5(Si_xGe_{1-x})_4$ have been extensively researched and the results have been published in various leading international journals or presented in major magnetics conferences. The project has revealed unusual behaviour in the properties of the material, and has provided better analytical tools for the future research on $Gd_5(Si_xGe_{1-x})_4$ and other magnetocaloric materials and has provided the necessary explanation of behaviour such as irreversible resistance changes. The major results of this thesis were as follows:

- Various methods of measurement of second order phase transition temperature were compared and it was concluded that the Arrott plot technique was the best method of determination of the second order phase transition temperature. A more advanced technique based on the Arrott plots was developed to estimate the second order phase transition temperature of the orthorhombic phase of $Gd_5(Si_xGe_{1-x})_4$ when it is suppressed by the first order phase transition. The Arrott plot technique was also extended to determine the transition temperature of individual phases in the mixed phase of $Gd_5(Si_xGe_{1-x})_4$.

- The field induced first order phase transition was examined at various fields strengths and the change of transition temperature with respect to the applied field was confirmed to be 5 K per Tesla.

- Magnetostriction measurements were carried out on various compositions and fine structure was observed in magnetostriction for the composition $Gd_5Si_{1.95}Ge_{2.05}$ ($x=0.475$) for both single and polycrystalline samples, but not on the other measured compositions.

- A giant thermally induced strain/ magnetostriction was obtained for the polycrystalline $Gd_5Si_{2.09}Ge_{1.91}$ sample by varying the temperature using a Peltier cell. This removed the need for bulky equipment such as PPMS (Physical Properties Measurement System) to induce the first order phase transition and obtain a giant magnetostriction.

- Electrical transport properties of single and polycrystalline $Gd_5(Si_xGe_{1-x})_4$ samples were measured. Irreversible increase in the resistivity was observed when the samples were thermally cycled through the first order phase transition temperature. The irreversible change in coercivity of $Gd_5(Si_xGe_{1-x})_4$ samples were also observed when the sample was thermally cycled through the first order phase transition temperature.

- A theoretical model was developed to explain the recovery in irreversible resistivity in the samples that were cycled through the first order phase transition. This was experimentally verified by holding the samples at higher temperatures for a longer period of time and comparing the results with the predictions of the theory.

- The magnetocrystalline anisotropy constant, K_1 was determined to be $1.45x10^4$ J/m^3 for the composition $Gd_5Si_{2.7}Ge_{1.3}$. The easy axis was determined for the same sample to be the 'b' and the hard axes were determined to be 'a' and 'c'. The dependence of orientation of the sample with respect to the applied magnetic field on the transition temperature was determined to be negligible.

- Additionally in collaboration with the Materials and Metallurgy Department of the Birmingham University, UK, polycrystalline samples of $Gd_5Si_{1.8}Ge_{2.2}$ (x=0.45) and

$Gd_5Si_{1.9}Ge_{2.1}$ (x=0.475) have been prepared by arc-melting method. XRD measurements were carried out confirming the crystal structure of these samples.

- Heat treatment was carried out on the samples prepared at Birmingham University to obtain a single phase in the material which was tested using magnetic moment vs. temperature measurements.

- High field measurements were carried out at the Department of Engineering Materials of The University of Sheffield to test the Arrott plots.

8.2 Future Work Recommendations

The following future work can be recommended on $Gd_5(Si_xGe_{1-x})_4$ or on other magnetocaloric materials.

- Device development is crucial to demonstrate the feasibility of magnetic refrigeration. Although $Gd_5(Si_xGe_{1-x})_4$ exhibits one of the largest magnetocaloric effect, there have not been any devices built with this material except one attempt by using particles of $Gd_5(Si_xGe_{1-x})_4$ by Lu *et. al.*

- In order to utilise the magnetocaloric effect in a magnetic refrigerator it is important to have the knowledge of thermal conductivity of giant magnetocaloric materials which until now has not been reported in the literature or at conferences.

- The giant magnetocaloric effect is not widely studied in thin films and nano structures which might show interesting and promising properties for various refrigeration applications such as micro cooling in integrated circuits/microchips.

- The effect of cycling the material through the first order phase transition shows irreversible effects such as irreversible increase in resistivity and coercivity. This effect has not been reported so far in the adiabatic temperature or isothermal entropy changes which are important to investigate for the reliability of the magnetic refrigerator over longer life span.

- Although $Gd_5(Si_xGe_{1-x})_4$ exhibits a colossal magnetostriction/thermally induced strain of about 10,000 ppm along 'a' axis, there are few reports on its applications. Application study utilising the colossal strain for sensors and actuators might yield high performance sensor and actuator devices.

Appendix

Appendix I

A1.1 Polycrystalline Sample Preparation by Arc-Melting

Polycrystalline samples of composition $Gd_5Si_{1.8}Ge_{2.2}$ and $Gd_5Si_{1.9}Ge_{2.1}$ were prepared in the Materials and Metallurgy Department of the University of Birmingham by arc-melting. Procedures stated below were followed to prepare the samples:

1. Stoichiometric mass of 99.95% pure Gd, 99.99999% pure Si, and 99.99999% pure Ge was measured.

2. Gd, Si and Ge are put into the crucible together and purged with argon gas several times in order to vent out all the oxygen present in the crucible.

3. The arc is used to first melt gadolinium metal and the molten metal is allowed to surround silicon and germanium pieces. If the arc is passed to silicon and germanium pieces directly then the spluttering of germanium and silicon occurs.

4. Once all the constituents are melted the molten liquid is turned upside down (stirred) several times to ensure the homogeneity of the material.

5. Since the vapour pressure of germanium is higher than gadolinium and slightly higher than silicon small amount of germanium is vaporised during the process. In order to account for this loss 2% more germanium should be added.

6. The compositions have to be examined by the XRD measurement to ensure the constituents lattice structure is as expected.

The binary phase diagrams of Gd -Si and Gd-Ge are shown in the Fig. A1.1 and A1.2 respectively.

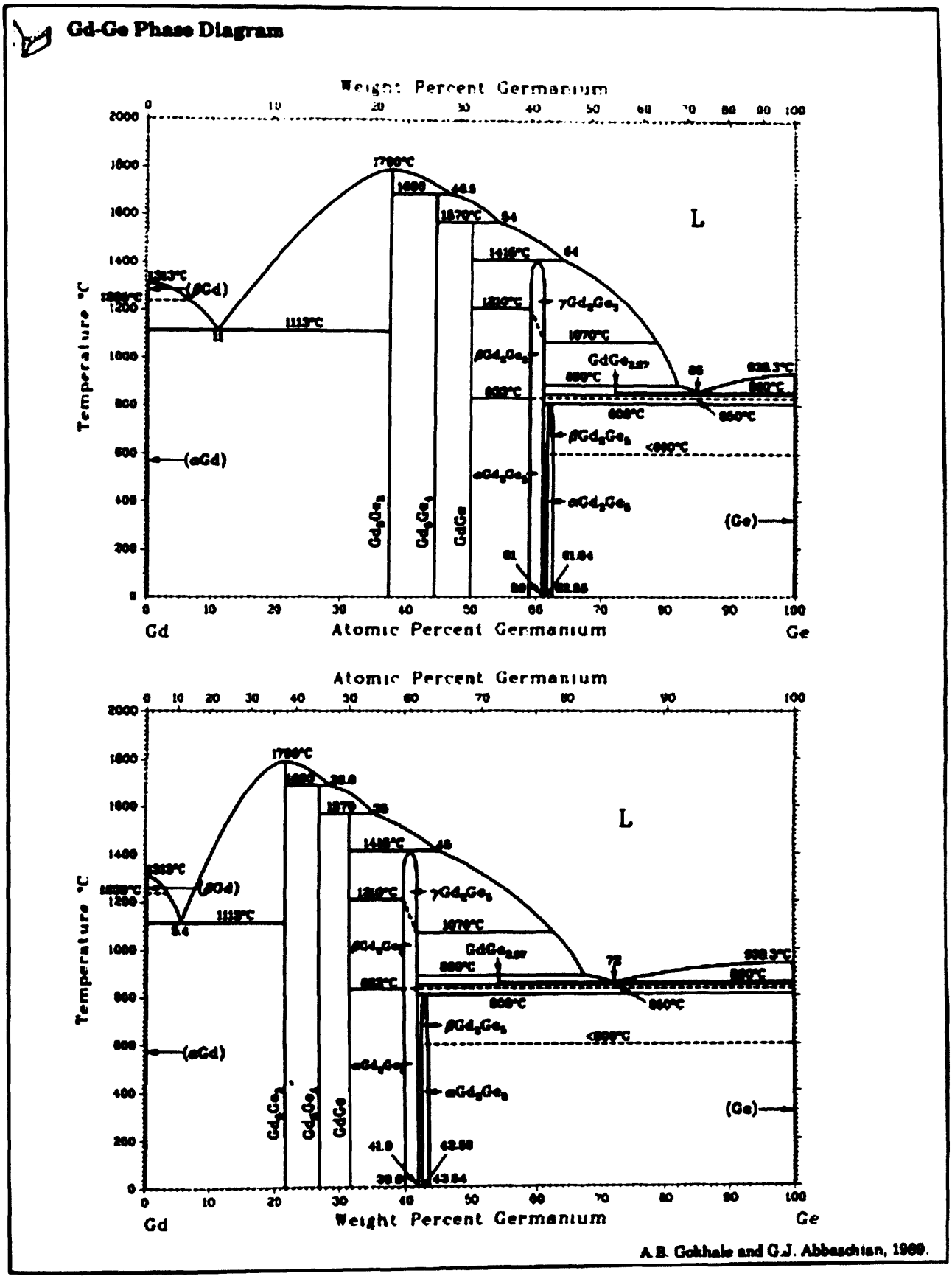

Fig. A1.1 Binary phase diagram of Gd and Ge in both weight percentage and atomic percentage.

Note that Gd_5Ge_4 has a narrow area in the phase diagram.

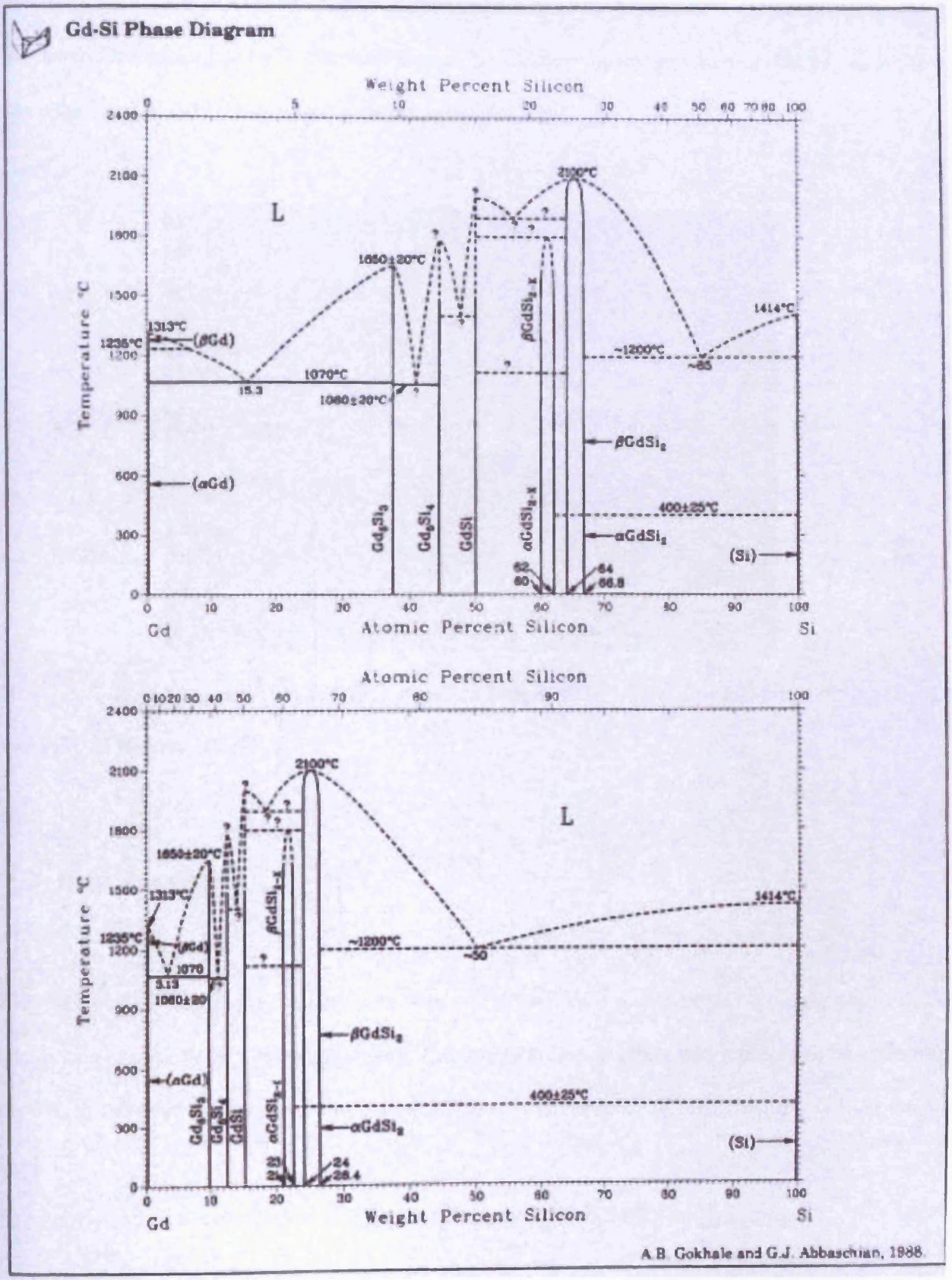

Fig. A1.2 Binary phase diagram of Gd and Si in both weight percentage and atomic percentage.

Note that Gd_5Si_4 has a narrow area in the phase diagram.

The samples are normally in the shape of a hemisphere after the preparation, as shown in Fig. A1.3. They should be cut either by a diamond saw or an electric discharge machine (EDM) in order to reduce the internal stresses during the cutting process.

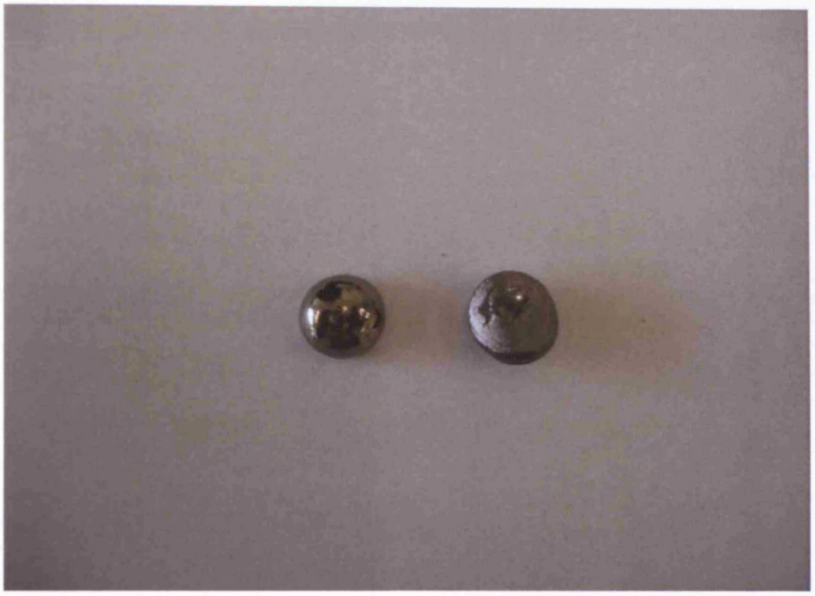

Fig. A1.3 $Gd_5Si_{1.8}Ge_{2.2}$ and $Gd_5Si_{1.9}Ge_2$ samples prepared by arc-melting before cutting at The University of Birmingham.

A1.2 Heat Treatment

Heat treatment of $Gd_5(Si_xGe_{1-x})_4$ samples was carried out in order to obtain a single phase in the material and to remove any residual phases. The magnetocaloric effect was reported to be extremely sensitive to the heat treatment of the samples hence it is essential to heat treat the $Gd_5(Si_xGe_{1-x})_4$ samples.

The following steps were carried out in order to heat treat the $Gd_5(Si_xGe_{1-x})_4$ samples.

1. The $Gd_5(Si_xGe_{1-x})_4$ samples were placed in the sample container with zirconium shavings as a getter material for any interstitial elements such as oxygen.

2. The $Gd_5(Si_xGe_{1-x})_4$ sample was wrapped in Tantalum foil to keep the sample separate from the Zirconium getter.
3. Heat the furnace to 1273 K in high purity Argon for 24 hours and cool to 553 K at 10 K/min and then hold the sample for 6 hours at this temperature.
4. Cool the sample to the room temperature at the rate of 10 K/min. Slower cooling is better as it removes more impurity phases than the faster cooling.

Appendix II

X-Ray Diffraction (XRD) Measurements

Polycrystalline samples of $Gd_5Si_{1.8}Ge_{2.2}$ and $Gd_5Si_{1.9}Ge_{2.1}$ which were prepared in the Materials and Metallurgy Department of the University of Birmingham by arc-melting. The samples were analysed using X-ray diffraction measurements for the corresponding lattice structure in the School of Engineering at Cardiff University. The samples were powdered to fine particles and mounted on a glass slide such that surface exposed to X-rays is completely covered by the particles. Both the samples were scanned between 5° and 80° with a step size of 0.02° as shown in Table A2.1. This range was chosen as the peaks for the monoclinic $Gd_5Si_2Ge_2$ crystal lattice occur in this range as shown in the reference Fig. A2.1. The reference peaks were then compared to the identified peaks of the polycrystalline samples of $Gd_5Si_{1.8}Ge_{2.2}$ and $Gd_5Si_{1.9}Ge_{2.1}$ shown in Fig. A2.2 and A2.3 respectively.

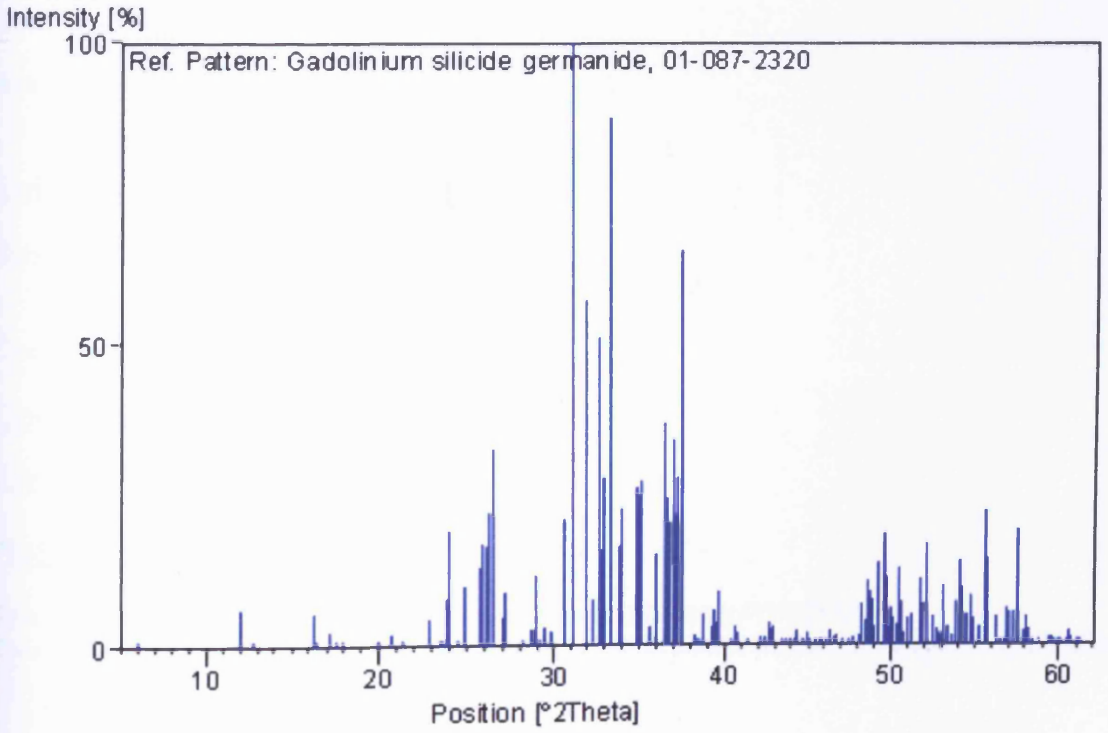

Fig. A2.1 Reference pattern of monoclinic $Gd_5Si_2Ge_2$ crystal lattice in the range of 0°-65°.

Reference pattern for the monoclinic $Gd_5Si_2Ge_2$.

Name and formula

Reference code:	01-087-2320
Common name:	Gadolinium silicide germanide
ICSD name:	Gadolinium Silicon Germanium
Empirical formula:	$Gd_5Ge_2Si_2$
Chemical formula:	$Gd_5(Si_2Ge_2)$

Crystallographic parameters

Crystal system:	Monoclinic
Space group:	P21/a
Space group number:	14
a (Å):	7.5808
b (Å):	14.8020
c (Å):	7.7799
Alpha (°):	90.0000
Beta (°):	90.0000
Gamma (°):	93.1900
Calculated density (g/cm^3):	7.52
Volume of cell (10^6 pm^3):	871.64
Z:	4.00
RIR:	1.83

Subfiles and Quality

Subfiles:	Inorganic Alloy, metal or intermetalic ICSD Pattern
Quality:	Calculated (C)

Comments

ICSD collection code:	084084

References

Primary reference:	*Calculated from ICSD using POWD-12++*
Structure:	Pecharsky, V.K., Gschneider, Jr., K.A., *J. Alloys Compds.* **260**, 98, (1997)

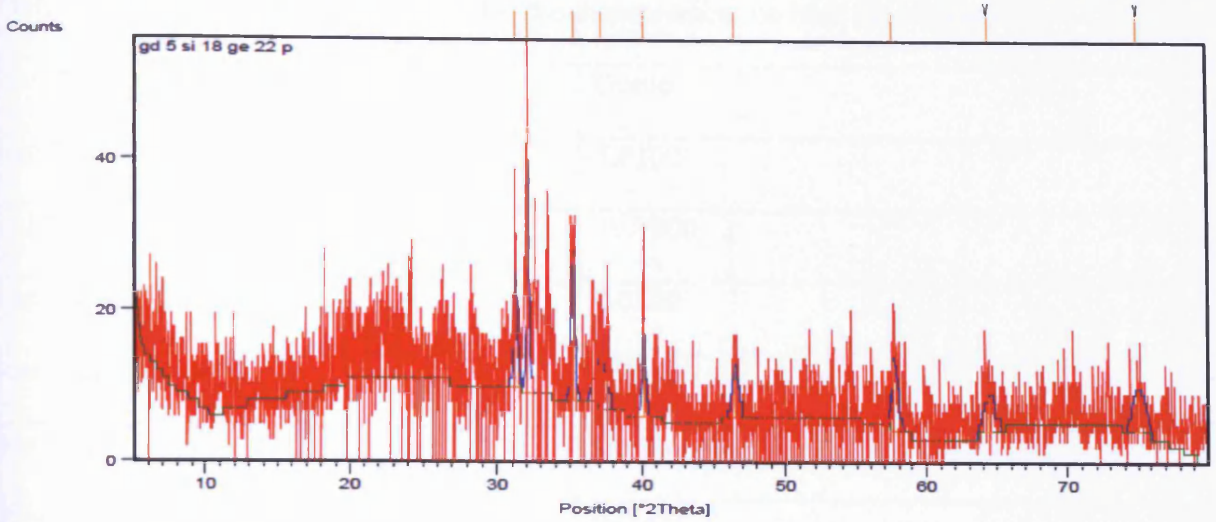

Fig.A2.2 Peaks identified are in Blue and the other diffracted intensities are in Red for a powdered sample of $Gd_5Si_{1.8}Ge_{2.2}$ and compared to the reference peaks of $Gd_5Si_2Ge_2$ shown on the top. Note that all the peaks are matching the peaks of the reference pattern except 2 minor peaks at the end of the range.

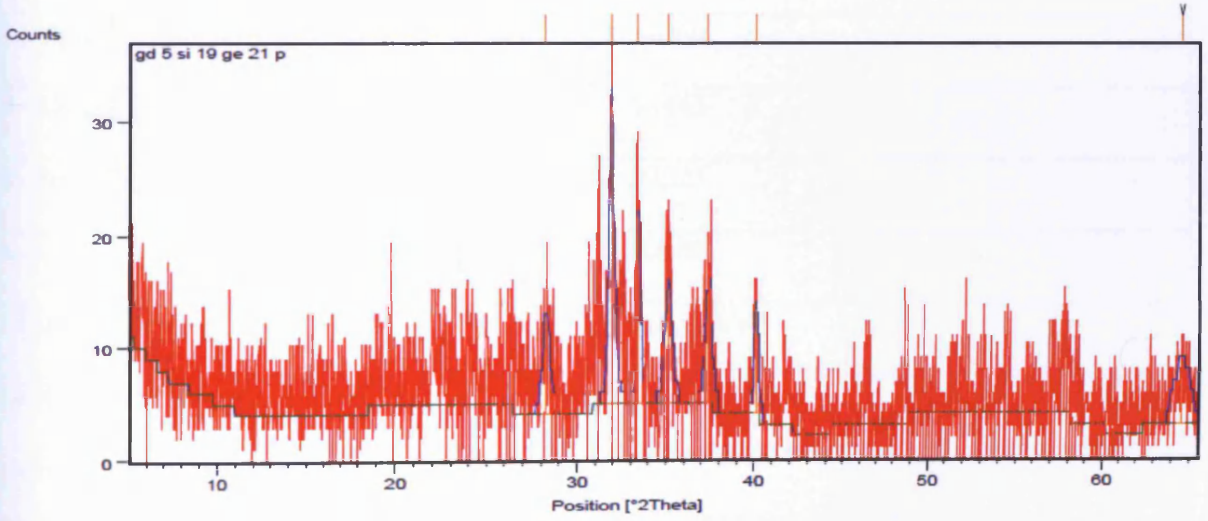

FigA2.3 Peaks identified are in Blue and the other diffracted intensities are in Red for a powdered sample of $Gd_5Si_{1.9}Ge_{2.1}$ and compared to the reference peaks of $Gd_5Si_2Ge_2$ shown on the top. Note that all the peaks are matching the peaks of the reference pattern except 1 minor peaks at the end of the range.

Table A2.1 XRD parameters selected for the measurement on both the samples.

Scan Axis	Gonio
Start Position [°2Th.]	5.0100
End Position [°2Th.]	79.9900
Step Size [°2Th.]	0.0200
Scan Step Time [s]	0.5000
Scan Type	Continuous
Offset [°2Th.]	0.0000
Irradiated Length [mm]	10.00
Specimen Length [mm]	10.00
Receiving Slit Size [mm]	0.0500
Measurement Temperature [°C]	295.00
Anode Material	Cu
K-Alpha1 [Å]	1.54060
K-Alpha2 [Å]	1.54443
K-Beta [Å]	1.39225
K-A2 / K-A1 Ratio	0.50000
Generator Settings	0 mA, 0 kV
Diffractometer Type	PW1710
Diffractometer Number	1
Goniometer Radius [mm]	173.00
Dist. Focus-Diverg. Slit [mm]	91.00
Incident Beam Monochromator	No
Spinning	No

Appendix III

Back Scattered Laue Diffraction

To index a single crystal sample with its principal axes, a technique called back scattered Laue diffraction is used. The pattern formed by the back scattered X-ray diffraction from any plane of a single crystal sample is unique. These unique patterns are known for the principal axes and are compared to the axes of the sample that is being indexed. Fig. A3.1 and A3.2 are the back scattered Laue diffractions carried out at the Ames Laboratory, USA by Dr. Deborah Schlagel on the planes of 'ac' and 'ab' of the single crystal $Gd_5Si_{1.5}Ge_{2.5}$ sample respectively. The procedure to index a single crystal sample is as follows:

- The single crystal ingot will normally have cleavages and these cleavage faces are normally perpendicular to one of the axes.

- The face with cleavage is then Laue imaged and the image is analysed to see what axis it is.

- If the Laue image is a 4 fold symmetric star pattern with clear lines connecting the dots as shown in Fig. A3.1, the face is perpendicular to b-axis otherwise it is either a-axis or c-axis. The sample is Laue imaged and oriented until the centre of the 4 fold symmetry falls on the centre of the film. The deviation of centre of symmetry of the image from the centre of the film is the measure of tilt of the crystal axis that is being aligned. The relation is given by $\beta = 0.5*\text{Arctan}(p/d)$ where d is the distance between film and the X-ray source (35 mm) and p is the deviation on the film.

- It is not possible to differentiate between a-axis and c-axis Laue images as they have similar crystal lattice parameters hence their Laue images will look similar. Fig. A3.2

shows a Laue image of the 'c' axis. To differentiate these axes, an XRD measurement of the single crystal sample has to be done. The sample has to be place with "a" or "c" axis parallel to the X-ray. The alignment of the axis should be accurate to 0.5 degrees.

- If the axis is "a" axis then we can see 2 peaks one very strong peak at 75° and a weak peak at 108°. If the axis is "b" axis then we can see a strong peak at 72° and a weak peak at 104°.

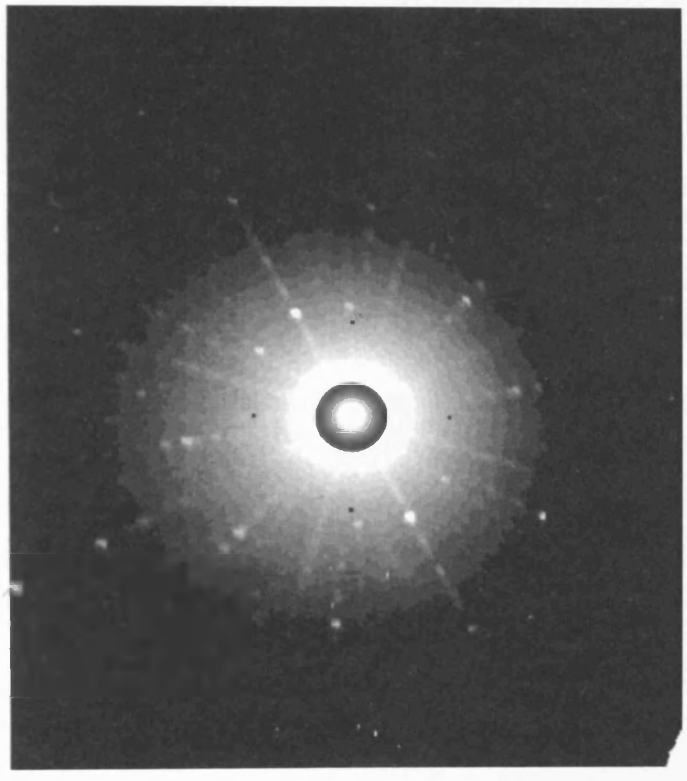

FigA3. 1 Back scattered Laue image from 'ac' ('b' perpendicular) on a single crystal $Gd_5Si_{1.5}Ge_{2.5}$ sample

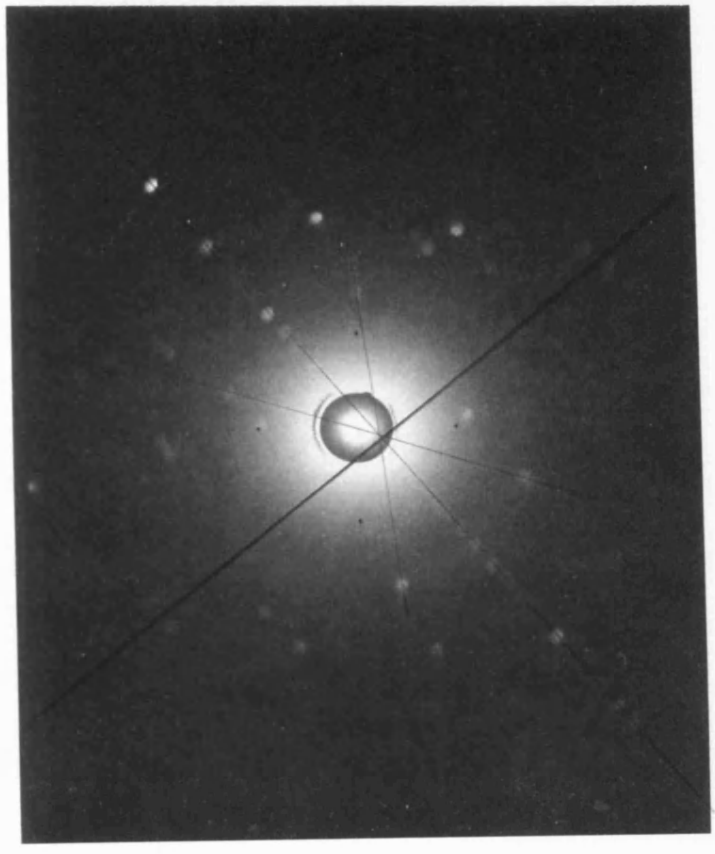

Fig. A3.2 Back scattered Laue image from 'ab' ('c' perpendicular) on a single crystal $Gd_5Si_{1.5}Ge_{2.5}$ sample

Appendix IV

Publications and Conference Presentations

Publications based on the work conducted for this thesis

1. R.L.Hadimani, Y Melikhov, J.E.Snyder, D.C.Jiles, "*Determination of the Projected Second Order Phase Transition Temperature of the Orthorhombic Phase of* $Gd_5(Si_xGe_{1-x})_4$", Journal of Applied Physics, **103**, pp. 033906, (2008).
2. R.L. Hadimani, D.C. Jiles, Y. Melikhov, J.E. Snyder, "*Determination of Curie Temperature by Arrott plot Technique in* $Gd_5(Si_xGe_{1-x})_4$", Journal of Magnetism and Magnetic Materials, **320**, Issue 20, pp. e696-698, (2008).
3. R. L. Hadimani, Y. Melikhov, J.E. Snyder, D.C. Jiles, "*Field induced phase transition at high temperatures above the Curie point in* $Gd_5(Si_xGe_{1-x})_4$" ,Journal of Applied Physics, **105**, pp. 07A927, (2009).
4. R. L. Hadimani, P. A. Bartlett, Y. Melikhov, J. E. Snyder and D. C. Jiles, "*Field and Temperature induced colossal strain in* $Gd_5(Si_xGe_{1-x})_4$ *for actuator applications* ", Journal of Magnetism and Magnetic Materials, Accepted, December 2009.
5. R. L. Hadimani, Y. Melikhov, J.E. Snyder, D.C. Jiles, "*Anomalous behaviour in electrical transport properties in single crystal* $Gd_5Si_{1.8}Ge_{2.2}$ *and polycrystalline* $Gd_5Si_{2.09}Ge_{1.91}$", IEEE Transaction on Magnetics, **45**, pp. 4368 – 4371, (2009).
6. R. L. Hadimani and D.C. Jiles, "*Resistivity recovery in* $Gd_5Si_{2.09}Ge_{1.91}$ *by annealing*", Journal of Applied Physics, **107**, pp. 09C501, (2010).
7. R. L. Hadimani and D.C. Jiles, *"Theory of Irrecoverable and Recoverable Resistivity in* $Gd_5(Si_xGe_{1-x})_4$*"*,IEEE Magnetics Letters, **Volume-1**, pp. 6000104, (2010).

Conference Presentations based on the work conducted for this thesis

1. R. L. Hadimani, Y. Melikhov, J. E. Snyder, D. C. Jiles, "*Estimation of first order and second order phase transition temperatures in* $Gd_5(Si_xGe_{1-x})_4$", Soft Magnetic Materials Conference, Cardiff 2-5, September 2007- *Awarded the best student poster presentation.*
2. R. L. Hadimani, Y. Melikhov, J. E. Snyder, D. C. Jiles, *"Determination of the Projected Second Order Phase Transition Temperature of Orthorhombic Phase of* $Gd_5(Si_xGe_{1-x})_4$", Magnetism and Magnetic Materials Conference, Tampa, Florida, USA, November 2007- Oral presentation.
3. R. L. Hadimani, Y. Melikhov, J. E. Snyder, D. C. Jiles, "*Magnetostriction close to the phase transition in* $Gd_5(Si_xGe_{1-x})_4$", APS March Meeting, New Orleans, Louisiana, March 10-14, 2008.
4. R. L. Hadimani, Y. Melikhov, J.E. Snyder, D.C. Jiles, *"Fine structure observation near critical temperature in* $Gd_5Si_{1.95}Ge_{2.05}$" , INTERMAG 2008 Conference, Madrid Spain, May 4-8, 2008- oral presentation.
5. R. L. Hadimani, Y. Melikhov, J. E. Snyder, D. C. Jiles, "*Determination of Transition Temperatures and Colossal Magnetostriction in* $Gd_5(Si_xGe_{1-x})_4$", IEEE Magnetic Society Summer School, Colorado Springs, USA, August 2008, poster presentation.
6. R.L.Hadimani, P.A.Bartlett, Y.Melikhov, J.E.Snyder and D.C.Jiles, "*Temperature induced Colossal magnetostriction in* $Gd_5(Si_xGe_{1-x})_4$ *for actuator applications*", European Magnetic Sensors and Actuators Conference, Cean, France, June 2008, Poster.
7. R. L. Hadimani, Y. Melikhov, J. E. Snyder, D. C. Jiles, *"Field induced phase transition in* $Gd_5(Si_xGe_{1-x})_4$ *series at high magnetic field strengths"*, International Workshop on 1&2 Dimensional Magnetic Measurement and Testing, Cardiff, 1-3 September 2008. Poster.

8. R. L. Hadimani, Y. Melikhov, J. E. Snyder, D. C. Jiles, "*Field induced structural phase transition at higher temperatures in* $Gd_5(Si_xGe_{1-x})_4$", Magnetism and Magnetic Materials Conference, Austin, Texas, USA, November 2008- Oral presentation.
9. R. L. Hadimani, Y. Melikhov, J. E. Snyder, D. C. Jiles, "*Examination of the Coupled Magnetic-Structural Phase Transition in Gadolinium-Silicon-Germanium Magnetocaloric alloys at temperatures well above Tc*", APS March Meeting, Pittsburgh, Pennsylvania, March 16-20, 2009. Oral presentation.
10. R. L. Hadimani, Y. Melikhov, J. E. Snyder, D. C. Jiles, "*Anomalous behaviour in electrical transport properties in single crystal* $Gd_5Si_{1.8}Ge_{2.2}$ *and polycrystalline* $Gd_5Si_{2.09}Ge_{1.91}$", INTERMAG 2009 Conference, Sacramento, California, USA, May 2009- oral presentation.
11. R. L. Hadimani, Y. Melikhov, J. E. Snyder, D. C. Jiles, "*Electrical transport and magnetic properties in giant magnetocaloric* $Gd_5(Si_xGe_{1-x})_4$", EUROMAT 2009, Glasgow, UK, September 2009- oral presentations.
12. R. L. Hadimani and D.C. Jiles, "*Resistivity recovery in* $Gd_5Si_{2.09}Ge_{1.91}$ *by annealing*", MMM-INTERMAG Joint Conference, Washington DC, January 2010- Poster.
13. R. L. Hadimani, Y. Melikhov, J. E. Snyder, D. C. Jiles, "*Magnetocrystalline anisotropy in single crystal* $Gd_5Si_{2.7}Ge_{1.3}$", APS March Meeting, Portland, Oregon, March 15-19, 2010. Oral presentation.